Characterization of dysregulated VHL-mediated pRb regulation in clear cell renal cell carcinoma

MERCY AKUMA

Thesis submitted to the University of Ottawa in partial Fulfillment of the requirements for the Doctorate in Philosophy degree in Cellular and Molecular Medicine

Department of Cellular and Molecular Medicine
Faculty of Medicine
University of Ottawa

Abstract

The von Hippel-Lindau (VHL) tumor suppressor plays a pivotal role in maintaining cellular homeostasis as a key component of E3 ubiquitin ligase complexes, which direct proteins for proteasomal degradation. Loss of VHL function, through mutation or transcriptional silencing, is a defining feature of most sporadic cases of clear cell renal cell carcinoma (ccRCC). VHL loss leads to the constitutive stabilization of its E3 ligase substrates, most notably hypoxia-inducible factor α (HIF-α), which drives ccRCC tumorigenesis through the activation of hypoxia-responsive genes. While HIF-α is well established as a driver of ccRCC, the HIF-independent functions of VHL in oncogenesis remain poorly understood. In this study, we sought to identify novel VHL targets and evaluate their therapeutic potential in ccRCC. Using proximity labeling to identify proteasome-sensitive VHL interactors, we discovered that retinoblastoma protein (pRb) is a novel substrate of VHL. Immunoprecipitation experiments revealed that VHL binds nuclear pRb under normoxic conditions in a phosphorylation-independent manner, facilitating its ubiquitin-mediated proteasomal degradation. In VHL-deficient ccRCC cells, pRb becomes hyperstabilized, leading to suppressed apoptosis and widespread transcriptional reprogramming that promotes tumorigenesis. Proteomic analysis of VHL-pRb interactors revealed an enrichment of proteins involved in genome-wide transcriptional remodeling, further implicating this pathway in ccRCC progression. To explore therapeutic strategies, we investigated pharmacological targeting of the VHL-pRb axis. Our findings revealed a pRb-dependent interaction between the CDK4/6 inhibitor Abemaciclib and the E2F1 activator β-lapachone, resulting in decreased viability across various ccRCC cell lines. While these results suggest a promising therapeutic approach, *in vivo* validation remains necessary. Overall, my work uncovers a previously unrecognized VHL-pRb pathway, providing new mechanistic insights into ccRCC pathogenesis and identifying a potential therapeutic strategy to mitigate tumor progression.

Contributions

This dissertation primarily contains findings from the following study:

Akuma, M., Kim, M., Zhu, C. *et al.* Loss of VHL-mediated pRb regulation promotes clear cell renal cell carcinoma. *Cell Death Dis* 16, 307 (2025). https://doi.org/10.1038/s41419-025-07623-y

Katayoun Sheikheleslamy and Caroline Vergette from StemCore Laboratories (Ottawa Hospital Research Institute, OHRI) performed Sanger sequencing. Sharlene Faulkes and Marjan Mahani from the Louise Pelletier Histology Core Facility performed immunohistochemistry staining and tissue microarray (TMA) construction. Fernando Ortiz and Shahriar Sheikholeslami from OHRI Flow Cytometry and Cell Sorting Facility performed flow cytometry and single-cell sorting. RNA-sequencing was performed by the McGill Applied Genomics Innovation Core at the McGill Genome Centre. Chenxuan Zhu from Dr. Ryan Russell's lab (University of Ottawa) assisted with the split-TurboID assay and generated the results in Figure 21B-D. Minjun Kim from Dr. Yasser Riazalhosseini's lab (McGill University) performed computational analysis of RNA-sequencing data. Zohreh Mehrjoo from Dr. Yasser Riazalhosseini's lab (McGill University) performed dose response and drug synergy testing on ccRCC patient-derived organoids. The OHRI Proteomics Core Facility performed liquid chromatography-mass spectrometry (LC-MS). Antoine Gaudreau-Lapierre from Dr. Laura Trinkle-Mulcahy's lab (University of Ottawa) performed LC-MS analysis. Ella Wiljer from Dr. William Stanford's lab (Ottawa Hospital Research Institute) performed tumor xenograft assay. All other experiments were performed by me.

Acknowledgements

I extend my heartfelt gratitude to my supervisor, Dr. Ryan Russell, for taking a chance on me during my third work term as a CO-OP student, and for convincing me to embark on a career path I'd never envisioned for myself. Thank you for constantly challenging me, embracing my ideas, encouraging me to think independently, and nurturing my curiosity. You have been a great mentor, and I appreciate the pivotal role you've played in shaping my research career.

To my thesis advisory committee members—Dr. Barbara Vanderhyden, Dr. Damien D'Amours, and Dr. Carolina Ilkow—thank you for sharing your expertise, insights, and guidance. Your advice was invaluable and helped me navigate this journey with confidence.

A special thank you goes to Dr. Chibuike Udenigwe for being both a mentor and a friend. Your wisdom and encouragement kept me grounded and inspired me to explore new possibilities for my future.

I am also immensely grateful to my lab members for their camaraderie and support. You all made even the toughest periods bearable with your humor and kindness. The bond we've created through shared struggles, triumphs, and countless ups and downs will always hold a special place in my heart.

To my family, I owe everything. Thank you for your unwavering emotional and financial support. Thank you for always encouraging me to chase my dreams, and for teaching me that giving up is never an option. To my sister Precious, thank you for being my confidante and for always lifting my spirits – I couldn't have done this without you. And to everyone I've lost along the way, thank you for being my reason to keep pushing forward. You remain my guiding light.

Finally, I thank God for guiding me through this journey and blessing me in ways I could never have imagined. Looking back, despite the challenges, the journey has been profoundly rewarding. To everyone who played a role in this chapter of my life, thank you from the bottom of my heart.

Table of Contents

List of Abbreviations

aa – Amino acid

ACAT1 - Acetyl-CoA acetyltransferase 1

AKT1 - RAC-alpha serine/threonine-protein kinase

ALDH1B1 - Aldehyde Dehydrogenase 1 Family Member B1

ANOVA – Analysis of variance

APAF1 - Apoptotic Peptidase Activating Factor 1

ARID1A - AT-Rich Interaction Domain 1A

aPKC - atypical protein kinase C

ARID1A - AT-Rich Interaction Domain 1A)

ARNT - Aryl hydrocarbon nuclear translocator

β2AR - β2-adrenergic receptor

BAP1 - BRCA1-associated protein-1

BNIP3 - Bcl-2 interacting protein 3

CARD1 - Caspase recruitment domain-containing protein 9

cBAF – canonical BRG1/BRM-associated factor

CBP – CREB-binding protein

ccRCC - Clear cell renal cell carcinoma

Cdc53 - Cell division control protein 53

CDK – Cyclin-dependent kinase

CLDN10 – Claudin-10

CK2 – Casein kinase 2

ColIV - collagen IV

CPTAC - Clinical Proteomic Tumor Analysis Consortium

CREB - cAMP Response Element-Binding Protein

CRISPR - Clustered regularly interspaced palindromic repeats

CRL - cullin-RING ligase

CTLA-4 - Cytotoxic T-lymphocyte associated protein 4

CUL2 – Cullin-2

CYFIP2 - Cytoplasmic FMR1 interacting protein 2

DCAF13 - DDB1 And CUL4 Associated Factor 13

DECR1 - 2,4-Dienoyl-CoA Reductase 1

DMSO - Dimethyl sulfoxide

DNA - Deoxyribonucleic acid

DNMT - DNA Methyltransferase

DPF1/2 - D4, zinc, and double PHD fingers family members 1/2

E1A - Adenovirus early region 1A

E2F1 - E2F Transcription Factor 1

ECM – Extracellular matrix

EDTA - Ethylenediamine tetraacetic acid

EGFR - Epidermal Growth Factor Receptor

EPO – Erythropoietin

FIH - Factor Inhibiting HIF

FN1 – Fibronectin 1

GAPDH - Glyceraldehyde 3-phosphate dehydrogenase

GEMM – Genetically engineered mouse model

GLUT1 - Glucose transporter 1

HA - hemagglutinin

HEK293 - human embryonic kidney 293

HMT - Histone methyltransferase

HDAC - Histone deacetylase

HECT - Homologous to the E6AP carboxyl terminus

HIF - Hypoxia inducible factor

HOXB8 - Homeobox B8

IgG - Immunoglobulin G

KDM5C - Lysine Demethylase 5C

KDM6A - Lysine Demethylase 6A

KRAS - Kirsten rat sarcoma virus

LC-MS - Liquid chromatography-mass spectrometry

MDM2 - Mouse double minute 2 homolog

MEFs – Mouse Embryonic Fibroblasts

mRNA – messenger RNA

MYOD - myoblast determination protein 1

NF-κB - Nuclear factor kappa B

ORR – Objective response rate

PBRM1 - Polybromo 1

PCR - Polymerase chain reaction

PD-1 - Programmed cell death protein 1

PD-L1 - Programmed cell death Ligand 1

PDGF - Platelet-derived growth factor

PFS – Progression-free survival

PP1 - Protein phosphatase 1

pRb – Retinoblastoma protein

PTM – Post-translational modification

qRT-PCR – Quantitative real-time PCR

RAPTOR - Regulatory-associated protein of mTOR

RB1 - RB Transcriptional Corepressor 1

RBL1 - RB Transcriptional Corepressor Like 1

RBL2 - RB Transcriptional Corepressor Like 2

Rbx-1 - RING box protein-1

RING - Really Interesting New Gene

RNA - Ribonucleic acid

SA-β-gal - senescence-associated β-galactosidase

SDS-PAGE - Sodium Dodecyl Sulfate Polyacrylamide Gel Electrophoresis

SETD2 - SET Domain Containing 2

SFMBT1 - Scm-like with four malignant brain tumor domains 1

sgRNA – single guide RNA

shRNA – short hairpin RNA

siRNA – small interfering RNA

SKIDA1 - SKI/DACH Domain Containing 1

SMARCA4 - SWI/SNF related BAF chromatin remodeling complex subunit ATPase 4

Spry2 - Sprouty2

SRB - Sulforhodamine B

SV40 - Simian Vacuolating Virus 40 TAg

SWI/SNF - Switch/sucrose non-fermentable

TCGA – The Cancer Genome Atlas

TGF-α - Transforming Growth Factor Alpha

TNF-α - tumor necrosis factor-alpha

TOP1 – Topoisomerase I

TKI – Tyrosine Kinase Inhibitor

TUNEL - terminal deoxynucleotidyl transferase dUTP nick end labeling

UALCAN - University of ALabama at Birmingham CANcer

UBR5 - Ubiquitin Protein Ligase E3 Component N-Recognin 5

VEGF – Vascular Endothelial Growth Factor

VEGFI – Vascular Endothelial Growth Factor Inhibitor

VHL – von Hippel-Lindau

ZHX2 - Zinc finger and homeobox 2

ZIP - zero interaction potency

List of Figures

List of Tables

Chapter 1: Introduction

1.1 The von Hippel Lindau (VHL) tumor suppressor

1.1.1 Discovery of *VHL*

In 1894, British ophthalmologist Treacher Collins first described familial retinal hemangioblastomas in pathologic specimens obtained from two siblings[1,2]. The term 'von Hippel Lindau disease' is derived from the descriptions of two authors: Eugene von Hippel, who studied the clinical appearance and progression of retinal lesions now referred to as retinal hemangioblastomas, and Arvid Lindau who found the association between cerebellar hemangioblastomas and retinal hemangioblastomas[2–4]. VHL disease is a hereditary cancer syndrome characterized by a range of benign and malignant tumors[5–11]. Its clinical manifestations include retinal and central nervous system hemangioblastomas, clear cell renal cell carcinoma (ccRCC), pheochromocytomas, pancreatic neuroendocrine tumors, and endolymphatic sac tumors[19–25]. Among these, ccRCC—a tumor of the kidney—is considered the most malignant and life-threatening complication of VHL disease.

The first hints about the identity and location of the *VHL* gene arose from cytogenetic studies of several unrelated families with an inherited susceptibility to ccRCC[1–3], and further supported by a series of studies that used cytogenetics and restriction fragment length polymorphism analysis to identify and characterize genetic abnormalities in sporadic ccRCC[4–8]. These studies consistently identified abnormalities in the short arm of chromosome 3 (3p) that were present in ccRCC tumors but absent in normal tissue and in patients with other histologic subtypes, such as papillary RCC[9,10]. Through genetic linkage analysis, researchers were able to narrow down the location of the *VHL* gene to a relatively small region on the short arm of chromosome 3 (3p), spanning approximately 4 centimorgans[11–13]. In 1993, the gene was successfully identified through positional cloning and mapped to chromosome 3p25–26[14]. VHL is a highly conserved

gene comprising three exons and encodes two ubiquitously expressed protein isoforms: $pVHL_{30}$ (amino acids 1-213) and $pVHL_{19}$ (amino acids 54–213), generated via alternative translation initiation[15,16]. These isoforms differ in their subcellular localization—$pVHL_{30}$ is predominantly cytoplasmic, whereas $pVHL_{19}$ is more evenly distributed between the nucleus and cytoplasm[15].

1.1.2 Classifications of VHL disease

VHL disease is an autosomal dominant condition with an incidence rate between 1/27,000 to 1/43,000 of live births[17–19]. VHL disease conforms to the Knudson's 'two-hit' hypothesis[20–22]. Germline mutations in *VHL* result in a defective allele, and this represents the first 'hit'. The second 'hit' is a somatic event that occurs in the second allele, leading to loss of heterozygosity at the *VHL* locus. Inactivation of both *VHL* alleles can lead to tumor development in the affected tissue. Missense mutations (27–38%) and nonsense mutations (13–27%) are the most common germline mutations, followed by rearrangements and large or microdeletions[23,24]. 'Second hit' events are typically caused by allelic loss (49%) or hypermethylation (35%) of the wild type allele, but could also be caused by point mutations in the wild type allele[25,26]. However, missense mutations in both alleles do not typically lead to ccRCC development, as VHL has been described to form homotypic complexes that function in a complementary fashion[27]. This compensation may potentially explain why VHL-associated tumors with the first *VHL* allele carrying a missense mutation are almost always accompanied by a second *VHL* allele containing a gross truncation or deletion.

Genotype-phenotype correlations exist in VHL disease. Clinically, VHL disease is classified into type 1 or type 2 depending on the absence or presence of pheochromocytomas (PCCs),

respectively[28] (Table 1). Type 1 disease is typically associated with ccRCC and the absence of pheochromocytomas[29]. Type 2 VHL disease is further subdivided into type 2A (low risk for ccRCC), type 2B (high risk for ccRCC), and type 2C (risk for PCCs only)[30–34]. Patients with type 2 VHL disease usually have a germline missense VHL mutation (84%), that is not predicted to remain conformationally intact[29,35,36]. In contrast, type 1 disease is often associated with truncating mutations or exon deletions, mutations that grossly alter VHL structure and function or that lead to its complete absence[29,35,36]. These observations have led to the hypothesis that type 2 VHL mutants acquire a gain-of-function that promotes pheochromocytoma development, or that complete loss of VHL function is incompatible with pheochromocytoma development[37,38].

Table 1. VHL disease subtypes, clinical phenotypes, and types of VHL mutations associated with each subtype.

VHL Disease Subtype	Clinical Phenotype	Type of VHL mutation
1	ccRCC; hemangioblastoma	Deletion, nonsense, frameshift, missense
2A	Hemangioblastoma; phaeochromocytoma	Missense
2B	ccRCC; hemangioblastoma; phaeochromocytoma	Missense
2C	Phaeochromocytoma	Missense

1.1.3 Other genetic mutations in clear cell renal cell carcinoma

RCC comprises a heterogeneous group of cancers originating from renal tubular epithelial cells, and accounts for more than 90% of kidney cancers[39,40]. Major subtypes of RCC include clear cell RCC (ccRCC)[41], papillary RCC (pRCC)[42], and chromophobe RCC (chRCC)[43]. Among these, ccRCC is the most common, making up 70-80% of cases[44], and is the leading cause of mortality

in VHL kindred[45]. The term 'clear cell' refers to the clear appearance of the cytoplasm following histological preparation of ccRCC tissue. Although VHL disease is rare, somatic mutations in the VHL gene are observed in up to 90% of sporadic ccRCC cases, highlighting its critical role in renal tumorigenesis[46–48]. However, VHL inactivation alone is insufficient to drive oncogenesis in most ccRCC cases, suggesting a requirement for additional cooperating mutations[49–51].

Mutations commonly observed in oncogenes and tumor suppressor genes associated with adult epithelial cancers, such as B-Raf proto-oncogene (*BRAF*), KRAS proto-oncogene (*KRAS*), and RB Transcriptional Corepressor 1 (*RB1*), are relatively rare in patients with ccRCC[52]. Before the development of massively parallel sequencing technology, VHL was the only known gene frequently found to be mutated in ccRCC. However, since 2010, large-scale exome sequencing studies have identified frequent recurrent mutations in genes encoding chromatin-modifying proteins. These include *PBRM1* (Polybromo-1)[53], *SETD2* (SET domain containing 2)[54], and *BAP1* (BRCA1 associated protein-1)[55,56], mutated in approximately 41–50%, 13–28%, and 11–17% of ccRCC cases, respectively. Germline mutations in both *BAP1* and *PBRM1* have been linked to increased susceptibility to ccRCC[57,58]. Notably, *PBRM1*, *SETD2*, and *BAP1* are located at the 3p21 locus on chromosome 3, close to *VHL*, which is located at the 3p25 locus[59]. This evidence supports the hypothesis that deletion of the 3p chromosome and the subsequent loss of heterozygosity at these loci plays a critical role in the development of ccRCC. Other frequent recurrent mutational targets in ccRCC include the histone modifying genes *KDM5C* and *KDM6A*[54], and genes involved in PI3K-AKT-mTOR signaling (~20% of the ccRCC tumors)[52]. Hence, while VHL inactivation is a critical early event in ccRCC initiation, additional genetic or epigenetic alterations may be required for full tumorigenic progression.

1.1.4 VHL targets cellular substrates for proteasomal degradation

1.1.4.1 The ubiquitin-proteasome pathway

Through a series of experiments in the late 1970s and early 1980s, Aaron Ciechanover, Avram Hershko, and Irwin A. Rose discovered and characterized the ubiquitin-mediated protein degradation system[60–62]. They later received the Chemistry Nobel prize for this discovery in 2004[63]. Ubiquitin is a small globular 76 amino acid protein, which is highly conserved across eukaryotes[64,65]. Ubiquitination, which involves the covalent attachment of a chain of ubiquitin molecules to the target substrate, facilitates targeting of the substrate to the 26S proteasome for rapid degradation. The 26S proteasome is a large, multi-catalytic ATP-dependent protease complex that acts as the degradation machinery of the ubiquitin system, which plays a major role in the regulated degradation of cytosolic, nuclear and membrane proteins across all eukaryotes[66]. The ubiquitination reaction is a multistep process achieved by three enzymes: the ubiquitin-activating enzyme (E1), the ubiquitin-conjugating enzyme (E2), and the ubiquitin ligase (E3)[64,65] (Figure 1). The E1 enzyme catalyzes the ATP-dependent formation of a covalent thioester bond between the carboxy-terminal glycine of ubiquitin and an E1 cysteine residue. Subsequently, the E1 transfers ubiquitin to the cysteine of an E2 enzyme forming another thioester bond. Finally, the E3 ligase catalyzes the transfer of ubiquitin from the E2 to a lysine residue or free N-terminal amino group of the target substrate, forming an isopeptide bond.

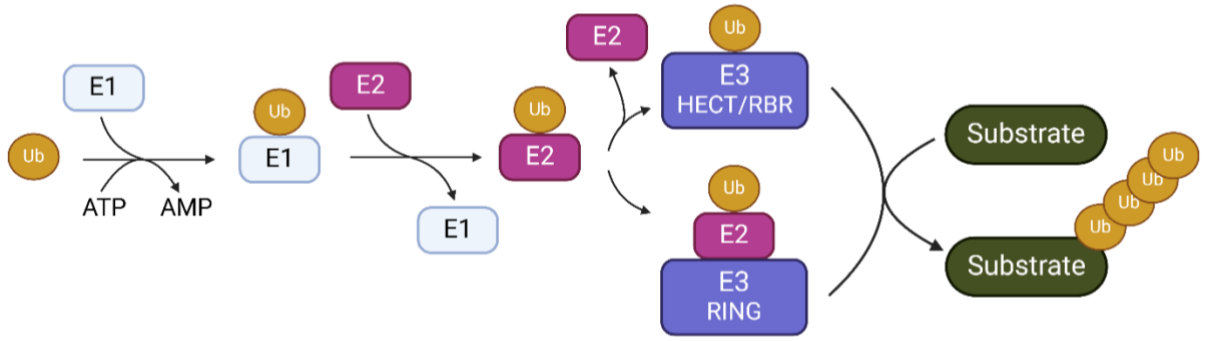

Figure 1. Schematic of the ubiquitination process. Ubiquitination involves a sequential cascade of enzymatic reactions. First, ubiquitin (Ub) is activated by the E1 Ub-activating enzyme in an ATP-dependent process and subsequently transferred to an E2 Ub-conjugating enzyme. Next, Ub is transferred from the Ub~E2 conjugate to a lysine residue of the substrate, either directly as mediated by a RING (Really Interesting New Gene) E3 Ub ligase or indirectly through an intermediate transfer to a HECT (homologous to the E6AP carboxyl terminus) or RBR (RING-between-RING) E3 Ub ligase. Created using BioRender.

Polyubiquitin chains are formed by covalent linkage of ubiquitin molecules typically on the Lys48 residue, or at the second most common position Lys63[67–71]. The specific lysine residue on which polyubiquitination occurs is also important in determining the fate of the protein. For instance, polyubiquitin chains linked at Lys-48 (well-studied) and Lys-29 (less studied) serve as signals for proteasome-mediated degradation. In contrast, ubiquitination at other lysine residues, such as Lys-63, may signal processes like DNA repair, transcription factor activation, etc.[65]. Meanwhile, mono-ubiquitination of proteins serves different functions, including regulation of endocytosis, histones, and virus budding[72]. Polyubiquitinated proteins are directed to the 26S proteasome, a large multi-subunit complex, where they are unfolded and channeled into its catalytic core for rapid degradation into short polypeptides in an ATP-dependent process[64,65].

1.1.4.2 Classification of E3 ligases

The human genome encodes over 600 E3 ligases[73]. E3 ligases can be classified into three categories depending on their structure and function: HECT, RBR, and RING E3 ligases[74] (Figure 2). HECT E3 ligases contain a conserved HECT domain located at the C-terminus, and diverse N-terminal domains that confers substrate specificity[75]. The N-terminal lobe of the HECT domain interacts with the ubiquitin-conjugated E2 enzyme, whereas the C-terminal lobe harbours the catalytic cysteine[76]. The HECT E3 ligases catalyze ubiquitin transfer via a two-step reaction: ubiquitin is first transferred to the catalytic cysteine on the C-terminal lobe and subsequently to the target substrate. RBR E3 ligases contain 3 domains: a RING1 domain that binds ubiquitin-charged E2, a RING2 domain with a cysteine residue that catalyzes a transthioesterification reaction to accept ubiquitin from RING1, and an in-between-RING (IBR) domain[77]. The process of ubiquitination by RBR E3 ligases involves recognition of the E2∼Ub conjugate by RING1, transfer of ubiquitin onto the catalytic cysteine in RING2 to form the thioester intermediate, and finally transfer of ubiquitin onto the substrate[78].

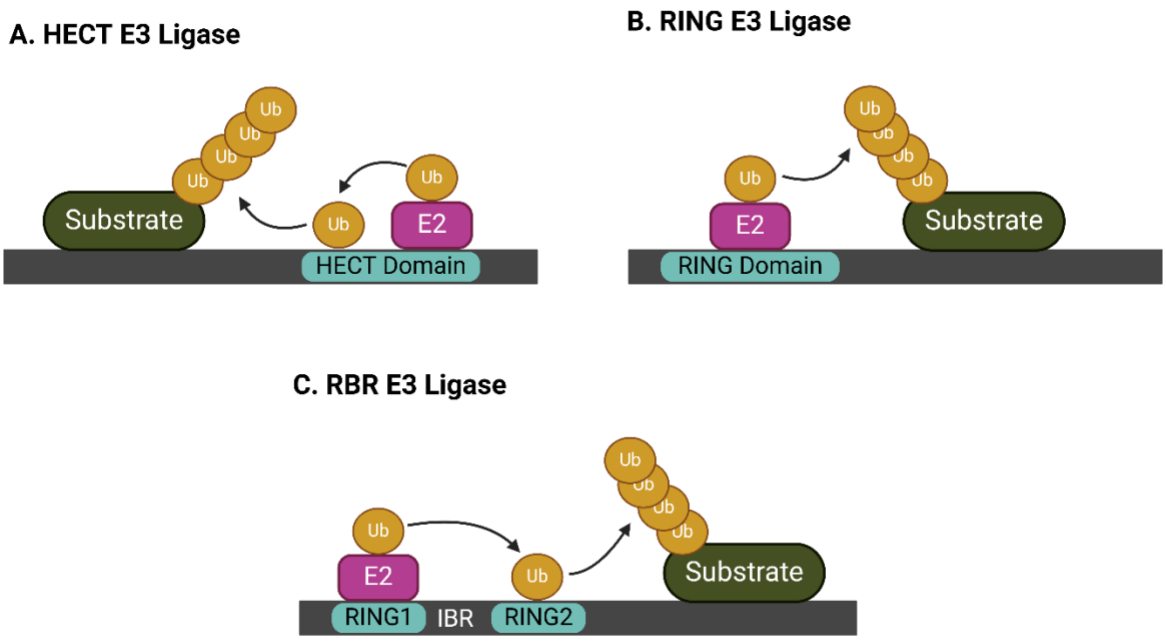

Figure 2. Classes of E3 ubiquitin ligases and their mechanism of action. (A) HECT type E3 ligases catalyze ubiquitin transfer through a two-step process: ubiquitin is transferred from the E2 ligase bound to the HECT domain (at the C-terminus) to a catalytic cysteine on the E3 ligase; the second step is the transfer of ubiquitin from the E3 ligase to the substrate. **(B)** RING E3 ligases mediate a direct transfer of ubiquitin from the E2 ligase to the substrate. **(C)** RBR E3 ligases catalyze ubiquitin transfer through a two-step process: ubiquitin is first transferred to a catalytic RING2 domain on the E3, the second step is the transfer of ubiquitin to the substrate. Created using BioRender.

RING (Really Interesting New Gene) E3 ligases are the most abundant type of ubiquitin ligases and are characterized by a zinc-binding domain called RING at the N-terminus[79–81]. In contrast to HECT E3s, RING E3s mediate the direct transfer of ubiquitin from the ubiquitin-charged E2 to the substrate, bypassing an E3-ubiquitin intermediate[82–84]. RING E3s are classified into two families: monomeric RING finger and multi-subunit E3 ligases. The cullin-RING ligases (CRLs) are a highly diverse class of multi-subunit RING E3 ligases with over 200 members, and may

contribute to ~20% of all ubiquitination in cells[85,86]. They consist of a cullin scaffold (CUL1, CUL2, CUL3, CUL4A/4B, CUL5, or CUL7), an N-terminal RING-box protein (RBX1 or RBX2), an adaptor protein, and a substrate receptor at the C terminus that confers substrate specificity[85,87].

1.1.4.3 VHL as an E3 ubiquitin ligase

E3 ligases confer substrate specificity in the ubiquitin-proteasome system by directly binding to their targets[80]. VHL is one such E3 ligase component, composed of two functional domains: the N-terminal β domain (residues 63–154), which is predicted to bind cellular substrates, and the α domain (residues 155–213), which binds to the Elongin B/C heterodimer[37,88,89]. VHL associates with adaptor proteins Elongin B/C, scaffold protein Cullin-2 (Cul2), and the RING finger protein Rbx1 to form the cullin-RING ligase complex, known as the ECV complex[89–91]. This complex facilitates ubiquitin transfer to target proteins. The ECV complex is structurally and functionally analogous to the yeast SCF (Skp1/Cdc53/F-box protein) complex that targets substrates recruited via the F-box protein[90,92] (Figure 3). Elongin C and Cul2 are similar to yeast Skp1 and Cdc53, respectively. Both complexes interact with Rbx1 and are classified as RING-type E3 ligases[91,93].

Within the ECV complex, VHL serves as the substrate recognition component that targets the α subunit of the hypoxia inducible factor (HIF-α) for proteasomal degradation under normoxic (normal oxygen) conditions[94,95]. This function is essential for cellular oxygen sensing. Notably, tumorigenic mutations frequently occur in both the α and β domains of VHL, highlighting the importance of its interactions with Elongin B/C and HIF-α in its tumor suppressor function[37,89,92,96]. Beyond HIF-α, VHL also mediates the degradation of various other substrates,

thereby conferring broader target specificity. These substrates include the Epidermal Growth Factor Receptor (EGFR), Zinc finger and homeobox 2 (ZHX2), β2-adrenergic receptor (β2AR), atypical protein kinase C (aPKC), Sprouty2 (Spry2), Scm-like with four malignant brain tumor domains 1 (SFMBT1), and Regulatory-associated protein of mTOR (RAPTOR)[97–104].

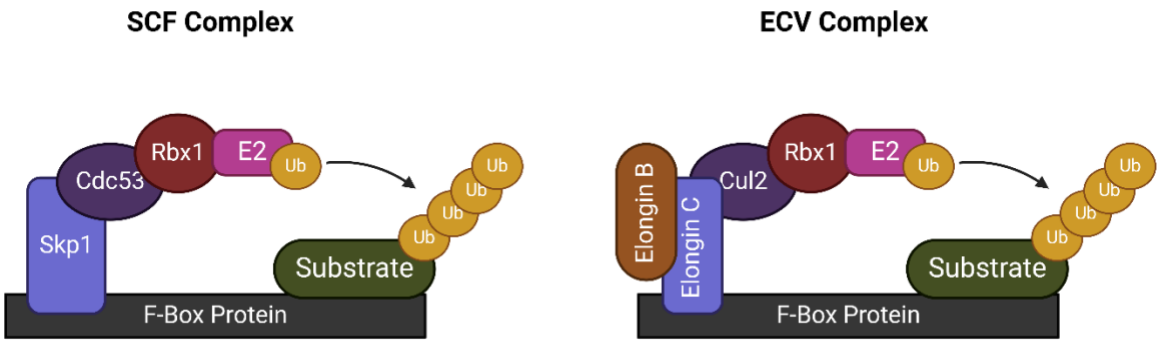

Figure 3. Schematic illustration of SCF and ECV complexes. The SCF and ECV complexes share a similar overall architecture and are both involved in the ubiquitin-dependent degradation of cellular proteins. Complex members that share sequence similarity (Skp1 and Elongin C; Cdc53 and Cullin-2) are represented by the same color. Rbx1 is common to both the SCF and VHL complexes. Created using BioRender.

1.1.5 VHL-mediated regulation of HIF and cellular oxygen sensing

1.1.5.1 HIF as an oxygen-dependent target of VHL

HIF is a heterodimeric transcription factor consisting of an oxygen-labile HIF-α subunit, and a stable HIF-β subunit that is constitutively expressed in the nucleus[105–107]. Three major HIF-α isoforms exist: HIF-1α, HIF-2α, and HIF-3α, of which HIF-1α and HIF-2α are the best studied[108]. Under normoxia, prolyl-4-hydroxylases (PHDs) use co-factors: 2-oxoglutarate (2-OG), Fe^{2+}, and ascorbate; and oxygen as a co-substrate to facilitate the hydroxylation of

conserved proline residues in the oxygen-dependent domain (ODD) of HIF-α[94,95,109] (Figure 4). These conserved residues are P402 and P564 in human HIF-1α; and P405 and P531 in human HIF-2α[94,95,110,111]. Hydroxylated proline residues on HIF-α serve as recognition sites for VHL, which in association with the ECV complex, facilitates the polyubiquitination of HIF-α, leading to its proteasomal degradation[94,95,110,111].

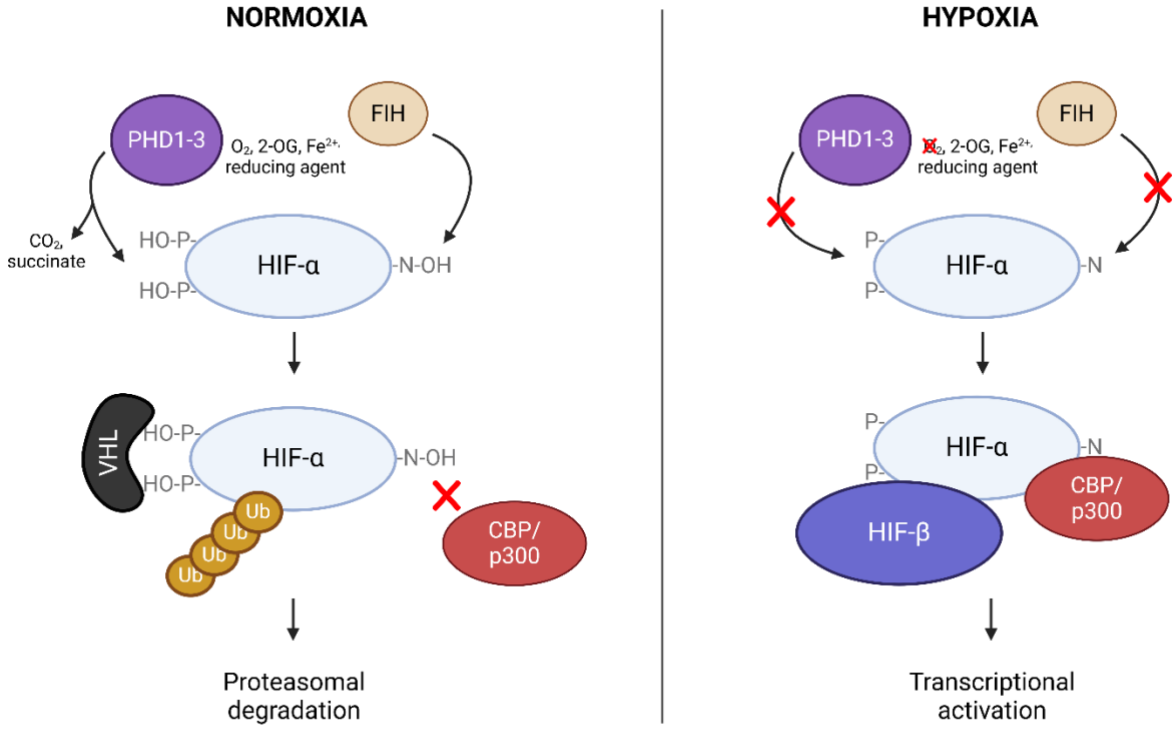

Figure 4. Regulation of HIF-α by the cellular oxygen sensors PHD and FIH. Prolyl-4-hydroxylases (PHDs) use co-factors: 2-oxoglutarate (2-OG), Fe^{2+} and ascorbate; and oxygen (O_2) as a co-substrate. Under normoxia, PHD-mediated hydroxylation of conserved proline residues in HIF-α, leads to the binding of VHL and recruitment of the ECV complex. Subsequently, HIF-α is polyubiquitinated and degraded by the proteasome, preventing transactivation of HIF-responsive genes. Factor Inhibiting HIF (FIH) also promotes hydroxylation of a specific asparagine residue on HIF-α, preventing the recruitment of transcriptional co-activators CBP/p300 to HIF-α. Under hypoxia (low oxygen), PHD and FIH can no longer catalyze the hydroxylation of HIF-α, allowing HIF-α to translocate to the nucleus, dimerize with HIF-β, and recruit CBP/p300, to promote the transactivation of hypoxia-responsive genes. Created using BioRender.

Under hypoxia, PHDs are unable to efficiently hydroxylate key proline residues on HIF-α (Figure 4). As such, HIF-α evades recognition by VHL and subsequent proteasomal degradation. Accumulated HIF-α subunits translocate into the nucleus where they dimerize with HIF-β (or ARNT) to promote transcription of hypoxia-response genes, which possess a hypoxia responsive element (HRE)[112]. The C-terminal activation domain (C-TAD) of HIF-α recruits co-activators CREB-binding protein (CBP) and p300 to promote the transactivation of hypoxia-responsive genes. The activity of the C-TAD domain is also regulated by FIH, a Fe^{2+}-dependent asparaginyl hydroxylase[113,114]. FIH-mediated hydroxylation of a conserved asparagine residue (Asn803 in human HIF-1α; Asn847 in human HIF-2α) within the C-TAD domain prevents the recruitment of CBP/p300, further suppressing HIF transcriptional activity under normoxia[113–115] (Figure 4). Dual regulation of HIF protein stability by PHD and FIH therefore controls the transcriptional activity of HIF in response to varying oxygen levels.

1.1.5.2 Dysregulation of VHL-HIF signaling axis in ccRCC

Somatic *VHL* gene mutations are observed in up to 90% of sporadic ccRCC[46–48]. The best-characterized function of VHL relates to its ability to target HIF-α for ubiquitination via the ECV complex, promoting its proteasomal degradation under normoxia[94,95]. Disruption of the VHL α domain, which nucleates the ECV complex, or the β domain, which binds HIF-α, results in the stabilization of HIF[116]. Hence, in ccRCCs with 'disruptive' *VHL* mutations, constitutive HIF stabilization is observed irrespective of oxygen levels[117,118]. A significant proportion of ccRCC-associated VHL mutants described either fail to bind HIF-α or to assemble the ECV ubiquitin ligase complex, underscoring the importance of HIF in mediating the ccRCC phenotype[119,120].

Both HIF-1 and HIF-2 heterodimers activate the transcription of target genes by binding to the same hypoxia-responsive element (HRE). However, they are not functionally redundant. Transcriptomic analyses reveal that HIF-1 primarily induces apoptotic pathways and regulates genes involved in glycolysis, whereas HIF-2 preferentially promotes growth and angiogenesis[121–123]. Both paralogues also share similar targets such as Vascular Endothelial Growth Factor A (VEGFA) and glucose transporter 1 (Glut-1)[124]. The activation of genes by HIF-1 and HIF-2 can also be context-specific and temporally regulated such that in certain cell lines, HIF-1 drives the acute response to hypoxia (< 24 hours), whereas HIF-2 regulates the chronic response (> 24 hours)[125]. As such, the relative contributions of HIF-1 and HIF-2 to the regulation of specific HIF target genes can vary depending on the cellular context[123].

Growing evidence suggests that HIF-2, rather than HIF-1, is the key driver of renal cancer progression[126]. Stable expression of a HIF-2α mutant lacking VHL recognition overrides VHL-mediated tumor suppression in ccRCC cells[127]. Furthermore, shRNA-mediated knockdown of HIF-2α was sufficient to suppress tumorigenesis in VHL-defective ccRCC cells[128]. Hence, HIF-2 is both necessary and sufficient for ccRCC tumorigenesis. HIF-2 also underlies much of the pathology observed in genetically engineered mouse models (GEMM) with VHL inactivation in specific tissues[129,130,130–134]. HIF-1α on the other hand, may function as a tumor suppressor in the context of ccRCC, as its expression is frequently lost in many VHL-defective ccRCC cell lines[119,120,122,127,128,134–137]. The overexpression of HIF-1α in VHL-defective ccRCC cell lines was shown to suppress tumor formation[122]. Furthermore, HIF-2α, but not HIF-1α, could override VHL's tumor suppressor activity[122,127,137]. Thus, although similar, HIF-1α and HIF-2α may have distinct and even opposing activities. HIF-driven expression of VEGF promotes the formation of new blood vessels that supply the tumor with oxygen and nutrients[138]. Glut-1 facilitates the

uptake of glucose into cancer cells to meet their increased metabolic demands[139]. Hence, the transactivation of HIF targets promotes tumor adaptation to hypoxic environments. Furthermore, HIF-activated genes not only facilitate the growth, survival, metastasis, and invasion of tumor cells, but also promote their resistance to chemotherapy and radiation[140].

1.1.6 Beyond HIF: Non-canonical functions of VHL

1.1.6.1 Non-HIF proteolytic functions of VHL

VHL has been reported to regulate additional substrates beyond the well-characterized HIF-α family (Figure 5). VHL promotes the ubiquitination and proteasomal degradation of activated EGFR[98], which may be critical for tumor growth of VHL-defective ccRCC cells[141,142]. VHL also mediates the ubiquitination and proteasomal degradation of activated aPKC[143], which is important in the regulation of cell polarity and cell growth[144], cellular functions often dysregulated in cancer cells. VHL promotes the degradation of β2AR, whose expression in tumors is closely associated with poor patient prognosis[145,146]. ZHX2, another proteasomal substrate of VHL, may promote ccRCC tumorigenesis through activation of Nuclear factor-kappa B (NF-κB)[99] and the MEK/ERK1/2 signaling pathway[147]. VHL mediates the ubiquitination and proteasomal degradation of SFMBT1[103], which regulates epithelial-to-mesenchymal transition and is linked to poor patient prognosis[104]. SFMBT1 also drives ccRCC oncogenesis via regulation of sphingosine kinase 1[103]. In 2021, RAPTOR was identified as a novel target of the VHL E3 ubiquitin ligase complex[97]. Downregulation of RAPTOR by VHL inhibits mTORC1 signalling, which plays a known role in the oncogenesis and progression of ccRCC[97,148].

Other proteasomal targets of VHL include Janus kinase 2 (JAK2)[149], erythropoietin receptor (EpoR)[150], Myb-binding protein 1A (MYBBP1A)[151], Sprouty2 (Spry2)[102], and RNA polymerase subunits RPB1[152] and RPB7[153]. In support of the biological relevance of HIF-independent VHL regulation in ccRCC, a synthetic VHL mutant that retains HIF degradation but is deficient in the regulation of some HIF-independent targets, was found to be incapable of suppressing ccRCC tumorigenesis[154,155]. Hence, HIF-independent VHL activity may play a role in ccRCC tumorigenesis. However, the extent to which these HIF-independent functions cooperate with HIF dysregulation to drive ccRCC tumorigenesis remains unclear.

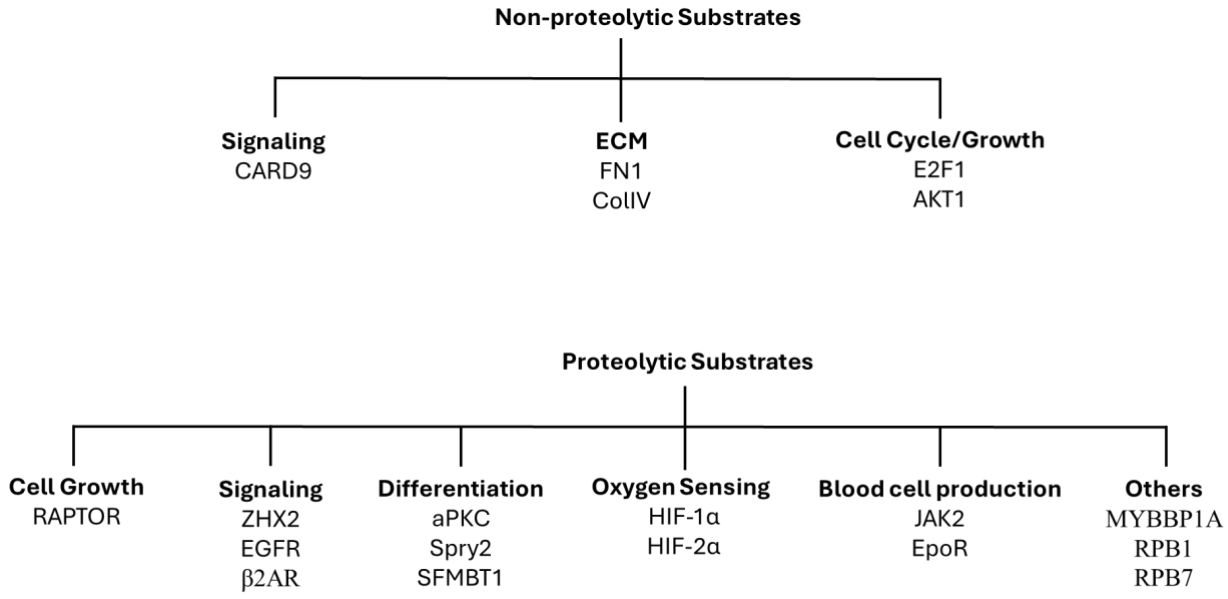

Figure 5. Proteolytic and non-proteolytic substrates of VHL. Grouping of proteolytic and non-proteolytic substrates of VHL based on their functions. Non-proteolytic targets of VHL are involved in cellular signalling, regulation of the ECM, cell growth, etc. Proteolytic targets of VHL are involved in cellular growth and differentiation, signaling, oxygen sensing, blood cell production, etc.

1.1.6.2 Non-proteolytic VHL activity

Studies show that VHL also regulates the activity of proteins in a non-proteolytic manner (Figure 5). For example, VHL promotes microtubule stabilization and primary cilia formation[156–162], and plays a critical role in controlling extracellular matrix (ECM) assembly by regulating the deposition of fibronectin (FN1)[163] and collagen IV (ColIV)[164]. VHL directly binds and inhibits AKT kinase activity in an E3 ligase-independent manner[165]. VHL acts as an adaptor to promote the phosphorylation of the Caspase recruitment domain-containing protein 9 (CARD9) C terminus by CK2 (Casein Kinase 2), leading to CARD9 inhibition, and ultimately suppression of NF-κB signalling[166]. VHL inhibits E2F1 expression at the mRNA and protein level[167] and binds to E2F1 to inhibit its transcriptional activity[168]. VHL regulates apoptosis via activation of p53 transcriptional activity[169,170], modulation of NF-κB activity[166], and downregulation of transcription factor Jun B Proto-Oncogene[171]. Finally, VHL regulates cellular senescence via the retinoblastoma protein (pRb) and the SWI2/SNF2 chromatin remodeller p400[49,172]. These findings highlight the diverse roles of VHL beyond the regulation of protein stability through ubiquitination.

1.1.7 Epidemiology of RCC and treatment landscape

Kidney cancer ranks among the top 10 most common cancers in both men and women in the United States, accounting for 3.7% of all new cancer diagnoses as of 2017[173]. RCC is the most prevalent type of kidney cancer, observed in up to 85% of cases, and with higher frequency in men and the older population[173–175]. Approximately one-third of kidney cancer patients present with regional or distant metastases[176], and among those with localized tumors who undergo

nephrectomy with curative intent, about one-quarter experience relapses at distant sites[177–179]. For patients with localized RCC, prognosis is favorable with 5-year survival rates of 93%[176]. However, for patients with advanced disease, prognosis is poor, with 5-year survival rates decreasing to 75% among patients with locally advanced disease (regional spread), and 18% among patients with metastatic disease[176].

1.1.7.1 Traditional therapies for RCC

For localized RCC, surgical excision remains the standard approach; however, up to 30% of patients will present with advanced or metastatic disease at later stages[180–183]. RCC is highly resistant to traditional chemotherapeutic agents such as floxuridine and 5-fluorouracil (5-FU)[180,181]. Due to the limited efficacy of chemotherapy, systemic treatment for advanced RCC shifted for decades towards the use of cytokine-based immunotherapy, with interferon-α (IFN-α) and interleukin-2 (IL-2), either alone or in combination, being the standard of care for the treatment of advanced RCC[184,185] (Figure 6). However, the significant toxicity associated with these agents, coupled with their low response rates (~5 to 20%), limited their applicability in clinical settings[185–193]. As such, new and innovative approaches to RCC therapy were needed.

1.1.7.2 Emerging therapies for metastatic RCC

After decades of research, improved molecular characterization of RCC has led to the development of therapies that are now used in combination with classical chemotherapeutics (Figure 6). One of the consequences of VHL loss in ccRCC is HIF transactivation of VEGF, which promotes blood supply to the growing tumor[138]. Hence, inhibition of VEGF signaling

became a novel strategy to treat ccRCC. One approach involves the use of a recombinant, human monoclonal antibody such as bevacizumab that binds and sequesters VEGF, preventing it from interacting with its receptors[194].

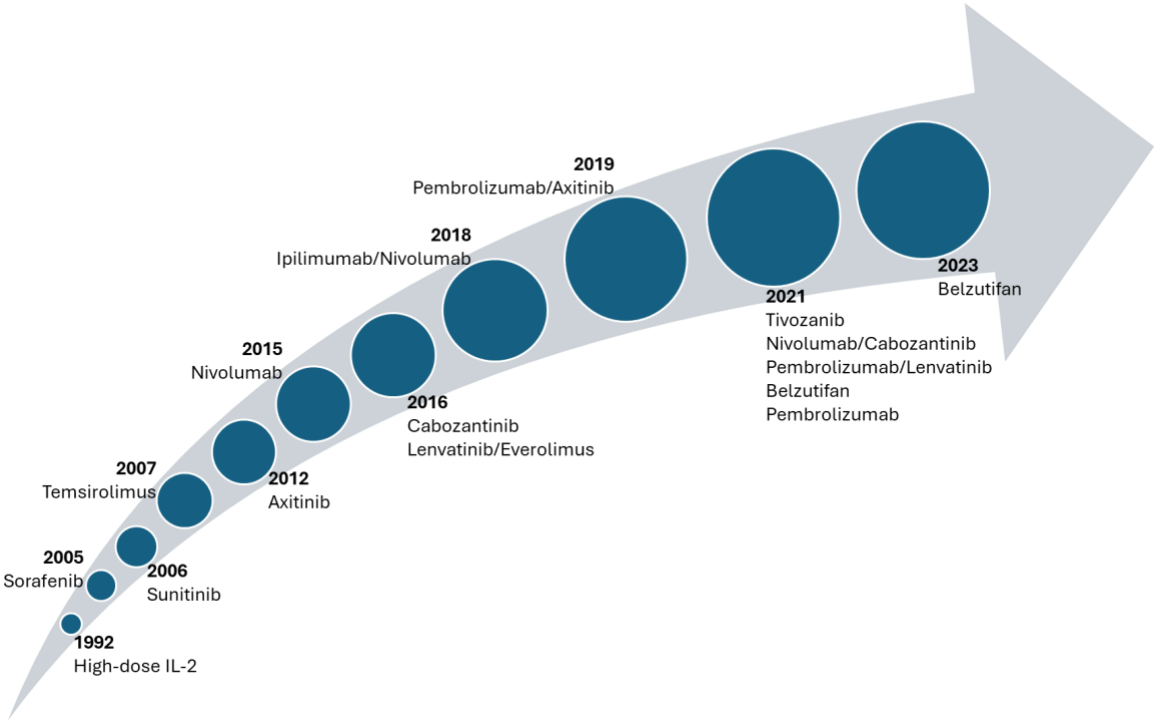

Figure 6. Timeline of FDA approved agents and combination treatments for metastatic renal cell carcinoma (RCC). Created using BioRender.

An alternative strategy for disrupting signaling events downstream of the VHL/HIF pathway involves targeting the receptor function rather than the ligand. Receptors for VEGF, PDGF (Platelet-derived growth factor), TGF-α (Transforming growth factor alpha), and similar molecules rely, at least partially, on tyrosine kinase activity for their signaling. Therefore, another approach involves inhibiting this tyrosine kinase activity, effectively blocking downstream signaling cascades initiated by these receptors[195–197]. Tyrosine Kinase Inhibitors (TKIs) have significantly improved progression-free survival (PFS) and overall survival (OS) in

both first-line and second-line RCC treatment settings[198]. The TKI sunitinib significantly improved the objective response rate (ORR) of RCC patients by 25% and median PFS by 6 months compared to the IFN-α treatment group[199].

Given that abnormalities in VHL leading to elevated HIF-α levels play a critical role in ccRCC, another therapeutic approach involves lowering the levels of HIF-α by using inhibitors of mTOR, positive regulators of HIF expression[200–204]. A selective HIF-2α inhibitor, Belzutifan, has also shown great promise in the clinical setting, demonstrating a 49% ORR in patients with VHL-associated RCC, a well-tolerated toxicity profile, and longer progression-free survival compared to mTOR inhibitor everolimus in pretreated advanced RCC[205–208]. More recently, the focus has shifted towards drugs targeting cytotoxic T-cell inhibitory molecules such as cytotoxic T-lymphocyte–associated protein 4 (CTLA-4), PD-1 (programmed cell death 1), and PD-L1 (programmed cell death ligand 1)[209–211]. These drugs, called immune checkpoint inhibitors, enhance the body's immune system by blocking inhibitory signals that prevent immune cells from attacking cancer cells.

In addition to immune checkpoint inhibitors, several novel immunotherapies are currently under investigation, including T-cell agonists, tumor vaccines, T-regulatory antagonists, and adoptive cell therapy[212]. The introduction of immune checkpoint inhibitors has led to significant advancements in the treatment of metastatic RCC, especially when used in combination with other therapies[209–211]. These combinations have led to significant improvements in PFS, OS, and ORR in patients with advanced and metastatic RCC[209–211]. For instance, the combination of tyrosine kinase inhibitor lenvatinib and anti–PD-1 monoclonal antibody pembrolizumab resulted in PFS of 23.9 months, and an ORR of 71%, significantly outperforming sunitinib monotherapy, which showed a PFS of 9.2 months and an ORR of 36.1%[213]. While combination therapies have

provided significant clinical benefits for many patients, resistance remains a major clinical challenge, and the long-term efficacy of these therapies is limited, spurring the search for novel therapeutic strategies[209,214,215]. Novel strategies currently under investigation for the treatment of advanced RCC include cyclin-dependent kinase 4 and 6 (CDK4/6) inhibitors[216,217], histone deacetylase (HDAC) inhibitors[218–220], glutaminase inhibitors[221], oncolytic viruses[222–224], and antibody-drug conjugates[225,226].

1.2 The multifaceted roles of the retinoblastoma protein (pRb) in cancer biology

Given the complexity and relevance of VHL's non-canonical functions, efforts have focused on identifying novel substrates and interacting partners of VHL that may contribute to ccRCC development. Among these, pRb (encoded by *RB1*) has emerged as a previously unrecognized substrate of VHL.

1.2.1 Discovery of the retinoblastoma susceptibility gene *RB1*

Retinoblastoma, a malignant tumor of the eye in children, can be inherited through a germline mutation or can arise sporadically due to somatic mutation[227–229]. Evaluation of the epidemiology of retinoblastoma led Alfred G. Knudson to postulate the "two-hit" hypothesis whereby two separate mutational 'hits' are required for the manifestation of retinoblastoma[230]. Early genetic studies of retinoblastomas occasionally identified tumors with deletions on chromosome 13, specifically in the 13q14 region[231–234]. Researchers then hypothesized that the alleles at this "retinoblastoma locus" acted as tumor suppressors, with their loss of function linked to malignancy[235]. This hypothesis established a model for identifying other tumor suppressor genes.

In 1986, two independent groups successfully cloned *RB1* from the q14 segment of chromosome 13[236,237]. *RB1* thus became the first described human tumor suppressor gene, with mutations at its locus recognized as a critical event in the development of retinoblastoma[236,237].

1.2.2 pRb structure and binding partners

RB1 is a relatively large gene, spanning 178,143 base pairs and containing 27 coding exons and 26 introns[238,239]. It encodes the protein pRb, which is composed of 928 amino acids, with a molecular weight of approximately 110 kilodaltons. pRb belongs to a larger 'pocket protein' family that comprises two other genes: RB transcriptional corepressor like 1 (*RBL1*) and RB transcriptional corepressor like 2 (*RBL2*), encoding proteins p107 and p130 respectively. pRb, p107 and p130 share extensive structural homology, with a conserved 'pocket' domain that binds various proteins[240]. Structurally, pRb contains an amino-terminal domain (pRbN), pocket domains A (pRbP A) and B (pRbP B), and a carboxy-terminal domain (pRbC)[238,241] (Figure 7). The A and B subdomains each form a single cyclin fold, separated by an unstructured flexible linker[242], and interact with each other to form the globular small pocket domain[243,244]. The large pocket consists of the small pocket and an unstructured C-terminal domain. The pocket domain of pRb has been shown to interact with E2F transcription factors[245], as well as LXCXE motif-containing proteins including HDACs[246], D-type cyclins[247], and viral oncoproteins[244]. The C-terminal domain of pRb contains binding sites for cyclin-CDK complexes[248] and protein phosphatase 1 (PP1)[249,249,250], and an E2F1-specific binding site[251,252].

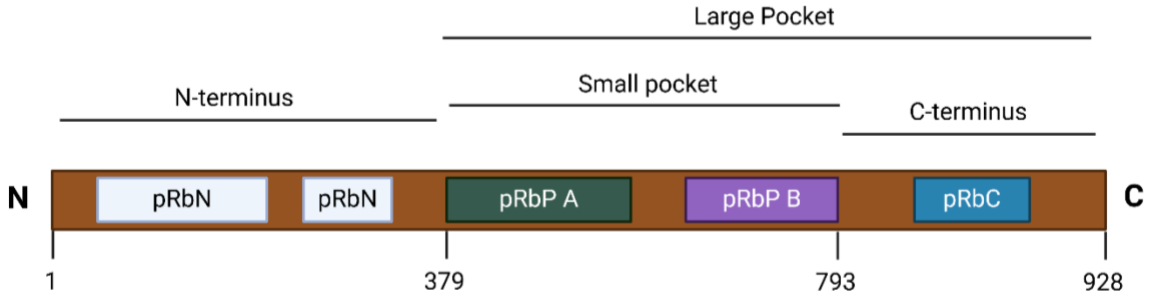

Figure 7. Schematic illustration indicating the structural regions of pRb and their associated residues. pRb comprises a N-terminal domain (aa1-379), a small pocket domain (aa379-793) and a C-terminal domain (aa793-928). The large pocket comprises the small pocket and the C-terminal domain. Full length pRb protein is 928aa. Created using BioRender.

1.2.3 pRb as a cell cycle regulator

Several lines of evidence indicate that the phosphorylation of pRb abrogates its cell cycle inhibitory function. Oncoproteins produced by DNA tumor viruses specifically sequester hypophosphorylated pRb, preventing its activity in controlling cell proliferation[253,254]. Furthermore, conditions that lead to pRb phosphorylation also favor cell proliferation[255]. pRb exists in its hypophosphorylated form throughout most of G1 and is predominantly found to be hyperphosphorylated in late G1, S, G2, and M phases of the cell cycle[255]. This oscillation suggests that pRb plays a role in regulating progression through specific stages of the cell cycle. Hypophosphorylated pRb prevents premature entry into the S phase by binding and inhibiting the E2F transcription factors, preventing the transcription of genes required for cell division[256–259]. pRb may also recruit chromatin-modifying factors, such as histone deacetylases[246,260–263] and histone methyltransferases[264], to promote active gene silencing at E2F-regulated promoters.

Interaction of D-type cyclins (cyclins D1, D2, and D3) with CDK4 or CDK6, cyclin E with CDK2, or cyclin A with CDK1 or CDK2, form complexes that are capable of phosphorylating pRb[265]. During mid-to-late G1, phosphorylation of multiple serine and threonine residues on pRb by mitogen-induced cyclin-dependent kinases (CDKs) inhibits the ability of pRb to sequester E2Fs, thereby allowing transcription of E2F targets and progression into the S phase[256,266–270] (Figure 8).

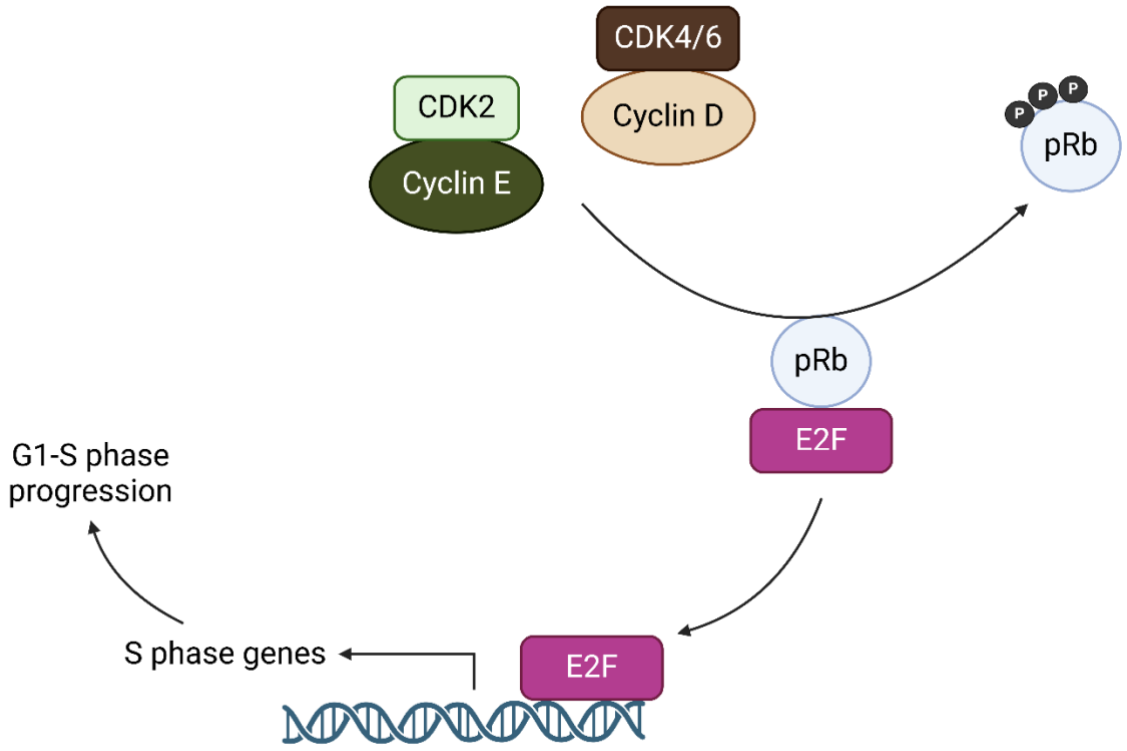

Figure 8. Schematic representation of cell cycle regulation via pRb phosphorylation. Active cyclin D–CDK4/6 and cyclin E-CDK2 complexes promote the phosphorylation (P) of pRb, triggering release of the E2F transcription factor. The free E2F activates the transcription of S phase genes, promoting cell cycle transition to the S phase. Created using BioRender.

pRb therefore regulates the G1 checkpoint in cells about to divide[271]. CDK-cyclin activity is tightly regulated by two families of CDK inhibitors: the INK4 family and the Cip/Kip family[272]. The INK4 family, which includes $p16^{INK4a}$, $p15^{INK4b}$, $p18^{INK4c}$, and $p19^{INK4d}$, specifically binds and inhibits CDK4/6-cyclin D complexes, promoting cell cycle arrest in the G1 phase[273]. In contrast, the Cip/Kip family, comprising $p21^{Cip1/Waf1}$, $p27^{Kip1}$, and $p57^{Kip2}$, can bind not only CDK4/6-cyclin D complexes but also CDK-cyclin A/B/E complexes, regulating multiple phases of the cell cycle[272,274–277].

1.2.4 Non-cell cycle functions of pRb

pRb is well known for its critical role in regulating the cell cycle by inhibiting E2F transcription factors and preventing premature entry into the S-phase[256–259]. However, accumulating evidence demonstrates that pRb also performs several non-cell cycle functions that contribute to senescence, differentiation, genomic stability, apoptosis, and cellular metabolism[278]. These functions extend beyond its classical role as a cell cycle regulator and highlight its broader significance in cellular regulation. Furthermore, the non-cell cycle functions of pRb highlight the complexity of its tumor-suppressive properties and suggest that its disruption in cancer cells may have far-reaching consequences beyond uncontrolled proliferation. Understanding these non-canonical roles of pRb may open new avenues for therapeutic interventions in cancer and other diseases associated with pRb dysfunction.

1.2.4.1 Regulation of genome stability

Several studies have shown that defects in pRb function may lead to chromosomal instability, a common feature of solid tumors[279–287]. Chromosomal instability resulting from pRb inactivation may be due to changes in the expression of mitotic proteins, chromatin remodeling, and/or defects in replication progression. pRb binding partners include HDACs, members of the SWItch/Sucrose NonFermentable (SWI/SNF) complex, heterochromatin protein 1 (HP1), DNA methyltransferase (DNMT), and DNA topoisomerase IIa (Topo II)[288]. pRb interaction with these chromatin remodeling factors may be important for the maintenance of genome stability. pRb interaction with centromere-associated protein HEC1 (highly expressed in cancer protein 1) suggests its involvement in chromosome segregation[289]. pRb is also necessary for the maintenance of constitutive heterochromatin features at telomeric and centromeric regions[286,287]. As a result, pRb can directly regulate chromosomal stability through the modulation of chromatin structure. However, chromosomal instability arising from pRb loss of function may be due to a secondary effect, caused by defects in cell cycle control[280]. Indeed, loss of pRb activity and activation of E2Fs, results in the overexpression of E2F target and mitotic checkpoint protein MAD2 (mitotic arrest deficient-like 2), whose overexpression results in mitotic defects leading to aneuploidy [280] and is sufficient to induce chromosomal instability *in vitro* and *in vivo*[290]. pRb also localizes to DNA double-strand breaks (DSBs) in an E2F1 and ATM (Ataxia-Telangiectasia Mutated) kinase-dependent manner, to promote DSB repair through homologous recombination. Consequently, its loss may impair this repair process and contribute to genomic instability[291].

1.2.4.2 Regulation of senescence

pRb plays a crucial role in the induction of cellular senescence, a state of irreversible growth arrest[292]. Re-expression of pRb in osteosarcoma, bladder carcinoma, and breast carcinoma cell lines deficient in both p53 and pRb led to growth arrest, inhibition of telomerase activity, morphological changes characteristic of senescent cells, and increased expression of the senescence-associated β-galactosidase biomarker SA-β-gal[293]. Similarly, ectopic expression of pRb in osteosarcoma cells induced morphological changes characteristic of senescent cells[294,295]. pRb was shown to be sufficient to maintain a senescent state, as acute pRb inactivation in senescent mouse embryonic fibroblasts (MEFs) promotes re-entry into the cell cycle[296]. Notably, in senescent cells, pRb predominantly exists in its active, hypophosphorylated form, in part due to high levels of p16 and p21, which inhibit the CDKs that phosphorylate pRb[292]. Consistently, ectopic expression of p16 in human prostate cancer cell lines induces senescence in a pRb-dependent manner[297]. p16 therefore plays a central role in pRb-induced cellular senescence. Furthermore, the pRb-p16 pathway plays a critical role in the formation of senescence-associated heterochromatin foci, which is associated with the stable repression of E2F target genes[298].

1.2.4.3 Regulation of cell death

Apoptosis is a type of programmed cell death characterized by distinct morphological features, including cell shrinkage, membrane blebbing, chromatin condensation, and DNA fragmentation[299–301]. pRb can promote both pro-apoptotic and anti-apoptotic functions depending on the cellular context. Several studies support the pro-apoptotic role of pRb. pRb-negative prostate cancer cells were highly resistant to apoptosis induced either by radiation or the addition

of ceramide[302]. pRb may promote apoptosis by inhibiting survivin, an antiapoptotic protein that is aberrantly expressed in many cancers[303]. pRb acetylation by the transcriptional coactivator CBP/p300 allows trimeric complex formation with Mouse double minute 2 homolog (MDM2) and p53[304]. This interaction prevents MDM2-dependent degradation of p53, thereby stabilizing p53 and rescuing its apoptotic functions[305].

Despite having some pro-apoptotic roles, pRb is generally considered an anti-apoptotic protein, and its inactivation through genetic mutations, sequestration by viral oncoproteins, or caspase-dependent degradation, is associated with increased levels of apoptosis[306]. Homozygous *Rb1* inactivation in mouse embryos leads to extensive apoptosis in the nervous system and the ocular lens[307–309]. Viral oncoproteins such as T antigen, E1A, and E7 sequester pRb, thereby releasing E2F1, which drives apoptosis through the regulation of apoptotic peptidase activating factor 1 (APAF1) and caspases 3, 7, 8, and 9[310,311]. Furthermore, a caspase degradation-resistant form of pRb can inhibit tumor necrosis factor-alpha (TNF-α)-mediated apoptotic induction in mice[312]. pRb may also repress apoptosis by binding to and inhibiting E2F1 via an E2F1-specific binding site located in its C-terminal domain[251,252].

Several studies demonstrate that the phosphorylation of pRb may promote resistance to apoptosis. Indeed, induction of apoptosis in some cell lines is associated with the transition of pRb from its inactive hyperphosphorylated state to the active hypophosphorylated form[313]. Furthermore, most sporadic cancers inactivate pRb through hyperphosphorylation, thus promoting resistance to apoptosis[314]. Dephosphorylation of pRb, mediated by protein phosphatase 1 alpha (PP1α), has been linked to the induction of apoptosis in leukemia cell lines[315]. Although the role that phosphorylation of pRb plays in protecting cells from apoptosis is not well understood, a possible mechanism has been postulated whereby hyperphosphorylated

pRb sequesters and inhibits the pro-apoptotic factor ANP32A (acidic nuclear phosphoprotein 32A), thereby preventing the induction of apoptosis[314]. In addition to apoptosis, pRb regulates other types of cell death. For instance, pRb represses HIF-mediated transcription of Bcl-2 interacting protein 3 (BNIP3), thus limiting the induction of hypoxia-induced autophagic cell death[316]. Furthermore, pRb restrains the induction of autophagic cell death in the *Vhl*-null mouse retina, specifically in photoreceptor cells[317]. These findings indicate that pRb plays a role in regulating both apoptotic and non-apoptotic forms of cell death.

1.2.4.4 Regulation of cellular differentiation

pRb plays a crucial role in promoting cellular differentiation, which is marked by permanent cell cycle withdrawal and activation of a cell-type specific gene program[318,319]. In *Rb1* knockout mice, lens cell differentiation was impaired and accompanied by reduced expression of differentiation markers[308]. pRb was shown to be involved in osteoblast differentiation[294,320], and is necessary for differentiation of adipocyte[321], keratinocyte[322], monocyte/macrophage and granulocyte cells[323]. pRb regulates differentiation by interacting not only with canonical E2F partners, but also tissue-specific transcription factors, inhibitors of differentiation, and chromatin modifiers[324]. For instance, pRb promotes muscle differentiation by negatively regulating E2F-responsive genes to maintain permanent cell cycle withdrawal, and by regulating the activity of muscle-specific genes[325]. When pRb is present, myoblast determination protein 1 (MYOD), a key transcription factor for muscle differentiation, stimulates the transcriptional activation of the muscle differentiation factor MEF2 (myocyte enhancer factor 2)[326]. Furthermore, the interaction between pRb and MYOD was fundamental for the onset and maintenance of myogenesis[327]. pRb disrupts transcriptional repression by the MYOD-HDAC1 complex by binding to HDAC1,

thereby allowing muscle-specific gene expression[328]. pRb also promotes proteasomal degradation of the E1A-like inhibitor of differentiation 1 (EID-1), a potent inhibitor of differentiation[329].

1.2.4.5 Regulation of metabolism

pRb has been shown to regulate cellular metabolism in different ways. For instance, pRb inhibits insulin production in pancreatic beta cells in response to glucose[330]. pRb inactivation by the oncogenic E1A adenoviral protein induces PDK4, which leads to decreased mitochondrial glucose oxidation[331]. Furthermore, *Rb1* deletion in the mouse hypothalamus promotes glucose intolerance and obesity[332]. The acute deletion of *Rb1* in mice erythrocytes led to reduced expression of oxidative metabolism genes and decreased mitochondrial biogenesis[333]. Decreased mitochondrial biogenesis was also observed in human myocytes following *RB1* loss[334]. There is likely some crosstalk between pRb and E2Fs in the regulation of cellular metabolism. For instance, in the absence of pRb, transcription of the E2F-regulated genes dyhidrofolate reductase, thymidylate synthase, ribonucleotide reductase, and thymidine kinase, which are involved in nucleotide synthesis, is increased[335–339]. Furthermore, E2F1 has been shown to regulate several genes involved in oxidative metabolism[340]. Hence, pRb may regulate these metabolic pathways through its antagonism of E2F1.

1.2.5 Context-dependent role of pRb in cancer

The first biochemical evidence that pRb may be crucial for tumor suppression in various tissues came from studies on viral oncoproteins. Oncoproteins such as adenovirus early gene 1A (E1A),

papillomavirus early gene 7 (E7), and simian virus 40 (SV40) large T (tumor) antigen, inactivate pRb during oncogenic transformation of cells, suggesting a tumor suppressive function for pRb[253,254,341,342]. In several cancer cells, loss of pRb function was linked to a loss of cell proliferation control as the exogenous expression of wild-type *RB1* in cells with mutant *RB1* led to a significant reduction in proliferation, colony formation in agar, and tumorigenicity in nude mice[343–345].

The original tumor suppressive function described for pRb relates to its ability to inhibit cell cycle progression in its hypophosphorylated state[256–259]. As such, tumors may employ mechanisms that inactivate this tumor suppressive function of pRb. For example, cyclin D1 overexpression observed in VHL-defective ccRCC cells results in pRb hyperphosphorylation, which supports abnormal proliferation in cells deprived of growth factors[346]. Furthermore, in bladder tumors expressing abnormally high levels of pRb, pRb is functionally inactivated through increased cyclin D1 expression and/or loss of expression of the cyclin-dependent kinase inhibitor 2A (CDKN2A/p16)[347].

pRb can also regulate pathways that have the potential to contribute to oncogenesis[348–353]. For instance, pRb has been described to have anti-apoptotic functions, and its inactivation is associated with increased levels of apoptosis[306,310]. Homozygous *Rb1* mutant mice die before the 16th embryonic day and massive cell death is observed in multiple tissues[309]. Caspase-resistant pRb protects mice from tumor-necrosis factor-alpha type I receptor (TNFRI)-induced apoptosis[312]. pRb has also been shown to inhibit hypoxia-mediated induction of autophagic cell death[316], and in *Vhl-/-* mouse retinal cells, pRb restrained the induction of autophagic death of photoreceptors[317]. Hence, pRb may have the capacity to support oncogenesis depending on the context. Accordingly, pRb overexpression has been observed in multiple cancer types including

familial adrenocortical carcinomas and pancreatic adenocarcinomas[354,355]. Furthermore, transgene expression of phosphorylation-resistant constitutively active pRb in the mammary gland led to the development of mammary adenocarcinoma[356].

1.3 Interplay between VHL and pRb

Some functional links have been observed between VHL and pRb. One study showed that the combined deletion of *Vhl*, *Trp53* and *Rb1*, specifically in mouse renal epithelial cells gives rise to ccRCC[357]. Furthermore, conditional knockout of *Rb1* was shown to be synthetically lethal with *Vhl* loss in the murine retina—a tissue that models the retinal abnormalities observed in individuals with VHL disease[317]. VHL regulates the expression of cyclin D1[346], which directly affects the phosphorylation status of pRb and its ability to control the cell cycle, thereby linking VHL dysfunction to cell cycle dysregulation in ccRCC. Furthermore, VHL inactivation in MEFs induces a senescent-like phenotype that is dependent on pRb and p400[49]. Overexpression of pRb promoted the transcriptional activity of HIF-1α[358], whose abundance is regulated by VHL. pRb has also been described to restrict HIF target gene expression in the *Vhl-/-* mouse retina[317], thus creating a link between VHL and pRb in the regulation of the hypoxia response. Finally, deletion of *Vhl* suppressed retinoblastoma formation in murine *Rb1/Rbl1*–null retina[317]. In patients with ccRCC, mutations of the *RB1* gene are rarely observed[52]. However, the status and expression of pRb in VHL-associated ccRCC are not well studied. Interestingly, mass-spectrometry-based proteomic data obtained from the National Cancer Institute's Clinical Proteomic Tumor Analysis Consortium (CPTAC)[359,360] revealed greater pRb protein abundance in ccRCC primary tumors compared to normal tissue.

1.4 Rationale and objectives

The relatively low success rate of current treatments for metastatic RCC, including conventional approaches such as surgery, targeted therapy, and immunotherapy, has driven researchers to explore novel, druggable targets of VHL beyond HIFs and their downstream targets. Loss of VHL function, a hallmark of ccRCC, results not only in HIF accumulation, but also the dysregulation of various cellular processes that contribute to tumor growth and survival. My research aims to identify additional molecular pathways destabilized by VHL loss in ccRCC, with the goal of developing more effective and targeted therapies. To this end, I first investigate how the disruption of VHL-mediated regulation of pRb drives ccRCC progression. I then conduct a detailed biochemical characterization of the VHL-pRb interaction to elucidate the underlying molecular mechanisms. Finally, I explore pharmacological strategies aimed at exploiting the vulnerabilities uncovered through this work, to inform the development of novel therapeutic options for ccRCC.

Chapter 2: Materials and Methods

2.1 Cell Culture and Reagents

All cell lines used in cell culture were obtained from the American Type Culture Collection (ATCC). 786-O, 769-P and RCC4 cells were grown in RPMI 1640 medium (350-000-CL, Wisent) supplemented with 10% (vol/vol) fetal bovine serum (FBS). A-498, HEK293A and U2OS cells were grown in Dulbelcco's modified Eagle's medium (319-015-CL, Wisent) supplemented with 10% (vol/vol) FBS (12483020, Thermo Fisher Scientific). All cells were maintained in a humidified incubator at 37°C, 5% CO_2, and 21% O_2 (normoxia). Assays were performed on arrested cultures grown to confluence in order to control for pRb cell cycle function. Moreover, VHL-mediated pRb degradation was more prominent in confluent cells, suggesting a confluence-dependent mechanism for VHL-pRb regulation. For hypoxic treatments, cells were placed in a hypoxia chamber at 37°C, 5% CO_2, and 0.5% O_2 for 24 hours. MG132 (Peptides International) was used at 10μM. Cell lines were routinely tested for mycoplasma contamination.

2.2 Western Blot and Antibodies

Whole cell lysates were prepared by lysing cells in 1x Laemmli buffer. After boiling at 95°C for 10 minutes, samples were separated by Sodium Dodecyl Sulfate Polyacrylamide Gel Electrophoresis (SDS-PAGE) and transferred onto polyvinylidene fluoride (PVDF) membranes. After blocking with 5% non-fat milk in TBST (Tris-Buffered Saline with 0.1% Tween 20, membranes were incubated in primary antibody diluted in 5% bovine serum albumin (BSA) in TBST. Membranes were washed with TBST and incubated with the appropriate horseradish peroxidase (HRP)-conjugated secondary antibody diluted in 2% non-fat milk in TBST. After

additional washes with TBST, blots were developed using a chemiluminescent substrate and imaged with the Bio-Rad ChemiDoc imaging system.

Primary antibodies against pRb (9313, 1:1000), Hemagglutinin (HA) (2999, 1:1000), VHL (68547, 1:500), and Ubiquitin (3936, 1:1000) were from Cell Signaling Technology. Antibodies against Vinculin (V9131, 1:20000), β-actin (A5441, 1:15000), α-tubulin (T6199, 1:15000) and Flag (A8592, 1:1000) were from Sigma Aldrich. HIF-2α (NB100-122, 1:500) antibody was from Novus Biologicals. Glut-1 (115730, 1:5000) antibody was from Abcam. SKIDA1 (ARP69749_P050, 1:500) antibody was from Aviva Systems Biology. Peroxidase-conjugated sheep anti-mouse (NB1206808) and donkey anti-rabbit (NB7185) antibodies were purchased from Novus Biologicals. Antibodies used for co-immunoprecipitation include mouse anti-HA (homemade, 1:500), anti-Flag M2 (A2220, Sigma), mouse anti-pRb (554136, BD Biosciences, 1:500), and mouse anti-VHL (556347, BD Biosciences, 1:500). High-Capacity Streptavidin Agarose beads (20359, Thermo Fisher Scientific) were used for biotin affinity purification.

2.3 Subcellular fractionation

Cells were scraped from 10 cm plates into 500 µL fractionation buffer (20 mM HEPES pH7.4, 10 mM KCl, 2 mM $MgCl_2$, 1 mM EDTA, 1 mM EGTA), and incubated on ice for 15 min. The cell suspension was passed through a 27-gauge needle 10 times and left on ice for 20 min. The sample was centrifuged at 720 x g for 5 minutes. The pellet (nuclei) was washed once with 500 µL fractionation buffer and extracted using 0.1% SDS in TBS. The supernatant was centrifuged at 10,000 x g for 5 minutes to remove the mitochondria. The remaining supernatant was used as the cytoplasmic fraction.

2.4 Quantitative real-time polymerase chain reaction (qRT-PCR)

Total RNA was extracted from cells using the PureLink RNA Mini Kit (12183018A, Invitrogen) according to the manufacturer's protocol. On-column genomic DNA digestion was performed using the PureLink DNase Set (12185010, Invitrogen). First strand cDNA synthesis was performed with the iScript cDNA Synthesis Kit (#1708891, Biorad) according to provided protocol. qRT-PCR detection was performed using the Luna® Universal qPCR Master Mix (M3003, New England Biolabs) and the CFX96 Real-Time PCR System. 10 ng of cDNA was used as input for qRT-PCR reactions. Real-time PCR was performed in triplicate, and relative gene expression was calculated using the $2^{-\Delta\Delta Ct}$ method[361] following normalization of Ct values to a GADPH control. Gene-specific primers (Table 2) were designed using the IDT PrimerQuest tool and obtained from Thermo Fisher Scientific. The final concentration of each primer in the qRT-PCR reaction was 10 μM.

Table 2. Primer sets (forward and reverse) used for RT-PCR amplification of target genes.

Gene	**Forward primer (5'->3')**	**Reverse primer (5'->3')**
RB1	AATCAGATGGTATGTAACAGCGA	TGAAATTTGGACTCTCCTGGG
SKIDA1	GTCCTGAATTTGCTACGGATTTG	CAGGGATTCTCGGCTTTAGTT
ACAT1	TGAACAGGACGCTTATGCTATT	CCACTACATCTGGTTGACCTTT
DECR1	GTGATTCAACCAGGGCCTATAA	CAGGGAATTCTGCCAATCATTTC
PSAT1	GCTTGGTTCTGGAGTGGATTA	CTCCACTGGACAAACGTAGAA
PNPO	TGATCGGGAGTATCTGAGAAAGA	ACCTGAGGGTACAGGACATAG
OAT	GTAGATGGCTGGCTGTTGATTA	CACTGCAGACACAGGGTATAAG

E2F1	CCTGCAGAGCAGATGGTTAT	GCTCTTAAGGGAGATCTGAAAGT
GAPDH	GGTGTGAACCATGAGAAGTATGA	GAGTCCTTCCACGATACCAAAG

2.5 Lentivirus production and transduction

Lentiviral particles were produced using a third-generation packaging system in HEK293T cells. Briefly, HEK293T cells were seeded at 40% confluency in 10 cm dishes 24 hours prior to adherent transfection. Cells were co-transfected with the lentiviral transfer plasmid (pLVX-M-puro (#125839, Addgene), lentiCas9-Blast (#52962, Addgene), or pCLIP-dual-SFFV-ZsGreen (Transomic technologies)), and the packaging plasmids psPAX2 (#12260, Addgene) and pMD2.G (#12259, Addgene) using PolyJet transfection reagent (#SL100688, SignaGen Laboratories) according to the manufacturer's instructions. The plasmids were used at a ratio of 4:3:1 (transfer:psPAX2:pMD2.G). After 6–8 hours, the transfection medium was replaced with fresh DMEM supplemented with 10% FBS. Viral supernatants were collected at 48- and 72-hours post-transfection, filtered through a 0.45 μm PVDF filter, and immediately used to infect target cells. Filtered viral supernatant was added to the cells in the presence of 8 μg/mL polybrene (Sigma-Aldrich) to improve transduction efficiency. Cells were incubated with virus-containing medium for 18 hours before replacing with fresh culture medium. Transduced cells were selected with 2 μg/ml puromycin or 10 μg/ml blasticidin as appropriate for 3–7 days beginning 48 hours post-transduction. Transduction efficiency was determined by western blot or qPCR.

2.6 Transfection and Co-immunoprecipitation assays

HEK293 cells were transfected using polyethylenimine (PEI) (23966-1, Polyscience) reagent 48 hours prior to lysis. Transfection of 786-O cells was achieved by electroporation using the Amaxa Nucleofector 2b device (Lonza) and the manufacturer's recommended conditions. Reverse siRNA transfection was performed using Lipofectamine RNAiMAX transfection reagent (13778030, Thermo Fisher Scientific) according to the manufacturer's instructions. Briefly, 3 pmol siRNA was diluted in 20 µl Opti-MEM Reduced Serum Medium (31985062, Gibco) in one well of a 96-well plate and mixed gently. 0.25 µl Lipofectamine RNAiMAX was added to each well containing the diluted siRNA molecules, mixed gently, and incubated for 10-20 minutes at room temperature. To each well, added 100 µl of appropriate cells diluted in complete growth medium without antibiotics, bringing the final siRNA concentration to 25 nM. Cells were cultured for 48–96 hours post-transfection before being harvested for downstream applications.

For immunoprecipitation, cells were harvested in mild lysis buffer (10mM Tris pH 7.5, 100mM NaCl, 10mM EDTA, 50mM NaF, 1% NP-40) supplemented with complete protease inhibitor. Lysates were clarified by centrifugation and then incubated with the appropriate antibody and beads for 1 hour. Bound complexes were washed with mild lysis buffer and eluted by boiling in 1x Laemmli buffer at 95°C for 10 minutes. Bound proteins were then resolved using SDS-PAGE followed by western blot analysis.

For immunoprecipitation under denaturing conditions, cells were lysed in mild lysis buffer and clarified by centrifugation. SDS was added to cell lysate to a final concentration of 1%, after which the lysate was boiled at 95°C for 5 minutes to denature proteins and disrupt protein-protein interactions. The cooled lysate was then diluted with mild lysis buffer to a final

concentration of 0.1% SDS prior to immunoprecipitation. Mouse anti-pRb antibody (554136, BD Biosciences) was used to pull down denatured pRb.

2.7 Proximity labeling assay

Mammalian cells were transfected with plasmids encoding VHL-Flag-BirA, NTID-Flag-pRb, or CTID-Myc-VHL (as indicated) and incubated for 24 hours. Cells were then treated with 10 μM MG132 or dimethyl sulfoxide (DMSO) vehicle for 4 hours, followed by 50 μM biotin (as appropriate) for an additional hour. Subsequently, cells were lysed using high-salt (500 mM NaCl) RIPA buffer and snap-frozen in liquid nitrogen. For the split-TurboID assay, the nuclear fraction was isolated as described in section 2.3 and lysed using high-salt RIPA buffer. Lysates were thawed rapidly in a 37°C water bath and clarified by sonication followed by centrifugation. Salt concentration of lysates was halved using no-salt RIPA buffer. Lysates were then pre-cleared using protein G agarose beads (16-266, Sigma Aldrich) at 4°C for 10 minutes. Pre-cleared lysates were incubated with streptavidin-agarose beads (20359, Thermo Fisher Scientific) at 4 °C for 4 hours to affinity-purify biotinylated proteins. Bound proteins were eluted using 30 mM biotin (B4639, Sigma-Aldrich). For complete protein denaturation, eluates were treated with dithiothreitol (DTT) and iodoacetamide (IAA) to reduce and alkylate disulfide bonds. Samples were then resolved on a NuPAGE 10% Bis-Tris gel (NP0315BOX, Thermo Fisher Scientific) and visualized using the SimplyBlue SafeStain (465034, Thermo Fisher Scientific). Bands were then excised and destained, followed by in-gel trypsin digestion.

An aliquot of each tryptic digest was analyzed by liquid chromatography–tandem mass spectrometry on an Orbitrap Fusion Lumos system (Thermo Scientific) coupled to a Dionex

UltiMate 3000 RSLC nano HPL. The raw files were searched against the Human UniProt Database using MaxQuant software v1.2.4.0 and the following criteria were used: peptide tolerance = 10 ppm, trypsin as the enzyme (2 missed cleavages allowed), and carboxyamidomethylation of cysteine as a fixed modification. Variable modifications are oxidation of methionine and N-terminal acetylation. The peptide and protein False Discovery Rate (FDR) was 0.01.

2.8 Live/Dead cell staining

Live/dead cell staining was performed using the ReadyProbes® Cell Viability Imaging Kit (Blue/Green) (R37609, Thermo Fisher Scientific). 2 drops of each reagent were added to 1 ml of cell culture media. Cells on a 12-well plate were then incubated with reagent-containing media for 15 minutes at room temperature. The NucBlue® Live reagent stains all nuclei, whereas the NucGreen® Dead reagent stains only the nuclei of cells with compromised plasma membrane integrity. Images were obtained using the EVOS M5000 microscope at 10x objective. The Fiji (ImageJ) software was used for image analysis – conversion to 8-bit grayscale, cell detection via thresholding, and quantification using the 'Analyze Particles' function, with appropriate particle size filters applied to exclude artifacts. For each well, average cell counts were determined from 10 randomly selected fields of view. All quantifications were performed on at least three biological replicates, and images were processed uniformly across experimental groups.

2.9 TUNEL assay

Adherent cells on a 96-well plate were rinsed twice with PBS and fixed with 4% paraformaldehyde (PFA) for 1 hour at room temperature. Cells were rinsed with PBS, then permeabilized with 0.1% Triton X-100 in 0.1% sodium citrate for 2 minutes on ice. Cells were rinsed twice with PBS. 50 µl TUNEL (terminal deoxynucleotidyl transferase dUTP nick end labeling) reaction mixture (11684795910, Sigma Aldrich) was added to cell monolayer and incubated for 60 minutes at 37°C in a humidified atmosphere in the dark. Cells were then rinsed 3 times with PBS and counterstained with 1 µg/ml 4′,6-diamidino-2-phenylindole (DAPI) reagent (D9542, Sigma Aldrich). For negative control, cells were incubated in 50 µl/well Label solution (without terminal transferase) instead of TUNEL reaction mixture. For positive control, cells were incubated with DNase I (3 U/ml in 50 mM Tris-HCl pH 7.5, 10 mM $MgCl_2$, 1 mg/ml BSA) for 10 minutes at room temperature to induce DNA strand breaks prior to labeling. Images were obtained using the EVOS M5000 microscope at 10x objective. The Fiji (ImageJ) software was used for image analysis – conversion to 8-bit grayscale, cell detection via thresholding, and quantification using the 'Analyze Particles' function, with appropriate particle size filters applied to exclude artifacts. For each well, average cell counts were determined from 10 randomly selected fields of view. All quantifications were performed on at least three biological replicates, and images were processed uniformly across experimental groups.

2.10 Sulforhodamine B (SRB) assay

The SRB assay was used to determine cell density based on total cellular protein content. Cells were fixed in media containing 10% trichloroacetic acid (TCA) (TB0968, Bio Basic) at 4°C for 2

hours. After washing off fixation solution, cells were stained with 0.04% (wt/vol) Sulforhodamine B sodium salt (HY-D0974, MedChemExpress) for 30 minutes. Cells were rinsed with 1% (vol/vol) acetic acid to remove unbound dye. 150 µl of 10 mM Tris base solution (pH 10.5) was then added to solubilize the protein-bound dye. Dye absorbance (570 nm) and background absorbance (650 nm) were obtained using a microplate reader. Final absorbance reading was obtained by subtracting background absorbance from dye absorbance.

2.11 Soft-agar colony formation assay

The soft agar colony formation assay was done on 6-well plates. The bottom layers consisted of 1.5 ml of 1% low melting point agarose (16520050, Thermo Fisher Scientific) in 1X RPMI media supplemented with FBS. The upper layers consisted of 7500 cells embedded in 1.5 ml of 0.5% agarose in 1X RPMI media supplemented with FBS. Both layers were allowed to solidify for 5 minutes at 4°C, then placed in a 37°C incubator for the remainder of the assay. Every 3 days, 200 µL of complete media were added onto the semi-solid media to prevent desiccation. After 5 weeks, colonies were stained with 200 µg/ml iodonitrotetrazolium chloride (IB0280**,** Bio Basic) solution. Images were obtained using the Bio-Rad ChemiDoc imaging system and the EVOS M5000 microscope, and analyzed using Fiji (ImageJ). Total colonies (> 100 µm) in each field of view were manually counted, and average counts for each well were obtained based on at least 10 fields of view. All quantifications were performed on at least three biological replicates, and images were processed uniformly across experimental groups.

2.12 Clonogenic assay

To assess colony formation, a total of 150 cells were seeded in each well of a 6-well plate and cultured for 10 days. Cell culture medium was replaced every 3-4 days. After incubation, cells were rinsed with PBS, fixed with a solution of 3 parts methanol to 1 part acetic acid for 5 minutes, and stained with 0.5% (wt/vol) crystal violet in methanol for 15 minutes. Excess stain was removed by rinsing with tap water until the background was clear. Images of the stained colonies were captured using the Bio-Rad ChemiDoc imaging system. Total colonies (> 1 mm) in each well were manually counted and recorded. All quantifications were performed on at least three biological replicates, and colonies were counted based on the same parameters across experimental groups.

When drug treatment was combined with the clonogenic assay, the drug was applied to cells at the indicated concentration for 72 h after 24 h of cell culture. Cells were then rinsed once with PBS and replaced with complete media. After which, cells were incubated for an extra week prior to fixation and staining.

2.13 β-galactosidase assay

Cells in a 12-well plate were stained using a senescence-associated β-galactosidase (SA-β-gal) staining kit (602010, Cayman Chemical), according to the manufacturer's protocol. Briefly, cells were washed twice with PBS and fixed with 500 µL Fixative Solution (1X) for 15 minutes at room temperature. Cells were then washed twice with PBS, followed by incubation in cell staining solution containing the X-gal substrate (pH 6) at 37°C overnight. Blue-stained cells (caused by SA-β-gal cleavage of X-gal at pH 6) were marked as senescent. Brightfield images

were then obtained using the EVOS M5000 microscope and analyzed using Fiji (ImageJ). Total and senescent (blue) cells in each field of view were manually counted, and average counts for each well were obtained based on at least 10 fields of view. All quantifications were performed on at least three biological replicates, and images were processed uniformly across experimental groups.

2.14 RNA-sequencing and data analysis

Total RNA was extracted using Trizol reagent (15596026, Thermo Fisher Scientific). RNA was initially quality-controlled by Qubit and Tapestation. Libraries were prepared using the Truseq kit from Illumina using the manufacturer's protocol (https://www.illumina.com/products/by-type/sequencing-kits/library-prep-kits/truseq-stranded-mrna.html). Quantity and quality of libraries were assessed by qPCR and LabChip, respectively. All libraries were sequenced on 1 lane of NovaSeq S1 (PE100), to generate 50 million reads per condition.

Raw sequencing data was processed using GenPipes[362] with standard settings, which aligns reads to GRCh37 (hg19) with *STAR* 2-passes mode and counted to gene features using 'htseq-count' function from *HTSeq*. The raw count data was normalized and analyzed by *DESeq2*. RNA-sequencing data are deposited in the Gene Expression Omnibus (GEO) under accession number GSE293447. The differentially expressed genes (DEG) (adjusted p-value < 0.05, fold change > 1.5 or > 2.0) were compared to HIF-2α-activated genes (downloaded from GSE149005 and re-analyzed by *limma* for significant DEGs with adjusted p-value < 0.05), downregulated genes in ccRCC versus normal kidney tissues (downloaded from the International Cancer Genome Consortium (ICGC) and analyzed by DESeq2), and E2F1-regulated genes (downloaded from

TRANSFAC database from ChIP-X enrichment analysis[363,364]). The comparisons between the DEGs in each group were visualized using *ggvenn*, and the pathway enrichment analysis was done using *pathfindR*. The enriched pathways were filtered based on biological relevance and visualized in a dot plot.

2.15 Patient samples

Snap-frozen tumor and matched normal kidney tissue samples from ccRCC patients were obtained from the McGill/MUHC RCC Biobank. All samples were collected following informed written consent from patients. Ethics approval was provided by MUHC REB (local REB number: IRB00010120). Proteins were extracted from tissue samples using RIPA buffer and mechanical lysis in a dounce homogenizer. Lysates were then clarified by centrifugation and 4x Laemmli Sample Buffer added to 1x final concentration.

2.16 Tumor xenograft assay

For tumor xenografts, four male and four female *NOD-scid IL2Rg*^{null} (strain JAX:005557, Jackson Labs) mice at 6-8 weeks of age and 20 – 23 g average body weight were used. The mice were housed and maintained in laminar flow rooms under specific pathogen-free conditions. All animal procedures were performed according to the guidelines of the Canadian Council on Animal Care (CACC). The protocol for animal studies was approved by the Animal Care Committee of the University of Ottawa (OHRI-1666).

Briefly, 786-O control and *RB1* KO cells were harvested at exponential growth phase using 0.25% trypsin-EDTA (25200-056, Thermo Fisher Scientific). Cells were washed once and resuspended in PBS. The number of viable cells was determined by trypan blue exclusion assay. 8 million viable cells were resuspended in 50% (vol/vol) Matrigel to a final volume of 100 µL and injected subcutaneously into the left or right flank of each mouse. Mice were randomly allocated to control/*RB1* KO or *RB1* KO/*RB1* KO groups. Five control injections and ten *RB1* KO injections were performed. The injection sites were manually palpated twice weekly until tumors were established. Caliper measurements of tumor length and width were taken twice weekly from the onset of tumor growth until the experimental endpoint (tumor diameter of 2 cm). Mice weights were recorded every 3 days. All mice were euthanized at 11 weeks post-injection when the first mouse had reached the endpoint. Tumors from each group were excised and weighed. Tumor measurements were performed by a collaborator who was blinded to the expected results of the study.

2.17 Organoid culture and drug screening

Patient-derived xenograft (PDX) organoid cultures were enzymatically disrupted with an organoid harvesting solution followed by 0.25% Trypsin. Partially fragmented organoids were then plated on Matrigel-coated 384-well plates (~25 uL/well) in a 5% Matrigel/Organoid medium in quadruplicate for 10 pint-concentration per component. After 4 days of growth, organoids were treated with compounds using automated injections performed by Echo Acoustic Liquid Handling. After 7 days (with one step of media and drug refresh on day 4), cell viability was measured using the CellTiter-Glo 3D assay (Promega).

2.18 Immunohistochemistry (IHC) and hematoxylin-eosin (HE) staining

Formalin-fixed tumor tissues were embedded in paraffin prior to IHC and HE staining. Cores were obtained from various parts of the tumors and 4 μm thick sections used to create a tumor microarray (TMA), containing control and *RB1* KO tumors. Before staining, the sections were deparaffinized and rehydrated, followed by antigen-retrieval in citrate buffer (pH 6) or Tris-EDTA (pH 9) as appropriate for 20 minutes. Tissue sections were blocked for 30 minutes using 10% goat serum (ab7481, Abcam), then incubated with primary antibody, followed by HRP-conjugated secondary antibody. Slides were stained using 3, 3'-diaminobenzidine (DAB) as the chromogen, counterstained with hematoxylin, mounted and cover-slipped. The staining intensity was scored as follows: 0 (no staining), 1 (weak staining), 2 (moderate staining) and 3 (strong staining). The proportion of positively stained cells was scored according to the following criteria: 0 (< 10% positive cells), 1 (10–25% positive cells), 2 (26–50% positive cells), 3 (51–75% positive cells) and 4 (> 75% positive cells). The final staining score was calculated as the staining intensity score × the proportion score and ranged from 0 to 12. The following antibodies were used for IHC staining: pRb (554136, BD Biosciences) and SKIDA1 (BS-9776R, Thermo Fisher Scientific).

2.19 CRISPR/Cas9 Genome Editing

Monoclonal 786-O *RB1* KO cell lines were generated with CRISPR/Cas9 technology. 786-O cells were transfected with PX458 plasmid (#48138, Addgene) containing *RB1*-targeting single guide RNAs (sgRNAs). Transfected cells were selected by single-cell sorting of green fluorescent protein (GFP)-expressing cells. Monoclonal cells were screened for target gene

knockout by western blot and later, Sanger sequencing of the region of interest. Successful knockout clones were then selected and expanded.

The following guide RNAs (Table 3) were used to create monoclonal *RB1* knockout cell lines:

Table 3. Guides (without PAM sequence) used for the generation of monoclonal RB1 KO cell lines.

***RB1* sgRNA #1** (5'->3')	CGGTGGCGGCCGTTTTTCGG
***RB1* sgRNA #2** (5'->3')	GCTCTCTCTCTGACATGATC

Polyclonal knockout cell lines were generated by stable expression of Cas9 using lentiCas9-Blast plasmid (#52962, Addgene) in target cells, followed by transduction with lentivirus containing the corresponding guide RNAs in the pCLIP-dual-SFFV-ZsGreen vector backbone. Each pCLIP-dual-SFFV-ZsGreen vector contains 2 guides (gRNA_a and gRNA_b) targeting the gene of interest (Table 4). All guides were designed against human genes. pCLIP-dual-SFFV-ZsGreen sgRNAs were obtained from transEDIT-dual CRISPR Whole Genome Arrayed Library from Transomic technologies.

Target sequences were as follows:

Table 4. Guides (without PAM sequence) used for the generation of polyclonal gene knockout cell lines.

	gRNA_a (5'->3')	**gRNA_b (5'->3')**
SKIDA1 sgRNAs #1	GAAAATAAGCAGGGTCCGAG	AATCCACTGGCTCAAAGTCA
SKIDA1 sgRNAs #2	ACAACAAAGAATACTCCGAG	GCAACTCCTCCAGATCGCAG
E2F1 sgRNAs #1	GCAGCAGGTCAGGGTCGCAG	CCACAGGTGTGAAATCCCCG
E2F1 sgRNAs #2	CAAGCCCTGTCAGAAATCCA	GGGCAGCCTGCGGGCTCCCG

2.20 Plasmids and siRNA constructs

HA-VHL wt-pBabe-puro (#19234, Addgene) and pCMV HA hRB-wt (#58905, Addgene) plasmids were used for transient transfections. HA-VHL-pRc/CMV (#19999, Addgene) plasmid was used to create stable HA-VHL-expressing cell lines. Flag-pRb constructs for transient transfections were obtained by cloning into the pLVX-M-puro vector (#125839, Addgene). The Flag-VHL plasmid used for transient transfections was obtained by Gibson cloning into pcDNA3.1(+) (V790-20, Addgene). For SKIDA1 overexpression studies, *SKIDA1* was cloned into the pLVX-M-puro vector using Gibson cloning. All plasmids were sequenced to confirm validity. ON-TARGETplus Non-targeting Control siRNAs (D-001810-01-05) and siGENOME Human RB1 siRNA smartpool (M-003296-03-0005) were purchased from Dharmacon.

2.21 Statistical analysis

Statistical analyses were performed using the GraphPad Prism 6 software. Data are presented as mean ± standard deviation (SD) unless otherwise indicated. Statistical significance was evaluated by unpaired two-tailed t-test, ordinary one-way ANOVA or two-way ANOVA with Holm-Sidak's post-hoc test or Tukey's post-hoc test as described in figure legends. p-values < 0.05 were considered statistically significant. Statistical significance was represented as: * $p < 0.05$, ** $p < 0.01$, and *** $p < 0.001$. 'ns' denotes not significant. Experiments were performed in at least three biological replicates in order to establish statistical significance (unless otherwise stated).

Chapter 3:

Loss of VHL-mediated pRb regulation promotes clear cell renal cell carcinoma

3.1 pRb binds VHL in a proteasomal-sensitive manner

The interaction between VHL and HIF is stabilized in the presence of proteasome inhibitors[164,365,366]. To identify novel proteasome-sensitive VHL substrates that might contribute to disease, we performed a proximity-dependent biotin identification (BioID) assay using HEK293A cells expressing VHL fused to the biotin ligase BirA. Cells were pre-treated with the proteasome inhibitor MG132 or vehicle control for 4 hours followed by 1 hour of biotin addition. MG132 stabilizes ubiquitinated proteins marked for degradation by blocking the proteolytic activity of the 26S proteasome complex, and this is known to stabilize the interaction of VHL and its targets, including HIF-α[118]. Biotinylated proteins were captured using streptavidin-conjugated beads and resolved on a NuPAGE 10% Bis-Tris gel. Proteins were visualized following a Coomassie stain. Protein-containing gel slices were then excised, trypsin-digested, and analyzed by liquid chromatography-mass spectrometry (LC-MS) (Figure 9A). LC–MS analysis revealed several proteins that were enriched in MG132-treated cells compared to vehicle control. Interestingly, the tumor suppressor pRb was one of the proteins enriched following MG132 treatment, raising the possibility that pRb is a proteasomal target of VHL. Despite the apparent paradox of one tumor suppressor degrading another, the prior data describing the synthetic lethality of *Vhl* and *Rb1* loss[317], and pRb's role in modulating hypoxic cell death[316] led us to validate pRb as our top hit.

To validate our mass spectrometry results, we first sought to confirm the enrichment of pRb in samples preferentially biotinylated by VHL-BirA in MG132-treated cells. Cells were transfected with VHL-BirA and treated with biotin and MG132 or vehicle as described above. Biotinylated proteins were pulled down with streptavidin beads and eluted proteins were resolved by SDS-PAGE. Immunoblot for pRb in the eluent showed a significant stabilization of VHL interaction

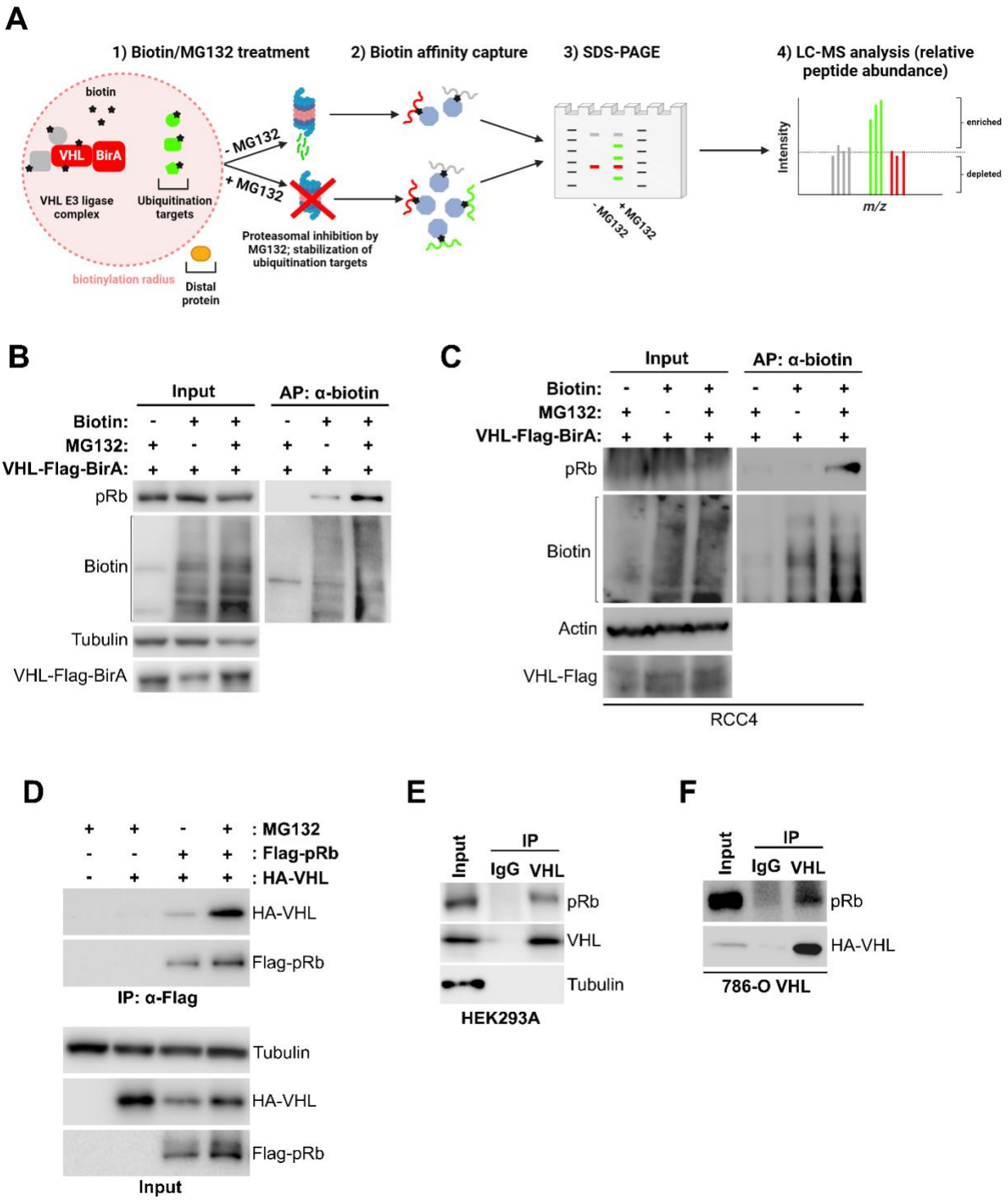

Figure 9. Proximity ligation analysis of VHL reveals pRb as a proteasome-sensitive VHL interactor.

Figure 9. Proximity ligation analysis of VHL reveals pRb as a proteasome-sensitive VHL interactor. (A) Schematic diagram illustrating BioID assay used to identify VHL interacting proteins. Figure was created with BioRender. In the experimental condition, 10 μM MG132 was added for 4 h, followed by 50 μM biotin for 1 h. In the control condition, 10 μM DMSO vehicle was added instead of MG132. Biotinylated proteins were captured using streptavidin-conjugated beads and resolved on SDS-PAGE gel. Gel chunks were then extracted separately from control and experimental lanes, trypsin digested and analyzed by mass spectrometry. **(B)** Affinity purification of biotinylated proteins using streptavidin-conjugated beads from HEK293A cells transfected with VHL-Flag-BirA plasmid and treated with 10 μM MG132 and 50 μM biotin as indicated for 4 h and 1 h respectively. **(C)** Affinity purification of biotinylated proteins using streptavidin-conjugated beads from RCC4 cells transfected with VHL-Flag-BirA plasmid and treated with 10 μM MG132 and 50 μM biotin as indicated for 4 h and 1 h respectively. **(D)** Immunoprecipitation of Flag-tagged pRb from HEK293A cells transfected with indicated plasmids and treated with 10 μM MG132 as indicated for 4 h. **(E)** Immunoprecipitation of endogenous VHL from HEK293A cells treated with 10 μM MG132 for 4 h. An IgG1 isotype control was included. MG132-treated HEK293A lysate was split equally between IgG1 and VHL pulldown conditions. **(F)** Immunoprecipitation of VHL from 786-O cells stably transfected with hemagglutinin (HA)-tagged VHL (HA-VHL), and treated with 10 μM MG132 for 4 h. An IgG1 isotype control was included. MG132-treated lysate was split equally between IgG1 and VHL pulldown conditions.

with pRb following proteasomal blockade (Figure 9B), consistent with our mass spectrometry data. Similar results were observed in ccRCC-derived (RCC4) cells, wherein the exogenous expression of VHL-BirA promoted endogenous pRb biotinylation in a MG132-sensitive manner (Figure 9C). To determine if VHL and pRb interact, we exogenously expressed Flag-tagged pRb and HA-tagged VHL in HEK293A cells in the presence or absence of MG132. Immunoprecipitation of pRb revealed increased co-precipitation of VHL in the presence of MG132, suggesting that inhibition of proteasomal degradation stabilizes the VHL-pRb interaction (Figure 9D). To determine if VHL and pRb interact endogenously, we performed immunoprecipitation on MG132-treated HEK293A lysates using either an anti-VHL antibody or a non-targeting isotype control antibody. Immunoblot analysis showed co-precipitation of pRb

with endogenous VHL (Figure 9E). Similarly, a VHL-targeting antibody applied to lysates from MG132-treated ccRCC (786-O) cells stably reconstituted with HA-VHL, specifically co-precipitated pRb as compared to an isotype control (Figure 9F). Together, these findings indicate that pRb is a novel binding partner of VHL that may be targeted by the ubiquitin-proteasome pathway, similar to HIF-α.

3.2 VHL regulates pRb stability via the ubiquitin-proteasome pathway

To determine the effect of VHL on pRb expression, HA-tagged VHL was reconstituted into two VHL-deficient ccRCC cell lines, 786-O and RCC4. Cells were lysed at confluence to mitigate cell cycle variation in log-phase growth and any associated variability in pRb regulation by cell-cycle-dependent factors. Western blot analysis in both ccRCC lines showed that VHL re-expression leads to downregulation of pRb protein levels (Figure 10A). This effect was determined to be post-transcriptional, as pRb mRNA levels were not affected by VHL reconstitution, as measured by qRT-PCR (Figure 10B). Next, we sought to determine the impact of endogenous VHL knockdown in HEK293A and U2OS cells, which have functional VHL expression. In both cell lines, knockdown of VHL led to an increase in pRb protein expression (Figure 10C). Consistent with our results in the ccRCC cell lines, VHL status did not affect pRb mRNA levels (Figure 10D). Collectively, these results indicate that VHL regulates pRb at the post-transcriptional level.

Given that VHL interaction with pRb is stabilized by proteasomal inhibition, we next asked whether VHL could promote ubiquitination of pRb. To analyze VHL-mediated ubiquitination of pRb, we immunoprecipitated pRb under denaturing conditions from VHL-null and VHL-

reconstituted 786-O cells treated with MG132. Immunoblot analysis showed significant pRb ubiquitination only in cells expressing VHL (Figure 10E). Treatment of VHL-reconstituted 786-O cells with MG132 resulted in pRb protein accumulation comparable to VHL-null 786-O cells, whereas MG132 treatment of VHL-null cells did not significantly affect pRb protein levels (Figure 10F). Together, these data demonstrate that VHL promotes the ubiquitination of pRb, thereby facilitating its proteasomal degradation.

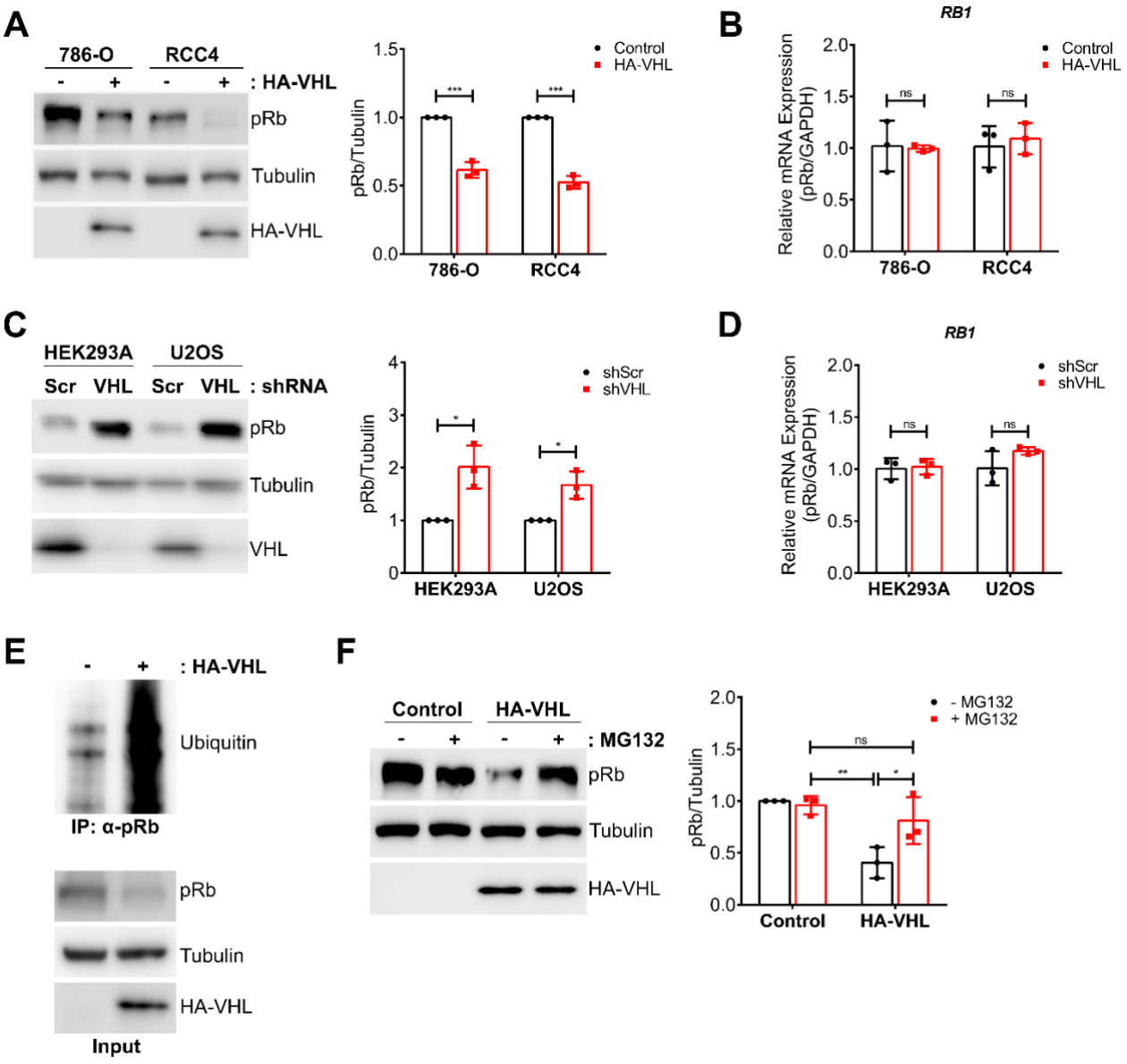

Figure 10. VHL promotes proteasomal degradation of pRb.

Figure 10. VHL promotes proteasomal degradation of pRb. (A) Immunoblot of lysates from 786-O and RCC4 cells stably transfected with either control vector (-) or HA- VHL. Quantification of pRb protein expression relative to tubulin is shown to the right. Statistical significance was calculated using unpaired t test and Holm-Sidak post-hoc test (n=3). **(B)** pRb mRNA expression (relative to GAPDH) in 786-O and RCC4 cells stably transfected with either control vector or HA-tagged VHL. Fold changes in gene expression were calculated using the delta delta Ct method and normalized to the control condition. Statistical significance was calculated using unpaired t test and Holm-Sidak post-hoc test (n=3). **(C)** Immunoblot of lysates from HEK293A and U2OS infected with lentivirus encoding either scrambled (Scr) or VHL-targeting shRNA. Quantification of pRb protein expression relative to tubulin is shown to the right. Statistical significance was calculated using unpaired t test and Holm-Sidak post-hoc test (n=3). **(D)** pRb mRNA expression (relative to GAPDH) in HEK293A and U2OS cells infected with lentivirus encoding either scrambled (Scr) or VHL-targeting shRNA. Fold changes in gene expression were calculated using the delta delta Ct method and normalized to the control condition. Statistical significance was calculated using unpaired t test and Holm-Sidak post-hoc test (n=3). **(E)** Immunoprecipitation under denaturing conditions of pRb from 786-O cells stably transfected with either control vector (-) or HA-tagged VHL and treated with 10 μM MG132 for 4 h. **(F)** Immunoblot of lysates from 786-O cells stably transfected with either control vector or HA-tagged VHL and treated as indicated with 10 μM MG132 or DMSO vehicle (-) for 4 h. Quantification of pRb protein expression relative to tubulin is shown to the right. Statistical significance was calculated using ordinary two-way ANOVA and Tukey's post-hoc test (n=3). **(A-F)** Data are represented as mean ± SD. *$p < 0.05$, **$p < 0.01$, ***$p < 0.001$. 'ns' denotes not significant.

3.3 Transcriptional regulation by the VHL-pRb and VHL-HIF pathways are largely distinct

The oxygen-dependent regulation of HIF-α stability is important in the transcriptional reprogramming of cells under hypoxia[367]. pRb has also been described to repress hypoxia-regulated transcription[316]. However, the mechanism for oxygen-dependent pRb transcriptional

regulation is not clearly understood. This led us to investigate whether VHL regulation of pRb was oxygen-sensitive. We analyzed the oxygen sensitivity of the pRb-VHL interaction in transfected cells. Immunoprecipitation of VHL showed that binding to pRb is inhibited by hypoxia (0.5% O_2 for 24 hours), demonstrating that VHL interaction with pRb is oxygen-dependent (Figure 11A). This suggests that VHL-mediated pRb regulation is involved in the cellular adaptation to hypoxia.

In response to oxygen limitation, cells upregulate pathways involved in angiogenesis, glucose metabolism and erythropoiesis to promote cellular adaptation to hypoxia[368]. pRb has also been described to regulate HIF-responsive genes in an oxygen-sensitive manner[316,317]. We first asked whether pRb and HIF coordinate to transcriptionally regulate the same target genes. To identify pRb-regulated genes in ccRCC, we first created a monoclonal *RB1* knockout (KO) cell line from 786-O cells using CRISPR/Cas9. Next, we determined global mRNA expression in 786-O control and *RB1* KO cells using RNA-sequencing. We were interested in genes that were upregulated following *RB1* KO, as pRb is known to repress transcription. We found 707 genes with significantly higher expression in *RB1* KO cells compared to control cells (Appendix A, fold change > 1.5, adjusted p-value (q) < 0.05) (Figure 11B). In contrast to pRb, HIF-α is a transcriptional activator. HIF-2α target genes were obtained from published datasets of RNA-sequencing analysis of 786-O control and *EPAS1* (HIF-2α) KO in 786-O cells[369] (fold change > 1.5, q < 0.05). Analysis of pRb-repressed and HIF-2α-activated genes showed little commonality, indicating that pRb regulates a distinct set of genes from HIF-2α (Figure 11B). Despite having few common targets at the level of individual genes, KEGG pathway analysis of HIF and pRb-regulated gene sets showed enrichment of similar pathways such as focal adhesion, extracellular matrix (ECM)-receptor interaction, cell cycle, cellular senescence, and apoptosis (Figure 11C).

These results indicate that the transcriptional influence of VHL deletion in ccRCC is impacted by a combined dysfunction in HIF-2α and pRb transcriptional regulation.

To assess pRb-regulated transcription in low vs high HIF-2α-expressing cells, we created *RB1* knockouts in both VHL-reconstituted and VHL-null 786-O cells (Figure 11D). Following RNA-sequencing, we analyzed transcripts that were significantly upregulated in *RB1* KO cells compared to corresponding controls, to identify pRb-repressed genes. We identified 670 genes that were significantly repressed by pRb in VHL-reconstituted cells (Appendix B, fold change > 1.5, $q < 0.05$), compared to the 707 genes repressed in VHL-null 786-O cells as described above. Interestingly, comparison of both gene sets showed roughly 6% overlap, suggesting that pRb transcriptionally regulates a distinct set of genes based on HIF expression (Figure 11E). However, KEGG pathway analysis of pRb-repressed transcripts in VHL-null and VHL-reconstituted cell lines showed enrichment of similar pathways such as focal adhesion, ECM-receptor interaction, necroptosis, oxidative phosphorylation, glycolysis, and cellular senescence (Figure 11F). These tumor-associated pathways raise the possibility of the involvement of pRb in ccRCC oncogenesis.

We next sought to identify which transcriptional targets of pRb may contribute to ccRCC development. To narrow down the list of potential candidates, stricter selection criteria of fold change > 2 and $q < 0.05$ were applied. We omitted the pRb-repressed genes in cells with low HIF and VHL reconstitution, which is not a relevant state in most ccRCC, leaving 395 genes (Figure 11G). We then removed genes whose expression were not sensitive to VHL status (251 genes removed), leaving 144 genes. Among these VHL and pRb differentially expressed genes, we removed any that were not regulated by E2F1 (obtained from ChIP-X Enrichment Analysis datasets[363]), as pRb has been described to repress apoptosis largely through E2F1[251] , leaving 45

genes. Finally, we asked which of these genes were repressed in ccRCC tumors versus normal tissue, which resulted in 6 genes (*PNPO*, *ACAT1*, *DECR1*, *OAT*, *SKIDA1* and *PSAT1*) that fulfilled the following criteria: (1) repressed by pRb in 786-O cells (2) downregulated in VHL-deficient vs VHL-reconstituted 786-O cells (3) downregulated in ccRCC tumor vs normal tissue, and (4) regulated by E2F1 (Figure 11G).

Among the selection criteria described above to identify physiologically relevant transcriptional targets of the VHL-pRb pathway, we have not demonstrated a requirement for E2F1 in our cell lines. To determine if the 6 narrowed down genes were regulated by E2F1 in ccRCC, we knocked out E2F1 from 786-O cells using CRISPR-Cas9 (Figure 11H) and examined the effect on mRNA expression for each gene. qRT-PCR analysis demonstrated that SKI/DACH domain containing protein 1 (SKIDA1) is transcriptionally repressed in ccRCC cells in an E2F1-dependent manner (Figure 11I). DECR1 and OAT mRNA levels were also increased upon *E2F1* KO but did not reach statistical significance. We next confirmed that SKIDA1 expression was upregulated by *RB1* deletion via qRT-PCR and immunoblot analyses of lysates from 786-O control and *RB1* KO cells (Figure 11J-K). These results suggest that SKIDA1 may be a downstream target of the VHL-pRb pathway that is functionally repressed in ccRCC patients. Kaplan-Meier[370] survival analysis of ccRCC patients revealed a positive correlation between SKIDA1 expression in tumors and patient survival (Figure 11L). These findings highlight SKIDA1 as a putative pRb target with prognostic significance in ccRCC, and whose repression upon VHL deletion may contribute to tumorigenesis.

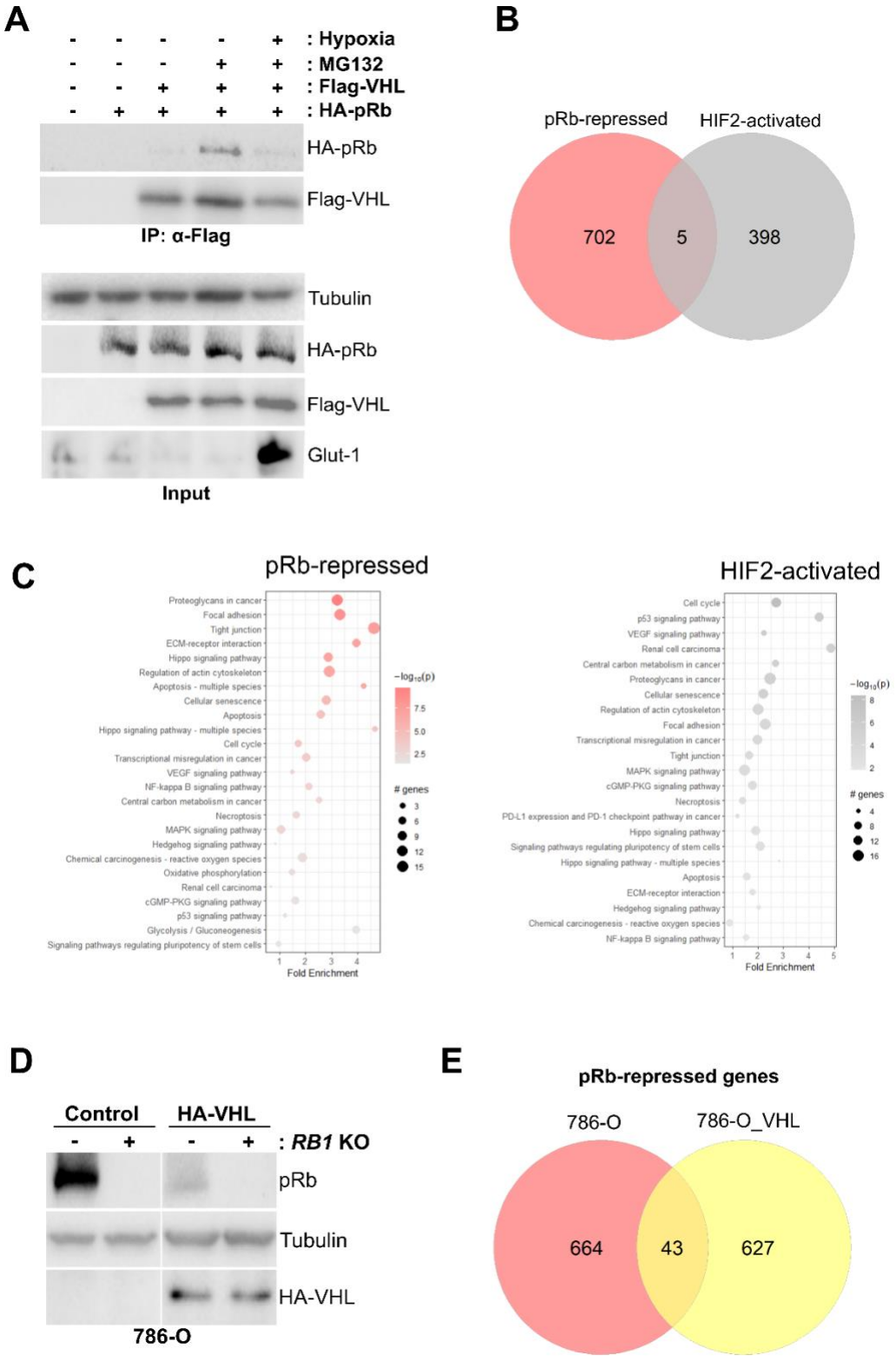

Figure 11. Transcriptional regulation by the VHL-pRb and VHL-HIF axes are distinct.

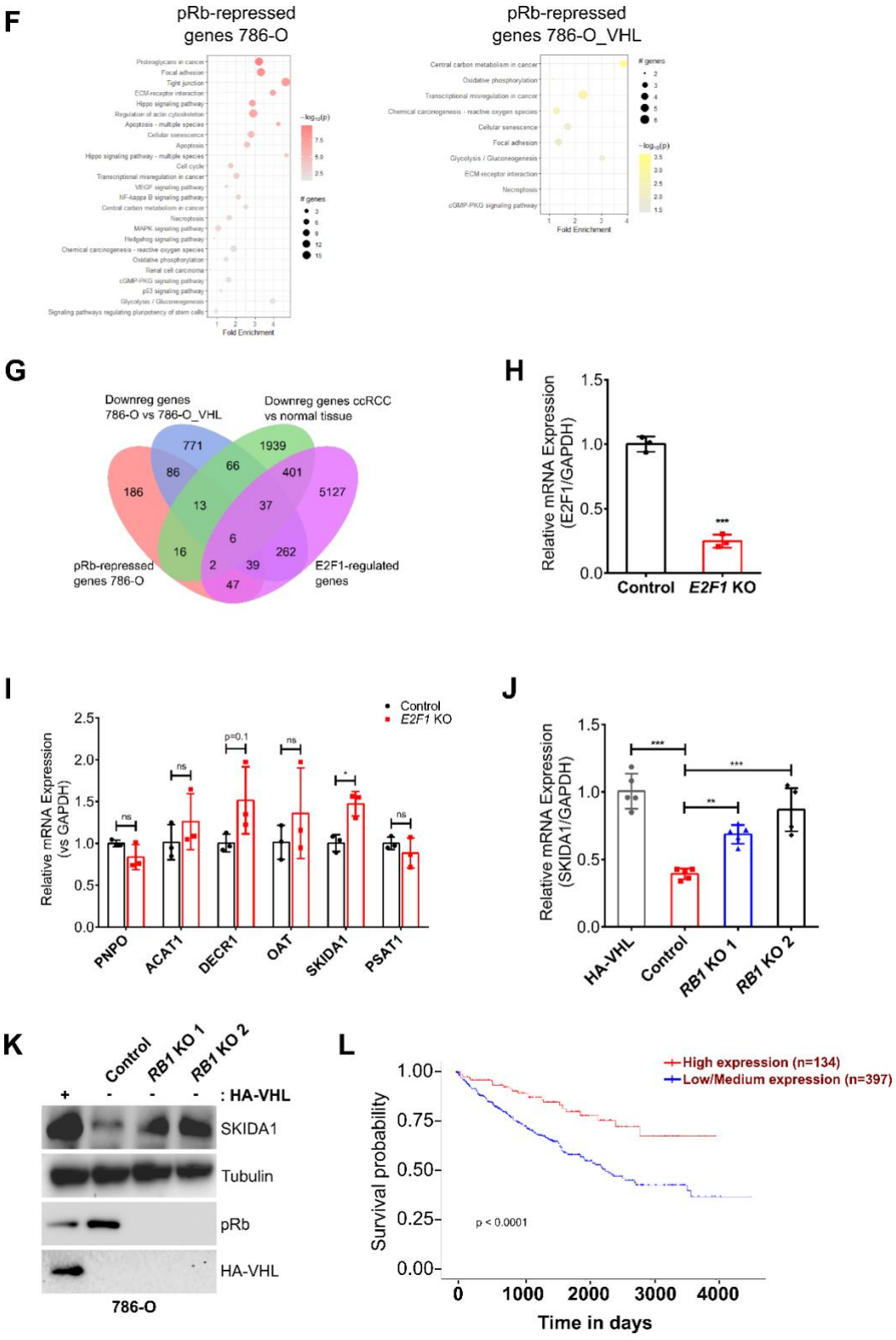

Figure 11 (continued). Transcriptional regulation by the VHL-pRb and VHL-HIF axes are distinct.

Figure 11. Transcriptional regulation by the VHL-pRb and VHL-HIF axes are distinct. (A) Immunoprecipitation of Flag-tagged VHL from HEK293A cells transfected with indicated plasmids and treated with 10 μM MG132 as indicated for 4 h. For hypoxia treatment, cells were placed in 0.5% O_2 for 24 h. Glut-1 expression serves as positive control to indicate HIF upregulation under hypoxia. **(B)** Venn diagram showing overlap between genes upregulated by *RB1* KO in 786-O cells (red), and genes activated by HIF2α as obtained from the GSE149005 RNA-sequencing dataset (grey). Fold change > 1.5, adjusted p-value < 0.05. **(C)** Pathway enrichment analysis of pRb-repressed (red) and HIF-activated (grey) genes in 786-O cells using *pathfindR*. Enriched pathways were filtered based on biological relevance and visualized in a dot plot. **(D)** Immunoblot of lysates from 786-O control and *RB1* KO cells stably transfected with either control vector or HAVHL. **(E)** Venn diagram showing overlap between genes upregulated by *RB1* KO in VHL-null (red) and VHL-reconstituted (yellow) 786-O cells. Fold change > 1.5, adjusted p-value < 0.05. **(F)** Pathway enrichment analysis of pRb-repressed genes in VHL-null (red) and VHL-reconstituted (yellow) 786-O cells using *pathfindR*. Enriched pathways were filtered based on biological relevance and visualized in a dot plot. **(G)** Four-way Venn diagram showing overlap between the indicated gene sets, visualized using *ggvenn*. Fold change > 2, adjusted p-value < 0.05. E2F1-regulated transcripts were obtained from TRANSFAC database from ChIP-X enrichment analysis[86,113]. Downregulated transcripts in ccRCC vs normal tissue were obtained from the International Cancer Genome Consortium (ICGC) data portal[12] and analyzed by DESeq2. **(H)** E2F1 mRNA expression (relative to GAPDH) in 786-O Cas9-expressing cells stably infected with virus encoding either control vector or *E2F1*-targeting guides. Fold changes in gene expression were calculated using the delta delta Ct method. Statistical significance was calculated using unpaired two-tailed t test (n=3). **(I)** Analysis of mRNA expression (relative to GAPDH) of indicated genes in 786-O Cas9-expressing cells stably infected with virus encoding either control vector or *E2F1*-targeting guides. Fold changes in gene expression were calculated using the delta delta Ct method and normalized to the control condition. Statistical significance was calculated using unpaired t test and Holm-Sidak post-hoc test (n=3).

Figure 11 (continued). Transcriptional regulation by the VHL-pRb and VHL-HIF axes are distinct. (J) SKIDA1 mRNA expression (relative to GAPDH) in 786-O control, VHL-expressing and *RB1* KO cells. Fold changes in gene expression were calculated using the delta delta Ct method and normalized to the control condition. Statistical significance was calculated using ordinary one-way ANOVA and Tukey's post-hoc test (n=5). **(K)** Immunoblot of lysates from 786-O control, VHL-expressing and *RB1* KO cells. **(L)** Kaplan-Meier analysis showing the correlation between SKIDA1 expression in ccRCC and OS or PFS in corresponding patients. Kaplan–Meier survival plots were obtained directly from the publicly available University of Alabama at Birmingham CANcer (UALCAN)[89] cancer analysis portal (http://ualcan.path.uab.edu), which provides access to pre-processed TCGA (The Cancer Genome Atlas) clinical data. Axes/texts were modified to increase legibility. Survival analysis was based on the stratification of patients into high and low/medium SKIDA1 expression groups. High expression was defined as the top 25% of patients with the highest gene expression levels, while the low/medium group comprised the remaining 75% (i.e., the bottom 25% and middle 50%). The log-rank test was used to evaluate statistical significance between survival curves. **(A-L)** Data are represented as mean ± SD. *$p < 0.05$, **$p < 0.01$, ***$p < 0.001$. 'ns' denotes not significant.

3.4 pRb inhibits apoptosis in ccRCC cells

We have demonstrated that VHL promotes the degradation of pRb in a proteasomal-sensitive manner. Therefore, pRb may be hyperstabilized in VHL-deficient tumors. Mass-spectrometry-based proteomic data obtained from the National Cancer Institute's CPTAC[359,360] confirmed that pRb protein abundance is higher in ccRCC primary tumors (n=110) compared to normal tissue (n=84) (Figure 12A). As expected, analysis of the same samples showed VHL protein downregulation in ccRCC compared to normal tissue (Figure 12A). Consistent with CPTAC data, immunoblot analysis showed that pRb was upregulated in the majority of ccRCC tumors compared to patient-matched normal tissue (Figure 12B). These patient-derived data are

consistent with our *in vitro* work in ccRCC cells, which showed a dramatic increase of pRb levels in cells lacking functional VHL (Figure 10A).

To determine the effect of pRb hyperstabilization on viability in ccRCC cells, we depleted pRb from several VHL-deficient ccRCC cell lines using pRb-targeting siRNAs (Figure 12C) and analyzed cell viability using the SRB colorimetric assay. We observed a significant decrease in cell viability following pRb depletion in all ccRCC cell lines (Figure 12D). By microscopy, we observed morphological changes associated with cell death including cell shrinkage, rounding, and increased cellular debris in pRb-depleted 786-O cells (Figure 12E). Live/dead cell staining of 786-O cells confirmed an increase in the proportion of dead cells upon siRNA-mediated knockdown of pRb (Figure 12F-G). Several reports have shown that pRb can repress apoptosis, while others have reported a repression of non-apoptotic cell death[251,309,316,371–375]. To determine if cell death induced by pRb depletion was apoptotic, we performed TUNEL staining on 786-O control and pRb knockdown cells. We observed a significant increase in the proportion of TUNEL-positive (or apoptotic) cells following pRb knockdown, suggesting that pRb inhibits apoptosis in ccRCC cells (Figure 12H-I).

Of note, pRb loss does not contribute to cellular senescence, a pathway that was enriched in our analysis of pRb transcriptional targets (Figure 12J-M). Interestingly, pRb knockdown in VHL-reconstituted 786-O cells did not lead to a similar decrease in cell viability, in stark contrast to the effect of pRb depletion in VHL-null cells (Figure 12N-O). These findings suggest that the anti-apoptotic function of pRb in ccRCC cells may be dependent on VHL or HIF expression, which is consistent with the differential transcriptional regulation by pRb in the presence or absence of VHL (Figure 11E) and the synthetic lethality observed between *Vhl* and *Rb1*[317].

We next asked whether the downstream VHL-pRb transcriptional target SKIDA1 contributes to the induction of cell death following pRb knockdown. Since SKIDA1 is upregulated upon knockout of *RB1*, we knocked out *SKIDA1* in 786-O cells and analyzed the effect of pRb depletion on cell viability as measured by the SRB assay. Knockout of *SKIDA1* rescued viability of 786-O cells depleted of pRb (Figure 12P). Next, we tested if overexpression of SKIDA1 alone was sufficient to induce cell death. Two ccRCC cell lines were infected with lentivirus encoding either control vector or SKIDA1 expression vector (Figure 12Q). Live/dead cell staining showed a significant increase in the proportion of dead cells following SKIDA1 overexpression in both cell lines (Figure 12R-S). Collectively, our results suggest that pRb suppresses cell death specifically in VHL-deficient renal cells, likely via regulation of downstream transcriptional targets such as SKIDA1 (Figure 12T).

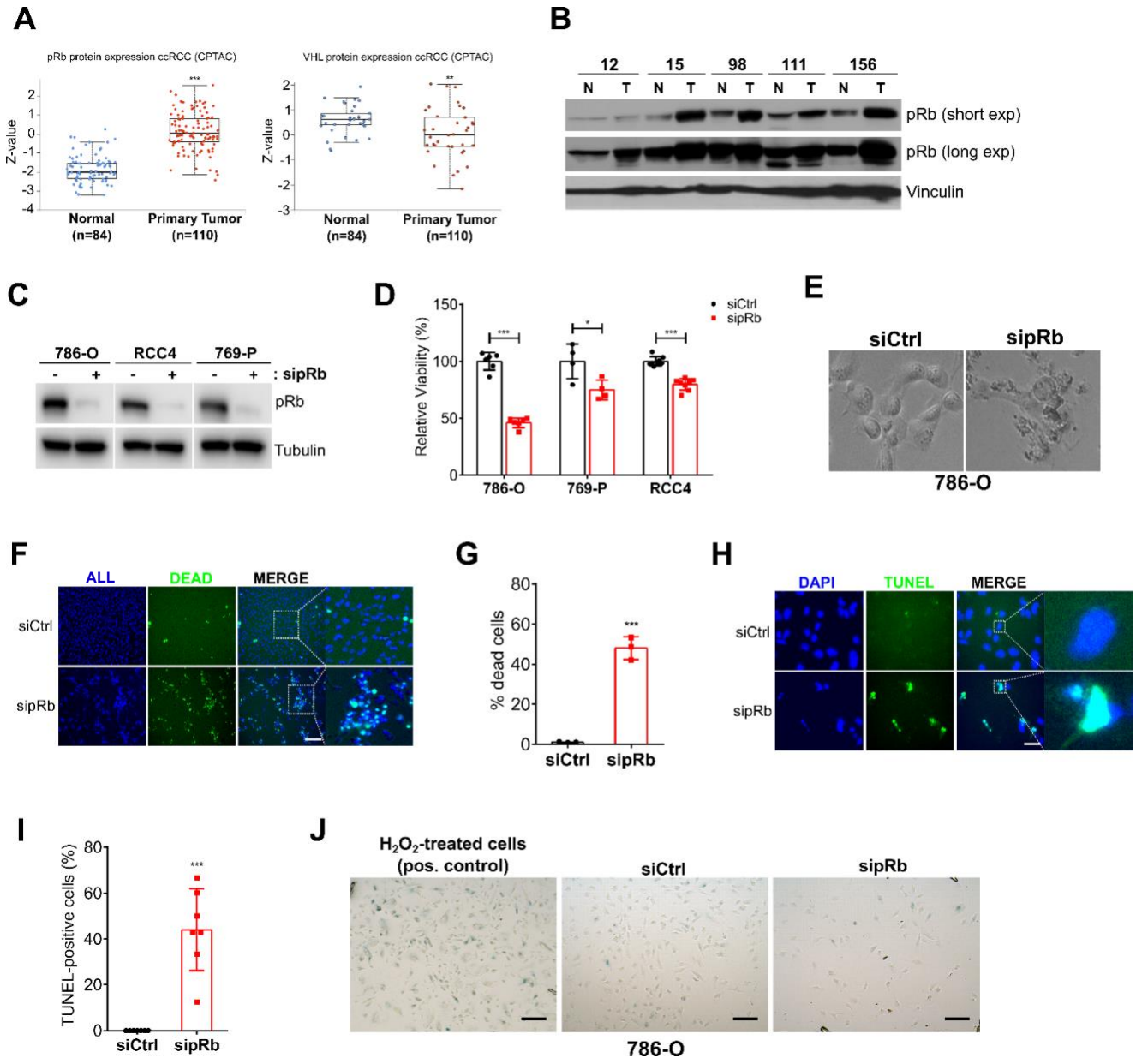

Figure 12. pRb suppresses apoptosis in ccRCC cells.

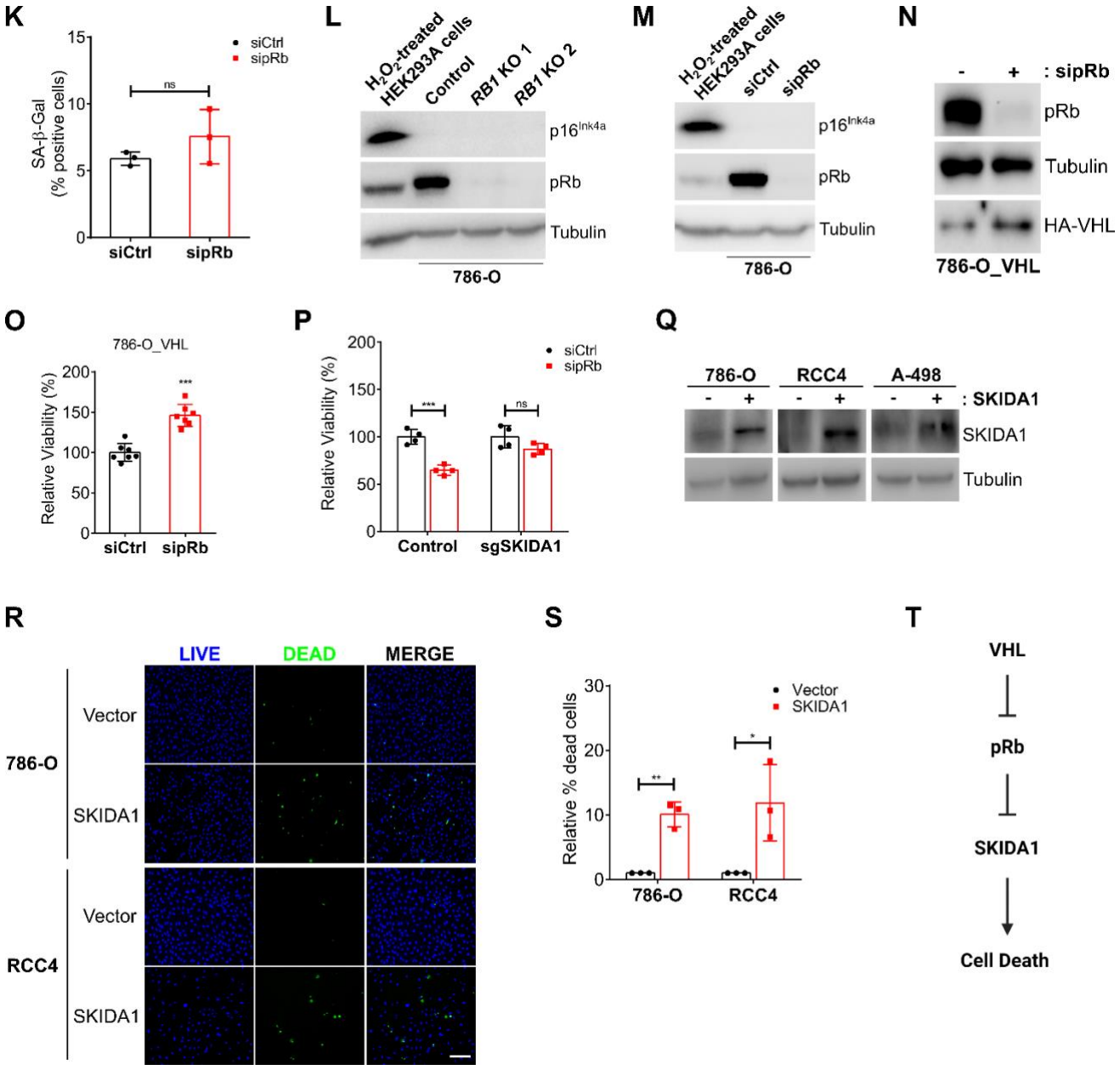

Figure 12 (continued). pRb suppresses apoptosis in ccRCC cells.

Figure 12. pRb suppresses apoptosis in ccRCC cells. (A) Analysis of pRb and VHL protein expression in ccRCC primary tumors and normal tissue. Patient data were obtained from Clinical Proteomic Tumor Analysis Consortium (CPTAC) dataset via the UALCAN data analysis portal. Z-values represent standard deviations from the median across normal and tumor samples. Log2 spectral count ratio values from CPTAC were first normalized within each sample profile, then normalized across samples. **(B)** Immunoblot of lysates from ccRCC primary tumor (T) and patient-matched normal tissue (N). **(C)** Immunoblot of lysates from indicated ccRCC cell lines transfected with either non-targeting control siRNA (siCtrl) or pRb targeting siRNA (sipRb). **(D)** Analysis of cell viability (relative to control) in indicated ccRCC cell lines transfected with either non-targeting control siRNA (siCtrl) or pRb-targeting siRNA (sipRb), measured via a sulforhodamine B (SRB) assay. Statistical significance was calculated using unpaired t test and Holm-Sidak post-hoc test (n>3). **(E)** Representative phase-contrast images of 786-O cells transfected with either non-targeting control siRNA (siCtrl) or pRb-targeting siRNA (sipRb). **(F)** Representative fluorescence images showing 786-O cells transfected with either non-targeting control siRNA (siCtrl) or pRb-targeting siRNA (sipRb), and stained using the ReadyProbes® Cell Viability Imaging Kit. The blue stain represents the total cells, while the green stain represents dead cells. Scale bar = 250 µm. **(G)** Quantification of percentage of dead cells relative to total number of cells in (F). Statistical significance was calculated using unpaired two-tailed t test (n=3). **(H)** Representative images showing TUNEL staining of 786-O cells transfected with either non-targeting control siRNA (siCtrl) or pRb targeting siRNA (sipRb). Scale bar = 250 µm. **(I)** Quantification of percentage of TUNEL-positive cells relative to total number of cells in (H). Statistical significance was calculated using unpaired two-tailed t test (n=7). **(J)** Representative images showing beta-galactosidase staining of 786-O cells transfected with either non-targeting control siRNA (siCtrl) or pRb-targeting siRNA (sipRb). Positive control cells were obtained by treating 786-O cells with 150 µM hydrogen peroxide (H_2O_2) for 2 hours, followed by recovery for five days. Scale bar = 250 µm. **(K)** Quantification of SA-β-gal positive cells in (J). Statistical significance was calculated using unpaired two-tailed t test (n=3). **(L)** Immunoblot analysis of $p16^{Ink4a}$ expression in 786-O control and *RB1* KO cells. HEK293A cells treated with 150 µM H_2O_2 for five days, were used as positive control for senescence induction and $p16^{Ink4a}$ expression.

Figure 12 (continued). pRb suppresses apoptosis in ccRCC cells. (M) Immunoblot analysis of p16Ink4a expression in 786-O cells transfected with either non-targeting control siRNA (siCtrl) or pRb-targeting siRNA (sipRb) (final concentration 25 nM). HEK293A cells treated with 150 μM H_2O_2 for five days, were used as positive control for senescence induction and $p16^{Ink4a}$ expression. **(N)** Immunoblot of lysates from VHL-expressing 786-O cells transfected with either non-targeting control siRNA (siCtrl) or pRb targeting siRNA (sipRb) (final concentration 25 nM). **(O)** Analysis of cell viability (relative to control) in VHL-expressing 786-O cells transfected with either non-targeting control siRNA (siCtrl) or pRb targeting siRNA (sipRb) (final concentration 25 nM), measured via the SRB assay. Statistical significance was calculated using unpaired two-tailed t test (n=7). **(P)** Analysis of cell viability in 786-O Cas9-expressing cells transduced with either empty vector (control) or sgSKIDA1-containing vector, and transfected with either non-targeting control siRNA (siCtrl) or pRb targeting siRNA (sipRb) (final concentration 25 nM). Cell viability was measured via the SRB assay and normalized to the siCtrl condition. Statistical significance was calculated using unpaired t test and Holm-Sidak post-hoc test (n=4). **(Q)** Immunoblot of lysates from 786-O, RCC4 and A-498 cells stably infected with lentivirus encoding either control plasmid (-) or SKIDA1 cDNA containing plasmid. **(R)** Representative fluorescence images of 786-O and RCC4 cells transduced with lentivirus containing either empty (control) plasmid (Vector) or SKIDA1 cDNA-encoding plasmid. Cells were stained using the ReadyProbes® Cell Viability Imaging Kit. The blue stain represents total cells, while the green stain represents dead cells. Scale bar = 250 μm. **(S)** Quantification (relative to control) of percentage of dead cells relative to total number of cells in (R). Statistical significance was calculated using unpaired t test and Holm-Sidak post-hoc test (n=3). **(T)** Schematic illustration showing the VHL-pRb-SKIDA1 signalling axis and the effect on cell death. **(A-T)** Data are represented as mean ± SD. *$p < 0.05$, **$p < 0.01$, ***$p < 0.001$. 'ns' denotes not significant.

3.5 pRb depletion inhibits ccRCC tumorigenesis

pRb-mediated repression of cell death in ccRCC may be indicative of oncogenic contribution of hyperaccumulated pRb in ccRCC. Therefore, we sought to determine the effects of pRb accumulation on ccRCC cancer phenotype. We first analyzed anchorage-independent growth of ccRCC cells in soft agar, which is an important hallmark of cancer[376–378]. 786-O cells are known to grow in an anchorage-independent manner[99,369], so in this background we created two independent *RB1* KO cell lines using CRISPR-Cas9 (Figure 13A). Next, using 786-O control and *RB1* KO cells, we measured anchorage-independent growth in the soft agar 3D culture model. We found that knockout of *RB1* significantly inhibited anchorage-independent growth of 786-O cells (Figure 13B-C). In contrast, knockout of *RB1* in VHL-reconstituted 786-O cells was sufficient to induce anchorage-independent growth (Figure 13D-E). Interestingly, knockdown of pRb in 786-O cells to levels similar to VHL-reconstituted cells, was sufficient to inhibit anchorage-independent growth (Figure 13F-H). These data are consistent with an oncogenic role for hyperaccumulated pRb specifically in VHL-deficient ccRCC.

We next assessed the clonogenic capacity of 786-O control and *RB1* KO cells by performing a clonogenic assay, a survival assay based on the ability of a single cell to grow into a colony. Consistent with our findings from the soft agar assay, we observed a significant decrease in clonogenic outgrowth following pRb depletion (Figure 13I-L). Together, these results indicate that pRb is required to maintain the tumorigenic potential of ccRCC cells. We next looked downstream at the potential impact of SKIDA1 on ccRCC clonogenicity and anchorage-independent growth. We found that upregulation of the pRb target SKIDA1 in ccRCC cells led to a significant decrease in clonogenic outgrowth (Figure 13M-N) and anchorage-independent growth in soft agar (Figure 13O-P). Furthermore, depletion of SKIDA1 in 786-O *RB1* KO cells

resulted in partial rescue of colony formation (Figure 13Q-R) and anchorage-independent growth in soft agar (Figure 13S-T). These results further emphasize that SKIDA1 may be an important downstream tumor suppressor target of the VHL-pRb pathway in ccRCC (Figure 13U).

To examine the effect of *RB1* knockout on ccRCC tumor growth *in vivo*, we injected 786-O control and *RB1* KO cells subcutaneously into the flanks of immunodeficient *NOD-scid IL2Rg*^{null} (NSG) mice. All mice were euthanized when the first tumor reached endpoint. Tumors were then excised and weighed. One control injection which failed to grow was considered an outlier and omitted during statistical analysis. We found that on average, tumors formed by 786-O control cells were significantly larger compared to those formed by *RB1* KO cells (Figure 13V). Furthermore, immunohistochemical staining of SKIDA1 in extracted tumors revealed increased SKIDA1 expression in *RB1* KO tumors compared to control tumors (Figure 13W-X). To further validate SKIDA1 as a clinically relevant target in ccRCC, we performed immunoblot analysis of additional ccRCC tumor and patient-matched normal samples, genotyped to confirm VHL mutation in all tumor samples. As expected, pRb protein expression was upregulated in the majority of tumors (Figure 13Y). And whilst SKIDA1 expression varied significantly between tumors, overall, we observed downregulation of SKIDA1 protein levels in most tumors compared to their matched normal tissue, further underscoring the clinical significance of our findings. Collectively, our results indicate that pRb hyperstabilization promotes ccRCC tumorigenesis, likely through transcriptional remodeling including the identified target SKIDA1 (Figure 14).

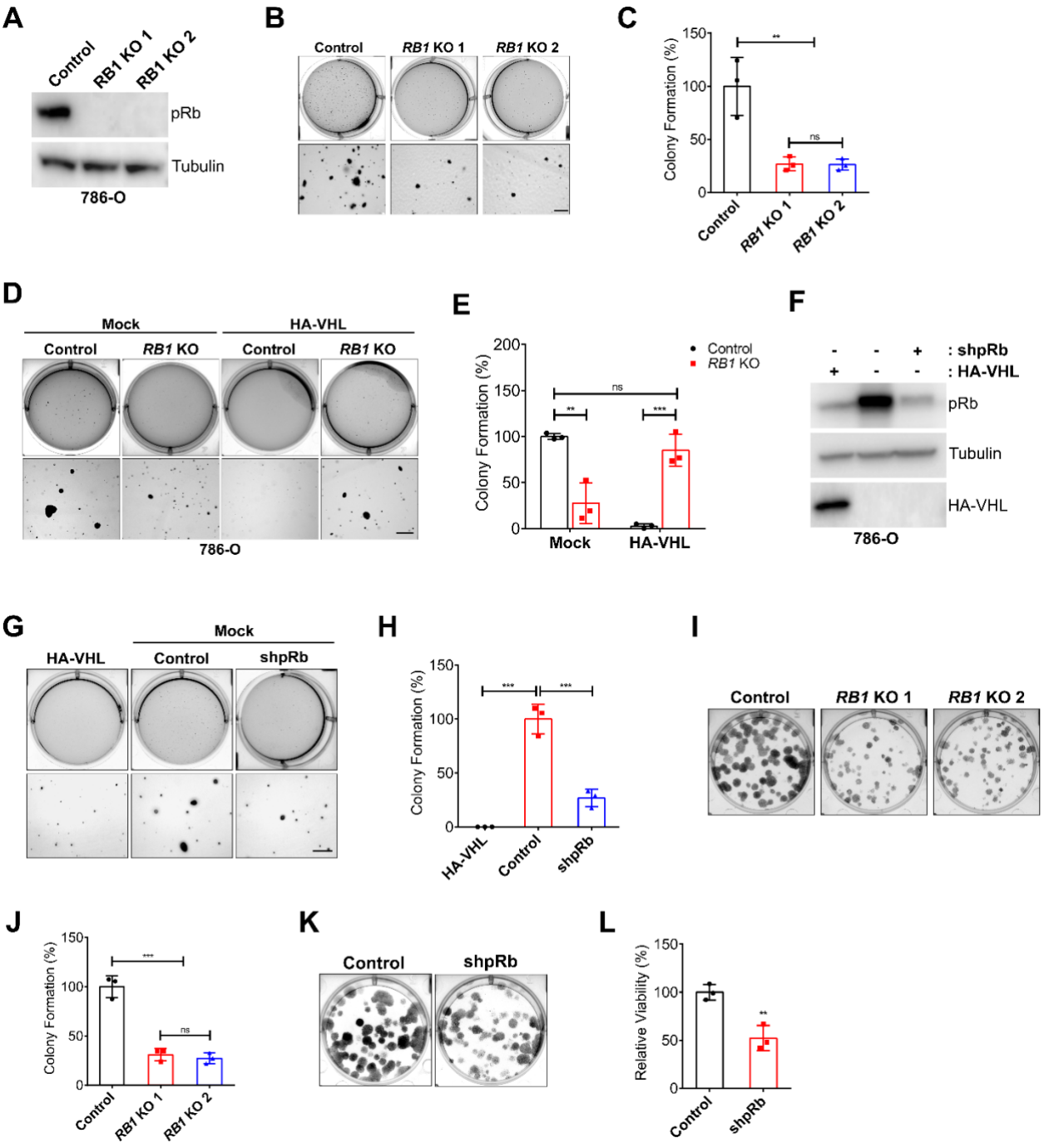

Figure 13. pRb hyperstabilization promotes ccRCC oncogenesis.

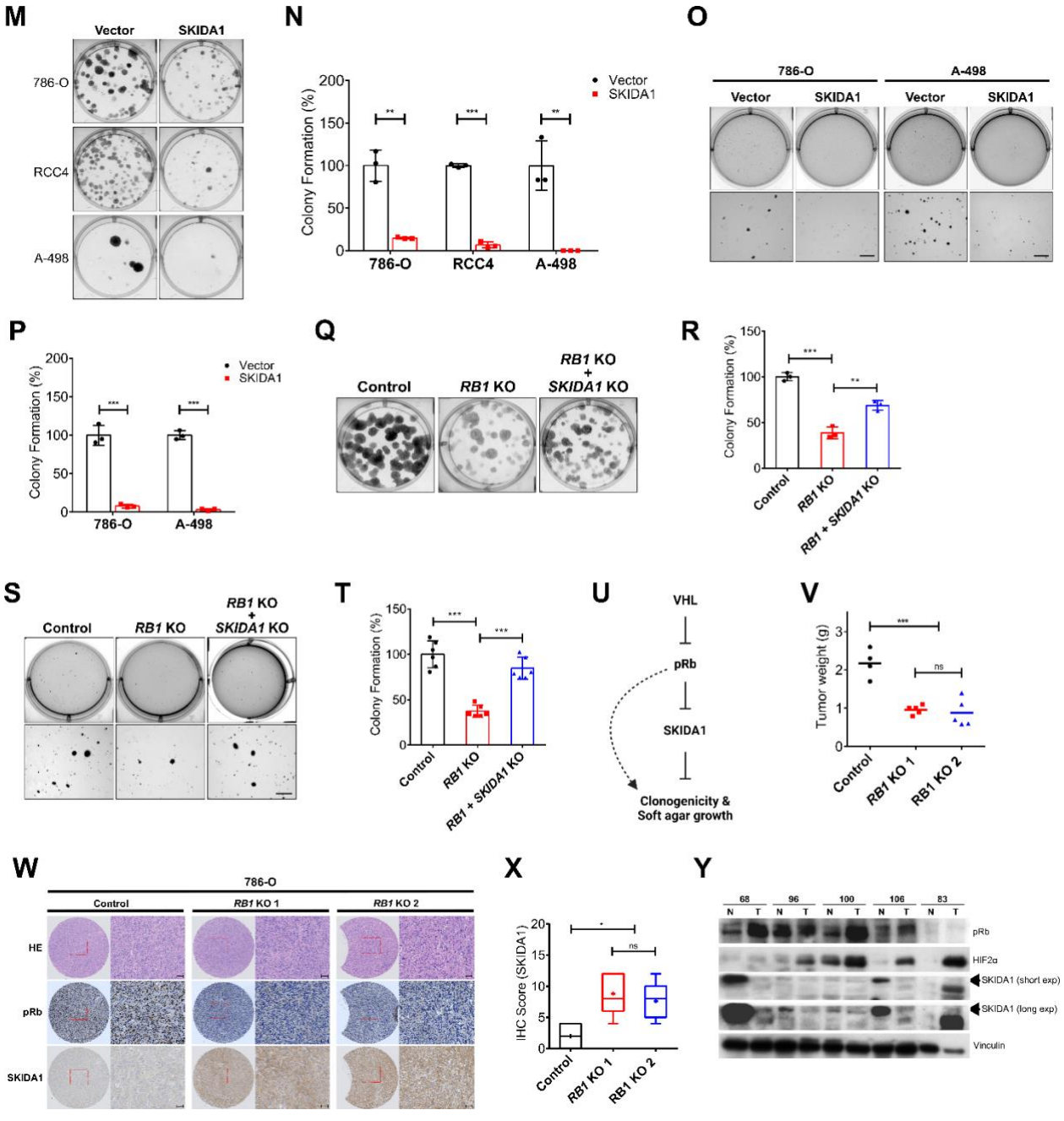

Figure 13 (continued). pRb hyperstabilization promotes ccRCC oncogenesis.

Figure 13. pRb hyperstabilization promotes ccRCC oncogenesis. (A) Immunoblot of lysates from 786-O control and *RB1* KO cells. **(B)** Representative images showing colony formation of 786-O control and *RB1* KO cells in soft agar. Scale bar = 500 μm. **(C)** Quantification (relative to control) of the number of colonies formed in (A). Colonies >100 μm were counted and quantified. Statistical significance was calculated using ordinary one-way ANOVA and Tukey's post-hoc test (n=3). **(D)** Representative images showing colony formation in soft agar of 786-O control and *RB1* KO cells stably transfected with either control vector (Mock) or HA-tagged VHL. Scale bar = 500 μm. **(E)** Quantification (relative to control) of the number of colonies formed in (D). Colonies >100 μm were counted and quantified. Statistical significance was calculated using ordinary two-way ANOVA and Tukey's post-hoc test (n=3). **(F)** Immunoblot of lysates from 786-O control, VHL-reconstituted, and pRb knockdown cells. For VHL reconstitution, 786-O cells were stably transfected with HA--VHL. pRb knockdown cells were made by infecting 786-O cells with lentivirus encoding pRb-targeting shRNA. **(G)** Representative images showing colony formation in soft agar of 786-O control, VHL-reconstituted, and pRb knockdown (shpRb) cells. Scale bar = 250 μm. **(H)** Quantification (relative to control) of the number of colonies formed in (G). Colonies >100 μm were counted and quantified. Statistical significance was calculated using ordinary one-way ANOVA and Tukey's post-hoc test (n=3). **(I)** Representative images showing clonogenic outgrowth of 786-O control and *RB1* KO cells. **(J)** Quantification (relative to control) of the number of colonies in (I). Statistical significance was calculated using ordinary one-way ANOVA and Tukey's post-hoc test (n=3). **(K)** Representative images showing clonogenic outgrowth of 786-O control and pRb knockdown cells. **(L)** Quantification (relative to control) of the number of colonies in (K). Statistical significance was calculated using unpaired two-tailed t test (n=3). **(M)** Representative images showing clonogenic outgrowth of 786-O, RCC4 and A-498 cells stably infected with lentivirus containing either control plasmid (Vector) or SKIDA1 cDNA containing plasmid. **(N)** Quantification (relative to control) of the number of colonies in (M). Statistical significance was calculated using unpaired t test and Holm-Sidak post-hoc test (n=3). **(O)** Representative images showing colony formation in soft agar of 786-O and A-498 cells stably infected with lentivirus containing either empty (control) plasmid (Vector) or SKIDA1 cDNA-encoding plasmid. c. **(P)** Quantification (relative to control) of the number of colonies formed in (O). Colonies >100 μm were counted and quantified. Statistical significance was calculated using unpaired t test and Holm-Sidak post-hoc test (n=3). **(Q)** Representative images showing clonogenic outgrowth of 786-O control, *RB1* KO and *RB1*/*SKIDA1* double KO cells.

Figure 13 (continued). pRb hyperstabilization promotes ccRCC oncogenesis. (R) Quantification (relative to control) of the number of colonies in (Q). Statistical significance was calculated using ordinary one-way ANOVA and Tukey's post-hoc test (n=3). **(S)** Representative images showing colony formation in soft agar of 786-O control, *RB1* KO and *RB1*/*SKIDA1* double KO cells. Scale bar = 500 µm. **(T)** Quantification (relative to control) of the number of colonies formed in (S). Colonies >100 µm were counted and quantified. Statistical significance was calculated using ordinary one-way ANOVA and Tukey's post-hoc test (n=6). **(U)** Schematic illustration showing the VHL-pRb-SKIDA1 signalling axis and the effect on clonogenicity and soft agar growth. The dotted line suggests alternate pathways. **(V)** Scatter dot plot showing quantification of weights of tumors formed by 786-O control and *RB1* KO cells injected subcutaneously into the flanks of immunodeficient *NOD-scid IL2Rg*^{null} mice, via a tumor xenograft assay. The line indicates the mean. Five injections were performed with control cells and ten injections with *RB1* KO cells (five for each clone). One control injection which failed to grow was considered an outlier and omitted during statistical analysis. Statistical significance was calculated using ordinary one-way ANOVA and Tukey's post-hoc test (n>3). **(W)** Representative images showing HE and IHC staining of the indicated proteins on tumor sections from mice xenograft injections of 786-O control or *RB1* KO cells. Scale bar = 50 µm. **(X)** Box and whisker plot showing semi-quantitative IHC scoring of SKIDA1 protein expression in tumor xenografts. Mean is shown as '+'. Statistical significance was calculated using ordinary one-way ANOVA and Tukey's post-hoc test (n>3). **(Y)** Immunoblot of lysates from ccRCC primary tumor (T) and patient-matched normal tissue (N). All tumors were genotyped and confirmed to have VHL mutations. **(A-Y)** Data are represented as mean ± SD. *$p < 0.05$, **$p < 0.01$, ***$p < 0.001$. 'ns' denotes not significant.

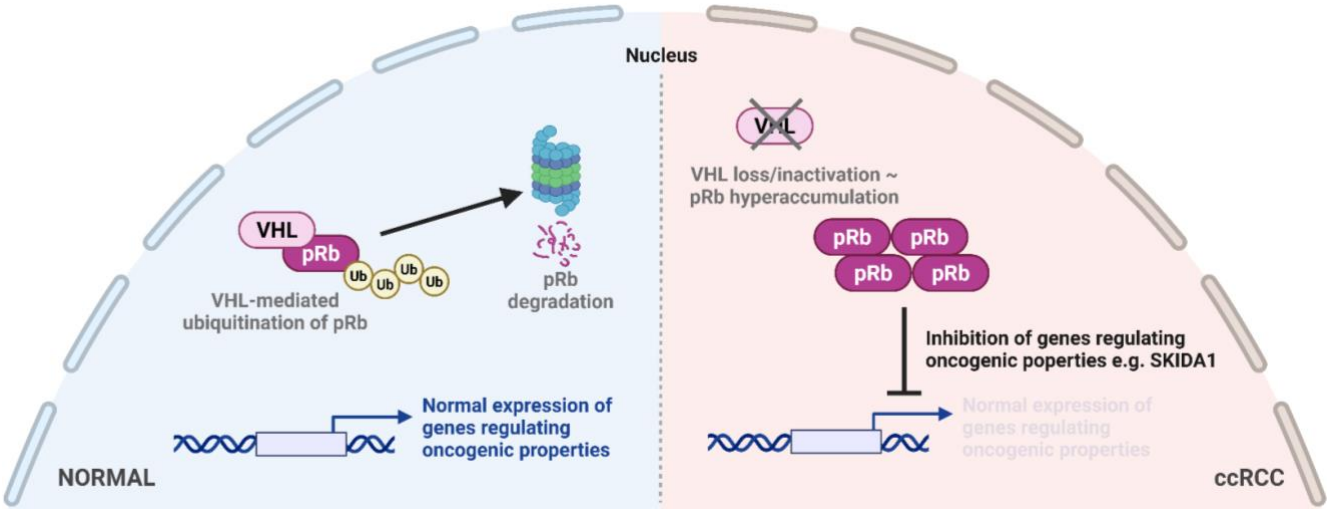

Figure 14. Schematic illustration of pRb regulation by VHL and effects on downstream targets. In normal kidney cells, VHL regulation of pRb promotes normal expression of genes regulating oncogenic properties. In ccRCC, VHL loss promotes pRb hyperaccumulation, which leads to the repression of genes regulating oncogenic properties. Created using BioRender.

Chapter 4:

Biochemical Characterization of VHL-pRb Interaction

4.1 Biochemical determinants of pRb regulation by VHL

To better understand pRb regulation by VHL, we sought to determine the conditions that favor VHL binding to pRb. Considering the known cellular and environmental factors influencing VHL-substrate interactions, as well as the established characteristics of pRb, we examined the effects of oxygen levels, phosphorylation status, and subcellular localization on VHL binding to pRb.

4.1.1 Effect of oxygen levels on VHL regulation of pRb

VHL has been described to regulate HIF-α (and other substrates) in an oxygen-sensitive manner[94,95,99,110,111]. We therefore asked whether VHL regulates pRb through a similar mechanism. To test this, we exogenously expressed pRb and VHL in HEK293A cells and performed VHL immunoprecipitation under normoxic and hypoxic (0.5% O_2 for 24 hours) conditions. As expected, pRb co-precipitated with VHL when cells were treated with MG132 (Figure 15A). However, this interaction was disrupted under hypoxia, suggesting that VHL targets pRb preferentially in normoxic conditions. Furthermore, in VHL-expressing 786-O cells, which express lower levels of pRb compared to their VHL-null counterparts, we observed a significant increase in pRb protein levels upon hypoxia treatment (Figure 15B). Together, these findings indicate that, similar to HIF-α, VHL regulates pRb in an oxygen-dependent manner. The oxygen-sensitive nature of this regulation suggests that pRb may play a critical role in the cellular adaptation response to hypoxia.

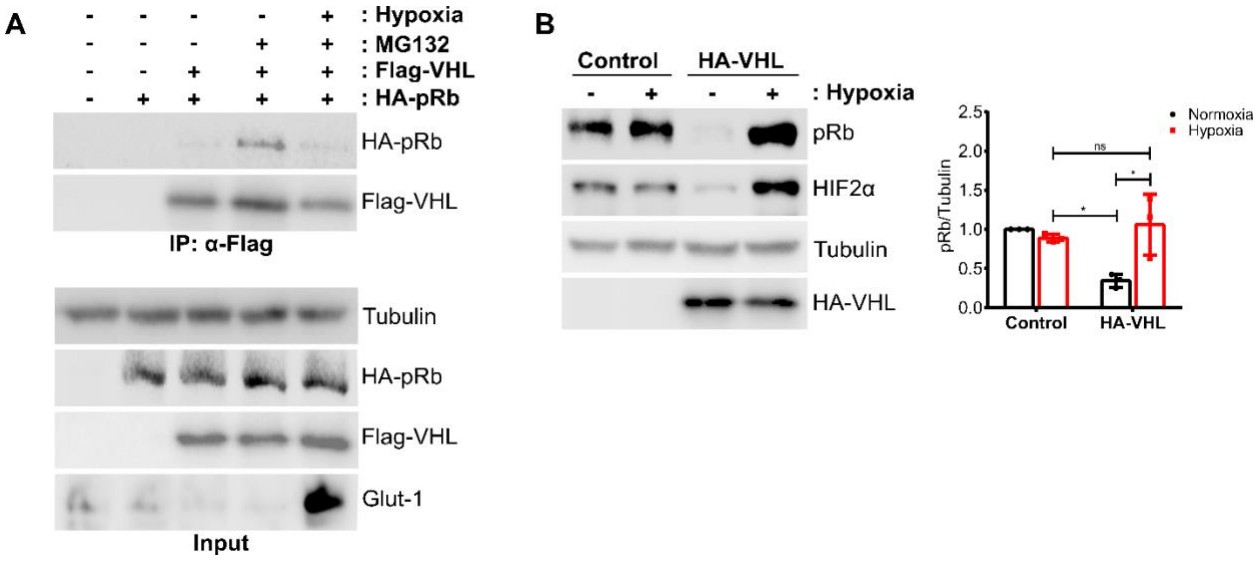

Figure 15. VHL targets pRb in an oxygen-dependent manner. (A) Immunoprecipitation of Flag-tagged VHL from HEK293A cells transfected with indicated plasmids and treated with 10 μM MG132 as indicated for 4 h. For hypoxia treatment, cells were placed in 0.5% O_2 for 24 h. Glut-1 expression serves as positive control to indicate HIF upregulation under hypoxia. **(B)** Immunoblot of lysates from 786-O cells stably transfected with either control vector or HA-tagged VHL and treated as indicated with hypoxia (0.5% O_2) for 24 h. Quantification of pRb protein expression relative to tubulin is shown to the right. Statistical significance was calculated using ordinary two-way ANOVA and Tukey's post-hoc test (n=3). Data are represented as mean ± SD. *$p < 0.05$, **$p < 0.01$, ***$p < 0.001$. 'ns' denotes not significant.

4.1.2 Effect of phosphorylation status on VHL regulation of pRb

The activity and function of pRb are largely governed by its phosphorylation state. In its hypophosphorylated form, pRb acts as a cell cycle repressor, whereas hyperphosphorylated pRb is strongly associated with uncontrolled cell division and cancer progression[256,266–270]. Given the critical role of phosphorylation in regulating pRb activity, we asked whether VHL targets pRb in

a phosphorylation-dependent manner. To test this, we co-expressed VHL with either wild-type (WT) pRb or a pRb mutant lacking all Ser/Thr CDK phosphorylation sites (ΔCDK) in HEK293A cells. Immunoprecipitation of WT and ΔCDK pRb revealed similar levels of VHL co-precipitation in the presence of MG132, suggesting that VHL binding to pRb is independent of CDK-mediated phosphorylation (Figure 16A). To further validate this, we generated 786-O cell lines stably expressing either Flag-tagged pRb or HA-tagged VHL and Flag-tagged pRb. In this system, we found that CDK4/6 inhibition with Palbociclib[366], which abrogates pRb phosphorylation, did not significantly impact VHL-pRb interaction (Figure 16B). Collectively, these findings indicate that pRb phosphorylation (at least by CDKs) does not play a major role in its recognition or targeting by VHL.

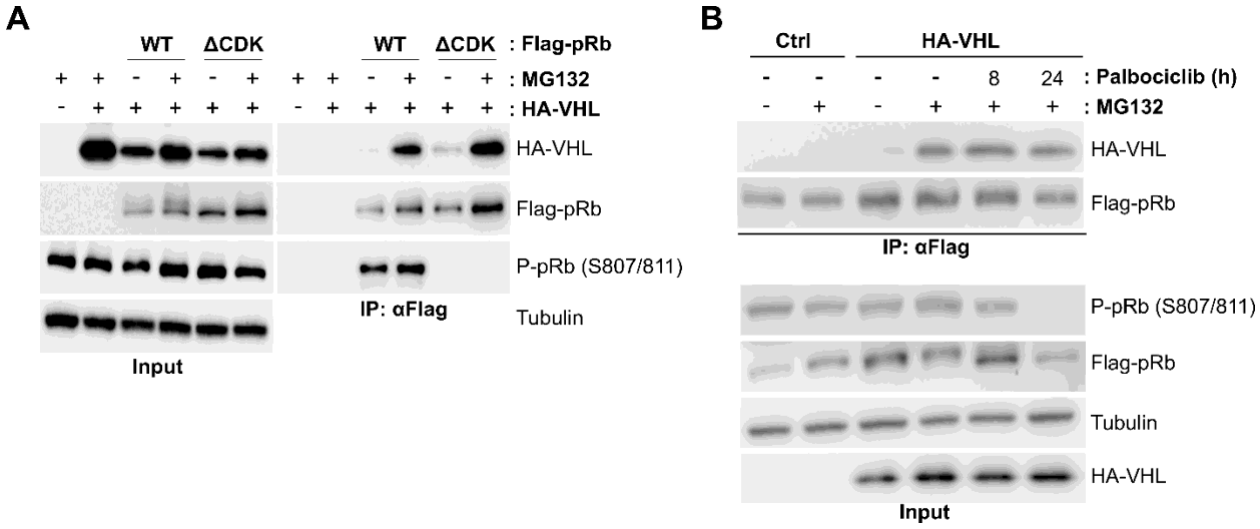

Figure 16. VHL targets pRb in a phosphorylation-independent manner. (A) Immunoprecipitation (IP) of Flag-tagged pRb wild-type (WT) or cyclin-dependent kinase (CDK) phospho-mutant from HEK293A cells transfected with indicated plasmids and treated with 10 μM MG132 as indicated for 4 h. **(B)** Immunoprecipitation of exogenous Flag-tagged pRb from 786-O cells stably transfected with either control vector (Ctrl) or HA-tagged VHL and treated with 10 μM MG132 as indicated for 4 h or 5 μM Palbociclib for the indicated time points.

4.1.3 Effect of subcellular localization on VHL regulation of pRb

Although primarily recognized as a nuclear protein, pRb shuttles between the nucleus and cytoplasm in response to factors such as mitotic phase and CDK activity[379,380]. Similarly, VHL has been reported to translocate between the nucleus and cytoplasm in a cell density-dependent manner[381]. Given these observations, we sought to determine whether VHL preferentially regulates pRb in specific cellular compartments. To investigate the subcellular distribution of VHL and pRb in VHL-reconstituted ccRCC cells, we performed immunoblot analysis on nuclear and cytoplasmic extracts from 786-O cells stably transfected with HA-tagged VHL. The results confirmed that VHL and pRb are present in both nuclear and cytoplasmic compartments (Figure 17A). To determine whether VHL binding to pRb was dependent on subcellular localization, we fractionated nuclear and cytoplasmic extracts from VHL-expressing ccRCC cells treated with MG132 and immunoprecipitated VHL under normoxic and hypoxic conditions. Notably, the MG132-sensitive interaction between VHL and pRb was observed only in the nuclear fraction, indicating that VHL preferentially targets nuclear pRb (Figure 17B). Consistent with previous observations, treatment with hypoxia (0.5% O_2 for 24 hours) disrupted this interaction. Together, our findings suggest that VHL specifically targets nuclear pRb for proteasomal degradation.

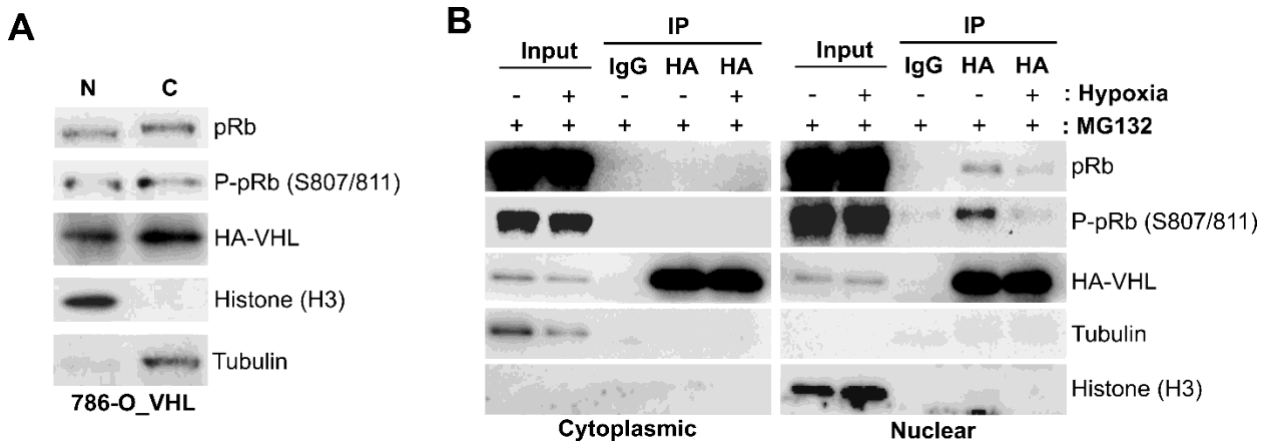

Figure 17. VHL predominantly targets nuclear pRb. (A) Immunoblot analysis of nuclear (N) and cytoplasmic (C) extracts from 786-O cells stably transfected with HA-VHL **(B)** Subcellular fractionation followed by immunoprecipitation (IP) of HA-tagged VHL stably transfected into 786-O cells and treated with 10 μM MG132 for 4 h and hypoxia (0.5% O_2 for 24 h) as indicated. An IgG isotype control was included to control for non-specific binding to primary (αHA) antibody. Tubulin was used as a cytoplasmic marker, while Histone (H3) was used as a nuclear marker.

4.2 Determination of VHL binding site on pRb

pRb is composed of 3 distinct domains: a N-terminal domain (aa1-379), a small pocket (aa380-787) that comprises subdomains pocket A and pocket B, and a C-terminal domain (aa787-928)[238,241], as depicted in Figure 18A. To identify the VHL binding site on pRb, we generated truncated pRb constructs and co-expressed them with full-length VHL in HEK293A cells. Immunoprecipitation of pRb was then performed to determine which fragments were capable of binding VHL. By analyzing overlapping VHL-binding pRb fragments, we identified a common region spanning amino acids (aa) 643-793 (pocket B), whose absence abolished VHL binding

(Figure 18B-C). This suggests that the pocket B domain of pRb is crucial for VHL recognition. To determine whether the pocket B domain is both necessary and sufficient for VHL binding, we co-expressed full-length VHL with either a pRb pocket B truncation mutant (Δ643-793) or the pocket B domain (aa643-793) alone. Immunoprecipitation of pRb revealed that the pocket B truncation mutant failed to bind VHL, whereas the isolated pocket B domain interacted with VHL to a similar extent as full-length pRb (Figure 18D). These findings demonstrate that the pocket B domain of pRb is not only necessary, but also sufficient for VHL binding.

To further refine the VHL binding site within the pRb pocket B domain, we generated small internal truncations within aa643-793 of pRb and assessed their interaction with VHL using immunoprecipitation assays. Deletion of aa778-793 or an expanded aa778-807 from full-length pRb was sufficient to disrupt VHL binding, indicating that this region is critical for VHL targeting (Figure 18E-F). It is also worth noting that all immunoprecipitation assays (Figure 18B,D,E) were performed following MG132 treatment to stabilize the VHL-pRb interaction. Collectively, our results demonstrate that VHL interacts specifically with the pocket B domain of pRb, targeting residues aa778-807. Alignment of this region across multiple species—including chicken (*Gallus gallus*), house mouse (*Mus musculus*), chimpanzee (*Pan troglodytes*), zebrafish (*Danio rerio*), and cattle (*Bos taurus*)—revealed a high degree of conservation (Figure 19). Among the fully conserved residues (highlighted in red), P781, P783, P786, P789, Y790, P796, P800, N803, and Y805 are potential sites for post-translational hydroxylation. Given the oxygen-sensitive regulation of pRb by VHL, hydroxylation of one or more of these residues may therefore serve as a signal for VHL binding.

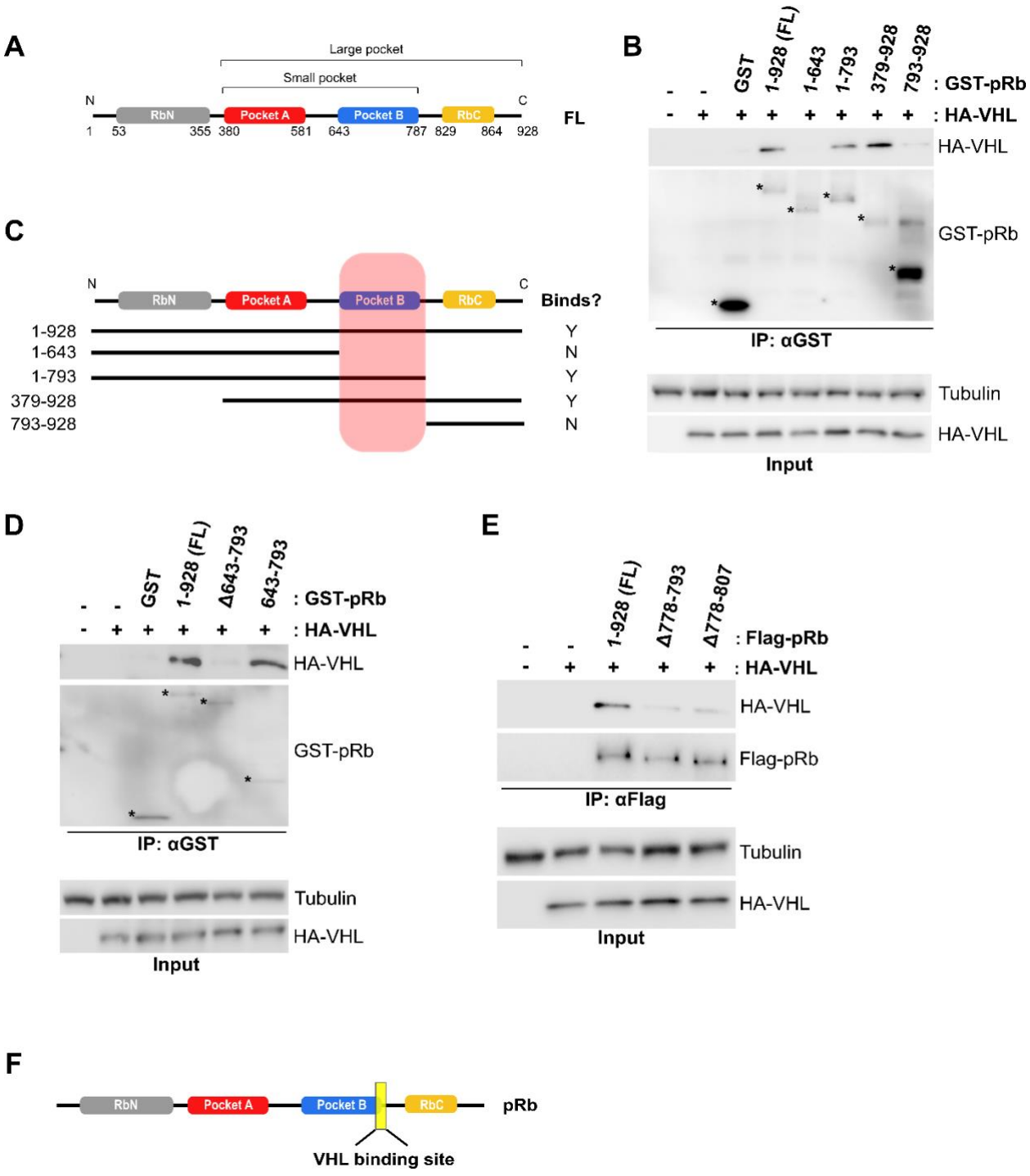

Figure 18. VHL interacts with the pocket B domain of pRb.

Figure 18. VHL interacts with the pocket B domain of pRb. (A) Schematic illustration of pRb domains: N-terminal domain (RbN), small pocket domain (Pocket A + Pocket B), and C-terminal domain (RbC); and associated amino acid residues. **(B, D)** Immunoprecipitation (IP) of Glutathione S-transferase (GST)-tagged pRb constructs from HEK293A cells transfected with indicated plasmids and treated with 10 μM MG132 for 4 hours. 'FL' denotes full length protein; 'Δ' denotes fragment truncation. **(C)** Schematic showing the estimated VHL binding site on pRb (pink box) based on the immunoprecipitation result from (B), and indicating the pRb fragments that bound (Y) or did not bind (N) to VHL. **(E)** Immunoprecipitation (IP) of Flag-tagged pRb constructs from HEK293A cells transfected with indicated plasmids and treated with 10 μM MG132 for 4 hours. 'FL' denotes full length protein; 'Δ' denotes fragment truncation. **(F)** Schematic illustrating narrowed down VHL binding site on pRb – yellow box.

SEQUENCE ALIGNMENT

```
                    778                                        807
Homo Sapiens          TLSPIPHIPRSPYKFPSSPLRIPGG-NIYIS
Gallus gallus         TLSPIPHIPRSPYQFSNSPRRVPAGNNIYIS
Mus musculus          TLSPIPHIPRSPYKFSSSPLRIPGG-NIYIS
Pan troglodytes       TLSPIPHIPRSPYKFPSSPLRIPGG-NIYIS
Danio rerio           PLSPIPHIPCSPYK--NSPLRVPGSNNVYVS
Bos taurus            TLSPIPHIPRSPYKFSSSPLRIPGG-NIYIS
                       ******** ***:  .** *:*.. *:*:*
```

Figure 19. pRb amino acid sequence alignment across different species. Sequence alignment of aa778-807 of pRb across different species as indicated using Clustal Omega Multiple Sequence Alignment tool. The asterisk '*' indicates that the residue is completely conserved across all the aligned sequences. The colon ':' indicates highly conserved residues that have strongly similar properties. The dot '.' indicates that the residues are weakly similar but still share some chemical properties.

4.3 Determination of the VHL-containing E3 ligase targeting pRb

VHL mediates the ubiquitin-dependent proteasomal degradation of HIF-α through the ECV complex, which consists of Elongin B/C, Cullin-2, and Rbx-1[89–91]. We asked whether VHL targets pRb via the same complex. To identify the E3 ligase complex associated with VHL and pRb, we ectopically expressed VHL and pRb in HEK293A cells and performed a sequential immunoprecipitation following MG132 treatment, as illustrated in Figure 20A. First, we immunoprecipitated Flag-tagged pRb and subsequently eluted it using 3× Flag peptides. The eluate was then subjected to a second immunoprecipitation for HA-tagged VHL, allowing us to coprecipitate proteins interacting with the VHL-pRb complex. In parallel, we purified the VHL-HIF-2α complex, which has a well-characterized E3 ligase, for comparative purposes. As expected, immunoblot analysis of VHL-HIF-2α-associated proteins indicated the presence of Elongin B, Cullin-2, and Rbx-1 (Figure 20B). However, these ECV complex proteins were notably absent from the VHL-pRb complex. Our findings therefore suggest that VHL targets pRb via a distinct, previously uncharacterized E3 ligase complex.

A

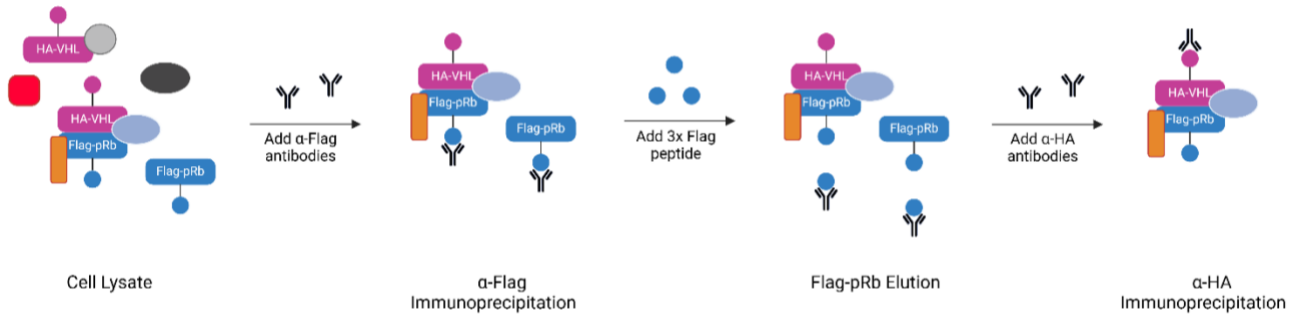

Figure 20. VHL targets pRb via a novel E3 ligase complex.

B

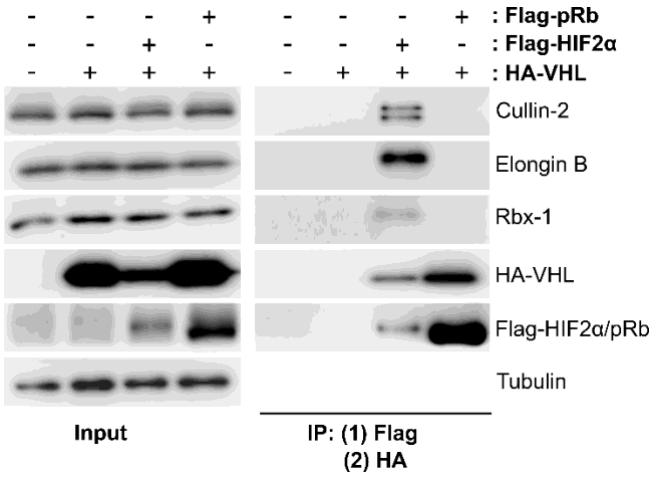

Figure 20. VHL targets pRb via a novel E3 ligase complex. (A) Schematic illustrating sequential immunoprecipitation to purify the VHL-pRb complex.Created using BioRender. **(B)** Immunoprecipitation (IP) of Flag-tagged HIF2α or pRb, followed by elution of Flag-tagged protein and IP of HA-tagged VHL in HEK293A cells. Cells were treated with 10 μM MG132 for 4 hours to stabilize VHL-pRb and VHL-HIF2α complexes.

4.4 Elucidation of VHL-pRb complex binding partners

To identify binding partners of the VHL-pRb complex, we employed the proximity labeling technique split-TurboID[382], with the N-terminal TurboID fragment (NTID) fused to Flag-tagged pRb and the C-terminal TurboID fragment (CTID) fused to Myc-tagged VHL. When pRb and VHL interact, the inactive NTID and CTID fragments are brought into close proximity, reconstituting enzymatic activity and enabling biotinylation of nearby proteins in the presence of biotin (Figure 21A). Following expression of NTID-Flag-pRb and CTID-Myc-VHL in HEK293A cells, and supplementation of the media with biotin, immunofluorescence analysis

revealed biotinylation signals predominantly localized to the nucleus (Figure 21B-C; data generated by Chenxuan Zhu). This observation aligns with our immunoprecipitation results, confirming that VHL and pRb specifically interact within the nuclear compartment (Figure 17BTo identify proteins associated with the VHL-pRb complex and assess their functional significance, we ectopically expressed NTID-Flag-pRb in HEK293A cells stably expressing CTID-Myc-VHL (control). Cells were treated with MG132 for 4 hours followed by 1 hour of biotin addition to promote the biotinylation of proteasomal-sensitive binding partners. Streptavidin affinity purification of biotinylated substrates was performed using nuclear fractions to minimize background protein contamination. As expected, immunoblot analysis of affinity-purified substrates revealed more pronounced protein biotinylation in cells co-expressing NTID-Flag-pRb and CTID-Myc-VHL compared to cells expressing CTID-Myc-VHL alone (Figure 21D; data generated by Chenxuan Zhu). Affinity-purified substrates were resolved on a NuPAGE 10% Bis-Tris gel and visualized following a Coomassie stain. Protein-containing gel slices were then excised, trypsin-digested, and analyzed by LC-MS. LC-MS analysis of biotinylated peptides enriched in cells co-expressing NTID-Flag-pRb and CTID-Myc-VHL, compared to those expressing CTID-Myc-VHL alone, identified several core components of the canonical BRG1/BRM-associated factor (cBAF) chromatin remodeling complex[383], including ARID1A (AT-Rich Interaction Domain 1A), SMARCA4 (SWI/SNF related BAF chromatin remodeling complex subunit ATPase 4), and DPF1/2 (D4, zinc, and double PHD fingers family members 1/2). This indicates a specific interaction between the VHL-pRb complex and chromatin remodeling proteins. Our findings thus suggest that the VHL-pRb interaction may have broader implications for global transcriptional regulation. Future studies employing techniques such as CUT&RUN (Cleavage Under Targets and Release Using Nuclease)[384,385] will enable precise

mapping of the genomic binding sites of the VHL-pRb-cBAF complex and provide further insights into its potential role in transcriptional regulation.

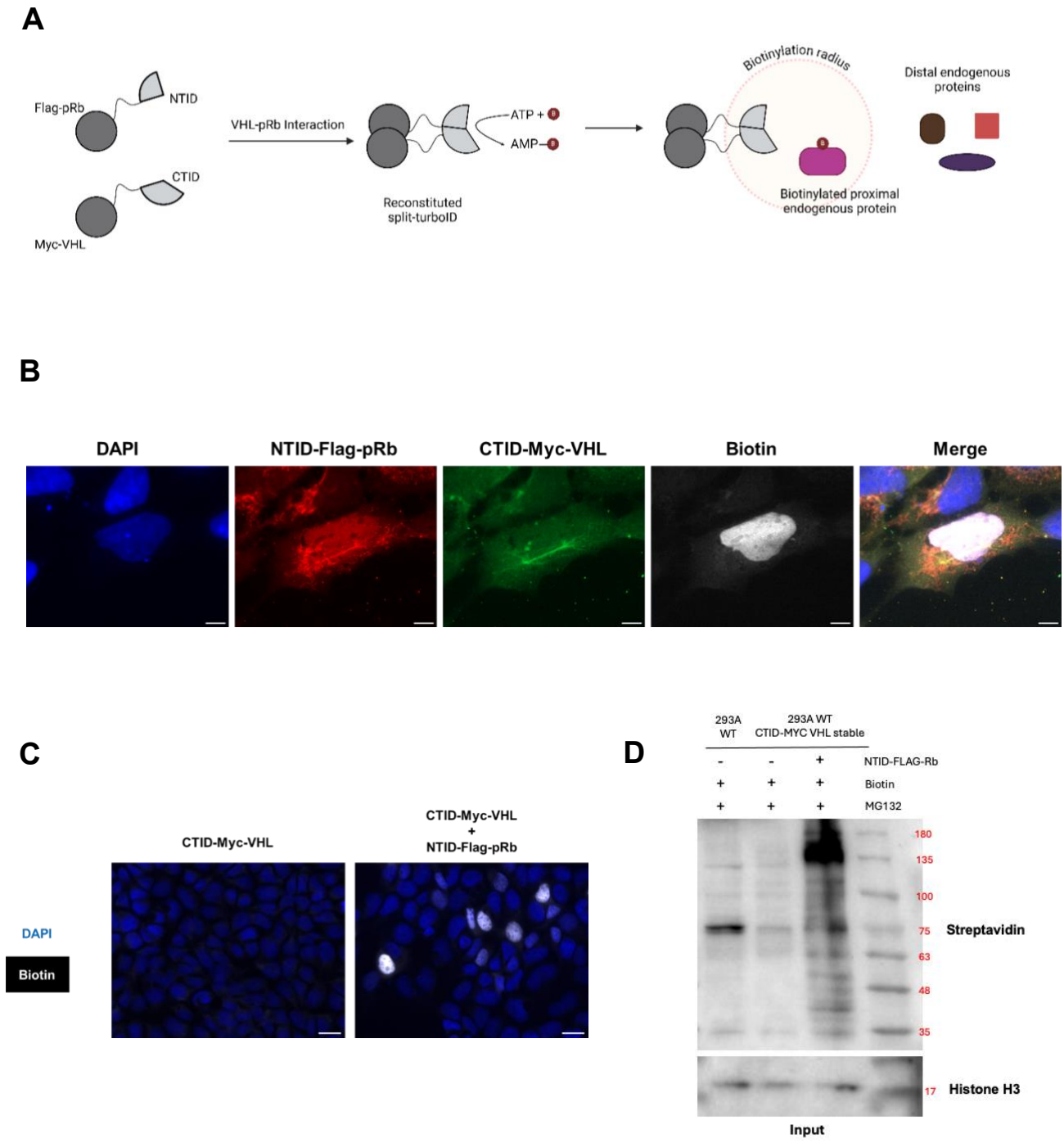

Figure 21. Split-TurboID reveals VHL-pRb complex interactors.

Figure 21. Split-TurboID reveals VHL-pRb complex interactors. (A) Split-TurboID consists of two TurboID fragments (NTID, an N-terminal fragment, and CTID, a C-terminal fragment), which can be brought together by protein–protein interaction (VHL-pRb interaction in this case) to reconstitute an active enzyme. Created using BioRender. **(B)** Immunofluorescence assay showing nuclear biotin staining (white) in HEK293A cells transiently expressing NTID-Flag-pRb (red) and CTID-Myc-VHL (green) and treated with 10 μM MG132 for 4 hours and 50 μM biotin for 1 hour. DAPI stain (blue). Scale bar = 5 μm. **(C)** Immunofluorescence staining of biotin (white) in HEK293A cells transiently expressing CTID-Myc-VHL alone or in combination with NTID-Flag-pRb, and treated with 10 μM MG132 for 4 hours and 50 μM biotin for 1 hour. . DAPI stain (blue). DAPI and biotin signals are merged. Scale bar = 20 μm. **(D)** Immunoblot analysis showing protein biotinylation in the nuclear lysates of untransfected HEK293A cells, and cells stably expressing CTID-Myc-VHL alone or together with NTID-Flag-pRb as indicated. Cells were treated with 10 μM MG132 for 4 hours and 50 μM biotin for 1 hour before harvesting. Histone H3 was used as a nuclear marker.

Chapter 5:

Pharmacological targeting of clear cell renal cell carcinoma

5.1 Abemaciclib in ccRCC

A synthetic lethal interaction exists between VHL loss and CDK4/6 inhibition across various human ccRCC cell lines *in vitro* and in tumor xenografts[386], making CDK4/6 inhibition a promising therapeutic avenue for ccRCC treatment. The CDK4/6 inhibitors Palbociclib, Ribociclib, and Abemaciclib are clinically approved for the treatment of patients with Hormone Receptor-Positive (HR+) / Human Epidermal Growth Factor Receptor 2-Negative (HER2−) advanced breast cancer[387]. However, their efficacy in ccRCC remains relatively understudied compared to other tumor types. Of the three approved CDK4/6 inhibitors, Abemaciclib was tested against ccRCC and was shown to have some activity *in vitro*, particularly when combined with the TKI Sunitinib[217]. To assess ccRCC sensitivity to Abemaciclib and its potential dependence on target pRb, we performed a dose-response assay using increasing concentrations of Abemaciclib to compare its activity in 786-O control cells versus *RB1* KO cells (Figure 22A). *RB1* deletion resulted in reduced sensitivity to Abemaciclib, as indicated by the upward shift of the curve (Figure 22B). However, this reduced sensitivity was only partial, suggesting that Abemaciclib may also exert pRb-independent effects. Using a 'drug-coupled' clonogenic assay, we further examined the effect of Abemaciclib on 786-O control, *RB1* KO, and VHL-expressing cells, which express significantly lower pRb levels compared to control cells. 24 hours after plating, cells were treated with either vehicle or 0.25 μM Abemaciclib for 3 days. Following treatment wash-off, cells were allowed to recover for an additional 7 days. Abemaciclib significantly reduced clonogenic outgrowth in control cells but had little effect on VHL-expressing and *RB1* KO cells (Figure 22C-D). These findings indicate that Abemaciclib may preferentially target cells with high pRb expression. Therefore, Abemaciclib may represent an effective therapeutic strategy for selectively targeting VHL-null, pRb-expressing ccRCC cells.

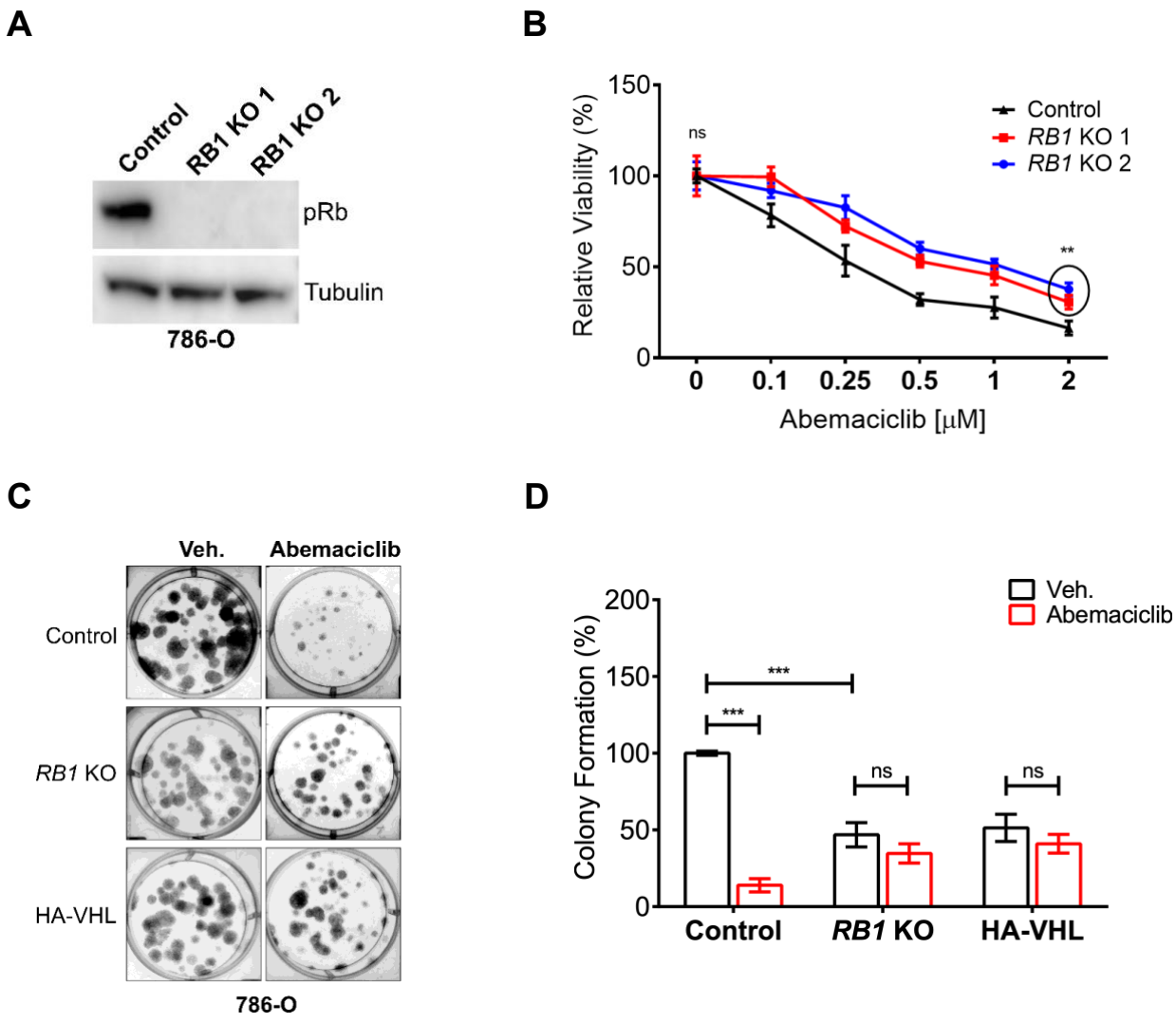

Figure 22. Abemaciclib targeting of ccRCC cells is pRb-dependent. (A) Immunoblot of lysates from 786-O control and *RB1* KO cells. **(B)** Analysis of cell viability in 786-O control and *RB1* knockout (KO) cells treated with increasing concentrations of Abemaciclib, measured via the SRB assay. Statistical significance was calculated using ordinary two-way ANOVA and Tukey's post-hoc test (n=4). **(C)** Representative images showing clonogenic capacity of 786-O control, *RB1* KO and VHL-reconstituted cells treated with vehicle (Veh.) or 0.25 μM Abemaciclib for 3 days. Colonies were allowed to form for 7 days following drug treatment and stained using crystal violet. **(D)** Quantification of the number of colonies in (C). Data are represented as mean ± SD. Statistical significance was calculated using ordinary two-way ANOVA and Tukey's post-hoc test (n=3). *p < 0.05, **p < 0.01, ***p < 0.001. 'ns' denotes not significant.

5.2 β-lapachone in ccRCC

5.2.1 E2F dependency of β-lapachone activity

β-Lapachone (3,4-dihydro-2,2-dimethyl-2H-naphtho[1,2-b]pyran-5,6-dione) is a natural ortho-naphthoquinone compound extracted from the bark of the lapacho tree (*Tabebuia avellanedae*)[388], and that has been shown to possess antitumor activity[389,390]. However, its mechanism of action is complex and not fully understood. Among the various proposed antitumor mechanisms, one study reported that β-lapachone induces E2F1-driven checkpoint-mediated apoptosis[391]. Given the well-established interplay between pRb and E2F1, we sought to investigate this mechanism further in the context of ccRCC. To determine the role of E2F1 in mediating β-lapachone sensitivity, we generated polyclonal *E2F1* KO 786-O cells using a lentiviral system and performed a dose-response assay using increasing concentrations of β-lapachone to compare its activity in 786-O control cells versus *E2F1* KO cells (Figure 23A). Loss of E2F1 resulted in a significant reduction in β-lapachone sensitivity, as indicated by the upward shift of the curve (Figure 23B). However, this effect was only partial, suggesting that β-lapachone also exerts E2F1-independent effects. To further assess the dependence of β-lapachone activity on E2F1 expression, we performed a 'drug-coupled' clonogenic assay using 786-O control and *E2F1* KO cells. 24 hours after plating, cells were treated with either vehicle or 1 μM β-lapachone for 3 days. Following treatment wash-off, cells were allowed to recover for an additional 7 days. *E2F1* knockout cells showed significant impairment in colony formation *in vitro*, likely due to an underlying cell cycle defect (Figure 23C). β-lapachone significantly inhibited clonogenic outgrowth in control cells but had little effect on *E2F1* KO cells (Figure 23C-D). These findings suggest that β-lapachone anti-cancer activity is at least partially

dependent on E2F1 expression. Therefore, β-lapachone may represent an effective therapeutic strategy for selectively targeting E2F1-expressing ccRCC cells.

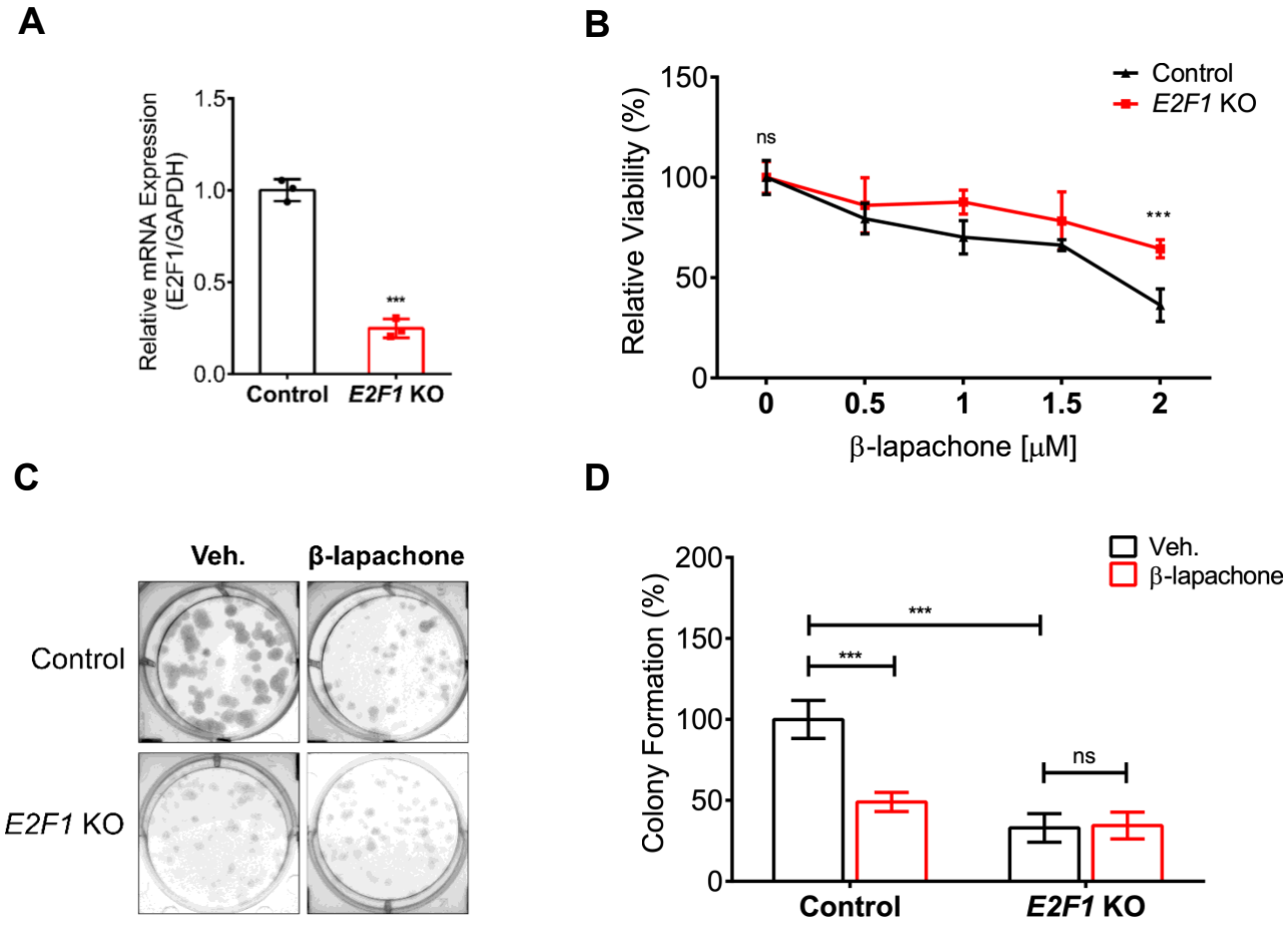

Figure 23. β-lapachone targeting of ccRCC cells is E2F1-dependent. (A) E2F1 mRNA expression (relative to GAPDH) in 786-O Cas9-expressing cells stably infected with virus encoding either control vector or *E2F1*-targeting guides. Fold changes in gene expression were calculated using the delta delta Ct method. Statistical significance was calculated using unpaired two-tailed t test (n=3). **(B)** Analysis of cell viability in 786-O control and *E2F1* knockout (KO) cells treated with increasing concentrations of β-lapachone, measured via the SRB assay. Statistical significance was calculated using ordinary two-way ANOVA and Sidak's post-hoc test (n=4). **(C)** Representative images showing clonogenic capacity of 786-O control and *E2F1* KO cells treated with vehicle (Veh.) or 1 μM β-lapachone for 3 days. Colonies were allowed to form for 7 days following drug treatment and stained using crystal violet. **(D)** Quantification of the number of colonies in (C). Data are represented as mean ± SD. Statistical significance was calculated using ordinary two-way ANOVA and Tukey's post-hoc test (n=3). *$p < 0.05$, **$p < 0.01$, ***$p < 0.001$. 'ns' denotes not significant.

5.2.2 pRb dependency of β-lapachone activity

To our knowledge, no studies have previously linked β-lapachone activity to pRb. Given β-lapachone's sensitivity to E2F1 and the well-established interaction between pRb and E2F1, we sought to determine whether β-lapachone functions in a pRb-dependent manner. To investigate this, we performed a 'drug-coupled' clonogenic assay to assess the effect of β-lapachone on 786-O control, *RB1* KO, and VHL-expressing cells, the latter of which exhibit markedly lower pRb levels compared to control cells. 24 hours after plating, cells were treated with either vehicle or 1 μM β-lapachone for 3 days. Following treatment wash-off, cells were allowed to recover for an additional 7 days. β-lapachone significantly inhibited clonogenic outgrowth in control cells but had no substantial effect on VHL-expressing or *RB1* KO cells (Figure 24B-C). Overall, our findings suggest that β-lapachone activity may be dependent on pRb expression. Therefore, β-lapachone may represent an effective therapeutic strategy for selectively targeting pRb-expressing ccRCC cells.

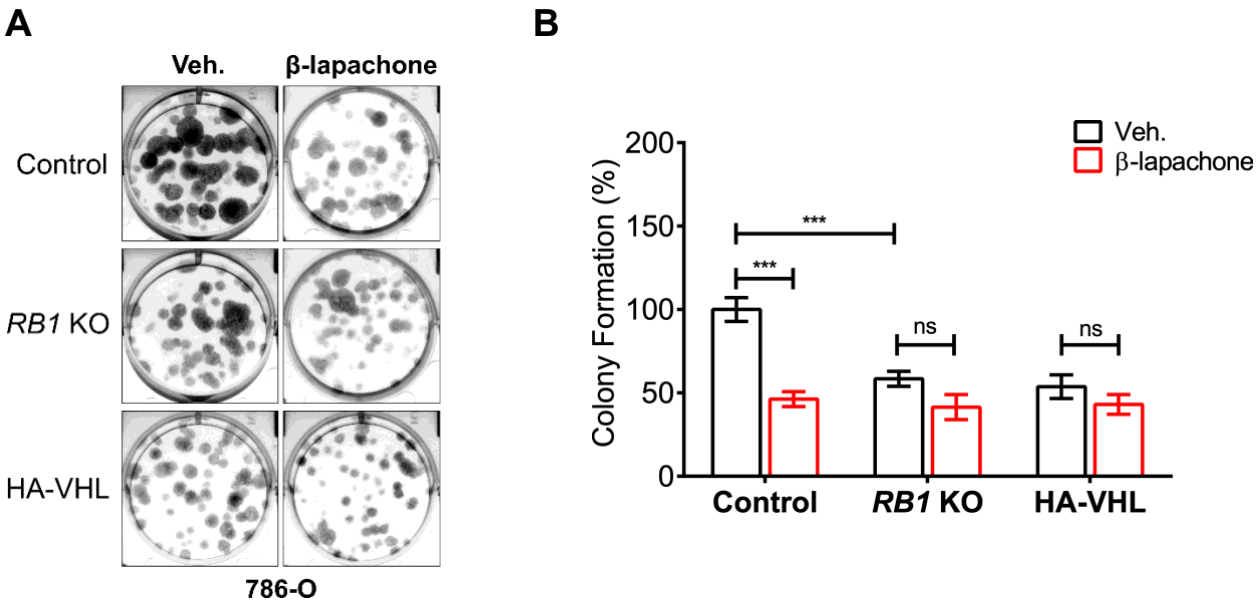

Figure 24. β-lapachone targeting of ccRCC cells is pRb-dependent.

Figure 24. β-lapachone targeting of ccRCC cells is pRb-dependent. (A) Representative images showing clonogenic capacity of 786-O control, *RB1* KO and VHL-reconstituted cells treated with vehicle (Veh.) or 1 μM β-lapachone for 3 days. Colonies were allowed to form for 7 days following drug treatment and stained using crystal violet. **(B)** Quantification of the number of colonies in (A). Data are represented as mean ± SD. Statistical significance was calculated using ordinary two-way ANOVA and Tukey's post-hoc test (n=3). *p < 0.05, **p < 0.01, ***p < 0.001. 'ns' denotes not significant.

5.3 Abemaciclib and β-lapachone in ccRCC

5.3.1 Drug combination in ccRCC cell lines (*in vitro* work)

Given the observed individual effects of Abemaciclib and β-lapachone, we next aimed to investigate their combined effects on ccRCC cell viability. To do this, we performed drug combination dose-response assays on several VHL-deficient ccRCC cell lines (786-O, 769-P, A498, and RCC4) using increasing concentrations of Abemaciclib, β-lapachone, or various combination doses of both drugs. Briefly, 24 hours after plating, cells were treated with either a single drug or a combination as indicated, and viability was assessed using the SRB assay after 3 days. To assess potential drug synergy, we analyzed the dose-response data using SynergyFinder+[392], identifying regions of synergy through the zero interaction potency (ZIP)[393] and Bliss independence (BLISS)[394] synergy models. Strong synergy between Abemaciclib and β-lapachone was observed in 786-O, 769-P, and A498 cells (Figure 25A-F). However, no significant synergy was detected in RCC4 cells (Figure 25G-H). Additionally, we examined the interaction between Abemaciclib and β-lapachone in primary Renal Proximal Tubule Epithelial Cells (RPTEC), which are normal kidney cells expressing VHL. Interestingly, SynergyFinder+ analysis revealed an antagonistic interaction (low synergy scores) in these cells (Figure 25I-J), suggesting that the synergistic effects of Abemaciclib and β-lapachone may be specific to VHL-

deficient cells. Further analysis using a clonogenic assay confirmed that combined treatment with Abemaciclib and β-lapachone resulted in greater toxicity in VHL-deficient ccRCC cells (786-O, 769-P, and A498) than either drug alone (Figure 26A-B). However, in pRb-depleted 786-O cells, the combined treatment showed no enhanced toxicity compared to single drug treatment (Figure 26C-D). These findings further support our previous observations that both Abemaciclib and β-lapachone exert their effects in a pRb-dependent manner.

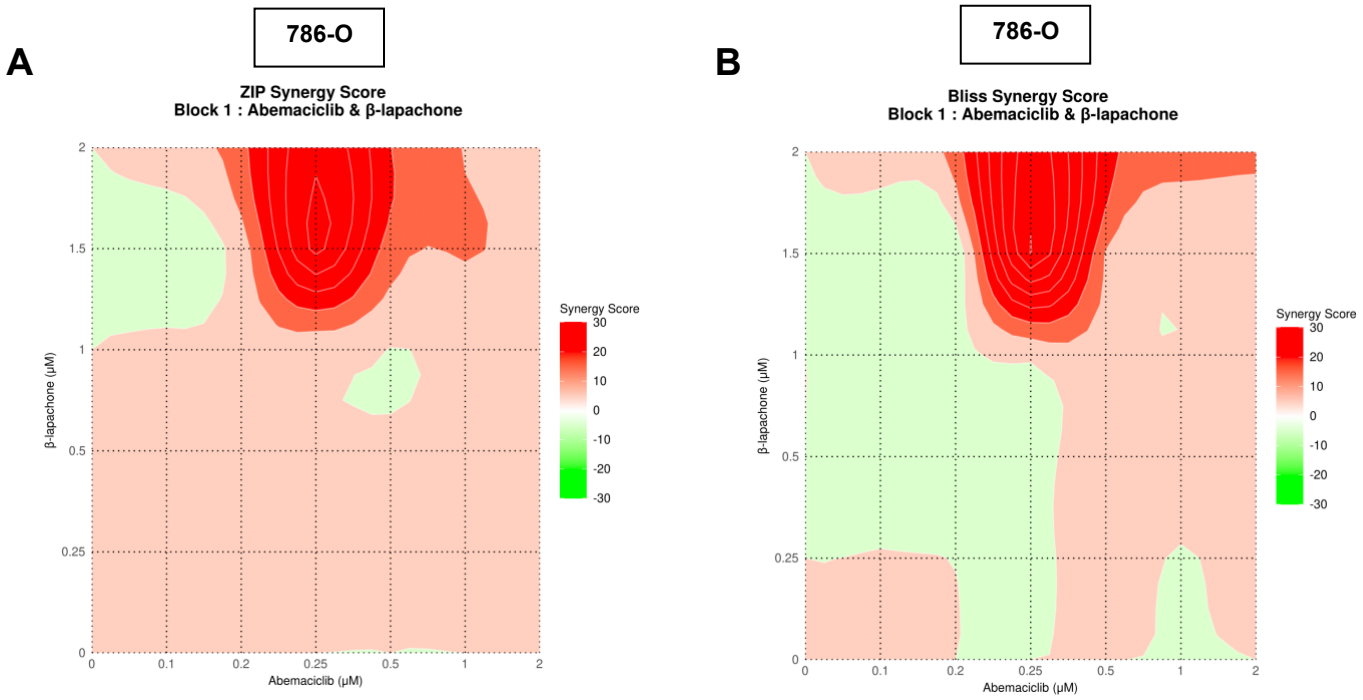

Figure 25. Synergy mapping of Abemaciclib and β-lapachone.

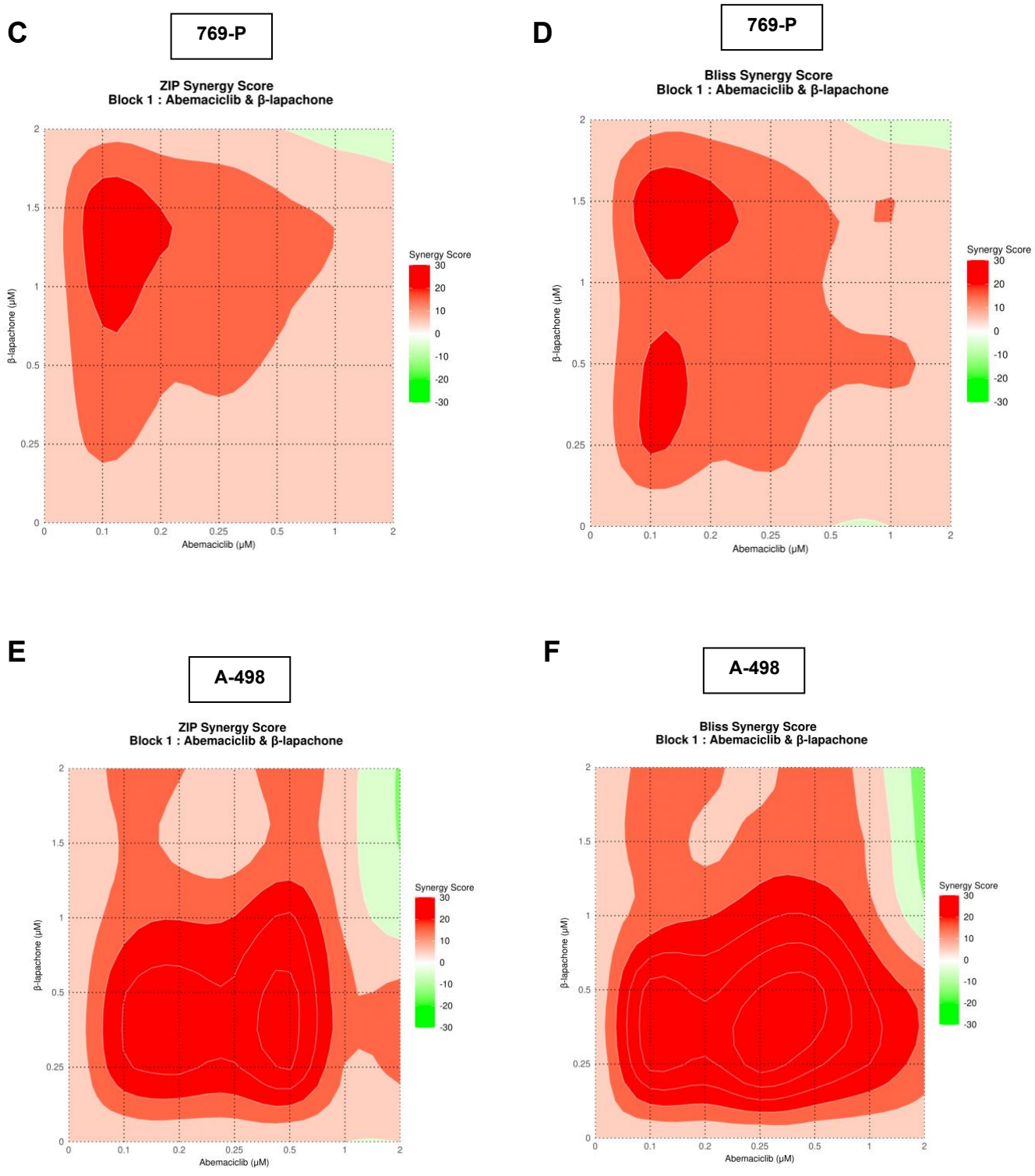

Figure 25 (continued). Synergy mapping of Abemaciclib and β-lapachone.

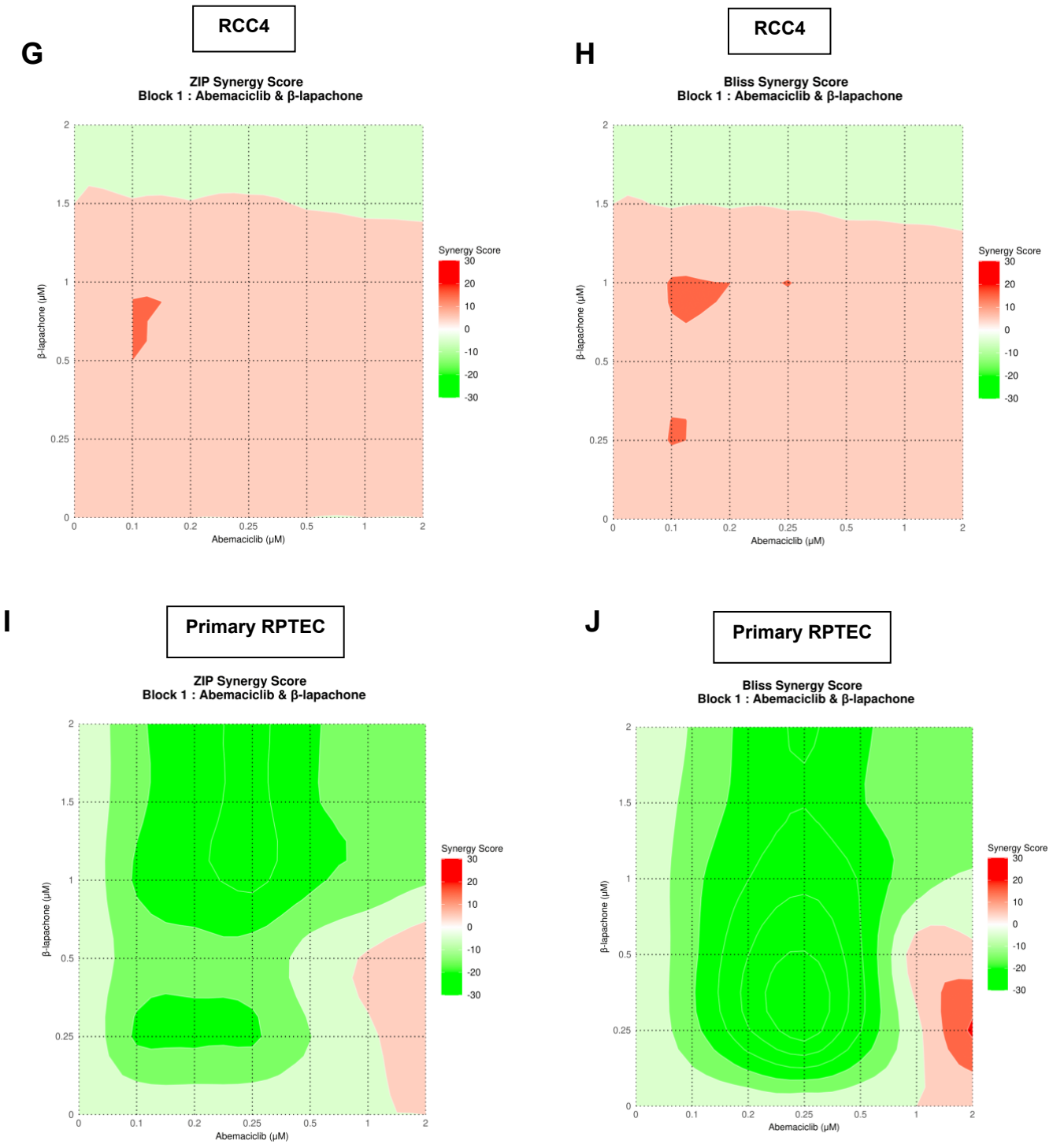

Figure 25. Synergy mapping of Abemaciclib and β-lapachone. (A-J) Synergy scoring and mapping between Abemaciclib and β-lapachone at increasing drug concentrations using the ZIP (left) and Bliss (right) synergy scoring methods as indicated. Results are from 3 replicates (n=3). Cells were treated for 3 days and cell viability was determined using the SRB assay. Strong areas of synergy are indicated in red, while strong areas of antagonism are indicated in green.

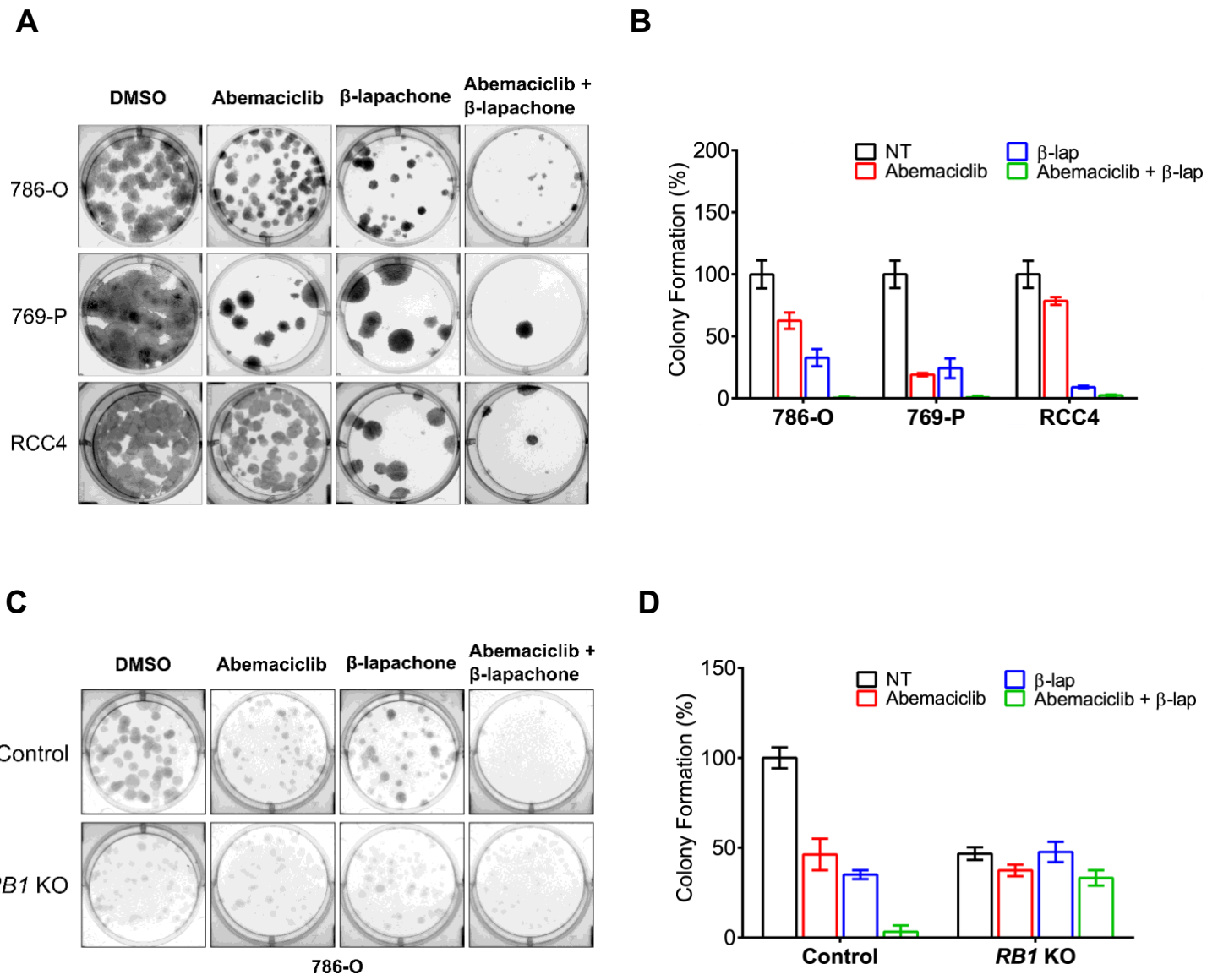

Figure 26. In vitro analysis of Abemaciclib and β-lapachone activity on ccRCC cells. (A) Representative images showing clonogenic capacity of ccRCC cell lines - 786-O, 769-P and RCC-4 treated with vehicle (DMSO), 0.25 μM Abemaciclib, 1 μM β-lapachone, or 0.25 μM Abemaciclib and 1 μM β-lapachone for 3 days. Colonies were allowed to form for 7 days following drug treatment and stained using crystal violet. **(B)** Quantification of the number of colonies in (A). Data are represented as mean ± SD (n=3). **(C)** Representative images showing clonogenic capacity of 786-O control and *RB1* KO cells treated with vehicle (DMSO), 0.25 μM Abemaciclib, 1 μM β-lapachone, or 0.25 μM Abemaciclib and 1 μM β-lapachone for 3 days. Colonies were allowed to form for 7 days following drug treatment and stained using crystal violet. **(D)** Quantification of the number of colonies in (C). Data are represented as mean ± SD (n=3).

5.3.2 Drug combination in patient-derived organoids

Given the promising synergy observed between Abemaciclib and β-lapachone in ccRCC cells (Figure 25A-F), we aimed to evaluate their effects on ccRCC patient-derived tissue organoids—a three-dimensional model with greater complexity than traditional two-dimensional cell culture. Using SynergyFinder+, we generated dose-response matrices based on the individual and combined effects of Abemaciclib and β-lapachone on the ccRCC tissue organoid KP90T and its matched normal kidney tissue organoid KP90N (Figure 27A-B) (experiment performed by Zohreh Mehrjoo) . Surprisingly, in contrast to our *in vitro* assays, drug combination dose-response analysis on normal organoids revealed strong synergy, as determined by the ZIP and BLISS synergy models (Figure 27C-D). Conversely, analysis on ccRCC organoids indicated mild antagonism (ZIP) or a mix of mildly synergistic and mildly antagonistic regions (BLISS) (Figure 27E-F). Overall, Abemaciclib and β-lapachone exhibited stronger synergy in normal organoids compared to their patient-matched ccRCC-derived counterparts. These results were unexpected based on our *in vitro* drug screening assays. However, it is important to note that this organoid experiment was performed only once (n=1) and on a single set of patient-derived organoids due to limitations in the expansion of available organoid samples. Therefore, while these findings are intriguing, they remain inconclusive and require validation through multiple replicates across diverse patient-derived organoid models.

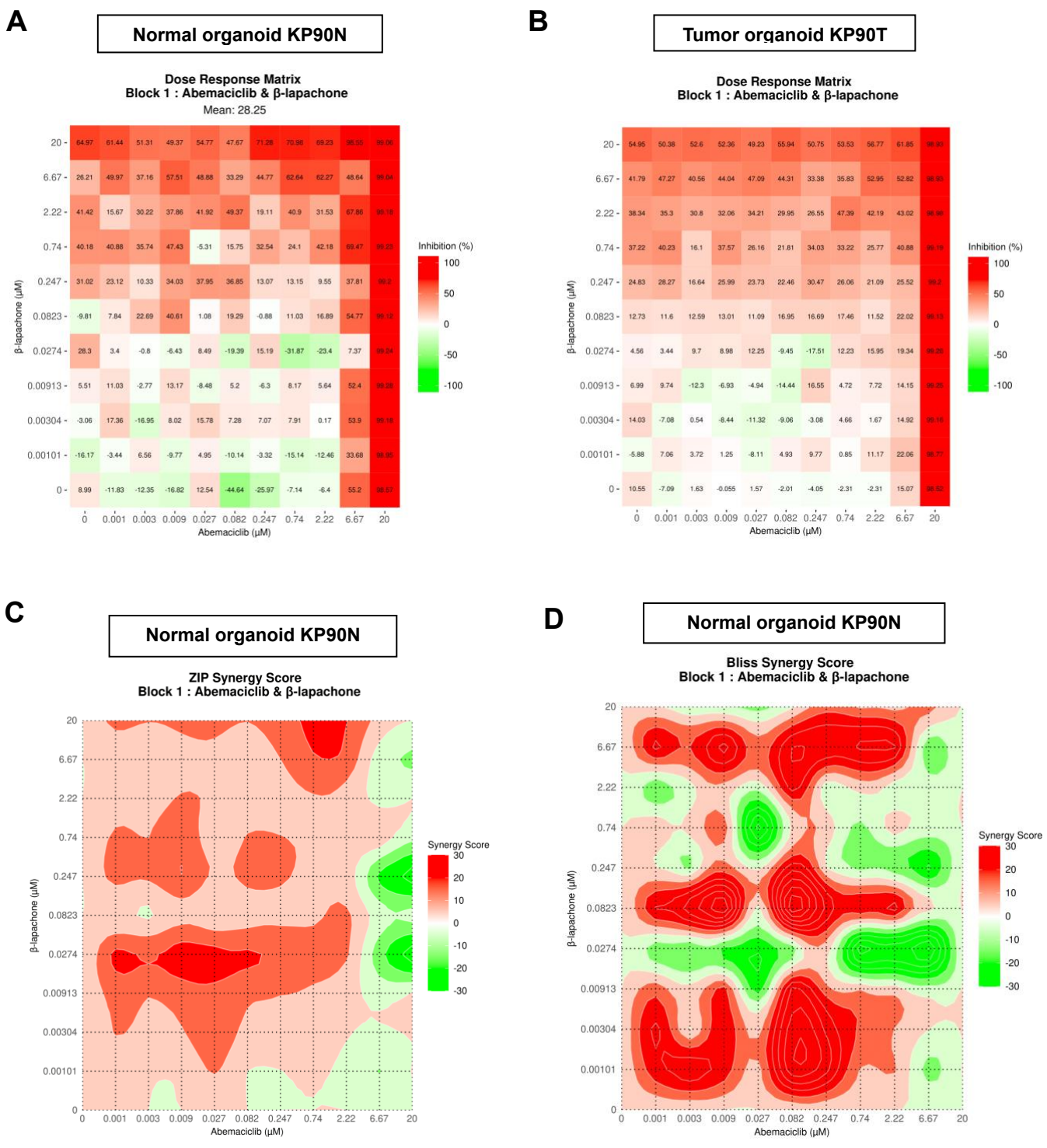

Figure 27. Abemaciclib and β-lapachone activity on patient-derived organoids.

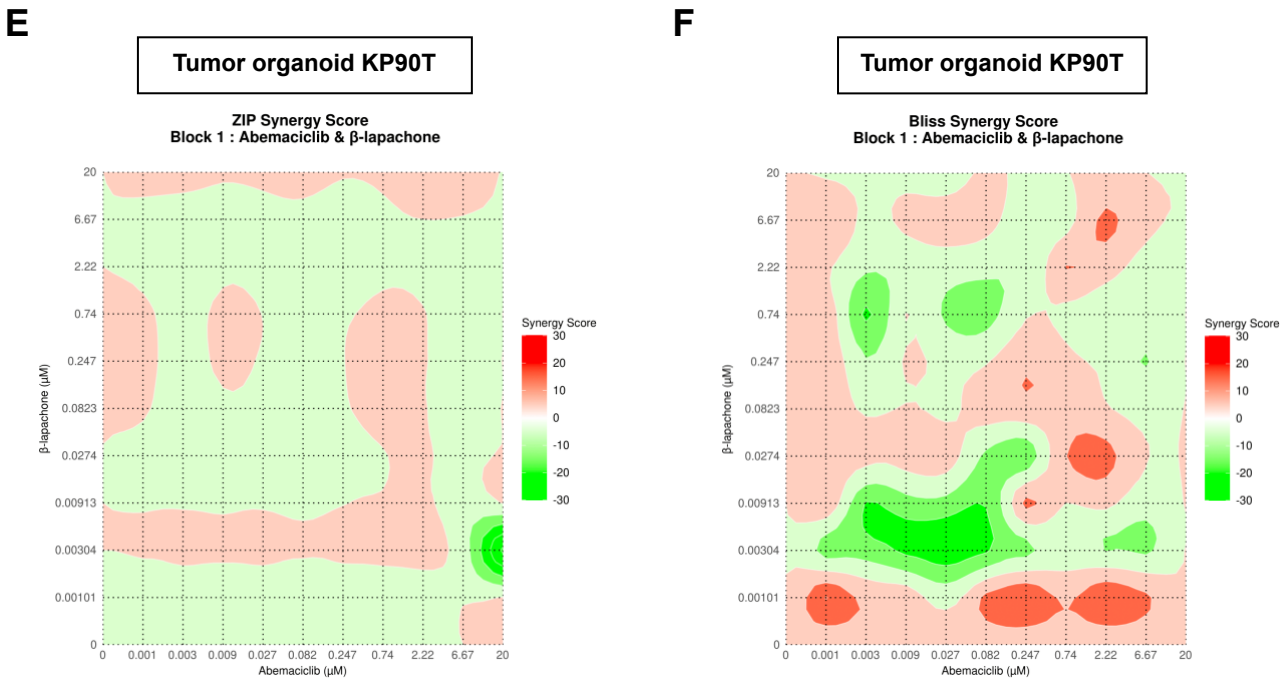

Figure 27. Abemaciclib and β-lapachone activity on patient-derived organoids. (A-B) Dose response matrix mapping of percentage inhibition of ccRCC patient-derived normal organoid (A) or tumor organoids (B) by Abemaciclib and β-lapachone. Results are from one replicate (n=1). Strong inhibitory activity is indicated in red. **(C-F)** Synergy scoring and mapping between Abemaciclib and β-lapachone at increasing drug concentrations using the ZIP and Bliss Synergy scoring methods as indicated on normal patient-derived organoids (C-D) and ccRCC patient-derived organoids (E-F). Results are from one replicate (n=1). Strong areas of synergy are indicated in red, while strong areas of antagonism are indicated in green.

Chapter 6: Discussion

6.1 Summary of findings

The findings presented in this thesis uncover a novel non-HIF VHL-regulated pathway involving the retinoblastoma protein pRb, offering new insights into ccRCC pathogenesis and potential therapeutic interventions. My research establishes that pRb is a substrate of a VHL-containing E3 ubiquitin ligase complex, which targets pRb for proteasomal degradation under normoxic conditions. Loss of VHL function results in pRb hyperstabilization, leading to the pathological repression of cell death and transcriptional reprogramming that promotes tumorigenesis. From a therapeutic perspective, my work demonstrates that targeting the VHL-pRb axis in ccRCC using CDK4/6 inhibitors such as Abemaciclib, in combination with the E2F1 activator β-lapachone, may be an effective strategy for selectively targeting VHL-deficient, pRb-expressing ccRCC cells. While these findings provide a strong rationale for continued study, further *in vivo* validation is required to determine the clinical applicability of these therapeutic strategies. Overall, my thesis explores the dysregulation of the VHL-pRb axis in ccRCC, providing novel insights into tumorigenic pathways and potential therapeutic strategies. Below, I provide a more in-depth discussion of my findings, including the implications, limitations, and future directions.

6.2 pRb plays a context-dependent role in ccRCC

Although pRb is traditionally recognized as a tumor suppressor, our study provides evidence for a context-dependent oncogenic function when dysregulated by VHL loss. Unlike other cancers where *RB1* is frequently mutated, ccRCC rarely harbors inactivating *RB1* mutations. Hence, in ccRCC cells, pRb should be able to suppress cell cycle. However, the cell cycle inhibitory function of pRb is mediated by its hypophosphorylated form and in ccRCC, pRb is inactivated

by hyperphosphorylation[247,266,395]. The hyperphosphorylation of pRb in ccRCC is likely due to the reported cyclin D1 overexpression, promoting CDK4/6 activity, as well as the inactivation of CDK inhibitors, which further promotes CDK activity[346,396]. Hyperphosphorylated pRb may thus promote tumorigenesis indirectly through its loss of cell cycle control, leading to uncontrolled cell division.

Several groups have described cell-cycle-independent functions of pRb that may contribute to tumorigenesis. For example, studies on homozygous *Rb1* deletion in mouse embryos showed significant cell death in several tissues including the eye lens, nervous system, and skeletal muscle[309,372,397]. pRb also inhibited HIF induction of autophagic cell death[316,317]. These findings demonstrate that pRb plays a crucial role in the repression of cell death, which could ultimately encourage tumorigenesis. In our study, we show that hyperstabilized pRb represses apoptosis in ccRCC cells (Figure 12H). Interestingly, *RB1* deletion promoted cell death in VHL-deficient (Figure 12D) but not VHL-expressing cells (Figure 12O), suggesting a context-dependent role for pRb in ccRCC whereby pRb functions as an 'oncogene' in the absence of VHL, and as a tumor suppressor in the presence of VHL. As such, pharmacological targeting of pRb in ccRCC may be particularly relevant for tumors that lack functional VHL expression. This is conceptually consistent with a recent study showing that dual inhibition of CDK4/6 (which promote pRb phosphorylation) is synthetically lethal with VHL loss, and acts in a pRb-dependent manner[386]. This synthetic lethality was observed in a conserved manner in mammals and is therefore relevant in our disease model. Additionally, dual knockout of *Vhl* and *Rb1* in the mouse retina resulted in synthetic lethality in rods and cone cells, further underscoring the epistatic links between *Vhl* and *Rb1*[317]. The synthetic lethality described between *Vhl* and *Rb1* may therefore explain our findings wherein *RB1* deletion promotes death in VHL-null but not VHL-expressing

ccRCC cells. Overall, our findings align with the context-dependent roles of pRb observed in other studies, whereby pRb can function as either a tumor suppressor or oncogenic factor depending on post-translational modifications (PTMs) and cellular context[306,309,310,314,343–345,354–356].

6.3 SKIDA1 as a potential tumor suppressor in ccRCC

My study highlights the role of pRb in transcriptional regulation beyond its classical function in cell cycle control. Transcriptomic analysis identified SKIDA1 as an important downstream target of pRb that is repressed in ccRCC (Figure 11G). Overexpression of SKIDA1 significantly decreased colony formation (Figure 13M) and anchorage-independent growth (Figure 13O) of ccRCC cells. Furthermore, SKIDA1 overexpression promoted ccRCC cell death (Figure 12R), highlighting its potential tumor suppressor activity. Accordingly, SKIDA1 expression is significantly repressed in ccRCC tumors.

The function of SKIDA1 remains relatively understudied, with only two findings reported so far. First, SKIDA1 was found to be differentially expressed in the regulatory T cells of Autoimmune polyendocrine syndrome type I (APS-1) patients compared to healthy patients[398]. Second, SKIDA1 is highly expressed in pediatric acute myeloid leukemia (AML), and this expression is predominantly observed in leukemias harboring mixed lineage leukemia 1 (MLL1) rearrangements[399]. These findings, however, are mainly associative, and the role of SKIDA1 in tumor development is not well-defined. The understudied nature of SKIDA1 and its prognostic value in ccRCC patient survival (Figure 11L), therefore made it a particularly interesting target to follow up on. In chapter 3, we describe a role for SKIDA1 in inhibiting ccRCC tumorigenesis

by promoting cell death. Mechanistically, SKIDA1 repression in ccRCC may be mediated by the pRb-E2F1 repressive complex, as depletion of either pRb or E2F1 rescues SKIDA1 expression in ccRCC cells (Figure 11I-J). This supports others' findings that pRb can regulate E2F1-driven transcription of cell death genes[251,400,401]. While our experiments point towards transcriptional regulation of SKIDA1 by the pRb-E2F1 complex, chromatin profiling methods such as ChIP (chromatin immunoprecipitation) or CUT&RUN may be employed to validate the direct regulation of SKIDA1 by these transcription factors.

6.4 Non-E2F1-regulated pRb targets may be involved in ccRCC tumorigenesis

In chapter 3, we validated *SKIDA1* as a potential pRb- and E2F1-regulated gene. However, RNA-sequencing of 786-O control and *RB1* KO cells identified additional pRb targets that may not be directly regulated by E2F1 but could still play a significant role in ccRCC oncogenesis. One such target is Rho-related BTB domain-containing protein 3 (RHOBTB3), which was not only identified as a pRb-regulated gene but also found to be repressed in ccRCC tumors. RHOBTB3 interacts directly with PHD2 (Prolyl hydroxylase domain protein 2) to promote HIF-α hydroxylation, triggering its degradation[402]. Additionally, RHOBTB3 interacts with VHL, facilitating HIF-α ubiquitination and subsequent proteasomal degradation[402]. By promoting HIF-α degradation, RHOBTB3 may inhibit ccRCC tumorigenesis. Supporting this hypothesis, RHOBTB3 depletion in MEFs led to accelerated xenograft tumor growth[402]. Further investigation of RHOBTB3 and other pRb-regulated genes is needed to appreciate the effects of pRb dysregulation in ccRCC, and may reveal additional therapeutically relevant targets, providing new avenues for potential ccRCC treatment strategies.

6.5 Functional interaction between pRb and HIF in ccRCC

Like HIF, pRb was also shown to be upregulated in VHL-deficient ccRCC cell lines (Figure 10A). RNA-sequencing reveals that pRb and HIF regulate largely distinct transcriptional targets (Figure 11B). However, gene ontology (GO) analysis of pRb and HIF targets indicates convergence on pathways such as apoptosis, cellular senescence, and focal adhesion (Figure 11C), which are notoriously linked to cancer development via regulation of cell death, cell proliferation, and cell-ECM interactions respectively[403–405]. pRb inhibits the induction of angiogenesis triggered by *Vhl* loss (and HIF-α stabilization) in the murine retina[317]. Additionally, pRb attenuates HIF-1α mediated induction of BNIP3 to inhibit hypoxia-induced autophagic cell death[316]. In contrast, overexpression of pRb was shown to drive the transcriptional activity of HIF-1α under normoxia[358]. These studies provide evidence of a functional interaction between pRb and HIF-1α (and potentially HIF-2α). However, whether pRb interacts functionally with HIF-2α remains to be ascertained. We found that VHL's interaction with pRb, like its interaction with HIF-α, is regulated by oxygen tension (Figure 15A), suggesting that both HIF and pRb are involved in the cellular hypoxia response. Notably, hypoxia-mediated loss of VHL regulation occurred more slowly for pRb (~24 hours) than for HIF (< 8 hours)[125], indicating that pRb regulation may be part of a prolonged adaptive mechanism. This pattern mirrors the differential stabilization of HIF-1α and HIF-2α, where HIF-1α is rapidly stabilized under acute hypoxia, while HIF-2α levels gradually increase, dominating under chronic hypoxia[125]. Given pRb's role in modulating HIF activity, its delayed regulation may serve to fine-tune HIF signaling across different oxygen conditions. Our findings highlight a complex interplay between pRb and HIF in hypoxia adaptation and tumorigenesis, warranting further investigation into their coordinated roles in normal physiology and ccRCC progression.

6.6 Proposed model - Hyperphosphorylated pRb drives ccRCC tumorigenesis via dual mechanisms

VHL binding to nuclear pRb under normal oxygen tension suggests that VHL regulates a specific, possibly oncogenic subset of pRb. In ccRCC, pRb is inactivated through hyperphosphorylation[247,266,395], which prevents it from exerting its role in cell cycle repression. However, hyperphosphorylation does not render pRb entirely inactive, as studies have shown that pRb phosphorylation can promote resistance to apoptosis[314,315,317]. In 2003, Dick et al. proposed a unique interaction between E2F1 and the C-terminal domain of pRb, which regulates E2F1-induced apoptosis[251,252,406,407]. Notably, this interaction was resistant to disruption by CDK phosphorylation[406,408]. Therefore, it is plausible that in ccRCC, hyperphosphorylated pRb bound to E2F1 may inhibit E2F1-induced apoptosis. According to our model, hyperphosphorylation of pRb may promote ccRCC via two mechanisms: indirectly by permitting uncontrolled cell division, and directly by repressing E2F1-driven apoptosis in response to various stimuli (Figure 28). Based on this model, we initially hypothesized that VHL would specifically target hyperphosphorylated pRb for proteasomal degradation, in line with the concept of a tumor suppressor degrading an 'oncogenic factor'. However, as discussed in chapter 4, our findings indicate that VHL does not target pRb in a phosphorylation-dependent manner (Figure 16). Other modifications to pRb may thus serve as signals for specific recognition and degradation by VHL.

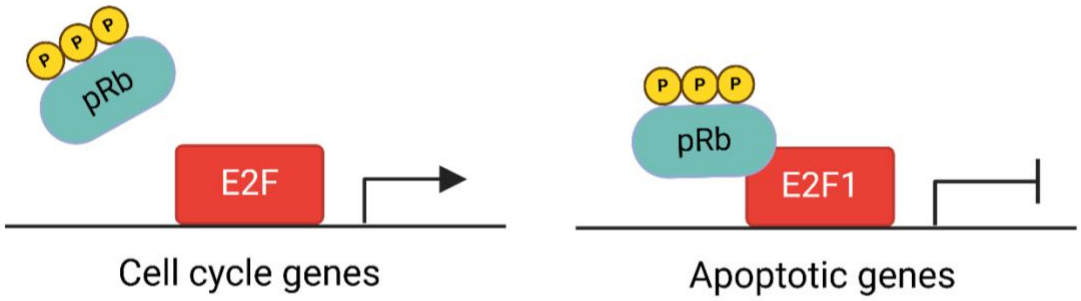

Figure 28. Effect of pRb hyperphosphorylation on cell cycle and apoptotic regulation. In many cancers including ccRCC, pRb is inactivated by phosphorylation (P). Hyperphosphorylation of pRb inhibits binding to E2Fs allowing the transcription of cell cycle genes. However, hyperphosphorylated pRb retains binding to E2F1 specifically, and this interaction results in the repression of apoptotic genes. Hyperphosphorylation of pRb therefore promotes ccRCC by allowing uncontrolled cell proliferation and by actively repressing apoptosis. Created using BioRender.

6.7 Analysis of the VHL-pRb interaction network reveals cBAF complex components and novel E3 ligase candidates

pRb is well-established as a transcriptional repressor[409]. Mechanisms of transcriptional repression by pRb include the recruitment of chromatin remodelling complexes such as HDACs[246,262,263], histone methyltransferases (HMTs)[264,410], DNMTs[411], and the SWI/SNF chromatin remodeling complex[412–414]. Notably, our split-TurboID assay designed to identify VHL-pRb binding partners, revealed several core components of the cBAF complex, a subtype of the mammalian SWI/SNF chromatin remodeling complex, which regulates chromatin accessibility by repositioning, mobilizing, and evicting nucleosomes[415,416]. Many cBAF subunits function as tumor suppressors, and their loss of function can drive oncogenic phenotypes across a wide range of cancers[417,418]. For instance, loss of ARID1A results in DNA damage

accumulation and genomic instability, activation of the interferon type I response, and chronic inflammation, ultimately promoting tumor formation in mice[419]. Our findings suggest that the VHL-pRb complex may regulate cBAF activity and its downstream targets, thereby influencing transcriptional programs. In ccRCC, inactivation of VHL may therefore result in dysregulation of the assembly and/or activity of the cBAF complex, promoting gene expression patterns that are critical for ccRCC progression. Thus, the interaction between VHL and pRb may play a broader role in tumor suppression through its association with cBAF components.

To define the gene regulatory landscape of the VHL-pRb-cBAF complex, we will employ CUT&RUN (Cleavage Under Targets and Release Using Nuclease)[384]. This technique utilizes micrococcal nuclease (MNase) to selectively cleave and release DNA fragments bound by the complex (Figure 29). The precise mapping of these target regions will enable further elucidation of the transcriptional activity of VHL-pRb-cBAF and the potential impact on ccRCC tumor suppression. Alternatively, the VHL-pRb-cBAF complex may inhibit ccRCC tumorigenesis by promoting DNA repair, preventing the accumulation of oncogenic mutations, which leads to genomic instability[420,421]. Accordingly, pRb has been described to recruit SMARCA4 (also known as BRG1), a core cBAF component, to facilitate DSB repair[291]. Furthermore, pRb-SMARCA4 interaction has been implicated in cell cycle arrest[412,422], reinforcing tumor suppression through proliferation control. Thus, multiple mechanisms may underlie potential regulation of tumor suppression by VHL-pRb-cBAF, including transcriptional regulation, DNA repair, and cell cycle control. Further studies are needed to elucidate these pathways and their implications in ccRCC pathogenesis.

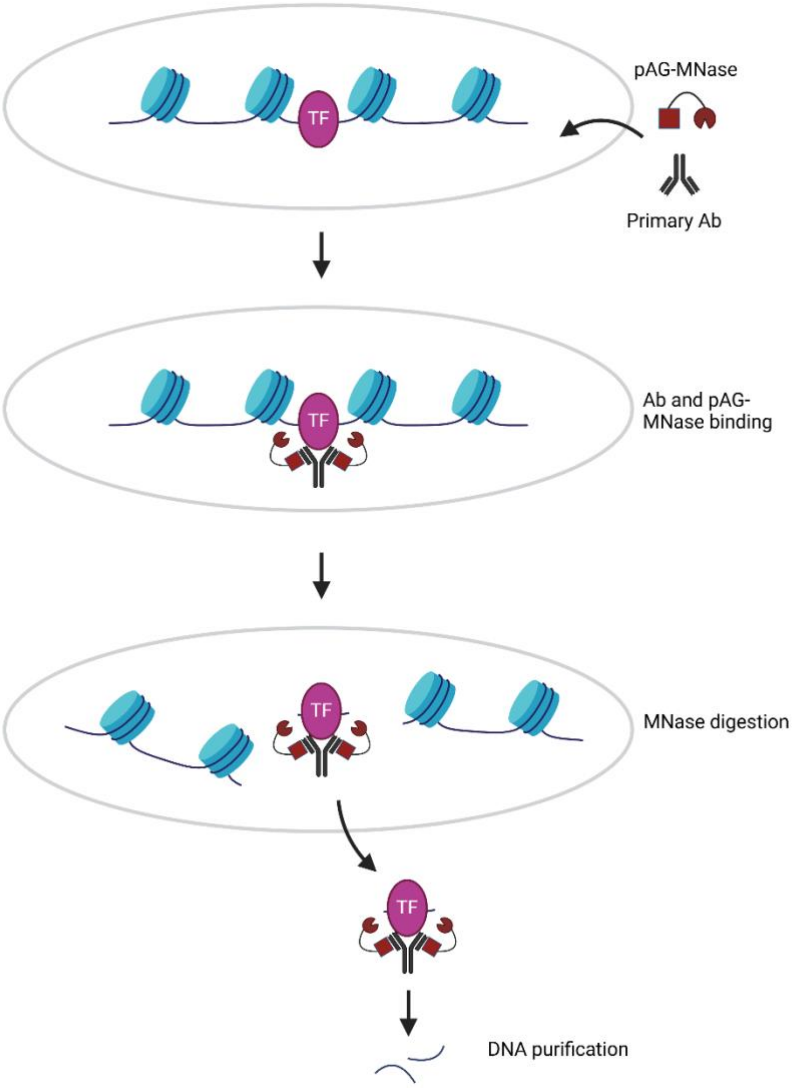

Figure 29. Schematic illustration of the CUT&RUN technique. CUT&RUN uses a target-specific primary antibody (Ab) and a Protein A-Protein G-Micrococcal Nuclease (pAG-MNase) to isolate specific protein-DNA complexes. Cell membranes are permeabilized to facilitate entry of the primary antibody into the nuclei, where it binds to the transcription factor (TF) of interest. The pAG domain of the pAG-MNase fusion protein then binds to the primary antibody heavy chain, targeting the enzyme to the chromatin region of interest to promoting cleavage. DNA bound to the TF can then be purified and used to construct a DNA sequencing library for next-generation sequencing (NGS) and whole-genome mapping. Created using BioRender.

In chapter 4, we showed that the ECV complex that targets HIFα for proteasomal degradation[94,95] was void from the VHL-pRb complex (Figure 20B), indicating that VHL targets pRb via a novel E3 mechanism. Our split-TurboID assay uncovered some potential E3 ligase proteins — DCAF13 (DDB1- and CUL4-associated factor 13) and UBR5 (Ubiquitin Protein Ligase E3 Component N-Recognin 5). These hits will be validated by immunoprecipitation to determine physical association with the VHL-pRb complex. Furthermore, functional association will be ascertained by depleting these hits in VHL-expressing cells to determine whether pRb is stabilized as a result. Our E3 ligase candidates were identified following the overexpression of VHL and pRb in mammalian cells. However, this approach has several limitations. First, overexpression of VHL can lead to an excess of free VHL that is not properly incorporated into the E3 ligase complex, resulting in VHL-pRb complexes that are not bound to an E3 ligase. Additionally, overexpression of both proteins may promote aberrant, non-physiological protein-protein interactions, increasing the likelihood of false positives. A more effective strategy would involve isolating proteins bound to endogenous VHL-pRb complexes to ensure the identification of physiologically relevant E3 ligase-associated proteins.

6.8 Exploring the VHL-pRb pathway for novel therapeutic opportunities

The identification of the VHL-pRb axis as a novel pathway in ccRCC provides an opportunity for therapeutic intervention. Although not clinically approved for the treatment of ccRCC, CDK4/6 inhibitors have shown promise when combined with other therapeutics in preclinical mouse models and clinical trials[216,217,386]. For instance, the CDK4/6 inhibitor Palbociclib and the HIF-2α inhibitor PT2399 have demonstrated synergy in suppressing the viability of HIF-2α–dependent ccRCC cell lines[386]. By inhibiting the phosphorylation of pRb, CDK inhibitors can

reverse the hyperphosphorylated pRb phenotype in ccRCC, thereby promoting cell cycle arrest. However, while this approach is conceptually sound, CDK inhibitors alone may not suffice due to the potential for acquired resistance. To address this, coupling CDK inhibitors with agents that induce apoptosis could enhance therapeutic outcomes. One such approach involves combination with E2F1 activators such as β-lapachone, which can promote checkpoint-mediated apoptosis in tumorigenic cells[423,424]. Our strategy was to couple Abemaciclib, a CDK4/6 inhibitor, with an inducer of cell death like β-lapachone to bypass potential resistance development to CDK inhibitors. According to our model, treatment with Abemaciclib inhibits pRb phosphorylation, resulting in the accumulation of hypophosphorylated pRb and consequent E2F-mediated cell cycle arrest. Conversely, β-lapachone promotes E2F1-specific activation, potentially bypassing pRb repression of E2F1-mediated apoptosis (Figure 30). The synergistic effects observed between the CDK4/6 inhibitor Abemaciclib and the E2F1 activator β-lapachone suggest that targeting pRb's regulatory network could overcome the apoptotic resistance conferred by pRb hyperstabilization. These findings are particularly relevant given the limited efficacy of current treatments for metastatic RCC, which often fail due to the development of resistance. While our *in vitro* findings suggest potential synergistic activity between Abemaciclib and β-lapachone in ccRCC cells, validating their specific activity against tumor organoids will provide a foundation for future studies using GEM models of ccRCC, such as mice with *Vhl/Pbrm1* or *Vhl/Bap1* codeletions[425,426], for drug testing.

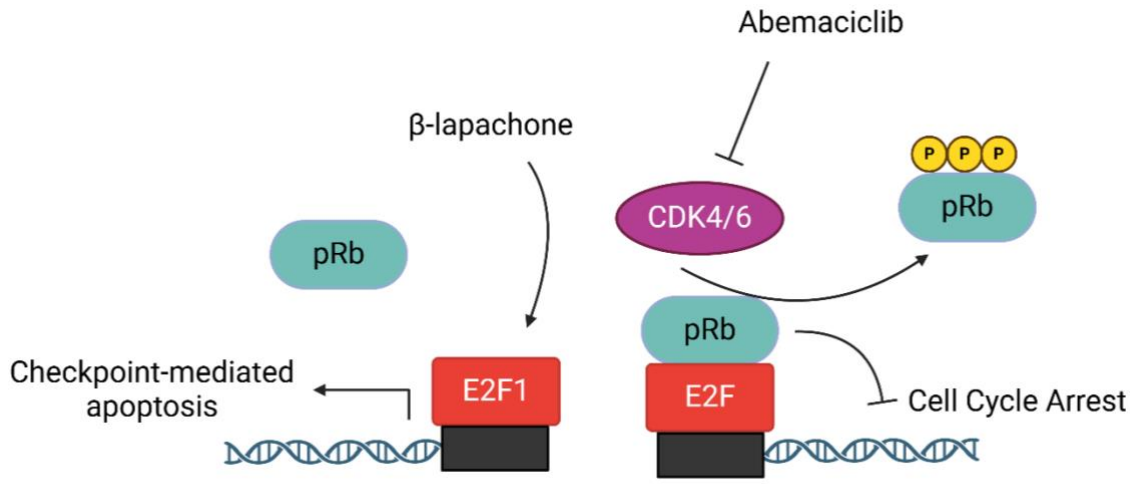

Figure 30. Proposed mechanism for the synergistic activity between Abemaciclib and β-lapachone in ccRCC. Abemaciclib inhibits CDK4/6, leading to hypophosphorylated pRb which is active in repressing cell cycle. On the other hand, β-lapachone activates E2F1, driving checkpoint-mediated apoptosis. Created using BioRender.

While Abemaciclib is already FDA-approved for other cancers[427–429], its combination with β-lapachone warrants further investigation. The dependency of β-lapachone's activity on E2F1 and pRb suggests a context-specific therapeutic window, which could minimize off-target effects. Moreover, the distinct mechanisms of action of these compounds may help mitigate the development of resistance, a common challenge in ccRCC treatment. Besides the activation of E2F1-driven checkpoint mediated apoptosis, β-lapachone may also exert its antitumor effects through other mechanisms. These include inhibition of DNA topoisomerase, which disrupts DNA replication and transcription[430], induction of a futile NQO1-mediated redox cycle, leading to excessive reactive oxygen species (ROS) production and DNA damage[431–435], and stimulation of apoptosis via both intrinsic (mitochondria-mediated) and extrinsic (death receptor-mediated)

pathways[436]. However, these mechanisms were not explored in our system. Given the dependency on pRb and E2F1 expression (Figures 23-24), it is unclear how β-lapachone interacts with both proteins to induce cell death in ccRCC. The clinical application of β-lapachone is limited by its poor aqueous solubility and low oral bioavailability, prompting the development of innovative formulation strategies to overcome these challenges and enable its broader therapeutic use[437–439]. Based on our findings, SKIDA1 activators—although not yet identified—represent another promising avenue for inducing tumor cell death. For increased efficacy and to minimize resistance, combining drugs with distinct mechanisms of action is essential. CDK4/6 inhibitors, E2F1 activators, and potential SKIDA1 activators could therefore be integrated with established frontline therapies such as immune checkpoint inhibitors, tyrosine kinase inhibitors, and mTOR inhibitors, which target different oncogenic pathways.

6.9 Implications of disrupted VHL–pRb interaction in ccRCC

In chapter 4, we identified a specific interaction between VHL and pRb, mediated by a previously uncharacterized binding site on pRb spanning amino acids 778–807, located at the junction of the small pocket and C-terminal domains (Figure 18E–F). Notably, expression of a HIF-2α variant that escapes VHL regulation was sufficient to promote tumorigenesis in VHL-expressing ccRCC cells[127]. This raises the intriguing possibility that expression of our VHL-interaction–deficient pRb variant (pRb Δ778–807) may similarly enhance tumorigenesis. However, based on our hypothesis that hyperphosphorylated pRb contributes to oncogenic signaling in ccRCC, it may be necessary to introduce phosphomimetic mutations into the CDK phosphorylation sites of the Δ778–807 pRb variant to observe a tumorigenic phenotype. Furthermore, it would be of interest to determine whether this VHL-interaction–deficient pRb

variant can potentiate the tumorigenic activity of the HIF-2α variant in VHL-expressing ccRCC cells, suggesting potential cooperative effects between deregulated HIF and pRb pathways in ccRCC progression.The pRb binding site on VHL remains to be elucidated. Type 1 and Type 2B VHL mutations, which severely impair HIF regulation, are strongly linked to ccRCC development[116,440]. These mutations may potentially also disrupt VHL-pRb interaction, contributing to ccRCC tumorigenesis via dysregulation of pRb and its targets. If VHL mutations associated with ccRCC also impair pRb binding and regulation, it could create a 'double-hit' mechanism driving tumorigenesis through HIF- and pRb-regulated pathways. To investigate whether VHL mutations linked to ccRCC are also associated with pRb dysregulation, pRb stability may be assessed in ccRCC cell lines expressing Type 1 and Type 2B VHL versus wild-type VHL. VHL residues critical for binding to pRb may also be identified and analyzed to determine whether these residues overlap with known Type 1 and Type 2B mutation sites.

6.10 Limitations and Future Directions

Several limitations in our characterization of the VHL-pRb pathway may be addressed in future studies. For example, *in vivo* studies are essential to validate the therapeutic potential of targeting the VHL-pRb axis. Further drug testing on genotyped patient-derived organoids is needed to determine how ccRCC mutational landscapes may impact therapeutic outcomes. Tumor xenograft models and GEM models) will provide critical insights into the pharmacokinetics, efficacy, and safety of combination therapies involving CDK4/6 inhibitors and E2F1 activators. These models could also help identify resistance mechanisms, informing the development of next-generation therapeutics.

Furthermore, the broader relevance of our findings across diverse ccRCC patient populations remains to be determined. In chapter 3, the 786-O ccRCC patient-derived cell line was used to evaluate the impact of pRb hyperstabilization on oncogenesis through soft agar assays, clonogenic assays, and tumor xenograft models. Notably, 786-O differs from other ccRCC cell lines used in this study, such as RCC4 and 769-P, as it exclusively expresses HIF-2α, with no detectable HIF-1α expression[128]. Previous studies have highlighted the tumorigenic potential of HIF-2α, but not HIF-1α, in the 786-O background[127,137]. Interestingly, overexpression of pRb was shown to promote transcriptional activation by HIF-1α[358], raising the question of how this regulation might influence tumorigenesis in HIF-1α-expressing ccRCC cells. Nonetheless, our findings revealed that depletion of pRb promoted cell death in both HIF-1α-expressing (RCC4 and 769-P) and HIF-1α-deficient (786-O) ccRCC cell lines (Figure 12D). This suggests that pRb depletion promotes ccRCC cell death in a HIF-1α-independent manner. Given the heterogeneity of ccRCC, it will be important to identify the molecular subtypes in which the VHL-pRb pathway is disrupted, to better inform targeted therapeutic strategies.

The precise molecular determinants governing VHL targeting of pRb remain undefined. Our preliminary data indicate that oxygen availability and subcellular localization may influence VHL interaction with pRb (Figures 15 & 17). However, the exact residues and PTMs involved require further investigation. Mutation of the hydroxylatable residues within the aa778-807 fragment of pRb, followed by immunoprecipitation assays to assess VHL binding, may help identify the critical residues and potential PTMs mediating this interaction. It is worth noting that the loss of pRb regulation by VHL under hypoxic conditions may not necessarily be due to the direct loss of hydroxylation on specific residues but may arise from secondary effects induced by

oxygen deprivation. These secondary effects may involve additional regulatory factors or PTMs, which could alter the functional dynamics of the VHL-pRb interaction.

The pocket protein family, which includes pRb, retinoblastoma-like 1 (*RBL1*/p107), and retinoblastoma-like 2 (*RBL2*/p130), shares a conserved pocket domain[240], raising the possibility that VHL may also target p107 and p130. While no physical interaction between VHL and p107 or p130 has been demonstrated, functional interactions have been reported between *Vhl* and *Rbl1*. In murine models, the combined loss of *Rb1* and *Rbl1* in the retina resulted in retinoblastoma formation, and deletion of *Vhl* in these *Rb1/Rbl1*-deficient retinas suppressed retinoblastoma formation but induced subretinal vascular growths[441–443]. Exploring potential interactions between VHL and other pocket proteins may enhance our understanding of their interconnected roles and how these potential interactions may contribute to disease development. Furthermore, while our study focused on the VHL-pRb axis, exploring how this pathway intersects with other HIF-independent substrates of VHL could uncover additional layers of regulation and novel therapeutic opportunities.

6.11 Broader implications of VHL-pRb regulation

The identification of pRb as a substrate for VHL-mediated proteasomal degradation expands our understanding of VHL's non-canonical functions and highlights the importance of HIF-independent pathways in ccRCC tumorigenesis. My investigation into the oncogenic contributions of pRb to ccRCC highlights the complexity of tumorigenic signaling and the need for a holistic approach to cancer research. The therapeutic strategies proposed in this study could be combined with each other or with current frontline ccRCC treatments to potentially enhance

efficacy and mitigate drug resistance. Moreover, targeting the VHL-pRb and pRb-SKIDA1 axes may serve as a model for precision medicine strategies in other cancers with similar pathway dysregulations. In conclusion, this thesis addresses a critical gap in our understanding of VHL function beyond its well-characterized role in regulating HIF-α, advancing our understanding of the molecular mechanisms underlying ccRCC tumorigenesis, and offering potential therapeutic strategies based on the VHL-pRb axis, paving the way for more effective treatments for metastatic RCC.

References

1. Pathak, S., Strong, L. C., Ferrell, R. E. & Trindade, A. Familial renal cell carcinoma with a 3;11 chromosome translocation limited to tumor cells. *Science* **217**, 939–941 (1982).

2. Kovacs, G., Brusa, P. & De Riese, W. Tissue-specific expression of a constitutional 3;6 translocation: development of multiple bilateral renal-cell carcinomas. *Int. J. Cancer* **43**, 422–427 (1989).

3. Cohen, A. J. *et al.* Hereditary renal-cell carcinoma associated with a chromosomal translocation. *N. Engl. J. Med.* **301**, 592–595 (1979).

4. Yoshida, M. A. *et al.* Cytogenetic studies of tumor tissue from patients with nonfamilial renal cell carcinoma. *Cancer Res.* **46**, 2139–2147 (1986).

5. de Jong, B. *et al.* Cytogenetics of 12 cases of renal adenocarcinoma. *Cancer Genet. Cytogenet.* **30**, 53–61 (1988).

6. Presti, J. C. *et al.* Histopathological, cytogenetic, and molecular characterization of renal cortical tumors. *Cancer Res.* **51**, 1544–1552 (1991).

7. Kovacs, G. & Frisch, S. Clonal chromosome abnormalities in tumor cells from patients with sporadic renal cell carcinomas. *Cancer Res.* **49**, 651–659 (1989).

8. Szücs, S., Müller-Brechlin, R., DeRiese, W. & Kovacs, G. Deletion 3p: the only chromosome loss in a primary renal cell carcinoma. *Cancer Genet. Cytogenet.* **26**, 369–373 (1987).

9. Zbar, B., Brauch, H., Talmadge, C. & Linehan, M. Loss of alleles of loci on the short arm of chromosome 3 in renal cell carcinoma. *Nature* **327**, 721–724 (1987).

10. Anglard, P. *et al.* Molecular analysis of genetic changes in the origin and development of renal cell carcinoma. *Cancer Res.* **51**, 1071–1077 (1991).

11. Seizinger, B. R. *et al.* Von Hippel-Lindau disease maps to the region of chromosome 3 associated with renal cell carcinoma. *Nature* **332**, 268–269 (1988).

12. Lerman, M. I. *et al.* Isolation and regional localization of a large collection (2,000) of single-copy DNA fragments on human chromosome 3 for mapping and cloning tumor suppressor genes. *Hum. Genet.* **86**, 567–577 (1991).

13. Hosoe, S. *et al.* Localization of the von Hippel-Lindau disease gene to a small region of chromosome 3. *Genomics* **8**, 634–640 (1990).

14. Latif, F. *et al.* Identification of the von Hippel-Lindau Disease Tumor Suppressor Gene. *Science* **260**, 1317–1320 (1993).

15. Iliopoulos, O., Ohh, M. & Kaelin, W. G. pVHL19 is a biologically active product of the von Hippel–Lindau gene arising from internal translation initiation. *Proc. Natl. Acad. Sci.* **95**, 11661–11666 (1998).

16. Schoenfeld, A., Davidowitz, E. J. & Burk, R. D. A second major native von Hippel–Lindau gene product, initiated from an internal translation start site, functions as a tumor suppressor. *Proc. Natl. Acad. Sci. U. S. A.* **95**, 8817–8822 (1998).

17. Maher, E. R. *et al.* Von Hippel-Lindau disease: a genetic study. *J. Med. Genet.* **28**, 443–447 (1991).

18. Binderup, M. L. M., Galanakis, M., Budtz-Jørgensen, E., Kosteljanetz, M. & Luise Bisgaard, M. Prevalence, birth incidence, and penetrance of von Hippel-Lindau disease (vHL) in Denmark. *Eur. J. Hum. Genet. EJHG* **25**, 301–307 (2017).

19. Evans, D. G. *et al.* Birth incidence and prevalence of tumor-prone syndromes: estimates from a UK family genetic register service. *Am. J. Med. Genet. A.* **152A**, 327–332 (2010).

20. Knudson, A. G. Genetics of Human Cancer. *Annu. Rev. Genet.* **20**, 231–251 (1986).

21. Knudson, A. G. & Strong, L. C. Mutation and cancer: neuroblastoma and pheochromocytoma. *Am. J. Hum. Genet.* **24**, 514–532 (1972).

22. Kaelin, W. G. Molecular basis of the VHL hereditary cancer syndrome. *Nat. Rev. Cancer* **2**, 673–682 (2002).

23. Stolle, C. *et al.* Improved detection of germline mutations in the von Hippel-Lindau disease tumor suppressor gene. *Hum. Mutat.* **12**, 417–423 (1998).

24. Friedrich, C. A. Von Hippel-Lindau Syndrome. *Cancer* **86**, 2478–2482 (1999).

25. Prowse, A. H. *et al.* Somatic inactivation of the VHL gene in Von Hippel-Lindau disease tumors. *Am. J. Hum. Genet.* **60**, 765–771 (1997).

26. Wait, S. D. *et al.* Somatic mutations in VHL germline deletion kindred correlate with mild phenotype. *Ann. Neurol.* **55**, 236–240 (2004).

27. Chung, J., Roberts, A. M., Chow, J., Coady-Osberg, N. & Ohh, M. Homotypic association between tumour-associated VHL proteins leads to the restoration of HIF pathway. *Oncogene* **25**, 3079–3083 (2006).

28. Chen, F. *et al.* Germline mutations in the von Hippel–Lindau disease tumor suppressor gene: Correlations with phenotype. *Hum. Mutat.* **5**, 66–75 (1995).

29. Nordstrom-O'Brien, M. *et al.* Genetic analysis of von Hippel-Lindau disease. *Hum. Mutat.* **31**, 521–537 (2010).

30. Neumann, H. P. *et al.* Consequences of direct genetic testing for germline mutations in the clinical management of families with multiple endocrine neoplasia, type II. *JAMA* **274**, 1149–1151 (1995).

31. Ritter, M. M. *et al.* Isolated familial pheochromocytoma as a variant of von Hippel-Lindau disease. *J. Clin. Endocrinol. Metab.* **81**, 1035–1037 (1996).

32. van der Harst, E. *et al.* Germline mutations in the vhl gene in patients presenting with phaeochromocytomas. *Int. J. Cancer* **77**, 337–340 (1998).

33. Crossey, P. A. *et al.* Molecular genetic diagnosis of von Hippel-Lindau disease in familial phaeochromocytoma. *J. Med. Genet.* **32**, 885–886 (1995).

34. Eng, C. *et al.* Mutations in the RET proto-oncogene and the von Hippel-Lindau disease tumour suppressor gene in sporadic and syndromic phaeochromocytomas. *J. Med. Genet.* **32**, 934–937 (1995).

35. Maher, E. R. *et al.* Phenotypic expression in von Hippel-Lindau disease: correlations with germline VHL gene mutations. *J. Med. Genet.* **33**, 328–332 (1996).

36. Crossey, P. A. *et al.* Identification of intragenic mutations in the von Hippel-Lindau disease tumour suppressor gene and correlation with disease phenotype. *Hum. Mol. Genet.* **3**, 1303–1308 (1994).

37. Stebbins, C. E., Kaelin, W. G. & Pavletich, N. P. Structure of the VHL-ElonginC-ElonginB complex: implications for VHL tumor suppressor function. *Science* **284**, 455–461 (1999).

38. Maher, E. R. & Kaelin, W. G. von Hippel-Lindau disease. *Medicine (Baltimore)* **76**, 381–391 (1997).

39. N, E. J. World Health Organization Classification of Tumours. *Pathol. Genet. Tumours Urin. Syst. Male Genit. Organs* 68–69 (2004).

40. Hsieh, J. J. *et al.* Renal cell carcinoma. *Nat. Rev. Dis. Primer* **3**, 1–19 (2017).

41. Creighton, C. J. *et al.* Comprehensive molecular characterization of clear cell renal cell carcinoma. *Nature* **499**, 43–49 (2013).

42. null, null. Comprehensive Molecular Characterization of Papillary Renal-Cell Carcinoma. *N. Engl. J. Med.* **374**, 135–145 (2016).

43. Davis, C. F. *et al.* The Somatic Genomic Landscape of Chromophobe Renal Cell Carcinoma. *Cancer Cell* **26**, 319–330 (2014).

44. Pandey, J. & Syed, W. Renal Cancer. in *StatPearls* (StatPearls Publishing, Treasure Island (FL), 2024).

45. Maher, E. R. *et al.* Clinical features and natural history of von Hippel-Lindau disease. *Q. J. Med.* **77**, 1151–1163 (1990).

46. Kondo, K. *et al.* Comprehensive mutational analysis of the VHL gene in sporadic renal cell carcinoma: Relationship to clinicopathological parameters. *Genes. Chromosomes Cancer* **34**, 58–68 (2002).

47. Gallou, C. *et al.* Mutations of the VHL gene in sporadic renal cell carcinoma: Definition of a risk factor for VHL patients to develop an RCC. *Hum. Mutat.* **13**, 464–475 (1999).

48. Gnarra, J. R. *et al.* Mutations of the VHL tumour suppressor gene in renal carcinoma. *Nat. Genet.* **7**, 85–90 (1994).

49. Young, A. P. *et al.* VHL loss actuates a HIF-independent senescence programme mediated by Rb and p400. *Nat. Cell Biol.* **10**, 361–369 (2008).

50. Rankin, E. B., Tomaszewski, J. E. & Haase, V. H. Renal cyst development in mice with conditional inactivation of the von Hippel-Lindau tumor suppressor. *Cancer Res.* **66**, 2576–2583 (2006).

51. Mitchell, T. J. *et al.* Timing the Landmark Events in the Evolution of Clear Cell Renal Cell Cancer: TRACERx Renal. *Cell* **173**, 611-623.e17 (2018).

52. Sato, Y. *et al.* Integrated molecular analysis of clear-cell renal cell carcinoma. *Nat. Genet.* **45**, 860–867 (2013).

53. Varela, I. *et al.* Exome sequencing identifies frequent mutation of the SWI/SNF complex gene PBRM1 in renal carcinoma. *Nature* **469**, 539–542 (2011).

54. Dalgliesh, G. L. *et al.* Systematic sequencing of renal carcinoma reveals inactivation of histone modifying genes. *Nature* **463**, 360–363 (2010).

55. Peña-Llopis, S. *et al.* BAP1 loss defines a new class of renal cell carcinoma. *Nat. Genet.* **44**, 751–759 (2012).

56. Guo, G. *et al.* Frequent mutations of genes encoding ubiquitin-mediated proteolysis pathway components in clear cell renal cell carcinoma. *Nat. Genet.* **44**, 17–19 (2012).

57. Benusiglio, P. R. *et al.* A germline mutation in PBRM1 predisposes to renal cell carcinoma. *J. Med. Genet.* **52**, 426–430 (2015).

58. Rai, K., Pilarski, R., Cebulla, C. M. & Abdel-Rahman, M. H. Comprehensive review of BAP1 tumor predisposition syndrome with report of two new cases. *Clin. Genet.* **89**, 285–294 (2016).

59. Hakimi, A. A. *et al.* Clinical and pathologic impact of select chromatin-modulating tumor suppressors in clear cell renal cell carcinoma. *Eur. Urol.* **63**, 848–854 (2013).

60. Ciechanover, A., Elias, S., Heller, H., Ferber, S. & Hershko, A. Characterization of the heat-stable polypeptide of the ATP-dependent proteolytic system from reticulocytes. *J. Biol. Chem.* **255**, 7525–7528 (1980).

61. Hershko, A., Eytan, E., Ciechanover, A. & Haas, A. L. Immunochemical analysis of the turnover of ubiquitin-protein conjugates in intact cells. Relationship to the breakdown of abnormal proteins. *J. Biol. Chem.* **257**, 13964–13970 (1982).

62. Hershko, A., Heller, H., Elias, S. & Ciechanover, A. Components of ubiquitin-protein ligase system. Resolution, affinity purification, and role in protein breakdown. *J. Biol. Chem.* **258**, 8206–8214 (1983).

63. Ciehanover, A., Hod, Y. & Hershko, A. A heat-stable polypeptide component of an ATP-dependent proteolytic system from reticulocytes. *Biochem. Biophys. Res. Commun.* **81**, 1100–1105 (1978).

64. Hershko, A. & Ciechanover, A. The ubiquitin system. *Annu. Rev. Biochem.* **67**, 425–479 (1998).

65. Weissman, A. M. Themes and variations on ubiquitylation. *Nat. Rev. Mol. Cell Biol.* **2**, 169–178 (2001).

66. Livneh, I., Cohen-Kaplan, V., Cohen-Rosenzweig, C., Avni, N. & Ciechanover, A. The life cycle of the 26S proteasome: from birth, through regulation and function, and onto its death. *Cell Res.* **26**, 869–885 (2016).

67. Kim, W. *et al.* Systematic and quantitative assessment of the ubiquitin-modified proteome. *Mol. Cell* **44**, 325–340 (2011).

68. Wagner, S. A. *et al.* A proteome-wide, quantitative survey of in vivo ubiquitylation sites reveals widespread regulatory roles. *Mol. Cell. Proteomics MCP* **10**, M111.013284 (2011).

69. Xu, P. *et al.* Quantitative proteomics reveals the function of unconventional ubiquitin chains in proteasomal degradation. *Cell* **137**, 133–145 (2009).

70. Dammer, E. B. *et al.* Polyubiquitin linkage profiles in three models of proteolytic stress suggest the etiology of Alzheimer disease. *J. Biol. Chem.* **286**, 10457–10465 (2011).

71. Ziv, I. *et al.* A perturbed ubiquitin landscape distinguishes between ubiquitin in trafficking and in proteolysis. *Mol. Cell. Proteomics MCP* **10**, M111.009753 (2011).

72. Hicke, L. Protein regulation by monoubiquitin. *Nat. Rev. Mol. Cell Biol.* **2**, 195–201 (2001).

73. Li, W. *et al.* Genome-Wide and Functional Annotation of Human E3 Ubiquitin Ligases Identifies MULAN, a Mitochondrial E3 that Regulates the Organelle's Dynamics and Signaling. *PLOS ONE* **3**, e1487 (2008).

74. Yang, Q., Zhao, J., Chen, D. & Wang, Y. E3 ubiquitin ligases: styles, structures and functions. *Mol. Biomed.* **2**, 23 (2021).

75. Sluimer, J. & Distel, B. Regulating the human HECT E3 ligases. *Cell. Mol. Life Sci. CMLS* **75**, 3121–3141 (2018).

76. Huang, L. *et al.* Structure of an E6AP-UbcH7 Complex: Insights into Ubiquitination by the E2-E3 Enzyme Cascade. *Science* **286**, 1321–1326 (1999).

77. Wenzel, D. M., Lissounov, A., Brzovic, P. S. & Klevit, R. E. UBCH7 reactivity profile reveals parkin and HHARI to be RING/HECT hybrids. *Nature* **474**, 105–108 (2011).

78. Walden, H. & Rittinger, K. RBR ligase–mediated ubiquitin transfer: a tale with many twists and turns. *Nat. Struct. Mol. Biol.* **25**, 440–445 (2018).

79. Deshaies, R. J. & Joazeiro, C. A. P. RING domain E3 ubiquitin ligases. *Annu. Rev. Biochem.* **78**, 399–434 (2009).

80. Zheng, N. & Shabek, N. Ubiquitin Ligases: Structure, Function, and Regulation. *Annu. Rev. Biochem.* **86**, 129–157 (2017).

81. Freemont, P. S., Hanson, I. M. & Trowsdale, J. A novel cysteine-rich sequence motif. *Cell* **64**, 483–484 (1991).

82. Joazeiro, C. A. & Weissman, A. M. RING finger proteins: mediators of ubiquitin ligase activity. *Cell* **102**, 549–552 (2000).

83. Bulatov, E. & Ciulli, A. Targeting Cullin-RING E3 ubiquitin ligases for drug discovery: structure, assembly and small-molecule modulation. *Biochem. J.* **467**, 365–386 (2015).

84. Nguyen, H. C., Wang, W. & Xiong, Y. Cullin-RING E3 Ubiquitin Ligases: Bridges to Destruction. *Subcell. Biochem.* **83**, 323–347 (2017).

85. Petroski, M. D. & Deshaies, R. J. Function and regulation of cullin–RING ubiquitin ligases. *Nat. Rev. Mol. Cell Biol.* **6**, 9–20 (2005).

86. Soucy, T. A. *et al.* An inhibitor of NEDD8-activating enzyme as a new approach to treat cancer. *Nature* **458**, 732–736 (2009).

87. Lydeard, J. R., Schulman, B. A. & Harper, J. W. Building and remodelling Cullin–RING E3 ubiquitin ligases. *EMBO Rep.* **14**, 1050–1061 (2013).

88. Diehl, C. J. & Ciulli, A. Discovery of small molecule ligands for the von Hippel-Lindau (VHL) E3 ligase and their use as inhibitors and PROTAC degraders. *Chem. Soc. Rev.* **51**, 8216–8257.

89. Kibel, A., Iliopoulos, O., DeCaprio, J. A. & Kaelin, W. G. Binding of the von Hippel-Lindau tumor suppressor protein to Elongin B and C. *Science* **269**, 1444–1446 (1995).

90. Pause, A. *et al.* The von Hippel-Lindau tumor-suppressor gene product forms a stable complex with human CUL-2, a member of the Cdc53 family of proteins. *Proc. Natl. Acad. Sci. U. S. A.* **94**, 2156 (1997).

91. Kamura, T. *et al.* Rbx1, a component of the VHL tumor suppressor complex and SCF ubiquitin ligase. *Science* **284**, 657–661 (1999).

92. Lonergan, K. M. *et al.* Regulation of Hypoxia-Inducible mRNAs by the von Hippel-Lindau Tumor Suppressor Protein Requires Binding to Complexes Containing Elongins B/C and Cul2. *Mol. Cell. Biol.* **18**, 732–741 (1998).

93. Ohta, T., Michel, J. J., Schottelius, A. J. & Xiong, Y. ROC1, a homolog of APC11, represents a family of cullin partners with an associated ubiquitin ligase activity. *Mol. Cell* **3**, 535–541 (1999).

94. Jaakkola, P. *et al.* Targeting of HIF-alpha to the von Hippel-Lindau ubiquitylation complex by O2-regulated prolyl hydroxylation. *Science* **292**, 468–472 (2001).

95. Ivan, M. *et al.* HIFalpha targeted for VHL-mediated destruction by proline hydroxylation: implications for O2 sensing. *Science* **292**, 464–468 (2001).

96. Stackhouse, M., Chen, F. & Lerman, I. Cellular Proteins That Bind the von Hippel-Lindau Disease Gene Product: Mapping of Binding Domains and the Effect of Missense Mutations.

97. Ganner, A. *et al.* VHL suppresses RAPTOR and inhibits mTORC1 signaling in clear cell renal cell carcinoma. *Sci. Rep.* **11**, 14827 (2021).

98. Zhou, L. & Yang, H. The von Hippel-Lindau Tumor Suppressor Protein Promotes c-Cbl-Independent Poly-Ubiquitylation and Degradation of the Activated EGFR. *PLOS ONE* **6**, e23936 (2011).

99. Zhang, J. *et al.* VHL substrate transcription factor ZHX2 as an oncogenic driver in clear cell renal cell carcinoma. *Science* **361**, 290–295 (2018).

100. Xie, L. *et al.* Oxygen-Regulated β2-Adrenergic Receptor Hydroxylation by EGLN3 and Ubiquitylation by pVHL. *Sci. Signal.* **2**, ra33–ra33 (2009).

101. Iturrioz, X. & Parker, P. J. PKCζII is a target for degradation through the tumour suppressor protein pVHL. *FEBS Lett.* **581**, 1397–1402 (2007).

102. Anderson, K. *et al.* Regulation of Cellular Levels of Sprouty2 Protein by Prolyl Hydroxylase Domain and von Hippel-Lindau Proteins*. *J. Biol. Chem.* **286**, 42027–42036 (2011).

103. Liu, X. *et al.* Genome-wide Screening Identifies SFMBT1 as an Oncogenic Driver in Cancer with VHL Loss. *Mol. Cell* **77**, 1294-1306.e5 (2020).

104. Tang, M. *et al.* The Malignant Brain Tumor (MBT) Domain Protein SFMBT1 Is an Integral Histone Reader Subunit of the LSD1 Demethylase Complex for Chromatin Association and Epithelial-to-mesenchymal Transition *. *J. Biol. Chem.* **288**, 27680–27691 (2013).

105. Wang, G. L. & Semenza, G. L. General involvement of hypoxia-inducible factor 1 in transcriptional response to hypoxia. *Proc. Natl. Acad. Sci. U. S. A.* **90**, 4304–4308 (1993).

106. Wang, G. L. & Semenza, G. L. Purification and Characterization of Hypoxia-inducible Factor 1 (∗). *J. Biol. Chem.* **270**, 1230–1237 (1995).

107. Wang, G. L. & Semenza, G. L. Characterization of hypoxia-inducible factor 1 and regulation of DNA binding activity by hypoxia. *J. Biol. Chem.* **268**, 21513–21518 (1993).

108. Lee, J.-W., Bae, S.-H., Jeong, J.-W., Kim, S.-H. & Kim, K.-W. Hypoxia-inducible factor (HIF-1)α: its protein stability and biological functions. *Exp. Mol. Med.* **36**, 1–12 (2004).

109. Epstein, A. C. *et al.* C. elegans EGL-9 and mammalian homologs define a family of dioxygenases that regulate HIF by prolyl hydroxylation. *Cell* **107**, 43–54 (2001).

110. Yu, F., White, S. B., Zhao, Q. & Lee, F. S. HIF-1α binding to VHL is regulated by stimulus-sensitive proline hydroxylation. *Proc. Natl. Acad. Sci.* **98**, 9630–9635 (2001).

111. Masson, N., Willam, C., Maxwell, P. H., Pugh, C. W. & Ratcliffe, P. J. Independent function of two destruction domains in hypoxia-inducible factor-α chains activated by prolyl hydroxylation. *EMBO J.* **20**, 5197–5206 (2001).

112. Kallio, P. J. *et al.* Signal transduction in hypoxic cells: inducible nuclear translocation and recruitment of the CBP/p300 coactivator by the hypoxia-inducible factor-1alpha. *EMBO J.* **17**, 6573–6586 (1998).

113. Lando, D., Peet, D. J., Whelan, D. A., Gorman, J. J. & Whitelaw, M. L. Asparagine hydroxylation of the HIF transactivation domain a hypoxic switch. *Science* **295**, 858–861 (2002).

114. Lando, D. *et al.* FIH-1 is an asparaginyl hydroxylase enzyme that regulates the transcriptional activity of hypoxia-inducible factor. *Genes Dev.* **16**, 1466–1471 (2002).

115. Mahon, P. C., Hirota, K. & Semenza, G. L. FIH-1: a novel protein that interacts with HIF-1alpha and VHL to mediate repression of HIF-1 transcriptional activity. *Genes Dev.* **15**, 2675–2686 (2001).

116. Miller, F., Kentsis, A., Osman, R. & Pan, Z.-Q. Inactivation of *VHL* by Tumorigenic Mutations That Disrupt Dynamic Coupling of the pVHL·Hypoxia-inducible Transcription Factor-1α Complex*. *J. Biol. Chem.* **280**, 7985–7996 (2005).

117. Maynard, M. A. & Ohh, M. Von Hippel-Lindau tumor suppressor protein and hypoxia-inducible factor in kidney cancer. *Am. J. Nephrol.* **24**, 1–13 (2004).

118. Maxwell, P. H. *et al.* The tumour suppressor protein VHL targets hypoxia-inducible factors for oxygen-dependent proteolysis. *Nature* **399**, 271–275 (1999).

119. Clifford, S. C. *et al.* Contrasting effects on HIF-1alpha regulation by disease-causing pVHL mutations correlate with patterns of tumourigenesis in von Hippel-Lindau disease. *Hum. Mol. Genet.* **10**, 1029–1038 (2001).

120. Hoffman, M. A. *et al.* von Hippel-Lindau protein mutants linked to type 2C VHL disease preserve the ability to downregulate HIF. *Hum. Mol. Genet.* **10**, 1019–1027 (2001).

121. Hu, C.-J., Wang, L.-Y., Chodosh, L. A., Keith, B. & Simon, M. C. Differential Roles of Hypoxia-Inducible Factor 1α (HIF-1α) and HIF-2α in Hypoxic Gene Regulation. *Mol. Cell. Biol.* **23**, 9361–9374 (2003).

122. Raval, R. R. *et al.* Contrasting Properties of Hypoxia-Inducible Factor 1 (HIF-1) and HIF-2 in von Hippel-Lindau-Associated Renal Cell Carcinoma. *Mol. Cell. Biol.* **25**, 5675–5686 (2005).

123. Carroll, V. A. & Ashcroft, M. Role of Hypoxia-Inducible Factor (HIF)-1α versus HIF-2α in the Regulation of HIF Target Genes in Response to Hypoxia, Insulin-Like Growth Factor-I, or Loss of von Hippel-Lindau Function: Implications for Targeting the HIF Pathway. *Cancer Res.* **66**, 6264–6270 (2006).

124. Loboda, A., Jozkowicz, A. & Dulak, J. HIF-1 and HIF-2 transcription factors — Similar but not identical. *Mol. Cells* **29**, 435–442 (2010).

125. Holmquist-Mengelbier, L. *et al.* Recruitment of HIF-1α and HIF-2α to common target genes is differentially regulated in neuroblastoma: HIF-2α promotes an aggressive phenotype. *Cancer Cell* **10**, 413–423 (2006).

126. Keith, B., Johnson, R. S. & Simon, M. C. HIF1α and HIF2α: sibling rivalry in hypoxic tumour growth and progression. *Nat. Rev. Cancer* **12**, 9–22 (2012).

127. Kondo, K., Klco, J., Nakamura, E., Lechpammer, M. & Kaelin, W. G. Inhibition of HIF is necessary for tumor suppression by the von Hippel-Lindau protein. *Cancer Cell* **1**, 237–246 (2002).

128. Kondo, K., Kim, W. Y., Lechpammer, M. & Kaelin, W. G. Inhibition of HIF2α Is Sufficient to Suppress pVHL-Defective Tumor Growth. *PLoS Biol.* **1**, e83 (2003).

129. Kim, W. Y. *et al.* Failure to prolyl hydroxylate hypoxia-inducible factor α phenocopies VHL inactivation in vivo. *EMBO J.* **25**, 4650–4662 (2006).

130. Rankin, E. B. *et al.* Hypoxia-inducible factor–2 (HIF-2) regulates hepatic erythropoietin in vivo. *J. Clin. Invest.* **117**, 1068–1077 (2007).

131. Rankin, E. B. *et al.* Inactivation of the Arylhydrocarbon Receptor Nuclear Translocator (Arnt) Suppresses von Hippel-Lindau Disease-Associated Vascular Tumors in Mice. *Mol. Cell. Biol.* **25**, 3163–3172 (2005).

132. Rankin, E. B. *et al.* Hypoxia-Inducible Factor 2 Regulates Hepatic Lipid Metabolism. *Mol. Cell. Biol.* **29**, 4527–4538 (2009).

133. Rankin, E. B. *et al.* Hypoxia-inducible factor-2 regulates vascular tumorigenesis in mice. *Oncogene* **27**, 5354–5358 (2008).

134. Zimmer, M., Doucette, D., Siddiqui, N. & Iliopoulos, O. Inhibition of Hypoxia-Inducible Factor Is Sufficient for Growth Suppression of VHL−/− Tumors1. *Mol. Cancer Res.* **2**, 89–95 (2004).

135. Gordan, J. D. *et al.* HIF-α Effects on c-Myc Distinguish Two Subtypes of Sporadic VHL-Deficient Clear Cell Renal Carcinoma. *Cancer Cell* **14**, 435–446 (2008).

136. Shen, C. *et al.* Genetic and Functional Studies Implicate HIF1α as a 14q Kidney Cancer Suppressor Gene. *Cancer Discov.* **1**, 222–235 (2011).

137. Maranchie, J. K. *et al.* The contribution of VHL substrate binding and HIF1-α to the phenotype of VHL loss in renal cell carcinoma. *Cancer Cell* **1**, 247–255 (2002).

138. Forsythe, J. A. *et al.* Activation of vascular endothelial growth factor gene transcription by hypoxia-inducible factor 1. *Mol. Cell. Biol.* **16**, 4604 (1996).

139. Wang, G. L., Jiang, B. H., Rue, E. A. & Semenza, G. L. Hypoxia-inducible factor 1 is a basic-helix-loop-helix-PAS heterodimer regulated by cellular O2 tension. *Proc. Natl. Acad. Sci. U. S. A.* **92**, 5510 (1995).

140. Semenza, G. L. Targeting HIF-1 for cancer therapy. *Nat. Rev. Cancer* **3**, 721–732 (2003).

141. de Paulsen, N. *et al.* Role of transforming growth factor-alpha in von Hippel--Lindau (VHL)(-/-) clear cell renal carcinoma cell proliferation: a possible mechanism coupling VHL tumor suppressor inactivation and tumorigenesis. *Proc. Natl. Acad. Sci. U. S. A.* **98**, 1387–1392 (2001).

142. Franovic, A. *et al.* Translational up-regulation of the EGFR by tumor hypoxia provides a nonmutational explanation for its overexpression in human cancer. *Proc. Natl. Acad. Sci. U. S. A.* **104**, 13092–13097 (2007).

143. Okuda, H. *et al.* The von Hippel-Lindau Tumor Suppressor Protein Mediates Ubiquitination of Activated Atypical Protein Kinase C *. *J. Biol. Chem.* **276**, 43611–43617 (2001).

144. Suzuki, A. *et al.* Atypical Protein Kinase C Is Involved in the Evolutionarily Conserved Par Protein Complex and Plays a Critical Role in Establishing Epithelia-Specific Junctional Structures. *J. Cell Biol.* **152**, 1183–1196 (2001).

145. Nilsson, M. B. *et al.* Stress hormones promote EGFR inhibitor resistance in NSCLC: Implications for combinations with β-blockers. *Sci. Transl. Med.* **9**, eaao4307 (2017).

146. Kaira, K. *et al.* Prognostic Impact of β2 Adrenergic Receptor Expression in Surgically Resected Pulmonary Pleomorphic Carcinoma. *Anticancer Res.* **39**, 395–403 (2019).

147. Zhu, L., Ding, R., Yan, H., Zhang, J. & Lin, Z. ZHX2 drives cell growth and migration via activating MEK/ERK signal and induces Sunitinib resistance by regulating the autophagy in clear cell Renal Cell Carcinoma. *Cell Death Dis.* **11**, 337 (2020).

148. Robb, V. A., Karbowniczek, M., Klein-Szanto, A. J. & Henske, E. P. Activation of the mTOR signaling pathway in renal clear cell carcinoma. *J. Urol.* **177**, 346–352 (2007).

149. Russell, R. C. *et al.* Loss of JAK2 regulation via a heterodimeric VHL-SOCS1 E3 ubiquitin ligase underlies Chuvash polycythemia. *Nat. Med.* **17**, 845–853 (2011).

150. Heir, P. *et al.* Oxygen-dependent Regulation of Erythropoietin Receptor Turnover and Signaling. *J. Biol. Chem.* **291**, 7357 (2016).

151. Lai, Y., Qiao, M., Song, M., Weintraub, S. T. & Shiio, Y. Quantitative Proteomics Identifies the Myb-Binding Protein p160 as a Novel Target of the von Hippel-Lindau Tumor Suppressor. *PLOS ONE* **6**, e16975 (2011).

152. Kuznetsova, A. V. *et al.* von Hippel–Lindau protein binds hyperphosphorylated large subunit of RNA polymerase II through a proline hydroxylation motif and targets it for ubiquitination. *Proc. Natl. Acad. Sci.* **100**, 2706–2711 (2003).

153. Na, X. *et al.* Identification of the RNA polymerase II subunit hsRPB7 as a novel target of the von Hippel—Lindau protein. *EMBO J.* **22**, 4249–4259 (2003).

154. Russell, R. C. & Ohh, M. NEDD8 acts as a 'molecular switch' defining the functional selectivity of VHL. *EMBO Rep.* **9**, 486–491 (2008).

155. Stickle, N. H. *et al.* pVHL Modification by NEDD8 Is Required for Fibronectin Matrix Assembly and Suppression of Tumor Development. *Mol. Cell. Biol.* **24**, 3251–3261 (2004).

156. Thoma, C. R. *et al.* Quantitative image analysis identifies pVHL as a key regulator of microtubule dynamic instability. *J. Cell Biol.* **190**, 991–1003 (2010).

157. Thoma, C. R., Frew, I. J. & Krek, W. The VHL tumor suppressor: riding tandem with GSK3beta in primary cilium maintenance. *Cell Cycle Georget. Tex* **6**, 1809–1813 (2007).

158. Lutz, M. S. & Burk, R. D. Primary cilium formation requires von hippel-lindau gene function in renal-derived cells. *Cancer Res.* **66**, 6903–6907 (2006).

159. Esteban, M. A., Harten, S. K., Tran, M. G. & Maxwell, P. H. Formation of primary cilia in the renal epithelium is regulated by the von Hippel-Lindau tumor suppressor protein. *J. Am. Soc. Nephrol. JASN* **17**, 1801–1806 (2006).

160. Schermer, B. *et al.* The von Hippel-Lindau tumor suppressor protein controls ciliogenesis by orienting microtubule growth. *J. Cell Biol.* **175**, 547–554 (2006).

161. Thoma, C. R. *et al.* VHL loss causes spindle misorientation and chromosome instability. *Nat. Cell Biol.* **11**, 994–1001 (2009).

162. Hergovich, A., Lisztwan, J., Barry, R., Ballschmieter, P. & Krek, W. Regulation of microtubule stability by the von Hippel-Lindau tumour suppressor protein pVHL. *Nat. Cell Biol.* **5**, 64–70 (2003).

163. Ohh, M. *et al.* The von Hippel-Lindau Tumor Suppressor Protein Is Required for Proper Assembly of an Extracellular Fibronectin Matrix. *Mol. Cell* **1**, 959–968 (1998).

164. Grosfeld, A. *et al.* Interaction of Hydroxylated Collagen IV with the von Hippel-Lindau Tumor Suppressor*. *J. Biol. Chem.* **282**, 13264–13269 (2007).

165. Guo, J. *et al.* pVHL suppresses kinase activity of Akt in a proline-hydroxylation–dependent manner. *Science* **353**, 929–932 (2016).

166. Yang, H. *et al.* pVHL acts as an Adapter to Promote the Inhibitory Phosphorylation of the NF-κB Agonist Card9 by CK2. *Mol. Cell* **28**, 15–27 (2007).

167. Mans, D. A. *et al.* Regulation of E2F1 by the von Hippel-Lindau tumour suppressor protein predicts survival in renal cell cancer patients. *J. Pathol.* **231**, 117–129 (2013).

168. Ji, W. *et al.* pVHL acts as a downstream target of E2F1 to suppress E2F1 activity. *Biochem. J.* **457**, 185–195 (2013).

169. Roe, J.-S. & Youn, H.-D. The positive regulation of p53 by the tumor suppressor VHL. *Cell Cycle Georget. Tex* **5**, 2054–2056 (2006).

170. Roe, J.-S. *et al.* p53 stabilization and transactivation by a von Hippel-Lindau protein. *Mol. Cell* **22**, 395–405 (2006).

171. Lee, S. *et al.* Neuronal apoptosis linked to EglN3 prolyl hydroxylase and familial pheochromocytoma genes: Developmental culling and cancer. *Cancer Cell* **8**, 155–167 (2005).

172. Welford, S. M., Dorie, M. J., Li, X., Haase, V. H. & Giaccia, A. J. Renal oxygenation suppresses VHL loss-induced senescence that is caused by increased sensitivity to oxidative stress. *Mol. Cell. Biol.* **30**, 4595–4603 (2010).

173. Siegel, R. L., Miller, K. D. & Jemal, A. Cancer Statistics, 2017. *CA. Cancer J. Clin.* **67**, 7–30 (2017).

174. Klatte, T., Pantuck, A. J., Kleid, M. D. & Belldegrun, A. S. Understanding the natural biology of kidney cancer: implications for targeted cancer therapy. *Rev. Urol.* **9**, 47–56 (2007).

175. Choueiri, T. K. & Motzer, R. J. Systemic Therapy for Metastatic Renal-Cell Carcinoma. *N. Engl. J. Med.* **376**, 354–366 (2017).

176. Cancer of the Kidney and Renal Pelvis - Cancer Stat Facts. *SEER* https://seer.cancer.gov/statfacts/html/kidrp.html.

177. Dabestani, S. *et al.* Renal cell carcinoma recurrences and metastases in primary non-metastatic patients: a population-based study. *World J. Urol.* **34**, 1081–1086 (2016).

178. Rabinovitch, R. A., Zelefsky, M. J., Gaynor, J. J. & Fuks, Z. Patterns of failure following surgical resection of renal cell carcinoma: implications for adjuvant local and systemic therapy. *J. Clin. Oncol. Off. J. Am. Soc. Clin. Oncol.* **12**, 206–212 (1994).

179. Sandock, D. S., Seftel, A. D. & Resnick, M. I. A new protocol for the followup of renal cell carcinoma based on pathological stage. *J. Urol.* **154**, 28–31 (1995).

180. Yagoda, A., Abi-Rached, B. & Petrylak, D. Chemotherapy for advanced renal-cell carcinoma: 1983-1993. *Semin. Oncol.* **22**, 42–60 (1995).

181. Motzer, R. J. & Russo, P. Systemic therapy for renal cell carcinoma. *J. Urol.* **163**, 408–417 (2000).

182. Dekernion, J. B., Ramming, K. P. & Smith, R. B. The natural history of metastatic renal cell carcinoma: a computer analysis. *J. Urol.* **120**, 148–152 (1978).

183. Heinzer, H., Huland, E. & Huland, H. Systemic chemotherapy and chemoimmunotherapy for metastatic renal cell cancer. *World J. Urol.* **19**, 111–119 (2001).

184. Bukowski, R. M. Cytokine therapy for metastatic renal cell carcinoma. *Semin. Urol. Oncol.* **19**, 148–154 (2001).

185. Garcia, J. A. & Rini, B. I. Recent progress in the management of advanced renal cell carcinoma. *CA. Cancer J. Clin.* **57**, 112–125 (2007).

186. Fisher, R. I., Rosenberg, S. A. & Fyfe, G. Long-term survival update for high-dose recombinant interleukin-2 in patients with renal cell carcinoma. *Cancer J. Sci. Am.* **6 Suppl 1**, S55-57 (2000).

187. McDermott, D. F. *et al.* Randomized phase III trial of high-dose interleukin-2 versus subcutaneous interleukin-2 and interferon in patients with metastatic renal cell carcinoma. *J. Clin. Oncol. Off. J. Am. Soc. Clin. Oncol.* **23**, 133–141 (2005).

188. Motzer, R. J. *et al.* Phase III trial of interferon alfa-2a with or without 13-cis-retinoic acid for patients with advanced renal cell carcinoma. *J. Clin. Oncol. Off. J. Am. Soc. Clin. Oncol.* **18**, 2972–2980 (2000).

189. Negrier, S. *et al.* Recombinant human interleukin-2, recombinant human interferon alfa-2a, or both in metastatic renal-cell carcinoma. Groupe Français d'Immunothérapie. *N. Engl. J. Med.* **338**, 1272–1278 (1998).

190. Yang, J. C. *et al.* Randomized study of high-dose and low-dose interleukin-2 in patients with metastatic renal cancer. *J. Clin. Oncol. Off. J. Am. Soc. Clin. Oncol.* **21**, 3127–3132 (2003).

191. Motzer, R. J., Bander, N. H. & Nanus, D. M. Renal-cell carcinoma. *N. Engl. J. Med.* **335**, 865–875 (1996).

192. Allard, C. B. *et al.* Contemporary trends in high-dose interleukin-2 use for metastatic renal cell carcinoma in the United States. *Urol. Oncol.* **33**, 496.e11–16 (2015).

193. Klapper, J. A. *et al.* High-dose interleukin-2 for the treatment of metastatic renal cell carcinoma : a retrospective analysis of response and survival in patients treated in the surgery branch at the National Cancer Institute between 1986 and 2006. *Cancer* **113**, 293–301 (2008).

194. Yang, J. C. *et al.* A randomized trial of bevacizumab, an anti-vascular endothelial growth factor antibody, for metastatic renal cancer. *N. Engl. J. Med.* **349**, 427–434 (2003).

195. Mendel, D. B. *et al.* In vivo antitumor activity of SU11248, a novel tyrosine kinase inhibitor targeting vascular endothelial growth factor and platelet-derived growth factor receptors: determination of a pharmacokinetic/pharmacodynamic relationship. *Clin. Cancer Res. Off. J. Am. Assoc. Cancer Res.* **9**, 327–337 (2003).

196. Fabian, M. A. *et al.* A small molecule-kinase interaction map for clinical kinase inhibitors. *Nat. Biotechnol.* **23**, 329–336 (2005).

197. Wilhelm, S. *et al.* Discovery and development of sorafenib: a multikinase inhibitor for treating cancer. *Nat. Rev. Drug Discov.* **5**, 835–844 (2006).

198. Barragan-Carrillo, R. *et al.* First and Second-line Treatments in Metastatic Renal Cell Carcinoma. *Eur. Urol.* **87**, 143–154 (2025).

199. Motzer, R. J. *et al.* Sunitinib versus Interferon Alfa in Metastatic Renal-Cell Carcinoma. *N. Engl. J. Med.* **356**, 115–124 (2007).

200. Atkins, M. B. *et al.* Randomized phase II study of multiple dose levels of CCI-779, a novel mammalian target of rapamycin kinase inhibitor, in patients with advanced refractory renal cell carcinoma. *J. Clin. Oncol. Off. J. Am. Soc. Clin. Oncol.* **22**, 909–918 (2004).

201. Reddy, G. K., Mughal, T. I. & Rini, B. I. Current data with mammalian target of rapamycin inhibitors in advanced-stage renal cell carcinoma. *Clin. Genitourin. Cancer* **5**, 110–113 (2006).

202. Boulay, A. *et al.* Antitumor efficacy of intermittent treatment schedules with the rapamycin derivative RAD001 correlates with prolonged inactivation of ribosomal protein S6 kinase 1 in peripheral blood mononuclear cells. *Cancer Res.* **64**, 252–261 (2004).

203. Cho, D., Signoretti, S., Regan, M., Mier, J. W. & Atkins, M. B. The role of mammalian target of rapamycin inhibitors in the treatment of advanced renal cancer. *Clin. Cancer Res. Off. J. Am. Assoc. Cancer Res.* **13**, 758s–763s (2007).

204. Smith, J. W. *et al.* Update of a phase 1 study of intravenous CCI-779 given in combination with interferon-α to patients with advanced renal cell carcinoma. *J. Clin. Oncol.* **22**, 4513–4513 (2004).

205. Albiges, L. *et al.* LBA88 Belzutifan versus everolimus in participants (pts) with previously treated advanced clear cell renal cell carcinoma (ccRCC): Randomized open-label phase III LITESPARK-005 study. *Ann. Oncol.* **34**, S1329–S1330 (2023).

206. Choueiri, T. K. *et al.* LBA87 Phase II LITESPARK-003 study of belzutifan in combination with cabozantinib for advanced clear cell renal cell carcinoma (ccRCC). *Ann. Oncol.* **34**, S1328–S1329 (2023).

207. Curry, L. & Soleimani, M. Belzutifan: a novel therapeutic for the management of von Hippel–Lindau disease and beyond. *Future Oncol.* (2024) doi:10.2217/fon-2023-0679.

208. Jonasch, E. *et al.* Belzutifan for Renal Cell Carcinoma in von Hippel–Lindau Disease. *N. Engl. J. Med.* **385**, 2036–2046 (2021).

209. Motzer, R. J. *et al.* Nivolumab plus Ipilimumab versus Sunitinib in Advanced Renal-Cell Carcinoma. *N. Engl. J. Med.* **378**, 1277–1290 (2018).

210. Motzer, R. J. *et al.* Avelumab plus Axitinib versus Sunitinib for Advanced Renal-Cell Carcinoma. *N. Engl. J. Med.* **380**, 1103–1115 (2019).

211. Rini, B. I. *et al.* Pembrolizumab plus Axitinib versus Sunitinib for Advanced Renal-Cell Carcinoma. *N. Engl. J. Med.* **380**, 1116–1127 (2019).

212. Carlo, M. I., Voss, M. H. & Motzer, R. J. Checkpoint inhibitors and other novel immunotherapies for advanced renal cell carcinoma. *Nat. Rev. Urol.* **13**, 420–431 (2016).

213. Motzer, R. *et al.* Lenvatinib plus Pembrolizumab or Everolimus for Advanced Renal Cell Carcinoma. *N. Engl. J. Med.* **384**, 1289–1300 (2021).

214. Xu, W., Atkins, M. B. & McDermott, D. F. Checkpoint inhibitor immunotherapy in kidney cancer. *Nat. Rev. Urol.* **17**, 137–150 (2020).

215. Wilky, B. A. Immune checkpoint inhibitors: The linchpins of modern immunotherapy. *Immunol. Rev.* **290**, 6–23 (2019).

216. Study Details | A Study of Abemaciclib in Combination With Sunitinib in Metastatic Renal Cell Carcinoma | ClinicalTrials.gov. https://clinicaltrials.gov/study/NCT03905889.

217. Small, J., Washburn, E., Millington, K., Zhu, J. & Holder, S. L. The addition of abemaciclib to sunitinib induces regression of renal cell carcinoma xenograft tumors. *Oncotarget* **8**, 95116–95134 (2017).

218. Pili, R. *et al.* Combination of the histone deacetylase inhibitor vorinostat with bevacizumab in patients with clear-cell renal cell carcinoma: a multicentre, single-arm phase I/II clinical trial. *Br. J. Cancer* **116**, 874–883 (2017).

219. Aggarwal, R. R. *et al.* Exceptional responders to abexinostat (ABX) plus pazopanib (PAZ) in pretreated renal cell carcinoma (RCC) and other solid tumors: Long-term follow-up of a phase 1b study. *J. Clin. Oncol.* **37**, 3022–3022 (2019).

220. Frampton, J. E. Pazopanib: a Review in Advanced Renal Cell Carcinoma. *Target. Oncol.* **12**, 543–554 (2017).

221. Meric-Bernstam, F. *et al.* CB-839, a glutaminase inhibitor, in combination with cabozantinib in patients with clear cell and papillary metastatic renal cell cancer (mRCC): Results of a phase I study. *J. Clin. Oncol.* **37**, 549–549 (2019).

222. Centre Leon Berard. *A Phase I Dose Escalation Trial Evaluating the Impact of an in Situ Immunization Strategy With Intra-Tumoral Injections of Pexa-Vec in Combination With Ipilimumab in Metastatic / Advanced Solid Tumors With Injectable Lesions.* https://clinicaltrials.gov/study/NCT02977156 (2022).

223. Breitbach, C. J., Bell, J. C., Hwang, T.-H., Kirn, D. H. & Burke, J. The emerging therapeutic potential of the oncolytic immunotherapeutic Pexa-Vec (JX-594). *Oncolytic Virotherapy* **4**, 25–31 (2015).

224. Kim, S.-G. *et al.* Phase II trial of pexa-vec (pexastimogene devacirepvec; JX-594), an oncolytic and immunotherapeutic vaccinia virus, in patients with metastatic, refractory renal cell carcinoma (RCC). *J. Clin. Oncol.* **36**, 671–671 (2018).

225. Astellas Pharma Global Development, Inc. *A Multi-Center, Open Label, Randomized Phase 2 Study of AGS-16C3F vs. Axitinib in Metastatic Renal Cell Carcinoma*. https://clinicaltrials.gov/study/NCT02639182 (2024).

226. Thompson, J. A. *et al.* Phase I Trials of Anti-ENPP3 Antibody–Drug Conjugates in Advanced Refractory Renal Cell Carcinomas. *Clin. Cancer Res.* **24**, 4399–4406 (2018).

227. Falls, H. F. & Neel, J. V. Genetics of retinoblastoma. *AMA Arch. Ophthalmol.* **46**, 367–389 (1951).

228. Schappert-Kimmijser, J., Hemmes, G. D. & Nijland, R. The heredity of retinoblastoma. *Ophthalmol. J. Int. Ophtalmol. Int. J. Ophthalmol. Z. Augenheilkd.* **151**, 197–213 (1966).

229. Smith, S. M. & Sorsby, A. Retinoblastoma: some genetic aspects. *Ann. Hum. Genet.* **23**, 50–58 (1958).

230. Knudson, A. G. Mutation and cancer: statistical study of retinoblastoma. *Proc. Natl. Acad. Sci. U. S. A.* **68**, 820–823 (1971).

231. Francke, U. & Kung, F. Sporadic bilateral retinoblastoma and 13q- chromosomal deletion. *Med. Pediatr. Oncol.* **2**, 379–385 (1976).

232. Lele, K. P., Penrose, L. S. & Stallard, H. B. CHROMOSOME DELETION IN A CASE OF RETINOBLASTOMA. *Ann. Hum. Genet.* **27**, 171–174 (1963).

233. Sparkes, R. S. *et al.* Regional assignment of genes for human esterase D and retinoblastoma to chromosome band 13q14. *Science* **208**, 1042–1044 (1980).

234. Yunis, J. J. & Ramsay, N. Retinoblastoma and subband deletion of chromosome 13. *Am. J. Dis. Child. 1960* **132**, 161–163 (1978).

235. Murphree, A. L. & Benedict, W. F. Retinoblastoma: clues to human oncogenesis. *Science* **223**, 1028–1033 (1984).

236. Friend, S. H. *et al.* A human DNA segment with properties of the gene that predisposes to retinoblastoma and osteosarcoma. *Nature* **323**, 643–646 (1986).

237. Lee, W. H. *et al.* Human retinoblastoma susceptibility gene: cloning, identification, and sequence. *Science* **235**, 1394–1399 (1987).

238. Di Fiore, R., D'Anneo, A., Tesoriere, G. & Vento, R. RB1 in cancer: Different mechanisms of RB1 inactivation and alterations of pRb pathway in tumorigenesis. *J. Cell. Physiol.* **228**, 1676–1687 (2013).

239. Berry, J. L. *et al.* The RB1 Story: Characterization and Cloning of the First Tumor Suppressor Gene. *Genes* **10**, 879 (2019).

240. Chan, H. M., Smith, L. & La Thangue, N. B. Role of LXCXE motif-dependent interactions in the activity of the retinoblastoma protein. *Oncogene* **20**, 6152–6163 (2001).

241. Dick, F. A. & Rubin, S. M. Molecular mechanisms underlying RB protein function. *Nat. Rev. Mol. Cell Biol.* **14**, 297–306 (2013).

242. Chow, K. N., Starostik, P. & Dean, D. C. The Rb family contains a conserved cyclin-dependent-kinase-regulated transcriptional repressor motif. *Mol. Cell. Biol.* **16**, 7173 (1996).

243. Gibson, T. J., Thompson, J. D., Blocker, A. & Kouzarides, T. Evidence for a protein domain superfamily shared by the cyclins, TFIIB and RB/p107. *Nucleic Acids Res.* **22**, 946 (1994).

244. Lee, J. O., Russo, A. A. & Pavletich, N. P. Structure of the retinoblastoma tumour-suppressor pocket domain bound to a peptide from HPV E7. *Nature* **391**, 859–865 (1998).

245. Stein, G. S. *The Molecular Basis of Cell Cycle and Growth Control*. (J. Wiley, 1999).

246. Luo, R. X., Postigo, A. A. & Dean, D. C. Rb Interacts with Histone Deacetylase to Repress Transcription. *Cell* **92**, 463–473 (1998).

247. Weinberg, R. A. The retinoblastoma protein and cell cycle control. *Cell* **81**, 323–330 (1995).

248. Adams, P. D. *et al.* Retinoblastoma protein contains a C-terminal motif that targets it for phosphorylation by cyclin-cdk complexes. *Mol. Cell. Biol.* **19**, 1068–1080 (1999).

249. Durfee, T. *et al.* The retinoblastoma protein associates with the protein phosphatase type 1 catalytic subunit. *Genes Dev.* **7**, 555–569 (1993).

250. Vietri, M., Bianchi, M., Ludlow, J. W., Mittnacht, S. & Villa-Moruzzi, E. Direct interaction between the catalytic subunit of Protein Phosphatase 1 and pRb. *Cancer Cell Int.* **6**, 3 (2006).

251. Dick, F. A. & Dyson, N. pRB Contains an E2F1-Specific Binding Domain that Allows E2F1-Induced Apoptosis to Be Regulated Separately from Other E2F Activities. *Mol. Cell* **12**, 639–649 (2003).

252. Julian, L. M., Palander, O., Seifried, L. A., Foster, J. E. G. & Dick, F. A. Characterization of an E2F1-specific binding domain in pRB and its implications for apoptotic regulation. *Oncogene* **27**, 1572–1579 (2008).

253. DeCaprio, J. A. *et al.* SV40 large tumor antigen forms a specific complex with the product of the retinoblastoma susceptibility gene. *Cell* **54**, 275–283 (1988).

254. Whyte, P. *et al.* Association between an oncogene and an anti-oncogene: the adenovirus E1A proteins bind to the retinoblastoma gene product. *Nature* **334**, 124–129 (1988).

255. Cobrinik, D., Dowdy, S. F., Hinds, P. W., Mittnacht, S. & Weinberg, R. A. The retinoblastoma protein and the regulation of cell cycling. *Trends Biochem. Sci.* **17**, 312–315 (1992).

256. Chellappan, S. P., Hiebert, S., Mudryj, M., Horowitz, J. M. & Nevins, J. R. The E2F transcription factor is a cellular target for the RB protein. *Cell* **65**, 1053–1061 (1991).

257. Helin, K. *et al.* A cDNA encoding a pRB-binding protein with properties of the transcription factor E2F. *Cell* **70**, 337–350 (1992).

258. Hiebert, S. W., Chellappan, S. P., Horowitz, J. M. & Nevins, J. R. The interaction of RB with E2F coincides with an inhibition of the transcriptional activity of E2F. *Genes Dev.* **6**, 177–185 (1992).

259. Nevins, J. R. E2F: a link between the Rb tumor suppressor protein and viral oncoproteins. *Science* **258**, 424–429 (1992).

260. Dahiya, A., Gavin, M. R., Luo, R. X. & Dean, D. C. Role of the LXCXE Binding Site in Rb Function. *Mol. Cell. Biol.* **20**, 6799–6805 (2000).

261. Lai, A. *et al.* RBP1 Recruits Both Histone Deacetylase-Dependent and -Independent Repression Activities to Retinoblastoma Family Proteins. *Mol. Cell. Biol.* **19**, 6632–6641 (1999).

262. Magnaghi-Jaulin, L. *et al.* Retinoblastoma protein represses transcription by recruiting a histone deacetylase. *Nature* **391**, 601–605 (1998).

263. Brehm, A. *et al.* Retinoblastoma protein recruits histone deacetylase to repress transcription. *Nature* **391**, 597–601 (1998).

264. Nielsen, S. J. *et al.* Rb targets histone H3 methylation and HP1 to promoters. *Nature* **412**, 561–565 (2001).

265. Lundberg, A. S. & Weinberg, R. A. Functional Inactivation of the Retinoblastoma Protein Requires Sequential Modification by at Least Two Distinct Cyclin-cdk Complexes. *Mol. Cell. Biol.* **18**, 753–761 (1998).

266. Goodrich, D. W., Wang, N. P., Qian, Y.-W., Lee, E. Y.-H. P. & Lee, W.-H. The retinoblastoma gene product regulates progression through the G1 phase of the cell cycle. *Cell* **67**, 293–302 (1991).

267. Bagchi, S., Weinmann, R. & Raychaudhuri, P. The retinoblastoma protein copurifies with E2F-I, an E1A-regulated inhibitor of the transcription factor E2F. *Cell* **65**, 1063–1072 (1991).

268. Buchkovich, K., Duffy, L. A. & Harlow, E. The retinoblastoma protein is phosphorylated during specific phases of the cell cycle. *Cell* **58**, 1097–1105 (1989).

269. Ludlow, J. W., Shon, J., Pipas, J. M., Livingston, D. M. & DeCaprio, J. A. The retinoblastoma susceptibility gene product undergoes cell cycle-dependent dephosphorylation and binding to and release from SV40 large T. *Cell* **60**, 387–396 (1990).

270. DeCaprio, J. A. *et al.* The product of the retinoblastoma susceptibility gene has properties of a cell cycle regulatory element. *Cell* **58**, 1085–1095 (1989).

271. Dyson, N. The regulation of E2F by pRB-family proteins. *Genes Dev.* **12**, 2245–2262 (1998).

272. Sherr, C. J. & Roberts, J. M. CDK inhibitors: positive and negative regulators of G1-phase progression. *Genes Dev.* **13**, 1501–1512 (1999).

273. Ekholm, S. V. & Reed, S. I. Regulation of G1 cyclin-dependent kinases in the mammalian cell cycle. *Curr. Opin. Cell Biol.* **12**, 676–684 (2000).

274. Russo, A. A., Tong, L., Lee, J.-O., Jeffrey, P. D. & Pavletich, N. P. Structural basis for inhibition of the cyclin-dependent kinase Cdk6 by the tumour suppressor p16INK4a. *Nature* **395**, 237–243 (1998).

275. Blain, S. W., Montalvo, E. & Massagué, J. Differential Interaction of the Cyclin-dependent Kinase (Cdk) Inhibitor p27Kip1 with Cyclin A-Cdk2 and Cyclin D2-Cdk4 *. *J. Biol. Chem.* **272**, 25863–25872 (1997).

276. LaBaer, J. *et al.* New functional activities for the p21 family of CDK inhibitors. *Genes Dev.* **11**, 847–862 (1997).

277. James, M. K., Ray, A., Leznova, D. & Blain, S. W. Differential Modification of p27Kip1 Controls Its Cyclin D-cdk4 Inhibitory Activity. *Mol. Cell. Biol.* **28**, 498–510 (2008).

278. Indovina, P., Marcelli, E., Casini, N., Rizzo, V. & Giordano, A. Emerging roles of RB family: New defense mechanisms against tumor progression. *J. Cell. Physiol.* **228**, 525–535 (2013).

279. Zheng, L., Flesken-Nikitin, A., Chen, P.-L. & Lee, W.-H. Deficiency of Retinoblastoma gene in mouse embryonic stem cells leads to genetic instability. *Cancer Res.* **62**, 2498–2502 (2002).

280. Hernando, E. *et al.* Rb inactivation promotes genomic instability by uncoupling cell cycle progression from mitotic control. *Nature* **430**, 797–802 (2004).

281. van Harn, T. *et al.* Loss of Rb proteins causes genomic instability in the absence of mitogenic signaling. *Genes Dev.* **24**, 1377–1388 (2010).

282. Manning, A. L., Longworth, M. S. & Dyson, N. J. Loss of pRB causes centromere dysfunction and chromosomal instability. *Genes Dev.* **24**, 1364–1376 (2010).

283. Srinivasan, S. V., Mayhew, C. N., Schwemberger, S., Zagorski, W. & Knudsen, E. S. RB Loss Promotes Aberrant Ploidy by Deregulating Levels and Activity of DNA Replication Factors*. *J. Biol. Chem.* **282**, 23867–23877 (2007).

284. Iovino, F., Lentini, L., Amato, A. & Di Leonardo, A. RB acute loss induces centrosome amplification and aneuploidy in murine primary fibroblasts. *Mol. Cancer* **5**, 38 (2006).

285. Mayhew, C. N. *et al.* Liver-Specific pRB Loss Results in Ectopic Cell Cycle Entry and Aberrant Ploidy. *Cancer Res.* **65**, 4568–4577 (2005).

286. Gonzalo, S. *et al.* Role of the RB1 family in stabilizing histone methylation at constitutive heterochromatin. *Nat. Cell Biol.* **7**, 420–428 (2005).

287. Gonzalo, S. & Blasco, M. A. Role of Rb family in the epigenetic definition of chromatin. *Cell Cycle Georget. Tex* **4**, 752–755 (2005).

288. Weintraub, S. J. *et al.* Mechanism of active transcriptional repression by the retinoblastoma protein. *Nature* **375**, 812–815 (1995).

289. Zheng, L., Chen, Y., Riley, D. J., Chen, P.-L. & Lee, W.-H. Retinoblastoma Protein Enhances the Fidelity of Chromosome Segregation Mediated by hsHec1p. *Mol. Cell. Biol.* **20**, 3529–3537 (2000).

290. Sotillo, R. *et al.* Mad2 overexpression promotes aneuploidy and tumorigenesis in mice. *Cancer Cell* **11**, 9–23 (2007).

291. Vélez-Cruz, R. *et al.* RB localizes to DNA double-strand breaks and promotes DNA end resection and homologous recombination through the recruitment of BRG1. *Genes Dev.* **30**, 2500–2512 (2016).

292. Campisi, J. Cellular senescence as a tumor-suppressor mechanism. *Trends Cell Biol.* **11**, S27-31 (2001).

293. Xu, H.-J. *et al.* Reexpression of the retinoblastoma protein in tumor cells induces senescence and telomerase inhibition. *Oncogene* **15**, 2589–2596 (1997).

294. Thomas, D. M. *et al.* The retinoblastoma protein acts as a transcriptional coactivator required for osteogenic differentiation. *Mol. Cell* **8**, 303–316 (2001).

295. Dasgupta, P., Padmanabhan, J. & Chellappan, S. Rb function in the apoptosis and senescence of non-neuronal and neuronal cells: role in oncogenesis. *Curr. Mol. Med.* **6**, 719–729 (2006).

296. Sage, J., Miller, A. L., Pérez-Mancera, P. A., Wysocki, J. M. & Jacks, T. Acute mutation of retinoblastoma gene function is sufficient for cell cycle re-entry. *Nature* **424**, 223–228 (2003).

297. Steiner, M. S., Wang, Y., Zhang, Y., Zhang, X. & Lu, Y. p16/MTS1/INK4A suppresses prostate cancer by both pRb dependent and independent pathways. *Oncogene* **19**, 1297–1306 (2000).

298. Narita, M. *et al.* Rb-Mediated Heterochromatin Formation and Silencing of E2F Target Genes during Cellular Senescence. *Cell* **113**, 703–716 (2003).

299. Kerr, J. F., Wyllie, A. H. & Currie, A. R. Apoptosis: a basic biological phenomenon with wide-ranging implications in tissue kinetics. *Br. J. Cancer* **26**, 239–257 (1972).

300. Kerr, J. F., Winterford, C. M. & Harmon, B. V. Apoptosis. Its significance in cancer and cancer therapy. *Cancer* **73**, 2013–2026 (1994).

301. Wyllie, A. H., Kerr, J. F. & Currie, A. R. Cell death: the significance of apoptosis. *Int. Rev. Cytol.* **68**, 251–306 (1980).

302. Bowen, C., Spiegel, S. & Gelmann, E. P. Radiation-induced Apoptosis Mediated by Retinoblastoma Protein1. *Cancer Res.* **58**, 3275–3281 (1998).

303. Jiang, Y., Saavedra, H. I., Holloway, M. P., Leone, G. & Altura, R. A. Aberrant regulation of survivin by the RB/E2F family of proteins. *J. Biol. Chem.* **279**, 40511–40520 (2004).

304. Chan, H. M., Krstic-Demonacos, M., Smith, L., Demonacos, C. & Thangue, N. B. L. Acetylation control of the retinoblastoma tumour-suppressor protein. *Nat. Cell Biol.* **3**, 667–674 (2001).

305. Hsieh, J. K. *et al.* RB regulates the stability and the apoptotic function of p53 via MDM2. *Mol. Cell* **3**, 181–193 (1999).

306. Chau, B. N. & Wang, J. Y. J. Coordinated regulation of life and death by RB. *Nat. Rev. Cancer* **3**, 130–138 (2003).

307. Macleod, K. F., Hu, Y. & Jacks, T. Loss of Rb activates both p53-dependent and independent cell death pathways in the developing mouse nervous system. *EMBO J.* **15**, 6178–6188 (1996).

308. Morgenbesser, S. D., Williams, B. O., Jacks, T. & DePinho, R. A. p53-dependent apoptosis produced by Rb-deficiency in the developing mouse lens. *Nature* **371**, 72–74 (1994).

309. Lee, E. Y.-H. P. *et al.* Mice deficient for Rb are nonviable and show defects in neurogenesis and haematopoiesis. *Nature* **359**, 288–294 (1992).

310. Moroni, M. C. *et al.* Apaf-1 is a transcriptional target for E2F and p53. *Nat. Cell Biol.* **3**, 552–558 (2001).

311. Nahle, Z. *et al.* Direct coupling of the cell cycle and cell death machinery by E2F. *Nat. Cell Biol.* **4**, 859–864 (2002).

312. Chau, B. N. *et al.* Signal-dependent protection from apoptosis in mice expressing caspase-resistant Rb. *Nat. Cell Biol.* **4**, 757–765 (2002).

313. Glozak, M. A. & Rogers, M. B. Retinoic Acid- and Bone Morphogenetic Protein 4-Induced Apoptosis in P19 Embryonal Carcinoma Cells Requires p27. *Exp. Cell Res.* **268**, 128–138 (2001).

314. Adegbola, O. & Pasternack, G. R. Phosphorylated retinoblastoma protein complexes with pp32 and inhibits pp32-mediated apoptosis. *J. Biol. Chem.* **280**, 15497–15502 (2005).

315. Wang, R.-H., Liu, C. W. Y., Avramis, V. I. & Berndt, N. Protein phosphatase 1α-mediated stimulation of apoptosis is associated with dephosphorylation of the retinoblastoma protein. *Oncogene* **20**, 6111–6122 (2001).

316. Tracy, K. *et al.* BNIP3 is an RB/E2F target gene required for hypoxia-induced autophagy. *Mol. Cell. Biol.* **27**, 6229–6242 (2007).

317. Wei, R. *et al.* Rb1/Rbl1/Vhl loss induces mouse subretinal angiomatous proliferation and hemangioblastoma. *JCI Insight* **4**, e127889.

318. Burkhart, D. L. & Sage, J. Cellular mechanisms of tumour suppression by the retinoblastoma gene. *Nat. Rev. Cancer* **8**, 671–682 (2008).

319. Takahashi, C., Contreras, B., Bronson, R. T., Loda, M. & Ewen, M. E. Genetic interaction between Rb and K-ras in the control of differentiation and tumor suppression. *Mol. Cell. Biol.* **24**, 10406–10415 (2004).

320. Berman, S. D. *et al.* The retinoblastoma protein tumor suppressor is important for appropriate osteoblast differentiation and bone development. *Mol. Cancer Res. MCR* **6**, 1440–1451 (2008).

321. Classon, M., Kennedy, B. K., Mulloy, R. & Harlow, E. Opposing roles of pRB and p107 in adipocyte differentiation. *Proc. Natl. Acad. Sci.* **97**, 10826–10831 (2000).

322. Pickard, A., Wong, P.-P. & McCance, D. J. Acetylation of Rb by PCAF is required for nuclear localization and keratinocyte differentiation. *J. Cell Sci.* **123**, 3718–3726 (2010).

323. Bergh, G., Ehinger, M., Olsson, I., Jacobsen, S. E. & Gullberg, U. Involvement of the retinoblastoma protein in monocytic and neutrophilic lineage commitment of human bone marrow progenitor cells. *Blood* **94**, 1971–1978 (1999).

324. Skapek, S. X., Pan, Y.-R. & Lee, E. Y.-H. P. Regulation of cell lineage specification by the retinoblastoma tumor suppressor. *Oncogene* **25**, 5268–5276 (2006).

325. De Falco, G., Comes, F. & Simone, C. pRb: master of differentiation. Coupling irreversible cell cycle withdrawal with induction of muscle-specific transcription. *Oncogene* **25**, 5244–5249 (2006).

326. Novitch, B. G., Spicer, D. B., Kim, P. S., Cheung, W. L. & Lassar, A. B. pRb is required for MEF2-dependent gene expression as well as cell-cycle arrest during skeletal muscle differentiation. *Curr. Biol. CB* **9**, 449–459 (1999).

327. Schneider, J. W., Gu, W., Zhu, L., Mahdavi, V. & Nadal-Ginard, B. Reversal of terminal differentiation mediated by p107 in Rb-/- muscle cells. *Science* **264**, 1467–1471 (1994).

328. Puri, P. L. *et al.* Class I histone deacetylases sequentially interact with MyoD and pRb during skeletal myogenesis. *Mol. Cell* **8**, 885–897 (2001).

329. Miyake, S. *et al.* Cells degrade a novel inhibitor of differentiation with E1A-like properties upon exiting the cell cycle. *Mol. Cell. Biol.* **20**, 8889–8902 (2000).

330. Annicotte, J.-S. *et al.* The CDK4-pRB-E2F1 pathway controls insulin secretion. *Nat. Cell Biol.* **11**, 1017–1023 (2009).

331. Hsieh, M. C. F., Das, D., Sambandam, N., Zhang, M. Q. & Nahlé, Z. Regulation of the PDK4 Isozyme by the Rb-E2F1 Complex*. *J. Biol. Chem.* **283**, 27410–27417 (2008).

332. Lu, Z. *et al.* pRb is an obesity suppressor in hypothalamus and high-fat diet inhibits pRb in this location. *EMBO J.* **32**, 844–857 (2013).

333. Sankaran, V. G., Stuart H. Orkin & Walkley, C. R. Rb intrinsically promotes erythropoiesis by coupling cell cycle exit with mitochondrial biogenesis. *Genes Dev.* **22**, 463–475 (2008).

334. Ciavarra, G. & Zacksenhaus, E. Rescue of myogenic defects in Rb-deficient cells by inhibition of autophagy or by hypoxia-induced glycolytic shift. *J. Cell Biol.* **191**, 291–301 (2010).

335. DeGregori, J., Kowalik, T. & Nevins, J. R. Cellular targets for activation by the E2F1 transcription factor include DNA synthesis- and G1/S-regulatory genes. *Mol. Cell. Biol.* **15**, 4215–4224 (1995).

336. Dou, Q. P. *et al.* G1/S-regulated E2F-containing protein complexes bind to the mouse thymidine kinase gene promoter. *J. Biol. Chem.* **269**, 1306–1313 (1994).

337. Good, L., Chen, J. & Chen, K. Y. Analysis of sequence-specific binding activity of cis-elements in human thymidine kinase gene promoter during G1/S phase transition. *J. Cell. Physiol.* **163**, 636–644 (1995).

338. Good, L., Dimri, G. P., Campisi, J. & Chen, K. Y. Regulation of dihydrofolate reductase gene expression and E2F components in human diploid fibroblasts during growth and senescence. *J. Cell. Physiol.* **168**, 580–588 (1996).

339. Angus, S. P. *et al.* Retinoblastoma Tumor Suppressor Targets dNTP Metabolism to Regulate DNA Replication *. *J. Biol. Chem.* **277**, 44376–44384 (2002).

340. Blanchet, E. *et al.* E2F transcription factor-1 regulates oxidative metabolism. *Nat. Cell Biol.* **13**, 1146–1152 (2011).

341. Dyson, N., Howley, P. M., Münger, K. & Harlow, E. The human papilloma virus-16 E7 oncoprotein is able to bind to the retinoblastoma gene product. *Science* **243**, 934–937 (1989).

342. Whyte, P., Williamson, N. M. & Harlow, E. Cellular targets for transformation by the adenovirus E1A proteins. *Cell* **56**, 67–75 (1989).

343. Bookstein, R., Shew, J. Y., Chen, P. L., Scully, P. & Lee, W. H. Suppression of tumorigenicity of human prostate carcinoma cells by replacing a mutated RB gene. *Science* **247**, 712–715 (1990).

344. Huang, H. J. *et al.* Suppression of the neoplastic phenotype by replacement of the RB gene in human cancer cells. *Science* **242**, 1563–1566 (1988).

345. Takahashi, R. *et al.* The retinoblastoma gene functions as a growth and tumor suppressor in human bladder carcinoma cells. *Proc. Natl. Acad. Sci. U. S. A.* **88**, 5257 (1991).

346. Bindra, R. S., Vasselli, J. R., Stearman, R., Linehan, W. M. & Klausner, R. D. VHL-mediated hypoxia regulation of cyclin D1 in renal carcinoma cells. *Cancer Res.* **62**, 3014–3019 (2002).

347. Chatterjee, S. J. *et al.* Hyperphosphorylation of pRb: a mechanism for RB tumour suppressor pathway inactivation in bladder cancer. *J. Pathol.* **203**, 762–770 (2004).

348. Sage, J. The retinoblastoma tumor suppressor and stem cell biology. *Genes Dev.* **26**, 1409–1420 (2012).

349. Dyson, N. J. RB1: a prototype tumor suppressor and an enigma. *Genes Dev.* **30**, 1492–1502 (2016).

350. Kitajima, S. & Takahashi, C. Intersection of retinoblastoma tumor suppressor function, stem cells, metabolism, and inflammation. *Cancer Sci.* **108**, 1726–1731 (2017).

351. Ciavarra, G. & Zacksenhaus, E. Direct and indirect effects of the pRb tumor suppressor on autophagy. *Autophagy* **7**, 544–546 (2011).

352. Indovina, P., Pentimalli, F., Casini, N., Vocca, I. & Giordano, A. RB1 dual role in proliferation and apoptosis: cell fate control and implications for cancer therapy. *Oncotarget* **6**, 17873–17890 (2015).

353. Nicolay, B. N. & Dyson, N. J. The multiple connections between pRB and cell metabolism. *Curr. Opin. Cell Biol.* **25**, 735–740 (2013).

354. Warneford, S., Townsend, M., Rowe, P. B., Dalla-Pozza, L. & Symonds, G. Overexpression of the retinoblastoma gene in a familial adrenocortical carcinoma. *Cell Growth Differ. Mol. Biol. J. Am. Assoc. Cancer Res.* **2**, 439–445 (1991).

355. Plath, T. *et al.* Overexpression of pRB in human pancreatic carcinoma cells: function in chemotherapy-induced apoptosis. *J. Natl. Cancer Inst.* **94**, 129–142 (2002).

356. Jiang, Z. & Zacksenhaus, E. Activation of retinoblastoma protein in mammary gland leads to ductal growth suppression, precocious differentiation, and adenocarcinoma. *J. Cell Biol.* **156**, 185–198 (2002).

357. Harlander, S. *et al.* Combined mutation in Vhl, Trp53 and Rb1 causes clear cell renal cell carcinoma in mice. *Nat. Med.* **23**, 869–877 (2017).

358. Budde, A., Schneiderhan-Marra, N., Petersen, G. & Brüne, B. Retinoblastoma susceptibility gene product pRB activates hypoxia-inducible factor-1 (HIF-1). *Oncogene* **24**, 1802–1808 (2005).

359. Rudnick, P. A. *et al.* A Description of the Clinical Proteomic Tumor Analysis Consortium (CPTAC) Common Data Analysis Pipeline. *J. Proteome Res.* **15**, 1023–1032 (2016).

360. Chandrashekar, D. S. *et al.* UALCAN: A Portal for Facilitating Tumor Subgroup Gene Expression and Survival Analyses. *Neoplasia* **19**, 649–658 (2017).

361. Livak, K. J. & Schmittgen, T. D. Analysis of relative gene expression data using real-time quantitative PCR and the 2(-Delta Delta C(T)) Method. *Methods San Diego Calif* **25**, 402–408 (2001).

362. Bourgey, M. *et al.* GenPipes: an open-source framework for distributed and scalable genomic analyses. *GigaScience* **8**, giz037 (2019).

363. Matys, V. *et al.* TRANSFAC: transcriptional regulation, from patterns to profiles. *Nucleic Acids Res.* **31**, 374–378 (2003).

364. Rouillard, A. D. *et al.* The harmonizome: a collection of processed datasets gathered to serve and mine knowledge about genes and proteins. *Database J. Biol. Databases Curation* **2016**, baw100 (2016).

365. Park, M. H., Choi, K.-Y., Jung, Y. & Min, D. S. Phospholipase D1 protein coordinates dynamic assembly of HIF-1α-PHD-VHL to regulate HIF-1α stability. *Oncotarget* **5**, 11857–11872 (2014).

366. Kim, D.-S. *et al.* Cancer cells promote survival through depletion of the von Hippel–Lindau tumor suppressor by protein crosslinking. *Oncogene* **30**, 4780–4790 (2011).

367. Dengler, V. L., Galbraith, M. & Espinosa, J. M. Transcriptional Regulation by Hypoxia Inducible Factors. *Crit. Rev. Biochem. Mol. Biol.* **49**, 1–15 (2014).

368. Ke, Q. & Costa, M. Hypoxia-Inducible Factor-1 (HIF-1). *Mol. Pharmacol.* **70**, 1469–1480 (2006).

369. Hong, K. *et al.* USP37 promotes deubiquitination of HIF2α in kidney cancer. *Proc. Natl. Acad. Sci. U. S. A.* **117**, 13023–13032 (2020).

370. Kaplan, E. L. & Meier, P. Nonparametric Estimation from Incomplete Observations. *J. Am. Stat. Assoc.* **53**, 457–481 (1958).

371. Kasten, M. M. & Giordano, A. pRb and the Cdks in apoptosis and the cell cycle. *Cell Death Differ.* **5**, 132–140 (1998).

372. Clarke, A. R. *et al.* Requirement for a functional Rb-1 gene in murine development. *Nature* **359**, 328–330 (1992).

373. Haas-Kogan, D. A. *et al.* Inhibition of apoptosis by the retinoblastoma gene product. *EMBO J.* **14**, 461–472 (1995).

374. Haupt, Y., Rowan, S., Shaulian, E., Vousden, K. H. & Oren, M. Induction of apoptosis in HeLa cells by trans-activation-deficient p53. *Genes Dev.* **9**, 2170–2183 (1995).

375. Berry, D. E. *et al.* Retinoblastoma protein inhibits IFN-gamma induced apoptosis. *Oncogene* **12**, 1809–1819 (1996).

376. de Larco, J. E. & Todaro, G. J. Growth factors from murine sarcoma virus-transformed cells. *Proc. Natl. Acad. Sci.* **75**, 4001–4005 (1978).

377. Hamburger, A. W. & Salmon, S. E. Primary bioassay of human tumor stem cells. *Science* **197**, 461–463 (1977).

378. Roberts, A. B. *et al.* Type beta transforming growth factor: a bifunctional regulator of cellular growth. *Proc. Natl. Acad. Sci. U. S. A.* **82**, 119–123 (1985).

379. Szekely, L. *et al.* Subcellular localization of the retinoblastoma protein. *Cell Growth Differ. Mol. Biol. J. Am. Assoc. Cancer Res.* **2**, 287–295 (1991).

380. Jiao, W., Datta, J., Lin, H.-M., Dundr, M. & Rane, S. G. Nucleocytoplasmic Shuttling of the Retinoblastoma Tumor Suppressor Protein via Cdk Phosphorylation-dependent Nuclear Export*. *J. Biol. Chem.* **281**, 38098–38108 (2006).

381. Lee, S. *et al.* Nuclear/cytoplasmic localization of the von Hippel-Lindau tumor suppressor gene product is determined by cell density. *Proc. Natl. Acad. Sci. U. S. A.* **93**, 1770–1775 (1996).

382. Cho, K. F. *et al.* Proximity labeling in mammalian cells with TurboID and split-TurboID. *Nat. Protoc.* **15**, 3971–3999 (2020).

383. Varga, J., Kube, M., Luck, K. & Schick, S. The BAF chromatin remodeling complexes: structure, function, and synthetic lethalities. *Biochem. Soc. Trans.* **49**, 1489–1503 (2021).

384. Skene, P. J., Henikoff, J. G. & Henikoff, S. Targeted in situ genome-wide profiling with high efficiency for low cell numbers. *Nat. Protoc.* **13**, 1006–1019 (2018).

385. Skene, P. J. & Henikoff, S. An efficient targeted nuclease strategy for high-resolution mapping of DNA binding sites. *eLife* **6**, e21856 (2017).

386. Nicholson, H. E. *et al.* HIF-independent synthetic lethality between CDK4/6 inhibition and VHL loss across species. *Sci. Signal.* **12**, eaay0482 (2019).

387. Shah, M., Nunes, M. R. & Stearns, V. CDK4/6 Inhibitors: Game Changers in the Management of Hormone Receptor–Positive Advanced Breast Cancer? *Oncol. Williston Park N* **32**, 216–222 (2018).

388. Schaffner-Sabba, K., Schmidt-Ruppin, K. H., Wehrli, W., Schuerch, A. R. & Wasley, J. W. beta-Lapachone: synthesis of derivatives and activities in tumor models. *J. Med. Chem.* **27**, 990–994 (1984).

389. Ferraz da Costa, D. C. *et al.* Anticancer Potential of Resveratrol, β-Lapachone and Their Analogues. *Molecules* **25**, 893 (2020).

390. Moon, D.-O. *et al.* β-Lapachone (LAPA) Decreases Cell Viability and Telomerase Activity in Leukemia Cells: Suppression of Telomerase Activity by LAPA. *J. Med. Food* **13**, 481–488 (2010).

391. Li, Y., Sun, X., LaMont, J. T., Pardee, A. B. & Li, C. J. Selective killing of cancer cells by beta -lapachone: direct checkpoint activation as a strategy against cancer. *Proc. Natl. Acad. Sci. U. S. A.* **100**, 2674–2678 (2003).

392. Zheng, S. *et al.* SynergyFinder Plus: Toward Better Interpretation and Annotation of Drug Combination Screening Datasets. *Genomics Proteomics Bioinformatics* **20**, 587–596 (2022).

393. Yadav, B., Wennerberg, K., Aittokallio, T. & Tang, J. Searching for Drug Synergy in Complex Dose–Response Landscapes Using an Interaction Potency Model. *Comput. Struct. Biotechnol. J.* **13**, 504–513 (2015).

394. Bliss, C. I. The Toxicity of Poisons Applied Jointly. *Ann. Appl. Biol.* **26**, 585–615 (1939).

395. Connell-Crowley, L., Harper, J. W. & Goodrich, D. W. Cyclin D1/Cdk4 regulates retinoblastoma protein-mediated cell cycle arrest by site-specific phosphorylation. *Mol. Biol. Cell* **8**, 287–301 (1997).

396. Vidaurreta, M. *et al.* Inactivation of p16 by CpG hypermethylation in renal cell carcinoma. *Urol. Oncol.* **26**, 239–245 (2008).

397. Jacks, T. *et al.* Effects of an Rb mutation in the mouse. *Nature* **359**, 295–300 (1992).

398. Berger, A. H. *et al.* Transcriptional Changes in Regulatory T Cells From Patients With Autoimmune Polyendocrine Syndrome Type 1 Suggest Functional Impairment of Lipid Metabolism and Gut Homing. *Front. Immunol.* **12**, 722860 (2021).

399. Lopes, B. A. *et al.* Novel Diagnostic and Therapeutic Options for KMT2A-Rearranged Acute Leukemias. *Front. Pharmacol.* **13**, 749472 (2022).

400. Sun, B., Wingate, H., Swisher, S. G., Keyomarsi, K. & Hunt, K. K. Absence of pRb facilitates E2F1-induced apoptosis in breast cancer cells. *Cell Cycle Georget. Tex* **9**, 1122–1130 (2010).

401. Hsieh, J. K., Fredersdorf, S., Kouzarides, T., Martin, K. & Lu, X. E2F1-induced apoptosis requires DNA binding but not transactivation and is inhibited by the retinoblastoma protein through direct interaction. *Genes Dev.* **11**, 1840–1852 (1997).

402. Zhang, C.-S. *et al.* RHOBTB3 promotes proteasomal degradation of HIFα through facilitating hydroxylation and suppresses the Warburg effect. *Cell Res.* **25**, 1025–1042 (2015).

403. Thompson, C. B. Apoptosis in the pathogenesis and treatment of disease. *Science* **267**, 1456–1462 (1995).

404. Calcinotto, A. *et al.* Cellular Senescence: Aging, Cancer, and Injury. *Physiol. Rev.* **99**, 1047–1078 (2019).

405. Sleeboom, J. J. F. *et al.* The extracellular matrix as hallmark of cancer and metastasis: From biomechanics to therapeutic targets. *Sci. Transl. Med.* **16**, eadg3840 (2024).

406. Cecchini, M. J. & Dick, F. A. The biochemical basis of CDK phosphorylation-independent regulation of E2F1 by the retinoblastoma protein. *Biochem. J.* **434**, 297–308 (2011).

407. Rubin, S. M., Gall, A.-L., Zheng, N. & Pavletich, N. P. Structure of the Rb C-Terminal Domain Bound to E2F1-DP1: A Mechanism for Phosphorylation-Induced E2F Release. *Cell* **123**, 1093–1106 (2005).

408. Calbó, J. *et al.* G1 Cyclin/Cyclin-dependent Kinase-coordinated Phosphorylation of Endogenous Pocket Proteins Differentially Regulates Their Interactions with E2F4 and E2F1 and Gene Expression *. *J. Biol. Chem.* **277**, 50263–50274 (2002).

409. Helin, K. & Ed, H. The retinoblastoma protein as a transcriptional repressor. *Trends Cell Biol.* **3**, 43–46 (1993).

410. Vandel, L. *et al.* Transcriptional Repression by the Retinoblastoma Protein through the Recruitment of a Histone Methyltransferase. *Mol. Cell. Biol.* **21**, 6484–6494 (2001).

411. Robertson, K. D. *et al.* DNMT1 forms a complex with Rb, E2F1 and HDAC1 and represses transcription from E2F-responsive promoters. *Nat. Genet.* **25**, 338–342 (2000).

412. Dunaief, J. L. *et al.* The retinoblastoma protein and BRG1 form a complex and cooperate to induce cell cycle arrest. *Cell* **79**, 119–130 (1994).

413. Strober, B. E., Dunaief, J. L., Guha & Goff, S. P. Functional interactions between the hBRM/hBRG1 transcriptional activators and the pRB family of proteins. *Mol. Cell. Biol.* **16**, 1576–1583 (1996).

414. Zhang, H. S. *et al.* Exit from G1 and S phase of the cell cycle is regulated by repressor complexes containing HDAC-Rb-hSWI/SNF and Rb-hSWI/SNF. *Cell* **101**, 79–89 (2000).

415. Wang, W. *et al.* Purification and biochemical heterogeneity of the mammalian SWI-SNF complex. *EMBO J.* **15**, 5370–5382 (1996).

416. Whitehouse, I. *et al.* Nucleosome mobilization catalysed by the yeast SWI/SNF complex. *Nature* **400**, 784–787 (1999).

417. McBride, M. J. & Kadoch, C. Disruption of mammalian SWI/SNF and polycomb complexes in human sarcomas: mechanisms and therapeutic opportunities. *J. Pathol.* **244**, 638–649 (2018).

418. Kadoch, C. *et al.* Proteomic and bioinformatic analysis of mammalian SWI/SNF complexes identifies extensive roles in human malignancy. *Nat. Genet.* **45**, 592–601 (2013).

419. D'Ambrosio, A. *et al.* Increased genomic instability and reshaping of tissue microenvironment underlie oncogenic properties of Arid1a mutations. *Sci. Adv.* **10**, eadh4435 (2024).

420. Jackson, S. P. & Bartek, J. The DNA-damage response in human biology and disease. *Nature* **461**, 1071–1078 (2009).

421. Basu, A. K. DNA Damage, Mutagenesis and Cancer. *Int. J. Mol. Sci.* **19**, 970 (2018).

422. Strobeck, M. W. *et al.* BRG-1 is required for RB-mediated cell cycle arrest. *Proc. Natl. Acad. Sci. U. S. A.* **97**, 7748–7753 (2000).

423. Li, C. *et al.* A phase Ib trial of ARQ 501, a selective checkpoint activator, in combination with docetaxel in patients with advanced solid tumors. *J. Clin. Oncol.* **24**, 13053–13053 (2006).

424. Shapiro, G. I. *et al.* Phase I trial of ARQ 501, an Activated Checkpoint Therapy (ACT) agent, in patients with advanced solid tumors. *J. Clin. Oncol.* **23**, 3042–3042 (2005).

425. Gu, Y.-F. *et al.* Modeling Renal Cell Carcinoma in Mice: Bap1 and Pbrm1 Inactivation Drive Tumor Grade. *Cancer Discov.* **7**, 900–917 (2017).

426. Nargund, A. M. *et al.* The SWI/SNF Protein PBRM1 Restrains VHL-Loss-Driven Clear Cell Renal Cell Carcinoma. *Cell Rep.* **18**, 2893–2906 (2017).

427. Sledge, G. W., Jr *et al.* The Effect of Abemaciclib Plus Fulvestrant on Overall Survival in Hormone Receptor–Positive, ERBB2-Negative Breast Cancer That Progressed on Endocrine Therapy—MONARCH 2: A Randomized Clinical Trial. *JAMA Oncol.* **6**, 116–124 (2020).

428. Sledge, G. W. *et al.* MONARCH 2: Abemaciclib in Combination With Fulvestrant in Women With HR+/HER2− Advanced Breast Cancer Who Had Progressed While Receiving Endocrine Therapy. *J. Clin. Oncol.* **35**, 2875–2884 (2017).

429. Turner, N. C. *et al.* Palbociclib in Hormone-Receptor–Positive Advanced Breast Cancer. *N. Engl. J. Med.* **373**, 209–219 (2015).

430. Li, C. J., Averboukh, L. & Pardee, A. B. beta-Lapachone, a novel DNA topoisomerase I inhibitor with a mode of action different from camptothecin. *J. Biol. Chem.* **268**, 22463–22468 (1993).

431. Pink, J. J. *et al.* NAD(P)H:Quinone Oxidoreductase Activity Is the Principal Determinant of β-Lapachone Cytotoxicity *. *J. Biol. Chem.* **275**, 5416–5424 (2000).

432. Reinicke, K. E. *et al.* Development of β-Lapachone Prodrugs for Therapy Against Human Cancer Cells with Elevated NAD(P)H:Quinone Oxidoreductase 1 Levels. *Clin. Cancer Res.* **11**, 3055–3064 (2005).

433. Bey, E. A. *et al.* An NQO1- and PARP-1-mediated cell death pathway induced in non-small-cell lung cancer cells by β-lapachone. *Proc. Natl. Acad. Sci.* **104**, 11832–11837 (2007).

434. Li, L. S. *et al.* Modulating Endogenous NQO1 Levels Identifies Key Regulatory Mechanisms of Action of β-Lapachone for Pancreatic Cancer Therapy. *Clin. Cancer Res.* **17**, 275–285 (2011).

435. Bentle, M. S., Reinicke, K. E., Bey, E. A., Spitz, D. R. & Boothman, D. A. Calcium-dependent Modulation of Poly(ADP-ribose) Polymerase-1 Alters Cellular Metabolism and DNA Repair *. *J. Biol. Chem.* **281**, 33684–33696 (2006).

436. Yu, H. Y. *et al.* β-lapachone-Induced Apoptosis of Human Gastric Carcinoma AGS Cells Is Caspase-Dependent and Regulated by the PI3K/Akt Pathway. *Biomol. Ther.* **22**, 184–192 (2014).

437. Bermejo, M., Mangas-Sanjuan, V., Gonzalez-Alvarez, I. & Gonzalez-Alvarez, M. Enhancing Oral Absorption of β-Lapachone: Progress Till Date. *Eur. J. Drug Metab. Pharmacokinet.* **42**, 1–10 (2017).

438. Liu, C. *et al.* Oral bioavailability enhancement of β-lapachone, a poorly soluble fast crystallizer, by cocrystal, amorphous solid dispersion, and crystalline solid dispersion. *Eur. J. Pharm. Biopharm.* **124**, 73–81 (2018).

439. Kim, I. *et al.* Preclinical Pharmacokinetic Evaluation of β-Lapachone: Characteristics of Oral Bioavailability and First-Pass Metabolism in Rats. *Biomol. Ther.* **23**, 296–300 (2015).

440. Kaelin, W. G. Von Hippel–Lindau disease: insights into oxygen sensing, protein degradation, and cancer. *J. Clin. Invest.* **132**, e162480.

441. Zhang, J., Schweers, B. & Dyer, M. A. The First Knockout Mouse Model of Retinoblastoma. *Cell Cycle* **3**, 950–957 (2004).

442. MacPherson, D. *et al.* Cell type-specific effects of Rb deletion in the murine retina. *Genes Dev.* **18**, 1681–1694 (2004).

443. Chen, D. *et al.* Cell-specific effects of RB or RB/p107 loss on retinal development implicate an intrinsically death-resistant cell-of-origin in retinoblastoma. *Cancer Cell* **5**, 539–551 (2004).

Appendices

Appendix A: Genes upregulated by *RB1* KO in 786-O cells.

Gene name	Ensembl gene ID	log2FoldChange	p-value	Adjusted p-value
AP003064.1	ENSG00000255126	8.694973758	6.95E-13	6.18E-11
ZNF135	ENSG00000176293	8.33703019	8.67E-12	6.52E-10
AP003306.2	ENSG00000255118	7.735901911	4.09E-10	2.38E-08
SERPINB2	ENSG00000197632	6.741911011	2.09E-07	6.99E-06
AL354813.1	ENSG00000255438	6.735768471	2.46E-07	8.04E-06
CLDN10	ENSG00000134873	6.489948191	8.43E-07	2.51E-05
LEF1-AS1	ENSG00000232021	6.32809166	1.83E-06	5.09E-05
AC091814.1	ENSG00000255882	6.170867007	4.91E-06	0.000125608
AC069185.1	ENSG00000255046	5.977356655	1.16E-05	0.00026855
AL358333.3	ENSG00000259007	5.836659774	9.30E-08	3.35E-06
DZIP1	ENSG00000134874	5.745789162	4.03E-05	0.000791293
AC004594.1	ENSG00000240499	5.636530827	6.85E-05	0.00126449
AP001970.1	ENSG00000254710	5.495785843	0.000127883	0.002155611
AC104667.2	ENSG00000234949	5.359670908	4.51E-09	2.22E-07
AP002383.3	ENSG00000256469	5.148040835	5.85E-46	3.98E-43
SLC24A5	ENSG00000188467	5.14273037	1.59E-10	1.02E-08
AMOTL1	ENSG00000166025	5.102515276	4.55E-08	1.78E-06
AC004551.1	ENSG00000257452	5.038399607	7.59E-27	2.15E-24
AP002008.2	ENSG00000255093	5.035377362	0.000204676	0.003190503
MYO1F	ENSG00000142347	4.966174049	1.28E-05	0.000292519
NLRP9	ENSG00000185792	4.95954591	1.18E-28	3.64E-26
AC139491.5	ENSG00000251623	4.762985053	5.83E-05	0.001099938
UBE2L6	ENSG00000156587	4.653589682	0.000904364	0.010991113
PCSK7	ENSG00000160613	4.534840993	2.65E-149	4.51E-145
GP6	ENSG00000088053	4.354442063	7.47E-06	0.000182919
CXCL2	ENSG00000081041	4.332052571	0.002719982	0.026907213
DNAH5	ENSG00000039139	4.300452295	1.92E-08	8.20E-07
RDH13	ENSG00000160439	4.185727325	1.62E-39	8.60E-37
IFI27	ENSG00000165949	4.179838498	3.73E-05	0.000738387
LINC00705	ENSG00000225269	3.937496848	4.19E-13	3.82E-11
06-Sep	ENSG00000125354	3.891233119	0.00168179	0.018341011
TENM4	ENSG00000149256	3.810096758	0.000295388	0.004322938
AP002833.2	ENSG00000255317	3.792638303	3.00E-05	0.000613388
AL031658.1	ENSG00000226239	3.730059029	8.29E-27	2.31E-24
UCHL1	ENSG00000154277	3.659439548	1.86E-40	1.02E-37
RTN4IP1	ENSG00000130347	3.583265677	0.005703423	0.048112486

AC011476.2	ENSG00000267149	3.457845767	0.000307677	0.004483481
MPP7	ENSG00000150054	3.401698566	0.002169116	0.022431806
AC068385.1	ENSG00000255498	3.37911652	5.00E-09	2.42E-07
TRPC4	ENSG00000133107	3.370962018	0.001770484	0.019057459
LINC01578	ENSG00000272888	3.35630255	4.72E-24	1.13E-21
AC010525.1	ENSG00000267117	3.142355678	1.99E-14	2.16E-12
PLAU	ENSG00000122861	3.127606757	1.72E-13	1.65E-11
AC125793.1	ENSG00000260832	3.122561057	0.004935959	0.043173312
PNPO	ENSG00000108439	2.921977492	3.72E-09	1.86E-07
HDDC3	ENSG00000184508	2.894250373	0.001710006	0.018577178
ERO1B	ENSG00000086619	2.869381769	1.52E-06	4.29E-05
FAM86FP	ENSG00000164845	2.852917774	3.54E-18	5.78E-16
WSCD1	ENSG00000179314	2.850925959	7.17E-05	0.001312641
C11orf88	ENSG00000183644	2.820046855	7.16E-13	6.34E-11
IRAK2	ENSG00000134070	2.790016184	0.000396905	0.005542083
AC027097.2	ENSG00000267787	2.780863874	5.13E-10	2.95E-08
AC068152.1	ENSG00000262879	2.741159607	1.65E-07	5.65E-06
PRR26	ENSG00000180525	2.738389315	0.000118272	0.002023529
AC027097.1	ENSG00000267040	2.720485651	1.35E-09	7.21E-08
BNIP3L	ENSG00000104765	2.670322151	3.66E-10	2.14E-08
AC008591.1	ENSG00000251680	2.641424736	1.44E-07	5.01E-06
TUBA1A	ENSG00000167552	2.622967995	5.99E-07	1.82E-05
HOXB9	ENSG00000170689	2.612695169	1.46E-05	0.000329119
YTHDF2P1	ENSG00000270503	2.598317555	1.62E-10	1.03E-08
CDK5RAP3	ENSG00000108465	2.572145489	1.81E-05	0.000397684
LAYN	ENSG00000204381	2.564278437	1.35E-09	7.21E-08
IL18R1	ENSG00000115604	2.557634717	0.001164819	0.013565076
ANKRD1	ENSG00000148677	2.547876601	3.10E-05	0.000628507
CD274	ENSG00000120217	2.526356145	8.12E-05	0.001458731
AC104667.1	ENSG00000227107	2.471347905	0.003596895	0.033616523
LRRC37A7P	ENSG00000265158	2.471225252	0.000225817	0.003456623
CCDC80	ENSG00000091986	2.46560864	6.40E-21	1.29E-18
HOXB8	ENSG00000120068	2.46525225	0.00052693	0.006989119
AC003092.2	ENSG00000236938	2.450149401	2.64E-30	9.55E-28
C10orf55	ENSG00000222047	2.449340168	1.67E-79	5.69E-76
MRC2	ENSG00000011028	2.445524523	1.73E-11	1.26E-09
SSH1	ENSG00000084112	2.441924228	0.002162819	0.0223803
MCCC2	ENSG00000131844	2.431169224	0.001187235	0.0137601
BMS1P22	ENSG00000232775	2.36615425	0.000236678	0.003590533
CAPRIN2	ENSG00000110888	2.365128486	0.001395555	0.015734484
PCSK5	ENSG00000099139	2.351295579	8.65E-05	0.001536881
BDNF-AS	ENSG00000245573	2.349411885	1.44E-55	1.75E-52
PGAM1P1	ENSG00000248271	2.341125122	5.72E-05	0.001082218

RGS3	ENSG00000138835	2.331651539	6.95E-06	0.000171437
EPHA5-AS1	ENSG00000250846	2.323397015	8.09E-06	0.000196249
MRPL50	ENSG00000136897	2.313600973	0.000318466	0.004612999
ITGB3	ENSG00000259207	2.313182221	3.38E-23	7.86E-21
NSF	ENSG00000073969	2.27530999	3.50E-12	2.75E-10
HS3ST5	ENSG00000249853	2.273487214	0.000261448	0.003913881
KCNA7	ENSG00000104848	2.24120395	5.37E-06	0.000135816
TMEM218	ENSG00000150433	2.238957345	0.000471669	0.006395918
SEMA3C	ENSG00000075223	2.219488552	2.15E-21	4.46E-19
KDR	ENSG00000128052	2.207219467	0.005472235	0.04667608
NPDC1	ENSG00000107281	2.199111139	0.00040062	0.005588616
TFPI2	ENSG00000105825	2.155988533	2.80E-10	1.71E-08
TGM4	ENSG00000163810	2.149720041	0.005664601	0.047931887
ARHGAP22	ENSG00000128805	2.12644342	3.09E-05	0.000627527
SNX11	ENSG00000002919	2.114084833	2.42E-05	0.000509353
KLHL35	ENSG00000149243	2.096099069	0.005345647	0.045826382
DAAM2	ENSG00000146122	2.094651713	0.003605231	0.03367591
MEGF6	ENSG00000162591	2.06689507	0.00083134	0.010250583
AC018521.4	ENSG00000264701	2.026172659	5.15E-49	4.38E-46
TWF2	ENSG00000247596	2.022005633	0.000105101	0.001824075
RNF2P1	ENSG00000231381	2.017827906	0.000168883	0.002707064
CALCOCO2	ENSG00000136436	2.008752309	3.17E-10	1.90E-08
EDIL3	ENSG00000164176	2.007124079	1.97E-14	2.15E-12
NPY4R	ENSG00000204174	1.999879848	0.003613361	0.033688648
FRG1HP	ENSG00000276291	1.998645497	0.004592507	0.040896897
CBX1	ENSG00000108468	1.989964443	4.41E-31	1.70E-28
ITGB2-AS1	ENSG00000227039	1.988570751	0.00514482	0.04446865
ALKBH8	ENSG00000137760	1.988068569	0.003521194	0.033146041
RASA3	ENSG00000185989	1.976491984	0.004213087	0.03828051
AC003092.1	ENSG00000236453	1.975491309	1.18E-08	5.33E-07
AL445645.1	ENSG00000224992	1.972334232	0.000658287	0.008384527
SLC9C1	ENSG00000172139	1.970305812	1.28E-09	6.91E-08
AC005670.2	ENSG00000262633	1.96859539	1.78E-31	7.20E-29
WBP1L	ENSG00000166272	1.951547112	0.002612461	0.026012718
MAMDC2-AS1	ENSG00000204706	1.93557697	6.23E-30	2.16E-27
AC040934.1	ENSG00000253347	1.935250785	1.08E-16	1.45E-14
GNGT1	ENSG00000127928	1.933267964	1.48E-48	1.20E-45
AC103702.2	ENSG00000272763	1.931173535	7.14E-05	0.001309515
AC080038.3	ENSG00000279713	1.912844312	2.26E-46	1.60E-43
AL645939.2	ENSG00000225864	1.910964226	4.51E-17	6.60E-15
AC113383.1	ENSG00000250320	1.907570281	2.23E-37	1.11E-34
SERPINE1	ENSG00000106366	1.894111176	3.77E-32	1.56E-29
NFE2L1	ENSG00000082641	1.885278234	1.48E-20	2.90E-18

PHACTR2-AS1	ENSG00000235740	1.881480231	0.003075107	0.029783629
RMRP	ENSG00000269900	1.87769361	0.004999936	0.04358846
AL645929.1	ENSG00000230521	1.871646518	7.81E-08	2.88E-06
RNU7-186P	ENSG00000238419	1.870582851	2.46E-08	1.02E-06
STK10	ENSG00000072786	1.858887033	3.85E-08	1.54E-06
HOXB-AS2	ENSG00000239552	1.858529704	0.002706758	0.026844936
ATP5G1	ENSG00000159199	1.845718914	1.75E-06	4.89E-05
SHISA2	ENSG00000180730	1.843915708	1.20E-06	3.46E-05
CLEC4E	ENSG00000166523	1.834277579	7.13E-14	7.12E-12
SQOR	ENSG00000137767	1.829601936	0.004295806	0.038824487
LRRC37A4P	ENSG00000214425	1.822763474	1.68E-08	7.24E-07
HLA-B	ENSG00000234745	1.797739572	5.57E-14	5.64E-12
THCAT158	ENSG00000263293	1.79754506	2.31E-34	1.03E-31
AKAP12	ENSG00000131016	1.781339414	1.18E-19	2.17E-17
AL669841.1	ENSG00000233021	1.774106654	0.001165704	0.013566078
BIRC2	ENSG00000110330	1.769702951	2.41E-06	6.53E-05
GOSR2	ENSG00000108433	1.767810804	6.08E-07	1.84E-05
LRRC37A2	ENSG00000238083	1.745124402	5.38E-28	1.58E-25
ZC3H12C	ENSG00000149289	1.740531646	0.000589666	0.007605003
MT2A	ENSG00000125148	1.738445061	3.67E-08	1.48E-06
ELL2	ENSG00000118985	1.737639358	3.19E-05	0.00064572
CHCHD1	ENSG00000172586	1.73478026	0.005674925	0.04798971
TUFT1	ENSG00000143367	1.727587512	0.000577656	0.007509533
CXCL8	ENSG00000169429	1.725310661	0.000211366	0.003273764
SLC35F2	ENSG00000110660	1.717053353	8.35E-06	0.000201426
BTN3A1	ENSG00000026950	1.71596889	0.005119018	0.044366931
DHODH	ENSG00000102967	1.706765558	3.46E-09	1.76E-07
UBE2Z	ENSG00000159202	1.705988955	4.80E-09	2.33E-07
SERTAD4-AS1	ENSG00000203706	1.704041682	0.00082119	0.0101549
SUN1	ENSG00000164828	1.701562928	0.000284058	0.004189606
PRR15L	ENSG00000167183	1.699772825	7.78E-06	0.000189642
CGB7	ENSG00000196337	1.695115106	0.00028898	0.004243788
HOXA11-AS	ENSG00000240990	1.665229114	1.79E-07	6.08E-06
SCN9A	ENSG00000169432	1.664112616	0.002457151	0.024826831
LMF2	ENSG00000100258	1.661572226	0.003575159	0.033468613
AC004233.2	ENSG00000270168	1.644517682	0.000142148	0.002345497
AC004241.1	ENSG00000257433	1.630725037	0.002514231	0.025218003
HOXB-AS3	ENSG00000233101	1.627962513	1.58E-29	5.17E-27
AC012413.1	ENSG00000253664	1.62315416	7.32E-07	2.20E-05
CDH13	ENSG00000140945	1.621121712	0.001423959	0.016022844
SMC5-AS1	ENSG00000268364	1.619972893	3.45E-19	6.16E-17
PLAC4	ENSG00000280109	1.617606899	1.54E-06	4.34E-05
PLK2	ENSG00000145632	1.600902217	2.22E-06	6.07E-05

AL353768.1	ENSG00000224764	1.598484901	0.005124344	0.044377024
CLDN14	ENSG00000159261	1.598351613	8.27E-09	3.82E-07
ARHGEF28	ENSG00000214944	1.597266716	0.000551482	0.007246894
FZD4	ENSG00000174804	1.589811583	1.91E-15	2.35E-13
DOCK2	ENSG00000134516	1.588704539	0.000882348	0.010777839
AC004477.3	ENSG00000278765	1.588179407	1.60E-05	0.000355867
ALDH1B1	ENSG00000137124	1.581289694	4.67E-06	0.000120337
AC004477.2	ENSG00000266341	1.574963458	5.64E-42	3.31E-39
LINC00514	ENSG00000262152	1.573220741	0.000113106	0.001943164
ABL1	ENSG00000097007	1.571890495	5.07E-08	1.95E-06
HOXB-AS1	ENSG00000230148	1.569441804	3.94E-16	5.11E-14
ISCA1	ENSG00000135070	1.565746513	0.003614526	0.033688648
LRRC37A17P	ENSG00000263142	1.556554847	1.35E-34	6.18E-32
FBP2	ENSG00000130957	1.552643736	0.000455726	0.006219476
TBC1D2	ENSG00000095383	1.541718126	0.002562095	0.025622457
HOXB7	ENSG00000260027	1.541670055	7.35E-07	2.21E-05
CD27	ENSG00000139193	1.540875159	2.53E-06	6.83E-05
MT-TW	ENSG00000210117	1.540665765	0.005377078	0.046049359
AC090673.1	ENSG00000197301	1.540299763	5.90E-08	2.22E-06
TNFRSF14-AS1	ENSG00000238164	1.535981754	6.19E-07	1.87E-05
MORC4	ENSG00000133131	1.522184392	5.03E-05	0.000968365
IGFBP7-AS1	ENSG00000245067	1.522112818	1.73E-28	5.25E-26
AC018521.2	ENSG00000264019	1.518391958	9.35E-38	4.82E-35
DECR1	ENSG00000104325	1.515513078	0.000285259	0.004200028
AC025580.1	ENSG00000259342	1.511338981	3.53E-24	8.57E-22
EREG	ENSG00000124882	1.505019554	1.16E-11	8.57E-10
CASP4	ENSG00000196954	1.500673569	0.005180672	0.044713885
LRRC8A	ENSG00000136802	1.497307515	0.00200264	0.02116098
MEF2C	ENSG00000081189	1.494528106	0.000500023	0.006689678
SUPV3L1	ENSG00000156502	1.493220878	0.003272643	0.031188746
AC018754.1	ENSG00000272367	1.49026422	6.45E-34	2.81E-31
STXBP1	ENSG00000136854	1.480891734	2.98E-09	1.53E-07
SNHG22	ENSG00000267322	1.477929769	0.002341642	0.023895998
MIR3074	ENSG00000207617	1.477080084	3.47E-05	0.00069048
RPS3	ENSG00000149273	1.475526857	2.16E-14	2.32E-12
LIMA1	ENSG00000050405	1.474770431	4.14E-05	0.000811107
RPL3P1	ENSG00000228149	1.471242418	0.000512253	0.006823334
RPSAP52	ENSG00000241749	1.470870848	0.00170097	0.018490836
FAM198B	ENSG00000164125	1.468641844	0.000606138	0.007778622
GCSAM	ENSG00000174500	1.464215003	1.85E-18	3.09E-16
CLTB	ENSG00000175416	1.455048176	6.36E-05	0.001185605
BTN2A2	ENSG00000124508	1.449920343	0.005314975	0.045678679
AL512413.1	ENSG00000272088	1.448567295	0.0056174	0.047603616

NUPR1	ENSG00000176046	1.446788643	0.001840238	0.01965272
PANX1	ENSG00000110218	1.442530067	0.002091097	0.021860925
TUBA1C	ENSG00000167553	1.441553378	1.72E-21	3.60E-19
TAGLN	ENSG00000149591	1.435110921	0.000253703	0.003811381
CCNH	ENSG00000134480	1.432837919	1.10E-24	2.91E-22
HMGA1	ENSG00000137309	1.421499549	0.001979643	0.020944029
CASP7	ENSG00000165806	1.414112157	0.000687393	0.008670744
SIK2	ENSG00000170145	1.407646896	7.72E-17	1.06E-14
HOXB3	ENSG00000120093	1.402247889	2.19E-11	1.56E-09
INHBA	ENSG00000122641	1.397534077	3.53E-12	2.77E-10
CYFIP2	ENSG00000055163	1.397429291	0.000813344	0.010065203
CDC27	ENSG00000004897	1.393520767	2.77E-12	2.21E-10
MCAM	ENSG00000076706	1.390699073	4.39E-09	2.16E-07
CHORDC1	ENSG00000110172	1.381216777	0.000202302	0.003156394
AL603839.1	ENSG00000227278	1.378646197	1.44E-11	1.06E-09
AC091133.1	ENSG00000230532	1.374251748	4.89E-29	1.54E-26
XPNPEP1	ENSG00000108039	1.360353478	0.003549759	0.033304224
AC103702.1	ENSG00000257178	1.347696257	0.001619212	0.017749694
AC098679.1	ENSG00000248429	1.345202021	4.90E-23	1.12E-20
SF3B6	ENSG00000115128	1.345197032	0.00316813	0.030412531
EFCAB13	ENSG00000178852	1.343705224	2.20E-07	7.30E-06
RHOBTB3	ENSG00000164292	1.337917257	3.97E-05	0.000781395
ANXA11	ENSG00000122359	1.335300302	0.000146434	0.002406254
PCBD1	ENSG00000166228	1.335049347	0.000430248	0.005933722
EHMT1	ENSG00000181090	1.334472541	5.70E-05	0.001080215
KCNIP1	ENSG00000182132	1.332085935	4.48E-08	1.77E-06
NANS	ENSG00000095380	1.331848984	2.88E-10	1.74E-08
TMEM123	ENSG00000152558	1.330252549	2.41E-12	1.98E-10
IFIT3	ENSG00000119917	1.325385135	0.000689674	0.008693062
C10orf90	ENSG00000154493	1.324853223	0.005727542	0.048272157
AC114760.2	ENSG00000272211	1.324099405	1.01E-08	4.60E-07
PARD3	ENSG00000148498	1.31675855	2.40E-12	1.98E-10
CHMP1A	ENSG00000131165	1.315334593	0.001847546	0.019703602
PTPRJ	ENSG00000149177	1.313367816	1.45E-05	0.000328082
PSAT1	ENSG00000135069	1.310830455	0.000418485	0.005785585
CBR3-AS1	ENSG00000236830	1.305818467	2.30E-22	5.01E-20
AC011611.3	ENSG00000257453	1.305530105	3.27E-19	5.91E-17
ARL17A	ENSG00000185829	1.304020464	4.46E-14	4.53E-12
TMEM178B	ENSG00000261115	1.30333293	0.002189616	0.022588804
CAMK2N2	ENSG00000163888	1.301301635	0.000466899	0.006341392
WDR11	ENSG00000120008	1.292726779	0.000557705	0.007317348
FOXD1-AS1	ENSG00000247993	1.290013722	1.15E-22	2.56E-20
COX7C	ENSG00000127184	1.286548525	0.00476445	0.042119031

ZDHHC6	ENSG00000023041	1.281752679	0.000937232	0.011334175
ANXA1	ENSG00000135046	1.277121948	6.68E-10	3.80E-08
MSC-AS1	ENSG00000235531	1.275883482	6.64E-17	9.17E-15
RPL12P14	ENSG00000224321	1.275416692	0.000144439	0.002378067
AFAP1	ENSG00000196526	1.275127289	0.002595985	0.025900401
HLA-A	ENSG00000206503	1.272020919	4.98E-09	2.42E-07
SLC25A39	ENSG00000013306	1.271229476	0.003206705	0.030695846
AL671883.3	ENSG00000271581	1.268674443	3.02E-28	9.02E-26
SWAP70	ENSG00000133789	1.266217368	0.000760724	0.009485634
POLR2B	ENSG00000047315	1.26290418	4.72E-19	8.27E-17
GLRX3	ENSG00000108010	1.260511077	0.000122485	0.002082974
BTN3A2	ENSG00000186470	1.258468859	0.002069289	0.021703266
AC124066.1	ENSG00000265263	1.257554964	1.08E-07	3.84E-06
MYL9	ENSG00000101335	1.257526081	3.56E-05	0.000706937
OPTN	ENSG00000123240	1.254574175	1.28E-07	4.50E-06
AC073072.1	ENSG00000179428	1.253105091	4.72E-12	3.66E-10
OCIAD2	ENSG00000145247	1.249271208	0.000971641	0.011700315
TXNRD1	ENSG00000198431	1.248844088	2.45E-11	1.72E-09
FN1	ENSG00000115414	1.244700033	9.88E-07	2.89E-05
AC090152.1	ENSG00000167912	1.244420932	0.005573969	0.047353655
EIF2S1	ENSG00000134001	1.244130443	7.52E-09	3.49E-07
AC245100.4	ENSG00000231551	1.226474034	5.03E-08	1.94E-06
CGNL1	ENSG00000128849	1.223620123	0.002455991	0.024826831
DNMBP-AS1	ENSG00000227695	1.221454662	5.35E-12	4.12E-10
UBA6	ENSG00000033178	1.220912291	9.63E-07	2.83E-05
AC024909.3	ENSG00000274021	1.219522661	0.001115787	0.013092777
STK17B	ENSG00000081320	1.210730777	0.00124919	0.014360617
GNAQ	ENSG00000156052	1.203114771	0.001159205	0.013518225
PRR7	ENSG00000131188	1.202938267	0.001950848	0.020665121
FPGS	ENSG00000136877	1.202127569	0.004277159	0.038697126
SNX9	ENSG00000130340	1.201729508	0.000275271	0.004095561
SH3PXD2B	ENSG00000174705	1.199735799	0.004295286	0.038824487
CTSD	ENSG00000117984	1.197905761	0.00358464	0.033538886
PROSER2-AS1	ENSG00000225778	1.196695941	1.57E-17	2.50E-15
SKIDA1	ENSG00000180592	1.196540543	0.000338271	0.00485027
LRRC37A	ENSG00000176681	1.19386351	7.14E-09	3.34E-07
SNX2	ENSG00000205302	1.193831099	0.003507024	0.033030952
LRRC46	ENSG00000141294	1.192438893	3.83E-14	3.97E-12
ZMYND19	ENSG00000165724	1.187902631	0.002981212	0.029044596
ACTA2-AS1	ENSG00000180139	1.186053483	1.67E-08	7.21E-07
PCED1B	ENSG00000179715	1.184276326	2.85E-14	3.02E-12
CEACAM1	ENSG00000079385	1.18332806	0.000444744	0.006098989
DPAGT1	ENSG00000172269	1.180669712	1.04E-06	3.04E-05

C9orf3	ENSG00000148120	1.170989628	0.000190515	0.00299726
GLRX	ENSG00000173221	1.170702383	0.002710187	0.026844936
SSPN	ENSG00000123096	1.167966515	0.00051331	0.006827834
AL135818.1	ENSG00000258875	1.165903423	0.001552197	0.017158998
DBN1	ENSG00000113758	1.158317453	3.11E-07	9.95E-06
APLP2	ENSG00000084234	1.154449541	8.56E-12	6.47E-10
ACTR1A	ENSG00000138107	1.152430681	1.76E-05	0.00038991
ITGAV	ENSG00000138448	1.151362213	1.08E-08	4.89E-07
SFXN1	ENSG00000164466	1.150497893	0.001081039	0.012746657
AC008840.1	ENSG00000250240	1.14997144	4.84E-17	7.03E-15
AHNAK	ENSG00000124942	1.149680483	4.89E-06	0.00012527
EIF4E	ENSG00000151247	1.14849082	0.000360521	0.005134633
OAT	ENSG00000065154	1.148189666	0.001522977	0.016890928
COTL1	ENSG00000103187	1.145540457	2.87E-05	0.000590689
NT5C2	ENSG00000076685	1.142403973	0.000228186	0.003489753
PSMB8	ENSG00000204264	1.141897262	0.001461165	0.016354849
INVS	ENSG00000119509	1.140407129	0.002710971	0.026844936
AC009884.1	ENSG00000253335	1.140356042	0.005074183	0.044167746
AC002558.2	ENSG00000261872	1.140307998	2.55E-20	4.87E-18
NNMT	ENSG00000166741	1.135240399	3.28E-06	8.70E-05
ACO1	ENSG00000122729	1.132018069	2.29E-07	7.55E-06
AC239868.4	ENSG00000272993	1.131938933	0.005932545	0.049526242
AL596202.1	ENSG00000235381	1.127919508	7.11E-10	4.00E-08
MYOF	ENSG00000138119	1.12622407	7.10E-07	2.14E-05
IER3	ENSG00000137331	1.125992217	0.000249226	0.003757405
AC021205.3	ENSG00000273007	1.124177929	0.001694139	0.018440174
AC011676.2	ENSG00000254019	1.124024705	0.00276068	0.027208073
ANXA6	ENSG00000197043	1.124010076	6.13E-07	1.86E-05
MT-RNR2	ENSG00000210082	1.122414766	3.03E-17	4.60E-15
AL590644.3	ENSG00000282843	1.121932116	0.000412072	0.005720195
AC003070.1	ENSG00000267344	1.120345639	0.000126509	0.002138819
LRRFIP1	ENSG00000124831	1.119887483	0.000186918	0.002954351
CLIC1	ENSG00000213719	1.119523112	2.24E-07	7.41E-06
NLN	ENSG00000123213	1.11702027	0.002130238	0.022124824
AC008686.1	ENSG00000267633	1.115684514	2.31E-09	1.21E-07
HYLS1	ENSG00000198331	1.114798698	0.00068549	0.008658008
LRP11	ENSG00000120256	1.114356241	0.000589924	0.007605003
SLC2A6	ENSG00000160326	1.111624747	0.003878471	0.035795277
PMPCA	ENSG00000165688	1.104452174	0.003408184	0.032260975
CBL	ENSG00000110395	1.104225504	0.001811753	0.019385072
STX4	ENSG00000103496	1.096360979	0.002295483	0.023523859
AL603839.2	ENSG00000238186	1.093740187	1.25E-05	0.000288117
PRSS23	ENSG00000150687	1.089151081	6.25E-08	2.34E-06

AMIGO2	ENSG00000139211	1.088983288	6.93E-06	0.000171234
ACAT1	ENSG00000075239	1.08861724	0.000211001	0.003271096
AL354733.1	ENSG00000226877	1.087893471	0.000462221	0.006303054
EML2	ENSG00000125746	1.084449574	3.89E-05	0.000766426
PSAP	ENSG00000197746	1.083574041	0.002608589	0.02601088
BIRC3	ENSG00000023445	1.081961474	2.08E-05	0.000448304
FLNB	ENSG00000136068	1.081810549	6.74E-09	3.16E-07
CLNS1A	ENSG00000074201	1.080852025	0.004934021	0.043173312
IFT46	ENSG00000118096	1.079994268	0.004533508	0.040520167
SNF8	ENSG00000159210	1.079971843	1.80E-16	2.37E-14
AL359955.1	ENSG00000197550	1.074891443	0.000187131	0.00295496
AC068234.2	ENSG00000276790	1.069934808	0.000240999	0.00364632
HOXB-AS4	ENSG00000242207	1.066567301	4.40E-11	3.03E-09
ANXA7	ENSG00000138279	1.066493961	0.000395584	0.005540051
QRFP	ENSG00000188710	1.065157437	0.000435702	0.005989492
HIST1H2BG	ENSG00000273802	1.059939202	0.000125857	0.002129911
TSTA3	ENSG00000104522	1.059370643	0.005386083	0.046069471
MFSD14B	ENSG00000148110	1.057964883	0.000794175	0.009863909
DDX10	ENSG00000178105	1.056466286	0.002347847	0.023930572
INHBA-AS1	ENSG00000224116	1.052746891	2.89E-05	0.000594196
AP2S1	ENSG00000042753	1.052233755	0.001949822	0.020665121
FANCC	ENSG00000158169	1.04743476	2.18E-06	5.98E-05
AC022445.1	ENSG00000233847	1.04596703	9.18E-07	2.71E-05
AL357033.4	ENSG00000277496	1.045954121	0.000137819	0.002288515
GNG11	ENSG00000127920	1.04553072	0.00037059	0.005256011
AL162742.2	ENSG00000270075	1.043373445	4.05E-08	1.61E-06
HOXB4	ENSG00000182742	1.039395463	0.00317807	0.030473241
ERAP2	ENSG00000164308	1.038838184	6.55E-05	0.00121645
RNASEH2B-AS1	ENSG00000233672	1.038207392	0.004195097	0.03816704
KAZALD1	ENSG00000107821	1.038064472	0.000252351	0.003797787
MIR3936HG	ENSG00000233006	1.036208949	2.48E-05	0.000521236
ATP6V0E1	ENSG00000113732	1.033305645	0.005380527	0.046055686
SMIM15	ENSG00000188725	1.030949986	0.000795804	0.009876917
SIL1	ENSG00000120725	1.030215405	5.21E-09	2.51E-07
ZFPM2	ENSG00000169946	1.029723145	3.57E-08	1.44E-06
ETS1	ENSG00000134954	1.029722555	1.37E-05	0.00031103
PICALM	ENSG00000073921	1.027140938	5.89E-05	0.001107867
CFAP157	ENSG00000160401	1.02679468	5.92E-17	8.38E-15
NOLC1	ENSG00000166197	1.026041928	5.78E-06	0.000145182
C12orf10	ENSG00000139637	1.025435973	0.004912072	0.043037415
TNIP1	ENSG00000145901	1.025055642	2.07E-05	0.000445983
MAMDC2	ENSG00000165072	1.024399315	0.0048889	0.042906662
RSF1	ENSG00000048649	1.019141465	0.003272882	0.031188746

TXN	ENSG00000136810	1.018614117	0.000127208	0.002148494
BICD2	ENSG00000185963	1.018086576	0.001031794	0.012278273
ANXA3	ENSG00000138772	1.016583481	0.000594758	0.007661508
ITGB1	ENSG00000150093	1.015484464	1.29E-14	1.47E-12
STK16	ENSG00000115661	1.014489997	1.71E-17	2.66E-15
CDK15	ENSG00000138395	1.007909876	0.000323519	0.004674245
SRGAP1	ENSG00000196935	1.007868973	0.003355743	0.031835532
SLC4A7	ENSG00000033867	1.007825919	0.001524989	0.016902213
SETD2	ENSG00000181555	1.007106862	0.005036636	0.043885887
SLC26A2	ENSG00000155850	1.006208742	0.000954791	0.01151374
RPL29	ENSG00000162244	1.005440849	3.57E-07	1.13E-05
DLGAP1-AS2	ENSG00000262001	1.00479832	0.002613366	0.026012718
MGEA5	ENSG00000198408	1.00299818	0.000608427	0.00779622
SNHG5	ENSG00000203875	1.00256225	0.000295329	0.004322938
STK25	ENSG00000115694	1.001798888	1.10E-05	0.000255854
KRT18	ENSG00000111057	0.99959264	2.07E-10	1.28E-08
LINC02225	ENSG00000249584	0.996281634	0.000799435	0.009907509
AC022784.7	ENSG00000254340	0.995912648	9.79E-06	0.000230986
ATOX1	ENSG00000177556	0.994903146	1.61E-05	0.000358007
MYC	ENSG00000136997	0.992793967	0.000134096	0.002242549
VIM	ENSG00000026025	0.9913115	2.43E-11	1.71E-09
MAPKAP1	ENSG00000119487	0.988761586	0.000723444	0.009078311
PFDN5	ENSG00000123349	0.988626008	0.004365521	0.039370789
ADAM12	ENSG00000148848	0.987181234	0.000150426	0.002453106
WDR36	ENSG00000134987	0.986945653	0.002394123	0.024353587
GLUD1	ENSG00000148672	0.98559281	7.96E-06	0.000193769
RPS9P1	ENSG00000214889	0.985077041	2.88E-05	0.000593195
AC100861.1	ENSG00000246582	0.984439741	6.21E-05	0.001161484
DDX21	ENSG00000165732	0.980050982	0.000888174	0.010838827
MICAL2	ENSG00000133816	0.9795377	4.70E-06	0.000121055
HIST1H4I	ENSG00000276180	0.976318681	9.16E-06	0.000218227
RPS25	ENSG00000118181	0.975526128	3.32E-10	1.97E-08
LIMS1	ENSG00000169756	0.975008054	0.00151168	0.016798528
SRPRA	ENSG00000182934	0.97250928	7.43E-06	0.000182189
AC245100.2	ENSG00000225871	0.972183161	0.002047299	0.021512465
PINK1-AS	ENSG00000117242	0.97086465	2.00E-16	2.62E-14
ARHGAP21	ENSG00000107863	0.970538601	0.001101096	0.012947211
RDX	ENSG00000137710	0.967448246	5.33E-06	0.000135621
KRR1	ENSG00000111615	0.967389429	3.93E-15	4.61E-13
RPS23	ENSG00000186468	0.965096817	2.37E-08	9.85E-07
SLU7	ENSG00000164609	0.963288793	0.001863208	0.019806083
ITPR2	ENSG00000123104	0.963021326	0.000154484	0.002502228
CTAGE7P	ENSG00000233122	0.962620297	1.45E-05	0.000328913

VPS26A	ENSG00000122958	0.959187544	0.001200332	0.013902408
DPYSL3	ENSG00000113657	0.957277936	1.55E-07	5.34E-06
HMOX2	ENSG00000103415	0.953845549	0.002662514	0.026470905
FAR1	ENSG00000197601	0.952871362	0.00591218	0.049417089
AL662797.2	ENSG00000272273	0.950761623	1.44E-15	1.82E-13
CUEDC2	ENSG00000107874	0.949750863	0.00423792	0.038444473
FJX1	ENSG00000179431	0.948819383	0.003005089	0.02926044
GAS2	ENSG00000148935	0.946517794	0.000465761	0.006337581
GSTO1	ENSG00000148834	0.945496123	0.000376844	0.005327937
ATP5C1	ENSG00000165629	0.943710161	0.0021133	0.022019858
HLA-C	ENSG00000204525	0.943659189	0.001146599	0.013389595
PRPS1P2	ENSG00000232630	0.941639603	2.23E-05	0.000474351
AL157392.3	ENSG00000239665	0.938622914	4.75E-13	4.31E-11
RAB18	ENSG00000099246	0.93250097	0.00204631	0.021512465
NUDT6	ENSG00000170917	0.92961243	8.39E-14	8.24E-12
RPS24	ENSG00000138326	0.928238609	3.53E-09	1.78E-07
RPL39	ENSG00000198918	0.928118163	0.000281694	0.004169213
HOMER2	ENSG00000103942	0.926005713	0.000136452	0.002270772
FRMD6	ENSG00000139926	0.923820304	0.000283932	0.004189606
NKX6-2	ENSG00000148826	0.922980349	1.93E-07	6.51E-06
SLCO4A1-AS1	ENSG00000232803	0.920126807	2.73E-09	1.41E-07
TJP2	ENSG00000119139	0.919999756	0.000107546	0.001860349
AP003392.2	ENSG00000254909	0.919179226	0.005941701	0.049526242
ADAMTS1	ENSG00000154734	0.91886867	8.12E-06	0.000196807
ARPC3	ENSG00000111229	0.918071472	0.003648433	0.033948806
ZMYND11	ENSG00000015171	0.917899898	0.002016761	0.021270507
CTNNAL1	ENSG00000119326	0.917038114	0.000312274	0.004538798
SNX6	ENSG00000129515	0.916246869	0.005949032	0.049526242
THBS1	ENSG00000137801	0.915721074	4.03E-06	0.000105085
HIST1H2AE	ENSG00000277075	0.915188172	1.33E-05	0.000303082
AP002812.5	ENSG00000255449	0.912283397	4.84E-08	1.88E-06
AC020912.1	ENSG00000284430	0.910320284	7.89E-11	5.24E-09
TNFAIP8	ENSG00000145779	0.900676534	0.003162511	0.030392656
AP003696.1	ENSG00000253385	0.898054739	8.37E-05	0.001496095
KLC3	ENSG00000104892	0.896987303	8.21E-10	4.56E-08
ATP2B1	ENSG00000070961	0.895313382	0.000992375	0.011899395
ANP32B	ENSG00000136938	0.894233859	0.000181927	0.002888897
BDP1	ENSG00000145734	0.893619268	0.005860065	0.049145292
PGAM1	ENSG00000171314	0.892908328	0.001570198	0.017279299
AP001972.1	ENSG00000254429	0.889611436	0.00015264	0.002481824
AL109613.1	ENSG00000224093	0.885402835	8.87E-09	4.06E-07
SEC61A2	ENSG00000065665	0.884705635	1.92E-13	1.83E-11
MOK	ENSG00000080823	0.884692927	0.000892358	0.010868858

MAPRE1	ENSG00000101367	0.884614446	0.00174691	0.018879676
NTN3	ENSG00000162068	0.883771185	0.004155779	0.037862901
AC005324.5	ENSG00000266261	0.882983991	5.36E-09	2.58E-07
BCCIP	ENSG00000107949	0.882892396	3.38E-13	3.14E-11
MCMBP	ENSG00000197771	0.882618361	0.004585067	0.040873492
YAP1	ENSG00000137693	0.882357802	0.001861363	0.019803648
CD44-AS1	ENSG00000255443	0.88151725	3.01E-10	1.81E-08
MAGED2	ENSG00000102316	0.881008194	0.001131885	0.013245078
PAFAH1B2	ENSG00000168092	0.880085946	0.000131554	0.002206548
SACS	ENSG00000151835	0.878413684	0.000268251	0.004001634
SPARC	ENSG00000113140	0.878284216	8.05E-06	0.00019566
NCS1	ENSG00000107130	0.877403934	0.004700244	0.041681551
SPIRE1	ENSG00000134278	0.876578774	0.002467046	0.024862151
CDC14B	ENSG00000081377	0.876446312	3.29E-12	2.61E-10
SYNE1	ENSG00000131018	0.874613332	0.00066013	0.008401699
KRT8	ENSG00000170421	0.872771963	2.32E-15	2.82E-13
POLE3	ENSG00000148229	0.870532929	9.14E-05	0.001614089
PDCD11	ENSG00000148843	0.870017394	0.000229646	0.003500773
CAMSAP1	ENSG00000130559	0.867728367	0.003885076	0.03583677
EIF3M	ENSG00000149100	0.867070462	0.001540834	0.017044472
GAB2	ENSG00000033327	0.865647325	0.001063542	0.012592785
MAP1B	ENSG00000131711	0.864763858	6.50E-05	0.001207878
ARID4A	ENSG00000032219	0.86337641	0.002711195	0.026844936
AC069547.1	ENSG00000279863	0.861864645	0.005257358	0.045247801
ACBD6	ENSG00000230124	0.861206297	0.000722103	0.009068181
GDI2	ENSG00000057608	0.861008428	3.33E-07	1.06E-05
PPA1	ENSG00000180817	0.860794702	0.005469854	0.04667608
TRAPPC4	ENSG00000196655	0.860596118	1.62E-10	1.03E-08
DNAJB6	ENSG00000105993	0.859821718	0.00104553	0.012431495
PRAL	ENSG00000279296	0.858520354	1.80E-10	1.13E-08
AL354733.2	ENSG00000231616	0.858126044	0.000673029	0.00854666
G3BP1	ENSG00000145907	0.853227677	1.54E-05	0.000344582
FKBP15	ENSG00000119321	0.851733557	4.66E-10	2.69E-08
HNRNPF	ENSG00000169813	0.848716343	0.000439282	0.006028957
UNC45A	ENSG00000140553	0.847024858	8.98E-08	3.26E-06
ZNF575	ENSG00000176472	0.846979355	0.000465872	0.006337581
AL355987.5	ENSG00000274356	0.845731491	0.003318923	0.031566422
FO681492.1	ENSG00000277758	0.844343294	0.0010288	0.012258306
CLIP1	ENSG00000130779	0.842918343	0.003934442	0.036213494
CD44	ENSG00000026508	0.841027225	0.002076075	0.021720807
AL162385.2	ENSG00000231521	0.83875457	0.004998199	0.04358846
RPS16	ENSG00000105193	0.838230696	0.003417842	0.032298419
10-Sep	ENSG00000186522	0.837035218	0.00212066	0.022064991

CCT2	ENSG00000166226	0.832868397	0.000566504	0.007398511
MT-TT	ENSG00000210195	0.830728312	0.00491393	0.043037415
RUVBL2	ENSG00000183207	0.830707813	0.003613302	0.033688648
A2ML1-AS1	ENSG00000256661	0.826834347	0.001332755	0.015147051
BTF3	ENSG00000145741	0.826286133	0.001785609	0.019141501
BX470102.1	ENSG00000238279	0.824029719	3.17E-05	0.000641478
MYL12A	ENSG00000101608	0.819918425	0.001345764	0.015243916
AC017101.1	ENSG00000227227	0.8197831	2.71E-12	2.19E-10
AC096772.1	ENSG00000272851	0.818668177	2.29E-07	7.55E-06
RPS14	ENSG00000164587	0.818332202	1.91E-07	6.46E-06
ADAMTS9-AS1	ENSG00000241158	0.817507863	8.56E-10	4.74E-08
AC002480.1	ENSG00000225541	0.816834067	6.14E-08	2.30E-06
RPP38	ENSG00000152464	0.816702998	3.90E-07	1.22E-05
VCAN	ENSG00000038427	0.815606529	1.85E-07	6.28E-06
RPL7A	ENSG00000148303	0.815447024	0.001519752	0.016866173
RPL23	ENSG00000125691	0.814966935	6.62E-06	0.000164314
IL21R-AS1	ENSG00000259954	0.814931097	0.00047927	0.006465863
ERLIN1	ENSG00000107566	0.814372401	9.44E-05	0.001661186
MAF1	ENSG00000179632	0.812731917	0.000452025	0.006178884
EDF1	ENSG00000107223	0.811941474	0.00021288	0.003294217
NHP2	ENSG00000145912	0.811310623	0.000494448	0.006620301
FAM129B	ENSG00000136830	0.809362018	0.000183377	0.002906485
RBM7	ENSG00000076053	0.808096948	0.000144172	0.002375979
RARS	ENSG00000113643	0.8080128	0.002505248	0.02514275
CEP295	ENSG00000166004	0.803813009	4.13E-09	2.05E-07
CNNM2	ENSG00000148842	0.802973536	3.49E-12	2.75E-10
RPL23AP64	ENSG00000240970	0.800513238	0.001774679	0.019084542
RN7SL4P	ENSG00000263740	0.799065263	0.002074778	0.021720617
AL512770.1	ENSG00000228302	0.797555386	2.43E-11	1.71E-09
ARPC2	ENSG00000163466	0.794453894	7.51E-05	0.001368358
HK1	ENSG00000156515	0.793780148	0.002856911	0.027977578
SGTB	ENSG00000197860	0.792440084	0.002458182	0.024826831
SPCS3	ENSG00000129128	0.79212815	0.002074338	0.021720617
AC008747.1	ENSG00000267024	0.791091062	0.002792427	0.027425508
SURF6	ENSG00000148296	0.789248431	0.005556337	0.047274769
LARS	ENSG00000133706	0.788143901	0.002345429	0.023920284
HINT1	ENSG00000169567	0.786981285	0.00013615	0.00226796
ALG1L13P	ENSG00000253981	0.785586803	0.000170587	0.002731812
RPS3A	ENSG00000145425	0.784626624	0.000166229	0.002669569
TIMM8B	ENSG00000150779	0.782672856	0.000104527	0.001817825
AC079328.2	ENSG00000259498	0.781452279	2.69E-10	1.64E-08
KLF6	ENSG00000067082	0.780845603	0.004738361	0.041975747
PSTK	ENSG00000179988	0.780744914	0.000472043	0.006395918

C1QBP	ENSG00000108561	0.780436277	0.003066522	0.029722352
RPL35	ENSG00000136942	0.780315633	1.53E-06	4.32E-05
KPNB1	ENSG00000108424	0.780308322	1.39E-06	3.96E-05
PDE8B	ENSG00000113231	0.780156173	4.31E-06	0.000111541
SLC26A1	ENSG00000145217	0.776973801	0.003087337	0.029841516
TPM1	ENSG00000140416	0.775988928	1.32E-06	3.76E-05
HSBP1	ENSG00000230989	0.767871023	0.000394909	0.005536225
AC018761.2	ENSG00000267062	0.767295705	1.96E-10	1.21E-08
DST	ENSG00000151914	0.765552211	0.000206885	0.003219027
NPM1	ENSG00000181163	0.764319905	3.89E-07	1.22E-05
UBR5	ENSG00000104517	0.76186006	0.000104766	0.001820113
AHSA1	ENSG00000100591	0.760996755	0.003638338	0.033873425
APP	ENSG00000142192	0.759146138	4.62E-08	1.80E-06
WDR20	ENSG00000140153	0.758572657	1.15E-05	0.000268064
PAWR	ENSG00000177425	0.756984155	0.002408625	0.024476639
PTPRF	ENSG00000142949	0.752529279	0.003747079	0.034714624
TUBB8P1	ENSG00000229298	0.751711549	0.00564513	0.047790935
TRAPPC13	ENSG00000113597	0.750864206	0.002172684	0.022441379
RACK1	ENSG00000204628	0.749759669	2.12E-08	8.94E-07
CACFD1	ENSG00000160325	0.749517068	0.003452002	0.032576734
ETFBKMT	ENSG00000139160	0.748752414	0.000127666	0.002154096
PSD3	ENSG00000156011	0.745882872	0.003531951	0.033192131
AL121928.1	ENSG00000273262	0.745831768	1.55E-08	6.75E-07
NACA	ENSG00000196531	0.743252894	6.73E-05	0.001245408
PSMB8-AS1	ENSG00000204261	0.742605556	7.78E-10	4.35E-08
ADAMTS9	ENSG00000163638	0.742318635	0.002692458	0.0267217
RANBP2	ENSG00000153201	0.740924519	0.001607113	0.017639829
ETF1	ENSG00000120705	0.738760511	0.001126384	0.013189788
AC004148.2	ENSG00000263272	0.737138367	9.49E-08	3.42E-06
SLK	ENSG00000065613	0.735730783	0.002979832	0.029044596
WWC1	ENSG00000113645	0.734515963	0.002384174	0.024271725
UST-AS1	ENSG00000227660	0.733872057	0.002012493	0.021238676
AC008105.1	ENSG00000233175	0.731986664	0.000247347	0.00373239
LOXL3	ENSG00000115318	0.729477807	3.26E-08	1.33E-06
CFAP70	ENSG00000156042	0.72913525	0.004590727	0.040896897
MT-RNR1	ENSG00000211459	0.727685156	1.53E-08	6.66E-07
FAM118B	ENSG00000197798	0.727246293	5.89E-07	1.79E-05
AC079880.1	ENSG00000270228	0.726608957	2.20E-08	9.23E-07
TLDC2	ENSG00000101342	0.726522573	5.46E-07	1.68E-05
NAP1L1	ENSG00000187109	0.724915685	1.01E-05	0.00023896
EEF1A1	ENSG00000156508	0.724023576	1.02E-05	0.00024048
PPM1N	ENSG00000213889	0.723524099	5.78E-05	0.001093111
CCDC84	ENSG00000186166	0.722871209	5.30E-10	3.04E-08

SEC11A	ENSG00000140612	0.7207416	0.00514801	0.04446865
ACTN1	ENSG00000072110	0.719077965	0.000513564	0.006827834
LSAMP	ENSG00000185565	0.718070112	0.001175332	0.013668766
MYL12B	ENSG00000118680	0.717230953	0.004748102	0.042035123
MYO1B	ENSG00000128641	0.716519912	0.000142185	0.002345497
TRIM14	ENSG00000106785	0.716265756	7.25E-09	3.38E-07
PTK2	ENSG00000169398	0.711377312	0.004169443	0.037965167
PGM5P2	ENSG00000277778	0.709279127	8.31E-05	0.001485903
MACF1	ENSG00000127603	0.708604367	0.000682379	0.008633134
ATP5B	ENSG00000110955	0.708390774	0.001492026	0.016645445
ARNTL2-AS1	ENSG00000245311	0.70331326	3.29E-07	1.05E-05
AL671277.1	ENSG00000227766	0.698972849	4.07E-11	2.82E-09
TMSB10	ENSG00000034510	0.69817428	0.004581835	0.040866116
FCHSD1	ENSG00000197948	0.697519326	2.27E-05	0.000482619
SNRPD2	ENSG00000125743	0.696683148	0.000327209	0.004719039
PSME2	ENSG00000100911	0.695690868	0.003079897	0.029800984
AC005046.1	ENSG00000273055	0.695228	0.000616486	0.007893529
CRYZP1	ENSG00000233025	0.694179783	0.004835733	0.042549946
GRK6	ENSG00000198055	0.693757566	1.11E-06	3.23E-05
IPO7	ENSG00000205339	0.691664389	0.003007548	0.029267612
RPL26	ENSG00000161970	0.689930937	0.000221996	0.003407351
FUBP3	ENSG00000107164	0.689727936	0.001648395	0.018034692
DDX31	ENSG00000125485	0.689706973	0.000327453	0.004719039
AC079329.1	ENSG00000254680	0.689536869	1.50E-08	6.58E-07
COX15	ENSG00000014919	0.686210771	0.000424197	0.005855019
TWNK	ENSG00000107815	0.685828304	5.57E-05	0.001057722
PFKP	ENSG00000067057	0.682160964	0.000140066	0.002315043
TAF1D	ENSG00000166012	0.681625855	1.98E-06	5.46E-05
MAP4K4	ENSG00000071054	0.681538257	2.78E-05	0.000574764
ARL10	ENSG00000175414	0.680981389	1.22E-08	5.47E-07
SURF4	ENSG00000148248	0.680284765	0.001098966	0.012931119
AC084125.2	ENSG00000255182	0.679483392	8.23E-08	3.01E-06
CSPG4P10	ENSG00000276710	0.675024942	2.84E-07	9.21E-06
AC233702.8	ENSG00000266466	0.67328911	0.004906165	0.043022074
CSNK1A1	ENSG00000113712	0.672854099	0.000287961	0.004232479
FBXO25	ENSG00000147364	0.672229478	5.80E-05	0.001095069
CFLAR-AS1	ENSG00000226312	0.671543008	7.96E-08	2.92E-06
ASB6	ENSG00000148331	0.670146869	1.25E-07	4.42E-06
RPL10A	ENSG00000198755	0.669031661	0.0024175	0.024552146
POLR3G	ENSG00000113356	0.668298763	0.005132801	0.044415977
CTNNA1	ENSG00000044115	0.666908226	5.51E-05	0.001047546
SLF2	ENSG00000119906	0.666029702	0.002112015	0.022019858
LIPE-AS1	ENSG00000213904	0.66218826	0.000671886	0.008544927

SERPINA1	ENSG00000197249	0.661269135	0.00053341	0.007059348
KBTBD3	ENSG00000182359	0.660592854	4.33E-05	0.000844142
DCBLD2	ENSG00000057019	0.659995307	0.000581245	0.007528299
PRELID1	ENSG00000169230	0.657705961	0.001848985	0.019703602
ARSG	ENSG00000141337	0.656984703	1.05E-07	3.74E-06
AP000943.3	ENSG00000255929	0.656157129	2.21E-06	6.07E-05
FOXH1	ENSG00000160973	0.654894213	1.03E-07	3.69E-06
AP002812.2	ENSG00000254459	0.650882119	0.000685874	0.008658008
MRPL19	ENSG00000115364	0.649660723	0.005866504	0.04917502
HSPA4	ENSG00000170606	0.648682897	0.000237288	0.003596572
VPS13A-AS1	ENSG00000232998	0.647502119	0.000150585	0.002453106
NQO1	ENSG00000181019	0.647355231	0.002758159	0.027198999
AP001029.2	ENSG00000267199	0.646443222	1.64E-07	5.65E-06
HSPA9	ENSG00000113013	0.645213885	6.90E-05	0.001272213
AP001001.1	ENSG00000254433	0.643726138	1.25E-07	4.42E-06
RPL18A	ENSG00000105640	0.642706715	0.000562672	0.00737682
BBIP1	ENSG00000214413	0.642025525	1.39E-05	0.000315422
RBBP4	ENSG00000162521	0.641552385	3.02E-06	8.10E-05
VDAC1	ENSG00000213585	0.641278402	0.003087598	0.029841516
ITGA3	ENSG00000005884	0.639941949	0.003203388	0.030681378
TGFB2-AS1	ENSG00000232480	0.638523782	3.67E-07	1.16E-05
TUBB4B	ENSG00000188229	0.638199028	0.00038692	0.005446699
GTPBP4	ENSG00000107937	0.637929464	0.004462709	0.040119515
C11orf57	ENSG00000150776	0.636988976	2.57E-05	0.000537803
TTL	ENSG00000114999	0.634961447	0.005677083	0.04798971
NOP56	ENSG00000101361	0.634861677	0.004027093	0.036946183
TAF5	ENSG00000148835	0.634377929	4.06E-07	1.27E-05
C11orf65	ENSG00000166323	0.634242329	0.000506397	0.006758986
AC025271.2	ENSG00000261265	0.634138362	0.000316276	0.004589108
TAP1	ENSG00000168394	0.633324886	0.000938245	0.011338356
LOXL1-AS1	ENSG00000261801	0.632101164	0.004864797	0.042761385
WDR43	ENSG00000163811	0.629941065	0.002871827	0.028091662
ARRDC1-AS1	ENSG00000203993	0.62733138	0.004662697	0.041391788
AC135457.1	ENSG00000272742	0.624810572	3.87E-08	1.55E-06
TKT	ENSG00000163931	0.623961611	0.001024133	0.012221668
CDH2	ENSG00000170558	0.622696675	0.005961077	0.049576439
AP002433.1	ENSG00000255467	0.622439757	3.29E-07	1.05E-05
DYNC1H1	ENSG00000197102	0.622215937	0.001225271	0.014143057
PPIB	ENSG00000166794	0.6186962	0.004051913	0.037133792
EEF2	ENSG00000167658	0.616863384	0.000158868	0.002563456
RPL32	ENSG00000144713	0.616243305	0.001233734	0.014221421
AC091117.1	ENSG00000259352	0.614319174	9.27E-05	0.001631636
AC025682.1	ENSG00000263766	0.613675342	2.28E-06	6.22E-05

HSPA8	ENSG00000109971	0.612480664	0.000183883	0.002911802
FAM35A	ENSG00000122376	0.612077446	1.40E-07	4.89E-06
CSPG4P12	ENSG00000259295	0.611165699	0.002139971	0.022211514
AC008906.1	ENSG00000248734	0.610394213	1.92E-05	0.000417982
SBF2	ENSG00000133812	0.609868663	0.003964344	0.036429509
AP001267.1	ENSG00000254873	0.608627959	5.80E-07	1.77E-05
FLNB-AS1	ENSG00000244161	0.608595692	1.43E-07	4.99E-06
LINC00943	ENSG00000189238	0.608290902	0.004775164	0.042169669
RPL38	ENSG00000172809	0.607668538	0.002298495	0.023540528
C6orf201	ENSG00000185689	0.606178332	4.44E-07	1.39E-05
C5orf56	ENSG00000197536	0.604477305	3.77E-06	9.86E-05
AL355490.2	ENSG00000231970	0.603578106	0.000279282	0.004140731
AL133415.1	ENSG00000234961	0.603295646	8.36E-08	3.05E-06
PARP8	ENSG00000151883	0.602477727	0.004260438	0.038586943
BTD	ENSG00000169814	0.599761352	0.000144833	0.00238224
ANKRD49	ENSG00000168876	0.599639866	0.000601455	0.007736051
ENO4	ENSG00000188316	0.597929136	0.00509467	0.044257614
ADIRF	ENSG00000148671	0.597659535	0.000580203	0.007528299
RPL27	ENSG00000131469	0.596207685	0.00438118	0.039491054
C8orf59	ENSG00000176731	0.59619351	1.91E-05	0.00041788
NMT2	ENSG00000152465	0.594587201	1.12E-05	0.000260079
RAG2	ENSG00000175097	0.592038204	0.004509972	0.040394804
RPL12	ENSG00000197958	0.590807472	0.000604676	0.007765716
ELP4	ENSG00000109911	0.58695554	0.00040921	0.005689758
PTTG1IP	ENSG00000183255	0.586779468	0.000388664	0.005457673
STC2	ENSG00000113739	0.585163295	0.002732596	0.026993917

Appendix B: Genes upregulated by *RB1* KO in 786-O VHL-reconstituted cells.

Gene name	**Ensembl gene ID**	**log2FoldChange**	**p-value**	**Adjusted p-value**
NCKAP5	ENSG00000176771	11.64181852	2.43E-21	7.55E-19
LRRC77P	ENSG00000244227	6.324998323	5.47E-07	1.58E-05
ZNF804A	ENSG00000170396	4.856741406	3.28E-09	1.75E-07
AC079117.1	ENSG00000234653	4.596090184	7.25E-10	4.48E-08
NRAP	ENSG00000197893	4.302877034	3.95E-07	1.22E-05
KRT19	ENSG00000171345	4.13486895	1.70E-18	4.26E-16
MYH8	ENSG00000133020	3.709710536	3.40E-20	1.03E-17
CERNA1	ENSG00000259577	3.703071458	1.20E-09	7.18E-08
MYH1	ENSG00000109061	3.437369119	1.49E-08	6.84E-07

FOLR3	ENSG00000110203	3.404639884	1.09E-10	8.08E-09
NALCN	ENSG00000102452	3.331405619	9.30E-25	3.33E-22
NCAM1-AS1	ENSG00000227487	3.206754209	6.71E-32	3.77E-29
MYH4	ENSG00000264424	3.18753312	7.86E-14	9.88E-12
SLC12A1	ENSG00000074803	3.030517614	2.96E-12	2.75E-10
OR7E47P	ENSG00000257542	3.030252676	1.26E-30	6.19E-28
LINC00559	ENSG00000261446	2.998135426	1.28E-09	7.57E-08
AC098798.1	ENSG00000250511	2.951712948	2.29E-36	1.59E-33
snoU13	ENSG00000238901	2.868029111	1.47E-14	2.16E-12
RPL7L1P1	ENSG00000234227	2.858049012	8.79E-35	5.47E-32
AL117339.4	ENSG00000272983	2.828142549	4.35E-08	1.74E-06
LINC00353	ENSG00000236176	2.783448913	4.36E-07	1.33E-05
PLXDC2	ENSG00000120594	2.75419812	1.05E-05	0.000194961
AC091948.1	ENSG00000247199	2.693533036	3.37E-07	1.06E-05
AC025165.1	ENSG00000224713	2.654264202	1.15E-16	2.38E-14
AP000802.1	ENSG00000247416	2.554582091	3.80E-11	3.07E-09
LINC02296	ENSG00000258859	2.496167844	1.63E-36	1.20E-33
AC016405.2	ENSG00000272043	2.371923087	4.19E-05	0.000613728
AC004130.1	ENSG00000271133	2.352026254	2.04E-10	1.40E-08
AC137056.1	ENSG00000262995	2.346585596	2.45E-07	7.97E-06
NTRK3-AS1	ENSG00000260305	2.341922284	1.32E-09	7.77E-08
PLA2G16	ENSG00000176485	2.326020678	5.23E-05	0.000739628
AC011337.1	ENSG00000271795	2.31752352	3.23E-14	4.39E-12
MED15P9	ENSG00000223760	2.31000023	5.19E-08	2.03E-06
LINC01695	ENSG00000236532	2.308338756	1.26E-08	5.86E-07
COL5A1	ENSG00000130635	2.236817352	1.45E-84	1.71E-80
AL033528.2	ENSG00000236528	2.18170406	3.87E-14	5.14E-12
AL603650.1	ENSG00000232355	2.178874948	9.41E-07	2.51E-05
AC093752.1	ENSG00000245958	2.159190016	0.000267773	0.002816029
AC113386.1	ENSG00000254138	2.142504462	2.79E-72	8.25E-69
AL512288.1	ENSG00000227050	2.097427654	2.92E-06	6.46E-05
MIR663AHG	ENSG00000227195	2.094082482	2.50E-26	9.78E-24
AC244517.5	ENSG00000279047	2.072124344	5.68E-08	2.18E-06
AC004846.2	ENSG00000258944	2.063586343	6.13E-43	6.58E-40
KLHDC7A	ENSG00000179023	2.046413286	4.50E-07	1.36E-05
CCDC183-AS1	ENSG00000228544	2.042513232	4.27E-18	9.89E-16
FLJ12825	ENSG00000248265	2.040654693	9.95E-08	3.61E-06
MAP7D2	ENSG00000184368	2.014370381	0.000104231	0.001317958
A1BG-AS1	ENSG00000268895	1.992730548	0.000181614	0.002048574
C21orf2	ENSG00000160226	1.965196747	7.52E-31	3.86E-28
AC011139.1	ENSG00000283458	1.95374381	5.43E-05	0.000761862
SNHG22	ENSG00000267322	1.920880571	2.57E-26	9.78E-24
MIR548XHG	ENSG00000224141	1.896681086	0.000196635	0.002186682

SPTBN5	ENSG00000137877	1.890175787	3.72E-11	3.03E-09
GRIK1	ENSG00000171189	1.885931761	0.000544457	0.00505109
AF240627.1	ENSG00000230233	1.862682621	8.62E-10	5.20E-08
AC011611.4	ENSG00000257839	1.831109775	0.000425651	0.004140805
PKDREJ	ENSG00000130943	1.80718883	0.001613639	0.011910675
PRRT2	ENSG00000167371	1.795334549	0.000477919	0.004537154
FSIP2	ENSG00000188738	1.793355067	0.000501825	0.004732416
AC027607.1	ENSG00000248936	1.789121262	0.001567023	0.011624714
AC087442.1	ENSG00000255091	1.78614815	3.59E-06	7.76E-05
AP002833.2	ENSG00000255317	1.785065962	0.000574384	0.005250368
AC110597.3	ENSG00000263424	1.773016561	5.35E-47	7.90E-44
MKX	ENSG00000150051	1.764454899	0.001302888	0.010083293
AC009955.4	ENSG00000269068	1.763922197	8.63E-09	4.16E-07
AC010149.1	ENSG00000235419	1.757300253	0.003808174	0.022786461
NCAM1	ENSG00000149294	1.75219133	9.39E-05	0.001208542
RPS14P8	ENSG00000239528	1.744108882	1.23E-05	0.000221183
TSEN54	ENSG00000182173	1.722005656	1.81E-05	0.000310979
ITIH4-AS1	ENSG00000239799	1.718194025	0.001433337	0.010844144
AC012499.1	ENSG00000229941	1.712010027	1.34E-07	4.72E-06
PITX2	ENSG00000164093	1.690679099	0.002299239	0.015695959
KCNQ1OT1_2	ENSG00000276105	1.679001927	5.41E-05	0.000760071
AC010261.2	ENSG00000251187	1.678538081	1.71E-13	2.02E-11
SEMA6A-AS1	ENSG00000248445	1.672366692	5.07E-44	6.65E-41
ITGA7	ENSG00000135424	1.667199131	0.001417963	0.010748483
MYO5B	ENSG00000167306	1.661272715	2.65E-05	0.000423107
AC114689.3	ENSG00000265533	1.660765493	0.000914602	0.007537649
AL033381.1	ENSG00000176515	1.646795649	0.003184594	0.020069401
AL390816.1	ENSG00000258842	1.636667096	2.54E-09	1.41E-07
AHDC1	ENSG00000126705	1.630919109	6.09E-11	4.73E-09
AC073218.1	ENSG00000232153	1.629185947	0.000279512	0.002913538
PLD4	ENSG00000166428	1.616044038	2.91E-12	2.73E-10
SNX10	ENSG00000086300	1.601681383	1.71E-06	4.06E-05
AL137804.1	ENSG00000255525	1.599472219	0.003517828	0.021526188
ARRDC3-AS1	ENSG00000281357	1.588992178	3.89E-17	8.34E-15
FOXQ1	ENSG00000164379	1.584685495	0.005426432	0.02965439
AC004233.2	ENSG00000270168	1.581583916	0.005056591	0.028195629
AL603839.1	ENSG00000227278	1.577621012	2.50E-16	4.92E-14
LINC02211	ENSG00000245662	1.575256745	0.004884698	0.027523038
CHODL	ENSG00000154645	1.569263547	3.26E-13	3.71E-11
AL162497.1	ENSG00000275741	1.560964329	1.93E-06	4.49E-05
NEFL	ENSG00000277586	1.558495246	1.85E-15	3.21E-13
AGAP2-AS1	ENSG00000255737	1.557196025	1.18E-22	3.76E-20
AC007919.1	ENSG00000224611	1.552813119	0.000549541	0.005075204

AC098848.1	ENSG00000267112	1.550585366	9.40E-14	1.16E-11
SEC1P	ENSG00000232871	1.550447534	0.000572062	0.005237251
AC089984.1	ENSG00000257410	1.540503477	2.97E-05	0.00046446
AL390816.2	ENSG00000258903	1.540282112	1.19E-06	3.03E-05
PAPPA	ENSG00000182752	1.533946643	4.34E-06	9.09E-05
AL139260.1	ENSG00000228436	1.530139058	2.26E-05	0.000371838
PAPPA-AS1	ENSG00000256040	1.529316603	0.005237725	0.028878402
C1orf167	ENSG00000215910	1.516993791	4.34E-27	1.90E-24
C10orf10	ENSG00000165507	1.515815301	2.01E-07	6.73E-06
AL590428.1	ENSG00000231652	1.510209791	7.74E-14	9.84E-12
SLC35F4	ENSG00000151812	1.508203027	0.006710272	0.034727569
AC092171.3	ENSG00000234432	1.508196816	0.000535041	0.00497938
GPR39	ENSG00000183840	1.503209164	4.48E-34	2.64E-31
AC010359.1	ENSG00000269961	1.496160357	0.000110511	0.001381099
MIR6080	ENSG00000278581	1.493916842	0.002625288	0.017379291
DNAJB3	ENSG00000227802	1.49386377	5.24E-05	0.000739628
AC004846.1	ENSG00000258376	1.492372491	5.13E-14	6.74E-12
AL139035.1	ENSG00000280710	1.492226893	0.001362525	0.010462559
AC004551.1	ENSG00000257452	1.484713728	6.02E-10	3.78E-08
ZBTB7C	ENSG00000184828	1.48344094	0.00155944	0.011583013
MIR587	ENSG00000207577	1.47891843	0.002158191	0.01488799
AC091906.1	ENSG00000248537	1.47563523	0.000124827	0.00151824
MAL2	ENSG00000253972	1.473263075	6.82E-77	4.03E-73
MEF2C	ENSG00000081189	1.467271417	0.002120922	0.014682353
AC020763.2	ENSG00000279122	1.461296475	0.001928176	0.013717924
PREPL	ENSG00000138078	1.45948843	8.96E-20	2.58E-17
AC024243.1	ENSG00000272969	1.452669732	0.005822352	0.031170432
MGAT4A	ENSG00000071073	1.451846622	0.00203101	0.014201435
ALOX12B	ENSG00000179477	1.446617317	2.24E-06	5.10E-05
SEMA6A-AS2	ENSG00000249167	1.445929683	1.48E-09	8.63E-08
OGG1	ENSG00000114026	1.445489929	2.35E-39	1.98E-36
NCBP2L	ENSG00000170935	1.444465678	0.000142377	0.00169333
DENND1C	ENSG00000205744	1.425241344	1.10E-19	3.09E-17
AL645939.2	ENSG00000225864	1.418733183	5.48E-10	3.48E-08
SLC16A12-AS1	ENSG00000234452	1.415831036	3.00E-05	0.000467796
AC012313.2	ENSG00000268049	1.415315842	0.001103191	0.008818689
ZNF37A	ENSG00000075407	1.411901981	5.08E-05	0.000722343
FAM46B	ENSG00000158246	1.410227359	7.30E-07	2.01E-05
FLG-AS1	ENSG00000237975	1.409909288	1.84E-76	7.26E-73
AC114812.2	ENSG00000224814	1.408147691	4.80E-48	8.10E-45
POC1B-GALNT4	ENSG00000259075	1.405736417	0.0086834	0.04201186
AL603839.2	ENSG00000238186	1.405159462	1.35E-07	4.74E-06
AL136084.2	ENSG00000267026	1.400091193	1.42E-07	4.94E-06

AC005697.2	ENSG00000266527	1.398016706	1.06E-06	2.75E-05
AC135048.4	ENSG00000279196	1.390285328	7.66E-10	4.71E-08
SLC26A10	ENSG00000135502	1.384495406	2.40E-10	1.61E-08
RELL1	ENSG00000181826	1.379611338	1.18E-08	5.48E-07
AL034399.2	ENSG00000236064	1.378634804	0.004716097	0.026867391
AC007271.1	ENSG00000226925	1.373947638	1.27E-23	4.42E-21
GPRC5C	ENSG00000170412	1.361620312	0.009819898	0.046204382
IGFBP7-AS1	ENSG00000245067	1.361087622	1.38E-31	7.41E-29
MIR514B	ENSG00000252583	1.340650071	0.006875786	0.035321024
GLIPR1L1	ENSG00000173401	1.339824031	0.003535163	0.021598696
AC098869.2	ENSG00000250893	1.335283469	2.43E-06	5.48E-05
C9orf163	ENSG00000196366	1.328695204	0.007880917	0.039127036
AP000757.2	ENSG00000254844	1.328072499	9.01E-57	2.13E-53
AC073389.2	ENSG00000271848	1.319017077	0.003472272	0.021335866
MTCO1P12	ENSG00000237973	1.318780268	0.000225547	0.002459565
ZSCAN30	ENSG00000186814	1.318223155	0.00038169	0.003772179
AC005837.1	ENSG00000261335	1.314088159	0.010328175	0.048042713
SPNS3	ENSG00000182557	1.309203266	0.006551339	0.034104539
MYBPH	ENSG00000133055	1.306386775	2.96E-05	0.000464081
IGFBP3	ENSG00000146674	1.303523335	0.003625497	0.022036602
AC012309.2	ENSG00000267437	1.296132261	0.001952354	0.013848226
AL591684.2	ENSG00000254929	1.294580611	0.010858506	0.049782203
AC022400.7	ENSG00000279088	1.293579452	0.005957431	0.03169246
UTS2	ENSG00000049247	1.291033602	1.60E-16	3.20E-14
AC131888.1	ENSG00000280182	1.288643207	1.30E-07	4.57E-06
KRTAP16-1	ENSG00000212657	1.283169431	0.000206571	0.002283812
AC016405.3	ENSG00000272384	1.276128562	0.010674489	0.049205976
AC098829.1	ENSG00000249252	1.271486016	4.14E-18	9.78E-16
EXOC3L1	ENSG00000179044	1.270734615	0.000128532	0.001560087
AC117383.1	ENSG00000249417	1.26574914	0.004718287	0.026867391
AP001542.3	ENSG00000267480	1.261268858	6.11E-05	0.000833649
EPB41L4A-AS1	ENSG00000224032	1.258223269	1.94E-10	1.35E-08
AC104532.2	ENSG00000267571	1.256146168	0.000433794	0.004192394
TMEM51-AS1	ENSG00000175147	1.25587918	2.26E-06	5.12E-05
MELTF-AS1	ENSG00000228109	1.255077159	4.87E-20	1.44E-17
KAZN	ENSG00000189337	1.2542862	3.34E-08	1.37E-06
GRIP2	ENSG00000144596	1.250058445	1.36E-11	1.15E-09
AL355388.2	ENSG00000273002	1.249559808	6.76E-05	0.000913014
ANKRD55	ENSG00000164512	1.242180499	3.70E-06	7.96E-05
COL18A1-AS2	ENSG00000224574	1.232461261	0.000909777	0.00750836
AGMAT	ENSG00000116771	1.225238384	0.008280283	0.040559991
KRT78	ENSG00000170423	1.217952808	0.006725717	0.034777024
AL589743.5	ENSG00000277156	1.215647783	0.00399407	0.023679701

LINC00308	ENSG00000184856	1.211088938	9.59E-06	0.000180062
AC122129.1	ENSG00000197815	1.201646607	3.43E-08	1.40E-06
SPINT2	ENSG00000167642	1.199528854	0.006936737	0.035587689
RNU6-725P	ENSG00000252371	1.194213123	0.004660095	0.026690457
AL133284.1	ENSG00000230894	1.192168245	0.002424508	0.016306058
SLC22A18AS	ENSG00000254827	1.190438344	6.88E-06	0.000133646
GRAMD2A	ENSG00000175318	1.181930317	0.00102387	0.008287807
AC016825.1	ENSG00000232767	1.177789429	2.11E-40	1.92E-37
SPATA17-AS1	ENSG00000234070	1.177366103	0.005155066	0.028584193
CDH6	ENSG00000113361	1.170660174	2.62E-09	1.43E-07
AC024909.3	ENSG00000274021	1.167762048	1.84E-18	4.53E-16
AC060234.1	ENSG00000226576	1.16098362	9.77E-07	2.59E-05
RBBP4	ENSG00000162521	1.160764098	7.00E-38	5.51E-35
IFNWP19	ENSG00000238271	1.157676271	1.51E-10	1.08E-08
AL133480.1	ENSG00000233367	1.152506498	0.00730755	0.036976077
PDGFRL	ENSG00000104213	1.137675141	2.43E-07	7.94E-06
AC018529.2	ENSG00000278330	1.135261903	0.001027103	0.008302591
DENND6B	ENSG00000205593	1.131105398	0.010685583	0.049219774
AC024560.2	ENSG00000249626	1.126406604	0.005428687	0.02965439
BEND3P3	ENSG00000278616	1.119691662	2.42E-08	1.03E-06
AC132812.1	ENSG00000265298	1.117594088	2.03E-06	4.68E-05
SNRK	ENSG00000163788	1.117512721	6.00E-07	1.72E-05
EPB41L4A-AS2	ENSG00000278921	1.115566871	0.000777355	0.006667078
KAAG1	ENSG00000146049	1.112804861	4.61E-30	2.18E-27
CYP1B1-AS1	ENSG00000232973	1.106206144	2.97E-23	1.00E-20
COA3	ENSG00000183978	1.105640306	0.003859096	0.023029772
TXNDC12-AS1	ENSG00000228369	1.103521831	0.008080338	0.039828379
SMAD9	ENSG00000120693	1.10343193	0.001798256	0.012988299
CYTH4	ENSG00000100055	1.101579814	0.000710907	0.006168853
FAT2	ENSG00000086570	1.100909955	0.006811583	0.035098077
ZNF544	ENSG00000198131	1.0997434	1.29E-06	3.22E-05
TRIM32	ENSG00000119401	1.096117653	0.003559742	0.021681564
DFFBP1	ENSG00000232303	1.095493038	0.004060811	0.023921629
AL136131.3	ENSG00000272114	1.095368471	5.15E-29	2.34E-26
AC009166.1	ENSG00000261238	1.093596982	0.005519289	0.030010496
C1QL3	ENSG00000165985	1.09269242	1.56E-07	5.33E-06
DUX4L9	ENSG00000224807	1.087625583	0.005255075	0.028960537
MAF	ENSG00000178573	1.084417567	0.001721741	0.012534621
AC110749.1	ENSG00000244086	1.077200674	0.010081288	0.047246038
Z98884.1	ENSG00000236266	1.075875868	3.68E-09	1.91E-07
MORN4	ENSG00000171160	1.073739807	8.13E-11	6.11E-09
AL591684.1	ENSG00000224919	1.072586104	0.001249671	0.009748091
ALG1L7P	ENSG00000251271	1.070476091	0.001330894	0.010259698

SCRG1	ENSG00000164106	1.06960423	0.001260497	0.009806632
AL590677.1	ENSG00000227175	1.067432429	0.000427771	0.004154587
COL18A1-AS1	ENSG00000183535	1.067396783	0.003235252	0.020301979
U91328.3	ENSG00000272558	1.066879642	4.60E-27	1.94E-24
MT-CO1	ENSG00000198804	1.06301169	2.09E-35	1.37E-32
TMEM101	ENSG00000091947	1.060132598	0.005179594	0.028638111
DDIT4-AS1	ENSG00000269926	1.059766002	0.001693489	0.012361004
AC067945.3	ENSG00000231858	1.058502422	0.004817565	0.027280109
AC010127.1	ENSG00000236107	1.054411975	4.68E-23	1.54E-20
LAMA5-AS1	ENSG00000228812	1.052880761	1.21E-05	0.000218663
AL773572.1	ENSG00000225745	1.052189481	0.007716075	0.038515152
PGAM2	ENSG00000164708	1.05048218	1.08E-10	8.04E-09
TTC30B	ENSG00000196659	1.050243434	0.000895943	0.007404535
AHNAK2	ENSG00000185567	1.040114065	5.22E-07	1.52E-05
CTC1	ENSG00000178971	1.039739596	0.009208955	0.043995857
ZHX2	ENSG00000178764	1.037134567	0.01063589	0.049092945
C12orf57	ENSG00000111678	1.03614247	0.006781777	0.034978944
DRC3	ENSG00000171962	1.033318338	1.72E-08	7.81E-07
AC068385.1	ENSG00000255498	1.030014327	9.78E-13	1.00E-10
AL450003.2	ENSG00000234779	1.029731463	0.010595127	0.048973954
DNAH10	ENSG00000197653	1.029377433	2.54E-07	8.23E-06
VTI1B	ENSG00000100568	1.027678193	7.26E-12	6.45E-10
AP000753.2	ENSG00000256789	1.023569919	1.37E-12	1.36E-10
ENO1-AS1	ENSG00000230679	1.023521266	0.000277734	0.00290526
AC073896.5	ENSG00000258260	1.020716224	0.000133137	0.001604437
CCDC28B	ENSG00000160050	1.019187336	0.000318447	0.003249478
EPB42	ENSG00000166947	1.01686543	0.002784285	0.018157042
NDUFB9	ENSG00000147684	1.016657264	3.57E-16	6.91E-14
MMRN2	ENSG00000173269	1.014095546	0.000747085	0.006430814
NUMB	ENSG00000133961	1.012069851	4.67E-05	0.000673923
ZFHX4-AS1	ENSG00000253661	1.011177759	0.010308572	0.04798748
INCA1	ENSG00000196388	1.01093881	0.000262261	0.002770391
ST3GAL1P1	ENSG00000250656	1.007628165	0.008183916	0.040187961
ZNF575	ENSG00000176472	1.007598601	7.72E-18	1.75E-15
ARNTL	ENSG00000133794	1.001929788	3.10E-05	0.000479462
INPP5K	ENSG00000132376	0.999044312	0.001419295	0.010751682
AC127537.1	ENSG00000228000	0.998527525	0.002721512	0.01785614
ZNF496	ENSG00000162714	0.997913286	1.48E-12	1.46E-10
C17orf62	ENSG00000178927	0.995325054	0.00014801	0.001747994
AP006284.1	ENSG00000254815	0.995266451	0.003823192	0.022850151
AC114812.1	ENSG00000178836	0.99400091	0.008026289	0.039644699
PAXIP1	ENSG00000157212	0.992319652	0.001831875	0.013142018
ACTA2-AS1	ENSG00000180139	0.98988982	0.001972604	0.013924954

PCDH12	ENSG00000113555	0.9866712	0.002578333	0.017116423
TBC1D14	ENSG00000132405	0.984652007	6.88E-06	0.000133646
ZC2HC1A	ENSG00000104427	0.984421363	0.005149945	0.028584193
AC104365.2	ENSG00000267501	0.984359926	0.010907361	0.049909311
RAB7B	ENSG00000276600	0.982789105	7.09E-07	1.97E-05
PARD6G	ENSG00000178184	0.981006383	7.74E-07	2.11E-05
STARD4-AS1	ENSG00000246859	0.977337956	2.37E-18	5.71E-16
AC005865.2	ENSG00000250770	0.976976112	0.00051941	0.004864575
PITPNM2	ENSG00000090975	0.974391742	0.007511793	0.037718655
WFDC21P	ENSG00000261040	0.973680932	0.003343948	0.020752511
AC087482.1	ENSG00000259347	0.972736084	0.000798634	0.006795295
ANKH	ENSG00000154122	0.971151326	4.26E-16	7.99E-14
LGALS2	ENSG00000100079	0.969359252	0.003238198	0.020309675
C6orf223	ENSG00000181577	0.966082978	2.61E-05	0.000418316
AC138466.4	ENSG00000279480	0.9649354	6.02E-06	0.000118775
CLDN2	ENSG00000165376	0.964239052	0.001109517	0.00884767
AL122010.1	ENSG00000230163	0.963043525	0.008350144	0.040783788
LCA5L	ENSG00000157578	0.961946598	0.003153855	0.019923605
AC099795.1	ENSG00000283973	0.961840952	0.000321362	0.003269205
PICART1	ENSG00000246640	0.958362659	0.000112496	0.001392633
AC025048.4	ENSG00000267416	0.958082393	0.006723434	0.034777024
RPSAP52	ENSG00000241749	0.952045489	0.000329031	0.003332642
HRNR	ENSG00000197915	0.949193357	0.000114092	0.001407971
AC023355.1	ENSG00000259488	0.949118534	2.90E-13	3.33E-11
B9D1	ENSG00000108641	0.947118216	0.004723394	0.026883509
KIF28P	ENSG00000223519	0.944482579	0.005736144	0.030806666
AC068594.1	ENSG00000263718	0.94299454	0.000841431	0.007072809
TP53I3	ENSG00000115129	0.942207462	0.000767404	0.006591303
TMEM150A	ENSG00000168890	0.941817795	0.00024923	0.002661243
AL356095.2	ENSG00000279399	0.940181207	4.83E-07	1.44E-05
DEAF1	ENSG00000177030	0.935918404	7.18E-07	1.99E-05
AC022784.7	ENSG00000254340	0.93379331	1.08E-06	2.80E-05
SLITRK5	ENSG00000165300	0.933646839	4.05E-05	0.000595932
AC020779.2	ENSG00000260173	0.932937364	0.004061208	0.023921629
LDHAP2	ENSG00000235674	0.930463884	0.005984735	0.031780448
ATP8B1	ENSG00000081923	0.930169612	0.00018154	0.002048574
AL357033.4	ENSG00000277496	0.929981821	0.000133296	0.001604714
SEMA5A-AS1	ENSG00000251370	0.929873737	5.61E-08	2.17E-06
WDR88	ENSG00000166359	0.927758125	0.000247955	0.002650091
HOXA4	ENSG00000197576	0.927162787	0.00156318	0.011603494
POLR2B	ENSG00000047315	0.924837234	2.78E-14	3.82E-12
CGREF1	ENSG00000138028	0.923011803	0.001380905	0.010575098
AC084116.4	ENSG00000254010	0.921940676	1.24E-12	1.24E-10

RNF24	ENSG00000101236	0.921875113	6.85E-07	1.92E-05
B4GALT1-AS1	ENSG00000233554	0.919624839	0.005703075	0.030684881
POR	ENSG00000127948	0.918542814	0.007796324	0.038800922
CCDC192	ENSG00000230561	0.916934228	0.005112821	0.028442025
VLDLR-AS1	ENSG00000236404	0.913323686	4.95E-11	3.95E-09
CCDC57	ENSG00000176155	0.911833754	0.001121756	0.008927184
AC009126.1	ENSG00000247121	0.911487314	0.00343179	0.021142118
MED31	ENSG00000108590	0.910801103	1.37E-13	1.65E-11
ZNF436-AS1	ENSG00000249087	0.91002824	0.004407009	0.025482416
TMEM9B	ENSG00000175348	0.909229171	0.001643427	0.012085227
KCNQ1OT1_5	ENSG00000276015	0.9077337	2.24E-06	5.10E-05
AP001442.1	ENSG00000233783	0.907545871	0.000646613	0.005744302
C12orf73	ENSG00000204954	0.9038215	0.008759085	0.04229141
ACP4	ENSG00000142513	0.903264257	0.003027632	0.019348665
AC004889.1	ENSG00000244198	0.902558823	0.004249452	0.02474656
PSG4	ENSG00000243137	0.901938108	0.007061692	0.036087662
SLC19A1	ENSG00000173638	0.90004357	1.28E-26	5.21E-24
RNY3P8	ENSG00000223298	0.898763706	0.010462569	0.048551253
RNF220	ENSG00000187147	0.898540633	2.01E-10	1.39E-08
ZC3H12B	ENSG00000102053	0.896387579	0.000890518	0.007375184
HOXC10	ENSG00000180818	0.895964434	0.005213401	0.028784606
STPG3	ENSG00000197768	0.892251509	0.003431593	0.021142118
AC009542.1	ENSG00000231794	0.89224746	2.05E-08	9.09E-07
SPATA6L	ENSG00000106686	0.891594884	9.48E-05	0.001216361
SLC34A3	ENSG00000198569	0.889965046	0.003769032	0.022652556
RAB11B	ENSG00000185236	0.889373279	0.006916498	0.035499278
AC021088.1	ENSG00000250619	0.888573026	2.75E-17	6.02E-15
DUX4L50	ENSG00000232815	0.884848923	0.000643787	0.005729558
AC090617.6	ENSG00000263050	0.883970525	0.00041155	0.004030189
AL121753.2	ENSG00000279253	0.883221621	8.57E-10	5.19E-08
GPAT2	ENSG00000186281	0.881015136	5.76E-07	1.66E-05
AC004834.1	ENSG00000284523	0.878822891	0.000209767	0.002313121
CAMTA2	ENSG00000108509	0.876514046	1.83E-08	8.29E-07
IDUA	ENSG00000127415	0.876005991	0.000284641	0.002959159
DHDDS	ENSG00000117682	0.873580125	0.00018599	0.002093935
AC002472.2	ENSG00000284060	0.872605619	0.00014553	0.001723878
CACNA2D2	ENSG00000007402	0.871468229	0.009078928	0.043550827
ITGB8	ENSG00000105855	0.871343525	0.007881729	0.039127036
GEMIN4	ENSG00000179409	0.869933592	4.85E-07	1.44E-05
SELENOP	ENSG00000250722	0.869716608	6.50E-17	1.37E-14
GPRC5B	ENSG00000167191	0.867106782	2.58E-09	1.42E-07
TAP1	ENSG00000168394	0.866840867	1.94E-09	1.10E-07
ZNF32-AS1	ENSG00000226245	0.864406711	2.18E-05	0.000362032

LINC02029	ENSG00000241544	0.863180831	0.002288401	0.015640053
CLDN10	ENSG00000134873	0.859839339	0.000821266	0.006937148
ACVR2A	ENSG00000121989	0.859571593	0.002712713	0.017818207
NDRG1	ENSG00000104419	0.859565077	0.004399417	0.025456692
ODF3B	ENSG00000177989	0.856642492	0.004882197	0.027523038
ZNF32-AS2	ENSG00000230565	0.856270008	0.000186797	0.002101024
AC113189.1	ENSG00000262624	0.855528807	6.09E-07	1.73E-05
AC091132.5	ENSG00000267198	0.855277479	0.008484638	0.041202126
AC079226.1	ENSG00000248694	0.853362411	1.44E-16	2.93E-14
AL157935.1	ENSG00000227218	0.852471873	0.000322354	0.003276243
FAM20A	ENSG00000108950	0.852136081	1.47E-05	0.000259527
AC148477.3	ENSG00000256943	0.852099847	3.81E-06	8.15E-05
AC016683.1	ENSG00000234174	0.851937085	0.000458898	0.004376229
CA14	ENSG00000118298	0.847934112	0.002798738	0.018241223
AL671883.3	ENSG00000271581	0.847617088	1.20E-17	2.67E-15
DDB2	ENSG00000134574	0.842250373	7.49E-05	0.000995278
AC011495.3	ENSG00000268677	0.841725731	0.009089359	0.043565476
NDUFS7	ENSG00000115286	0.840936329	0.007187551	0.036588352
FLG	ENSG00000143631	0.838645956	5.08E-11	4.02E-09
SLC10A1	ENSG00000100652	0.837942951	0.00238828	0.016145153
AC011611.3	ENSG00000257453	0.835177161	1.85E-14	2.57E-12
C14orf166	ENSG00000087302	0.835161138	5.21E-12	4.77E-10
RNF215	ENSG00000099999	0.834565216	5.19E-06	0.00010609
AC002070.1	ENSG00000248636	0.8328637	0.00709912	0.036216243
CENPV	ENSG00000166582	0.831774915	0.007234399	0.036793527
PEX12	ENSG00000108733	0.831715496	0.004093035	0.024073078
ANXA2R	ENSG00000177721	0.831661532	3.11E-06	6.82E-05
HACD4	ENSG00000188921	0.828313731	0.000152383	0.001790686
PDCD4	ENSG00000150593	0.828066394	7.58E-15	1.21E-12
AC148477.2	ENSG00000256542	0.826648084	1.15E-13	1.40E-11
PIGCP1	ENSG00000213713	0.824442335	5.06E-06	0.000103505
DCAF6	ENSG00000143164	0.822626822	7.85E-16	1.43E-13
ZNF213	ENSG00000085644	0.822412928	0.007243006	0.036803096
AC129507.4	ENSG00000262920	0.82172459	6.87E-05	0.000924329
AC104365.3	ENSG00000267705	0.816707275	1.65E-10	1.16E-08
AP001615.1	ENSG00000236883	0.811669422	5.51E-11	4.34E-09
LTBP2	ENSG00000119681	0.811238145	0.000138014	0.001649742
BBOF1	ENSG00000119636	0.809858778	4.39E-08	1.75E-06
BRINP1	ENSG00000078725	0.808244888	1.91E-05	0.000325331
AVIL	ENSG00000135407	0.806425815	0.000107936	0.001356094
FER1L5	ENSG00000249715	0.805263626	0.002373398	0.016078329
LRRC37A	ENSG00000176681	0.804296223	0.001969038	0.013916418
METRN	ENSG00000103260	0.802901532	0.003799047	0.022754041

AC005540.1	ENSG00000235852	0.802213314	1.18E-18	3.02E-16
UBXN6	ENSG00000167671	0.800243044	1.98E-08	8.80E-07
AC015688.8	ENSG00000266872	0.799922285	1.58E-06	3.84E-05
AL133410.2	ENSG00000228843	0.799683691	3.13E-07	9.95E-06
AC141424.1	ENSG00000241525	0.798329678	6.79E-07	1.90E-05
LIPA	ENSG00000107798	0.79708851	2.25E-15	3.80E-13
ETV4	ENSG00000175832	0.794409117	0.008774673	0.042349363
AC104365.1	ENSG00000267476	0.79088965	7.11E-08	2.68E-06
AC091564.7	ENSG00000255680	0.790621383	0.00043615	0.004211716
PRIMPOL	ENSG00000164306	0.789430647	1.65E-06	3.93E-05
LRP2BP	ENSG00000109771	0.788845318	1.32E-05	0.000234084
AC073834.1	ENSG00000237655	0.788420202	0.000173811	0.001983042
AC072022.2	ENSG00000228804	0.786869567	0.007741398	0.038592616
SLC24A5	ENSG00000188467	0.786452468	1.40E-10	1.02E-08
SPAG7	ENSG00000091640	0.785484709	0.010496058	0.048686969
AC025171.2	ENSG00000215068	0.784710235	2.74E-06	6.14E-05
AL163636.1	ENSG00000258451	0.783031812	9.77E-05	0.00124789
PTPN18	ENSG00000072135	0.780239307	7.86E-06	0.000149276
GLS2	ENSG00000135423	0.779393176	1.83E-06	4.31E-05
AC108863.1	ENSG00000253645	0.778628957	5.53E-12	5.02E-10
NPB	ENSG00000183979	0.776561912	4.08E-10	2.65E-08
AL358852.1	ENSG00000278899	0.77652264	0.001897293	0.013538991
MXRA8	ENSG00000162576	0.775072102	1.03E-06	2.70E-05
AP006621.1	ENSG00000255108	0.774614921	1.75E-10	1.22E-08
ALDH6A1	ENSG00000119711	0.774089438	9.96E-05	0.00126709
CRACR2B	ENSG00000177685	0.773238859	1.67E-06	3.97E-05
EPS8L2	ENSG00000177106	0.770196496	4.65E-07	1.40E-05
KMO	ENSG00000117009	0.770083179	3.65E-12	3.37E-10
ZBTB5	ENSG00000168795	0.769877783	7.33E-05	0.000980109
LDHAL6B	ENSG00000171989	0.768325013	0.000878795	0.007307009
SRPK3	ENSG00000184343	0.767711539	0.00110479	0.008821885
LINC01465	ENSG00000221949	0.767382168	5.05E-07	1.49E-05
AL358333.3	ENSG00000259007	0.766887097	0.002896988	0.018736818
AC083964.1	ENSG00000272293	0.766068916	1.19E-07	4.28E-06
ZSWIM8	ENSG00000214655	0.765384826	3.80E-06	8.14E-05
AC010327.3	ENSG00000267577	0.764541763	5.77E-05	0.000798665
SLC6A6	ENSG00000131389	0.763996581	0.002694566	0.017725105
SLAMF8	ENSG00000158714	0.762424344	0.010685817	0.049219774
PTPMT1	ENSG00000110536	0.761567961	6.66E-15	1.08E-12
PP7080	ENSG00000188242	0.761025136	0.000576902	0.005269303
TRMT10B	ENSG00000165275	0.760521964	8.37E-08	3.09E-06
CCDC107	ENSG00000159884	0.758611305	1.20E-05	0.000217839
AL355916.1	ENSG00000250548	0.757603427	1.18E-10	8.58E-09

AC009034.1	ENSG00000261113	0.755457973	1.92E-06	4.47E-05
ST7-AS1	ENSG00000227199	0.75515831	0.000424486	0.004135981
VEGFA	ENSG00000112715	0.754677251	0.000923659	0.007601684
TMEM8B	ENSG00000137103	0.754371098	0.000555265	0.005119185
AC233723.2	ENSG00000280254	0.753573439	0.000351828	0.003536243
ARFGAP2	ENSG00000149182	0.752536983	0.00951434	0.045090031
INE2	ENSG00000281371	0.751720376	0.000895675	0.007404535
AC003075.1	ENSG00000237773	0.751259727	1.05E-07	3.78E-06
ARHGAP44	ENSG00000006740	0.748985567	0.004872815	0.027495435
AC003102.1	ENSG00000260793	0.748564414	0.00108181	0.008679466
SLC12A4	ENSG00000124067	0.747522668	0.0016348	0.012047508
LYPD1	ENSG00000150551	0.74723462	4.20E-15	6.94E-13
GCC2-AS1	ENSG00000214184	0.745947984	1.73E-05	0.000298615
KCNAB1	ENSG00000169282	0.745280346	2.19E-05	0.000363071
AC005046.1	ENSG00000273055	0.744792359	0.00515532	0.028584193
IMPDH1P10	ENSG00000232133	0.744230596	8.32E-10	5.07E-08
CXCL16	ENSG00000161921	0.744048356	5.02E-05	0.000715282
CICP14	ENSG00000281490	0.742636807	3.97E-05	0.000586381
AP006621.4	ENSG00000269915	0.742598553	5.23E-13	5.51E-11
GPR68	ENSG00000119714	0.742548419	0.000351136	0.0035323
AC137834.2	ENSG00000276727	0.742522978	3.49E-14	4.68E-12
PAX6	ENSG00000007372	0.741891511	0.000802931	0.006822029
AC010768.1	ENSG00000254693	0.741422523	6.39E-08	2.42E-06
PRKCA-AS1	ENSG00000264630	0.741326981	0.001258546	0.009797912
KCNMA1-AS1	ENSG00000236467	0.740678984	5.86E-14	7.52E-12
NR1H3	ENSG00000025434	0.740535171	2.98E-05	0.000464994
AC010776.2	ENSG00000267774	0.739253488	1.01E-10	7.58E-09
GNG12-AS1	ENSG00000232284	0.738331764	2.24E-05	0.000369492
C19orf71	ENSG00000183397	0.737629476	4.33E-10	2.79E-08
ZFPM2	ENSG00000169946	0.73669513	1.77E-06	4.19E-05
HK2	ENSG00000159399	0.736351218	1.19E-06	3.03E-05
BX470102.1	ENSG00000238279	0.735661724	0.000179779	0.002043491
AL133375.1	ENSG00000245261	0.735494303	0.000604191	0.005447868
NUDT4	ENSG00000173598	0.733160392	4.66E-06	9.65E-05
KF459542.1	ENSG00000231880	0.728822874	9.18E-08	3.36E-06
MARS	ENSG00000166986	0.728204485	1.45E-10	1.04E-08
AL391834.1	ENSG00000272842	0.727169484	0.000382264	0.0037747
AL807752.2	ENSG00000229257	0.725678342	2.15E-12	2.08E-10
AC025271.2	ENSG00000261265	0.724937375	0.000804085	0.006826923
RPS27AP13	ENSG00000244159	0.724273913	0.005507231	0.029972533
LETM2	ENSG00000165046	0.722851372	0.001692663	0.012361004
CXXC5-AS1	ENSG00000250635	0.72201451	0.003154711	0.019923605
LRRC28	ENSG00000168904	0.721767429	0.004203391	0.02457527

EPHA5-AS1	ENSG00000250846	0.721439616	5.91E-08	2.25E-06
MMP24-AS1	ENSG00000126005	0.720954878	5.24E-14	6.80E-12
NMRAL1	ENSG00000153406	0.720757353	0.003568843	0.021725789
BHLHE40-AS1	ENSG00000235831	0.718440087	1.41E-06	3.48E-05
AC004771.2	ENSG00000234203	0.717504449	0.006706528	0.034723406
C9orf139	ENSG00000180539	0.717216862	0.002917726	0.018798878
PPIL2	ENSG00000100023	0.714979077	0.007411567	0.037358345
PHLDA1	ENSG00000139289	0.714655364	0.000352641	0.003540788
PRSS54	ENSG00000103023	0.71369191	8.63E-06	0.000162504
PLPP5	ENSG00000147535	0.713530539	0.001896343	0.013538991
MSMP	ENSG00000215183	0.711555566	6.50E-09	3.20E-07
GFAP	ENSG00000131095	0.71060916	1.93E-06	4.48E-05
FRMD5	ENSG00000171877	0.709932232	0.003110362	0.019727916
AL109936.8	ENSG00000284726	0.708232048	0.00130688	0.010107565
CD44-AS1	ENSG00000255443	0.707645438	3.78E-13	4.21E-11
LOXL1-AS1	ENSG00000261801	0.70736087	0.000129956	0.001573602
AC010542.4	ENSG00000261519	0.706495523	0.005337826	0.02930717
CCR10	ENSG00000184451	0.706336241	0.002641006	0.017463766
TMEM80	ENSG00000177042	0.705135277	5.35E-07	1.55E-05
POLR2L	ENSG00000177700	0.703248847	6.56E-16	1.21E-13
ANKMY1	ENSG00000144504	0.702322701	2.46E-05	0.000400203
TMEM44-AS1	ENSG00000231770	0.699194755	0.001832761	0.013142018
MYLK-AS1	ENSG00000239523	0.697729503	0.000314617	0.003219776
CFAP52	ENSG00000166596	0.697605309	0.000379077	0.003755787
MYBBP1A	ENSG00000132382	0.697368976	5.06E-07	1.49E-05
GPX3	ENSG00000211445	0.696540256	3.60E-05	0.00053831
AC034236.2	ENSG00000271918	0.695179907	4.92E-06	0.000101308
AC087289.5	ENSG00000267801	0.695053408	9.07E-09	4.30E-07
CBR3	ENSG00000159231	0.69359647	0.007060047	0.036087662
AC090197.1	ENSG00000253837	0.693069427	2.63E-12	2.48E-10
AC008906.1	ENSG00000248734	0.692999026	5.88E-09	2.92E-07
ENTPD7	ENSG00000198018	0.692804143	0.002219302	0.015229492
SERINC4	ENSG00000184716	0.692443971	4.20E-08	1.69E-06
AC093591.2	ENSG00000261668	0.689475359	0.001937609	0.013768451
SHQ1P1	ENSG00000231588	0.688365017	0.009251	0.044161
HLA-V	ENSG00000181126	0.686073335	0.006312955	0.033195014
AC148477.4	ENSG00000277011	0.685694229	1.95E-07	6.58E-06
TTN	ENSG00000155657	0.685463667	0.008508338	0.041283269
THCAT158	ENSG00000263293	0.685111947	0.005597649	0.030283203
AC090510.1	ENSG00000246283	0.684700251	3.23E-08	1.33E-06
AC093462.1	ENSG00000277324	0.684149085	0.005427878	0.02965439
SDCCAG8	ENSG00000054282	0.683759407	3.54E-05	0.000531583
AC025165.2	ENSG00000257342	0.683738407	4.23E-15	6.94E-13

SBF2-AS1	ENSG00000246273	0.682707753	4.87E-09	2.46E-07
ZSCAN16-AS1	ENSG00000269293	0.68193376	0.003079655	0.019581381
FBXO8	ENSG00000164117	0.680554385	0.000170589	0.001955982
ACAP1	ENSG00000072818	0.679650771	1.85E-06	4.32E-05
MRPL34	ENSG00000130312	0.678570717	0.001669207	0.012236708
AC079922.2	ENSG00000237753	0.676358456	3.73E-06	8.00E-05
ABR	ENSG00000159842	0.676274418	3.19E-05	0.000490195
MIR3918	ENSG00000265558	0.675703224	0.001523908	0.011376328
TMEM87A	ENSG00000103978	0.675694805	0.000814218	0.006893125
C14orf93	ENSG00000100802	0.675332672	0.001462822	0.01102484
HDDC2	ENSG00000111906	0.674958902	3.10E-09	1.65E-07
SPTB	ENSG00000070182	0.674429273	1.99E-09	1.13E-07
VCAN-AS1	ENSG00000249835	0.674139014	1.04E-14	1.60E-12
AC100861.2	ENSG00000250714	0.673883455	1.66E-05	0.000287953
AC007485.2	ENSG00000279059	0.671759062	0.000876373	0.007298984
SLC25A4	ENSG00000151729	0.67158839	0.010895682	0.049875196
RDH10-AS1	ENSG00000250295	0.671516729	0.003326112	0.020685298
AL807752.3	ENSG00000231864	0.670179452	3.72E-16	7.09E-14
RNF2P1	ENSG00000231381	0.670110272	0.010929821	0.049973359
AL390719.1	ENSG00000217801	0.669057124	0.007921408	0.039275233
AC112211.1	ENSG00000272149	0.666679792	4.34E-06	9.09E-05
AC108058.1	ENSG00000238273	0.666481	3.04E-09	1.64E-07
TP53I13	ENSG00000167543	0.666201755	0.000734665	0.006340045
AC060780.1	ENSG00000267002	0.664578044	0.000606952	0.005467665
ELMOD3	ENSG00000115459	0.664544147	2.99E-10	1.95E-08
KCNIP1	ENSG00000182132	0.664110379	0.00336084	0.020835444
MNS1	ENSG00000138587	0.663980688	0.006612942	0.034344256
TMX2P1	ENSG00000213839	0.663212366	1.56E-09	9.04E-08
AC015849.3	ENSG00000270871	0.662763316	0.001451332	0.010959226
AP001178.3	ENSG00000266456	0.661338017	0.005697153	0.030668677
AL391421.1	ENSG00000204049	0.659683651	5.52E-05	0.000771259
EML2	ENSG00000125746	0.658918417	0.001380712	0.010575098
BDNF-AS	ENSG00000245573	0.658518534	8.06E-13	8.35E-11
RNF213	ENSG00000173821	0.657559971	1.95E-07	6.58E-06
SMIM27	ENSG00000235453	0.65743312	1.59E-06	3.85E-05
AC131971.1	ENSG00000183562	0.657045014	5.68E-05	0.000788056
ETFBKMT	ENSG00000139160	0.656861926	0.0025453	0.016944754
FRMD3	ENSG00000172159	0.65595657	0.001334651	0.010281951
KBTBD4	ENSG00000123444	0.6546953	1.14E-06	2.90E-05
C16orf45	ENSG00000166780	0.65457209	0.009651889	0.045613768
SLC9A3	ENSG00000066230	0.65448557	2.64E-08	1.11E-06
INO80D	ENSG00000114933	0.654334835	0.006683726	0.034650922
AC063952.1	ENSG00000240661	0.654142715	1.16E-10	8.49E-09

AC234782.2	ENSG00000231728	0.653796355	0.004906938	0.027556316
PYM1	ENSG00000170473	0.653371037	0.009444017	0.044835805
AC091053.1	ENSG00000254665	0.653164503	1.21E-07	4.31E-06
FAAP100	ENSG00000185504	0.652254618	0.004744247	0.026976197
SOX6	ENSG00000110693	0.651523649	0.001196406	0.00940716
AC005703.6	ENSG00000279660	0.651357886	3.45E-11	2.83E-09
UNKL	ENSG00000059145	0.649227556	4.33E-06	9.09E-05
YRDC	ENSG00000196449	0.648744068	4.45E-05	0.000647468
PSD4	ENSG00000125637	0.644458701	0.008182485	0.040187961
WDR6	ENSG00000178252	0.642632542	7.19E-06	0.000138724
SNAPC3	ENSG00000164975	0.641928285	6.71E-10	4.17E-08
TMC3	ENSG00000188869	0.641474837	0.005697466	0.030668677
AC007639.1	ENSG00000263680	0.641229375	2.81E-05	0.000443636
IL10RB-AS1	ENSG00000223799	0.640718918	4.24E-08	1.70E-06
KATNAL2	ENSG00000167216	0.640711145	0.009445511	0.044835805
AC068724.2	ENSG00000261687	0.640667009	5.87E-06	0.000116529
AL136980.1	ENSG00000225408	0.639147158	0.000257996	0.002732672
AL391834.2	ENSG00000273226	0.639079491	0.000154819	0.001808517
AC005696.2	ENSG00000272770	0.638783822	2.06E-15	3.52E-13
AC018413.1	ENSG00000265778	0.638305144	0.005907939	0.031528586
AL162419.1	ENSG00000228322	0.638285604	0.009705461	0.045808137
PEX10	ENSG00000157911	0.637730622	1.29E-11	1.10E-09
LACTB2-AS1	ENSG00000246366	0.637184167	2.08E-08	9.17E-07
MCM3AP-AS1	ENSG00000215424	0.636682163	1.13E-14	1.68E-12
AC092881.1	ENSG00000279530	0.635968431	0.000648478	0.005753963
IQCK	ENSG00000174628	0.635476158	7.48E-06	0.00014301
AL596223.2	ENSG00000231748	0.63540174	7.90E-08	2.94E-06
FERMT1	ENSG00000101311	0.63490561	3.59E-05	0.000537476
AC124066.1	ENSG00000265263	0.633651637	7.92E-12	6.98E-10
AC234582.1	ENSG00000231064	0.632468567	0.000447506	0.004293715
AC087276.4	ENSG00000255340	0.632309618	0.000492419	0.004656281
TAPBP	ENSG00000231925	0.631729073	0.002025941	0.014174387
TOM1L1	ENSG00000141198	0.629407552	2.25E-10	1.52E-08
TOPORS	ENSG00000197579	0.628824045	0.000391682	0.003858016
PPID	ENSG00000171497	0.628780172	0.0027649	0.018060544
NIP7	ENSG00000132603	0.628330514	0.007986581	0.039531234
AC019197.1	ENSG00000236283	0.626743398	0.003080627	0.019581381
GLIS3-AS1	ENSG00000237009	0.626041832	0.001997519	0.014033732
AC091153.4	ENSG00000261898	0.625473848	1.32E-06	3.29E-05
PLXNC1	ENSG00000136040	0.624809115	0.001462094	0.01102484
AC025262.3	ENSG00000280320	0.624726134	1.08E-06	2.80E-05
NAV2-AS2	ENSG00000254453	0.623172072	6.87E-05	0.000924329
SUN2	ENSG00000100242	0.623121299	1.23E-05	0.000221423

ARRDC1	ENSG00000197070	0.623084841	2.19E-05	0.00036265
ILK	ENSG00000166333	0.623061675	5.67E-09	2.83E-07
GLIPR1	ENSG00000139278	0.62273243	1.48E-14	2.16E-12
AP001178.2	ENSG00000265490	0.622672616	0.000306546	0.003153577
SLC6A9	ENSG00000196517	0.622273698	0.002694631	0.017725105
AL671277.1	ENSG00000227766	0.621627602	5.75E-10	3.63E-08
S100A1	ENSG00000160678	0.621321329	0.000916544	0.007548389
ANKRD37	ENSG00000186352	0.619279583	7.14E-06	0.000137994
PGM5P2	ENSG00000277778	0.618443627	3.44E-05	0.000520244
FBN1	ENSG00000166147	0.618334351	0.000180657	0.002044104
AC020934.2	ENSG00000267735	0.616173602	2.19E-06	5.01E-05
AC025171.1	ENSG00000177738	0.615668058	8.67E-07	2.33E-05
TSSK2	ENSG00000206203	0.615353886	0.003556152	0.021681564
AC093724.1	ENSG00000213222	0.615039164	3.76E-07	1.16E-05
HDAC5	ENSG00000108840	0.614330458	0.000929524	0.007633988
AC005324.5	ENSG00000266261	0.612660765	1.42E-10	1.03E-08
WDR73	ENSG00000177082	0.612225814	8.49E-06	0.000160343
TBC1D8	ENSG00000204634	0.611633926	7.12E-07	1.98E-05
AC007686.3	ENSG00000273729	0.611518251	2.81E-06	6.27E-05
AC090236.1	ENSG00000267396	0.610473797	0.000199151	0.002208423
ZNF2	ENSG00000275111	0.609168397	0.004043449	0.023864635
SEC14L2	ENSG00000100003	0.607928657	0.00697667	0.035730476
CLU	ENSG00000120885	0.606967508	0.006524665	0.034020438
NFE2L3	ENSG00000050344	0.605759243	3.06E-06	6.73E-05
PUSL1	ENSG00000169972	0.605748699	9.07E-05	0.001173343
MASP2	ENSG00000009724	0.605619078	0.000262847	0.002774108
LINC00621	ENSG00000262619	0.605519472	8.44E-08	3.10E-06
FAM57A	ENSG00000167695	0.60550105	3.24E-05	0.000495104
HSD17B6	ENSG00000025423	0.60514196	8.04E-07	2.19E-05
CPM	ENSG00000135678	0.603846071	2.64E-05	0.000422351
FNDC8	ENSG00000073598	0.603323247	0.003249202	0.020324725
MRPS7	ENSG00000125445	0.602749804	0.00012416	0.001511681
AL160408.2	ENSG00000228830	0.601949517	1.38E-13	1.65E-11
AL358790.1	ENSG00000282772	0.601536008	0.000646707	0.005744302
CDKN2C	ENSG00000123080	0.600709123	0.00306719	0.019527499
TUBGCP4	ENSG00000137822	0.600310807	1.13E-11	9.72E-10
EMC9	ENSG00000100908	0.599722837	4.70E-07	1.41E-05
AP1G2	ENSG00000213983	0.599240327	5.74E-06	0.000114605
TSPOAP1-AS1	ENSG00000265148	0.598990943	7.73E-11	5.85E-09
AC005775.1	ENSG00000266933	0.598868095	0.005370294	0.029458044
GGACT	ENSG00000134864	0.597598168	3.91E-06	8.33E-05
RNU6-395P	ENSG00000202532	0.596947114	0.000112343	0.001392633
ANKRD6	ENSG00000135299	0.596149566	0.00026728	0.002813344

AC012640.1	ENSG00000248968	0.595310433	6.21E-05	0.000842617
RCC1L	ENSG00000274523	0.594380513	0.000173957	0.001983042
RNF207	ENSG00000158286	0.592622008	0.001956108	0.013854164
PSMB10	ENSG00000205220	0.592529909	0.010805434	0.049622767
AL121748.2	ENSG00000238258	0.591836693	6.53E-12	5.84E-10
MTBP	ENSG00000172167	0.591523385	2.63E-10	1.74E-08
CRLS1	ENSG00000088766	0.590508081	1.75E-09	1.00E-07
Z94160.2	ENSG00000272694	0.58964097	5.35E-06	0.00010831
AC106786.2	ENSG00000249996	0.588779272	4.70E-05	0.000676893
LDLRAD2	ENSG00000187942	0.588534697	3.50E-09	1.85E-07
PHKG2	ENSG00000156873	0.588097685	0.000101065	0.001283413
SLC25A26	ENSG00000144741	0.58742285	2.65E-05	0.000423107
AC008734.1	ENSG00000269300	0.586516278	0.002802448	0.018255326
ITGB1BP1	ENSG00000119185	0.585976091	1.68E-14	2.39E-12
AC022966.2	ENSG00000267601	0.58590163	2.54E-12	2.42E-10
BCAN	ENSG00000132692	0.585231051	0.001164661	0.009194284

Appendix C: Genomic Sequencing at *RB1* locus in wild-type and *RB1* KO monoclonal cells